Zero-skew bridge deck behavior at expansion joints

by

Jeremy Lee Ryan, B.S.

Thesis

Presented to the Faculty of the Graduate School of

The University of Texas at Austin

in Partial Fulfillment

of the Requirements

for the Degree of

Master of Science in Engineering

The University of Texas at Austin

August 2003

Zero-skew bridge deck behavior at expansion joints

Approved by
Supervising Committee:

Oguzhan Bayrak, Supervisor

James O. Jirsa

Dedication

To my parents, who have always supported and encouraged me

Acknowledgements

I would like to thank Dr. Oguzhan Bayrak for his invaluable advice and insight as well as his dedication to the conclusion of this research project and thesis. Dr. James O. Jirsa was instrumental in the design and testing phase of the project as well as revising this thesis. The prompt and perceptive suggestions of Dr. Bayrak and Dr. Jirsa have enhanced this thesis significantly. In addition, thank you to Dr. Richard E. Klingner for the extensive experience in bridge deck research he brought to this research project. Dr. John E. Breen was a source of inspiration and friendly advice throughout this research as well as in the classroom. I would like to express my appreciation to the above professors and the rest of the structural engineering department at The University of Texas at Austin for the financial support during my time in Austin.

This research was funded by the Texas Department of Transportation (TxDOT). As the TxDOT contact for this research project, Dean Van Landuyt's advice and enthusiasm was much appreciated. Thank you to TxDOT for the extensive research funding they grant to The University of Texas at Austin.

I would like to thank Beth Woodward and Christin Coselli, the two graduate students who worked with me on this test specimen, for their assistance and friendship. Thank you to Jennifer Eggers and Cory Redding, the undergraduate assistants who worked on this bridge deck test specimen, for the hard work they dedicated to making this research a success. The expertise of

Blake Stasney, Mike Bell and Dennis Fillip, the Ferguson Laboratory's staff, was essential in the construction and testing of this bridge deck test specimen.

I owe a dept to Baris Binici, a fellow graduate student at The University of Texas at Austin, who performed the punching shear analysis and discussion for this bridge deck. His extensive knowledge of punching shear behavior as well as his eagerness to help were greatly appreciated.

I would like to thank my father, Bill Ryan, for always encouraging me to strive for more. I am grateful for his sound advice and edification through the years. Thank you to my mother, Jane Ryan-Cummings, who also helped to guide me and is always there for me. I would also like to express my sincere gratitude to my girlfriend, Jennifer Warren, for emotional support, which helped me remain focused on my goals. Thank you for patiently listening to my set backs, successes, and everything in between. I would not have been able to complete this thesis without all of you.

Jeremy Ryan

August, 11 2003

Abstract

Zero-skew bridge deck behavior at expansion joints

Jeremy Lee Ryan, M.S.E.

The University of Texas at Austin, 2003

Supervisors: Oguzhan Bayrak and James O. Jirsa

The TxDOT IBTS detail is a standard design for the slab end of bridge decks, which is commonly used at expansion joints. The IBTS detail creates a four-foot wide edge beam by increasing the section depth and reducing the spacing of the reinforcing steel. This detail has performed satisfactorily in the field; however, its origin as well as ultimate capacity is unknown. In addition, there is little previous research testing the edge of bridge decks.

For this reason, a zero-skew, full-scale bridge deck test specimen was constructed and loaded with AASHTO design loadings. This rectangular deck will simplify data analysis as well as providing a baseline for comparison to future, skewed test specimens. An un-thickened slab end detail, named the Uniform Thickness Slab End (UTSE) detail, was also tested with the aim of

increasing construction economy. The final specimen was a three-span, 18-foot by 32-foot composite bridge deck on steel girders. It contained four test areas and two variables, the deck span (eight and 10-foot) and the slab end detail (IBTS and UTSE). Influence lines were used to determine the critical loading locations to maximize positive and negative moment in the bridge deck. The tandem and truck loading configurations, given in the AASHTO LRFD Bridge Design Specification, were applied at the HS-20 and HS-25 design load levels. Then, typical design overloads of 20%, 75% and 200% were applied, and finally, the bridge deck was loaded to failure.

The failure mechanism for all tests was punching shear at the edge tire, although, after punching, significant reserve strength remained. The punching shear prediction given by AASHTO LRFD is unconservative for the edge tests performed on this test specimen. However, when the effect of unbalanced moment is included in the ACI 318-02 provisions, conservative and accurate predictions result.

At service load levels and overloads, when spanning eight-feet, the IBTS and UTSE details performed well as far as crack propagation, relative deflections, and strain magnitudes. The IBTS and UTSE details were un-cracked up to the 200% overload, when spanning eight-feet. However, when spanning 10-feet, both details cracked near the design load level. The UTSE detail was more flexible than the IBTS and had a lower punching capacity due to its smaller section depth. The reserve strength measured in the four test areas on this bridge deck test specimen ranged from 6.1 to 4.9 times the HS-25 design load.

Table of Contents

List of Tables

List of Figures

CHAPTER 1
Introduction

1.1 BACKGROUND

The IBTS detail (Figure 1-1 through Figure 1-3) is a standard design for the slab end of a bridge deck and is commonly used at expansion joints. The Texas Department of Transportation (TxDOT) uses its IBTS detail in the majority of the bridge decks they build. The origin of the detail is not well known, however, it has performed adequately in the field. TxDOT recently increased the required design loading for their bridge decks by 25%. This is partly due to the implementation of the North American Free Trade Agreement (NAFTA) on January 1, 1994. NAFTA increased trade with Mexico, which substantially increased truck traffic on the interstate highways in Texas. Another cause of the design load increase is that trucks are often operated at loads beyond the legal limit, as it is difficult to enforce the load restrictions. This has prompted the need to know the behavior of the IBTS detail at service load and overload conditions as well as its capacity.

In this research, the behavior of the free edge of bridge decks, typically occurring at expansion joints is examined. This is a complicated location because the deck acts as a two-way slab and is affected by torsional moments due to the free edge. An area in the middle of a typical deck has continuity on all sides to distribute loads in two directions. The loads applied on a typical free edge are transferred to supporting girders in a somewhat more complicated manner. In addition, the dynamic loads from truck tires pounding the expansion joint of the deck impose increased stresses on the free edge.

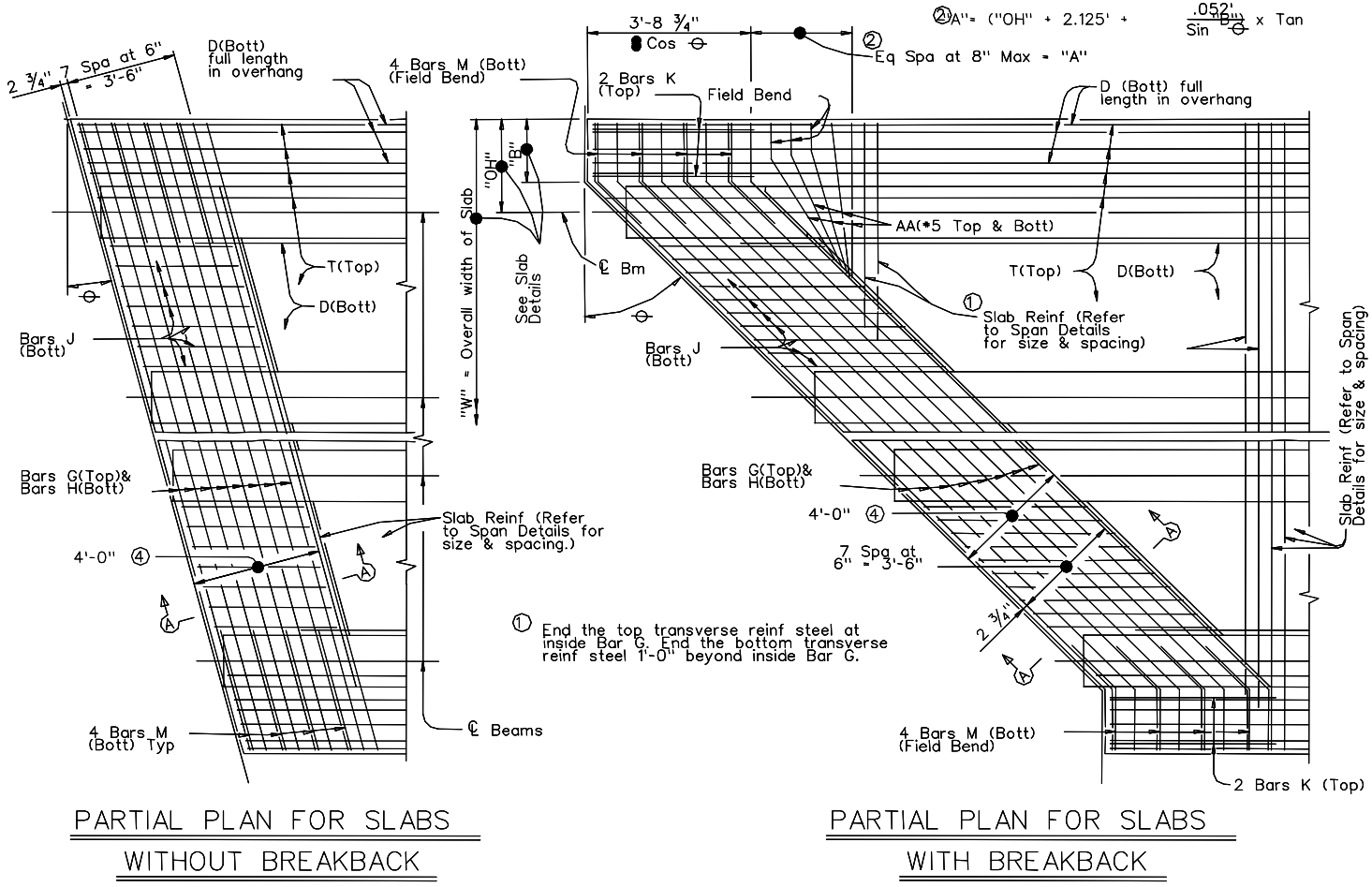

Figure 1-1: TxDOT IBTS detail, plan view

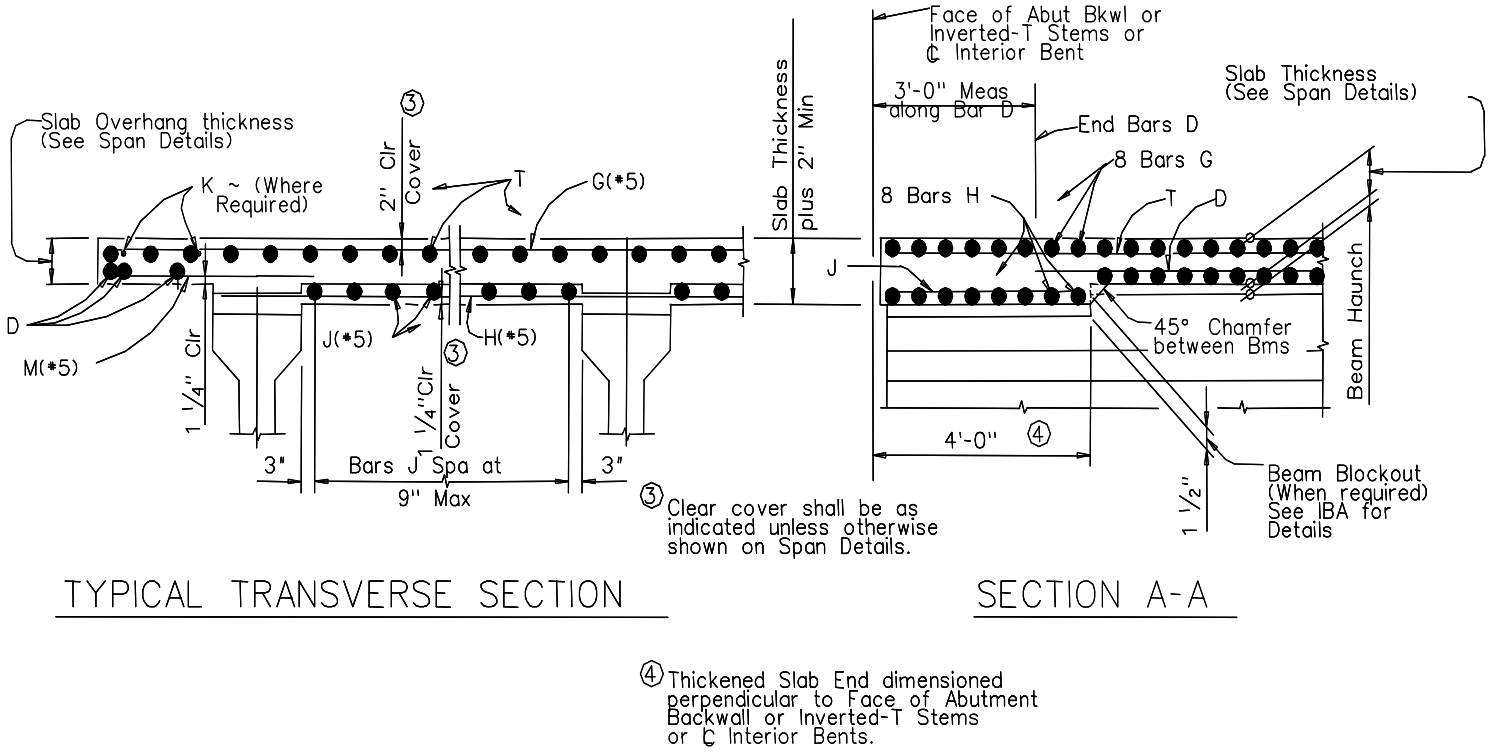

Figure 1-2: TxDOT IBTS detail, cross-sections

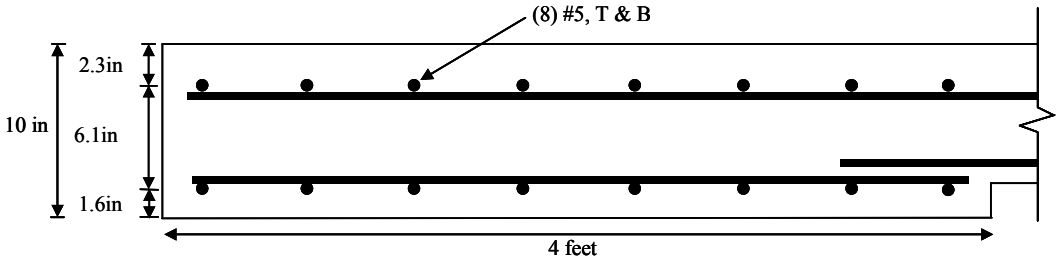

Figure 1-3: IBTS cross-section

Previous bridge deck research has focused on testing the interior of the deck as opposed to the free edge. However, the edge of the bridge deck is a critical location because it is not surrounded on all sides by concrete. The IBTS detail is two inches thicker and has a closer spacing of reinforcement than the typical deck in order to withstand the applied loads. The previous research (loads applied on the interior of the bridge deck) has found that the ultimate capacity of a bridge deck is often several times the service load level they are designed for (Youn and Chang, 2). The significant over-strength of bridge decks has been attributed to arching action (compressive membrane action), occurring due to lateral restraint created by the surrounding deck and girders. However, due to the lack of research on the edge of bridge decks, arching action has not been verified at this location.

Due to the size, and therefore, cost of constructing a full-scale bridge deck as a test specimen, most previous research has been on scale models. In order to test the IBTS detail as it exists in the field, a full-scale specimen was necessary. Therefore, the effects of scaling the test specimen will not be a factor.

The IBTS detail is not easy to construct, as the thickening of the edge requires additional formwork. If the increase in load capacity caused by arching action occurs at the free edge of the bridge deck, the thickened edge may be unnecessary for strength requirements. An alternate, possibly more economical detail was tested on one edge of the specimen, which is not thickened, but has a

similar capacity to the IBTS detail. Named the Uniform Thickness Slab End (UTSE) detail, it has been instrumented and tested in the same manner as the IBTS detail. Its behavior has been compared and contrasted with the IBTS detail. Serviceability (cracking, deflections, etc.) issues could be significant with an un-thickened edge detail. Significant cracking under increased loading may cause increased deflections and increase the possibility of corrosion of the reinforcing steel where deicing agents are used or the deck is exposed to the sea.

In the experimental program carried out during this research project, the IBTS detail was subjected to design loads as well as typical overloads to determine its serviceability performance. The specimen was then taken to failure to determine its ultimate capacity and failure mechanism. Performance of the bridge deck was evaluated using extensive instrumentation applied to the test specimen. Strain, deflection and load measurements were recorded through out testing. In addition, crack maps were created to show the extent of cracking at service loads as well as yield lines at failure.

In this thesis, the behavior of the edge of zero degree skew bridge decks was studied. Understanding the behavior of zero degree skew bridge decks at expansion joints provides a reference for interpreting the behavior of skewed bridge deck end details. Effects of skew on bridge deck behavior will be examined in subsequent tests of this ongoing research project.

1.2 OBJECTIVES AND SCOPE

The objectives of the overall research project are:

- To understand and explain the behavior of slab ends at expansion joints with special emphasis on skew ends.
- To determine the performance of the IBTS detail when loaded with design loads (HS-20 and HS-25) and typical overloads.

- To determine the ultimate capacity and failure mechanism of the IBTS detail.
- To test an alternate edge detail and compare the behavior with the IBTS detail
- To develop guidelines for TxDOT engineers to follow in designing bridge decks if current practice is shown to be inadequate.
- To present the results of the full scale bridge deck tests in order to allow comparisons with finite element model results.

Since this research project is ongoing, the scope of this thesis is limited and includes the load testing of four distinct areas of a full-scale bridge deck specimen. This bridge deck's edges were zero-skew to create a baseline for comparisons with future tests of skewed decks. The IBTS detail and an alternative edge detail were tested with the aim of increasing economy in bridge deck construction. Two girder spacings were tested since the deck span of bridges in the field varies widely.

1.3 IBTS DETAIL

The IBTS edge detail is used in the majority of TxDOT designed bridge decks (Figure 1-1 through Figure 1-3). This detail creates an edge beam in the bridge deck by increasing the depth of the section by two-inches and increasing the percentage of flexural reinforcement. The edge beam is four-feet wide and is discontinued in the overhangs. The increase in section depth is formed by lowering the bottom reinforcement, essentially keeping the same top and bottom cover as in the interior of the deck.

1.4 SITE VISITS

To simulate as-built conditions, two site visits were made prior to building the specimen. The first bridge was located on IH-35 in San Marcos, TX, spanning the San Marcos River. The second site visit was an overpass on Highway 290, crossing over Highway 183. The IBTS detail is rather complicated so witnessing a contractor experienced with construction was helpful.

Typical of most TxDOT bridge construction, prestressed panels were used as stay-in-place formwork in the interior of the deck, up to the IBTS detail. Bridge decks are typically supported on prestressed concrete girders. Figure 1-4 shows the top of a girder with shear stirrups extending into the deck.

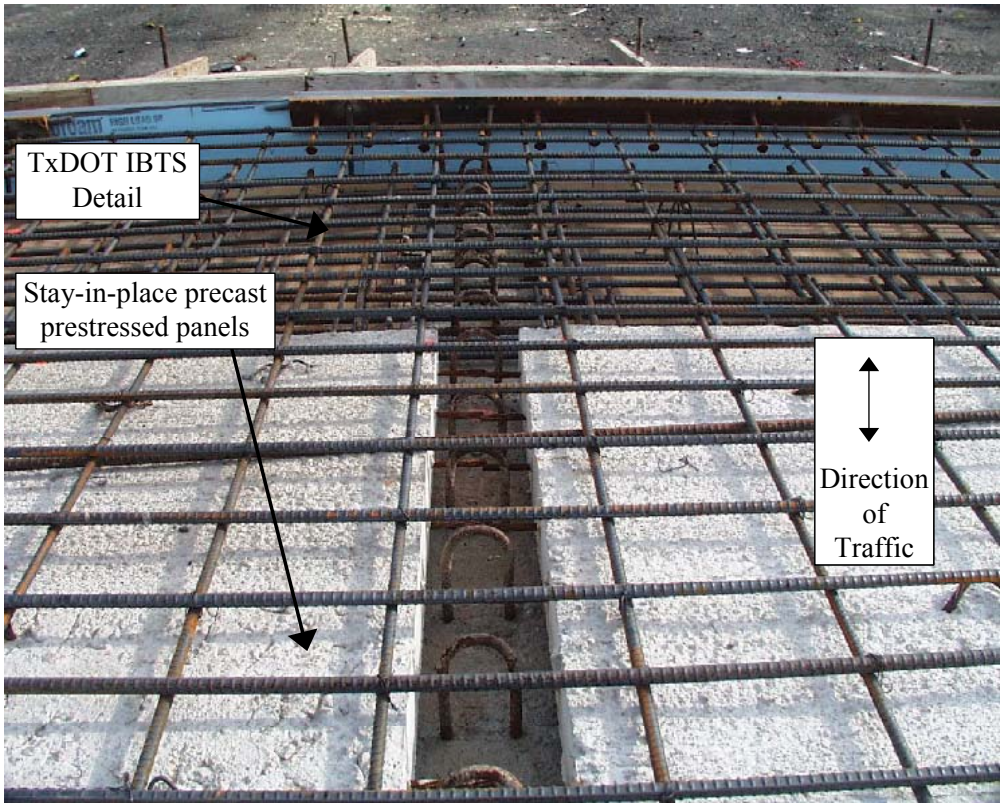

Figure 1-4: Prestressed panels and shear stirrups

Armored joint reinforcements were cast into the top edge of the decks at the expansion joints (Figure 1-5). They protect the edge of the expansion joint from deterioration if there is a differential displacement at the joint, causing a bump.

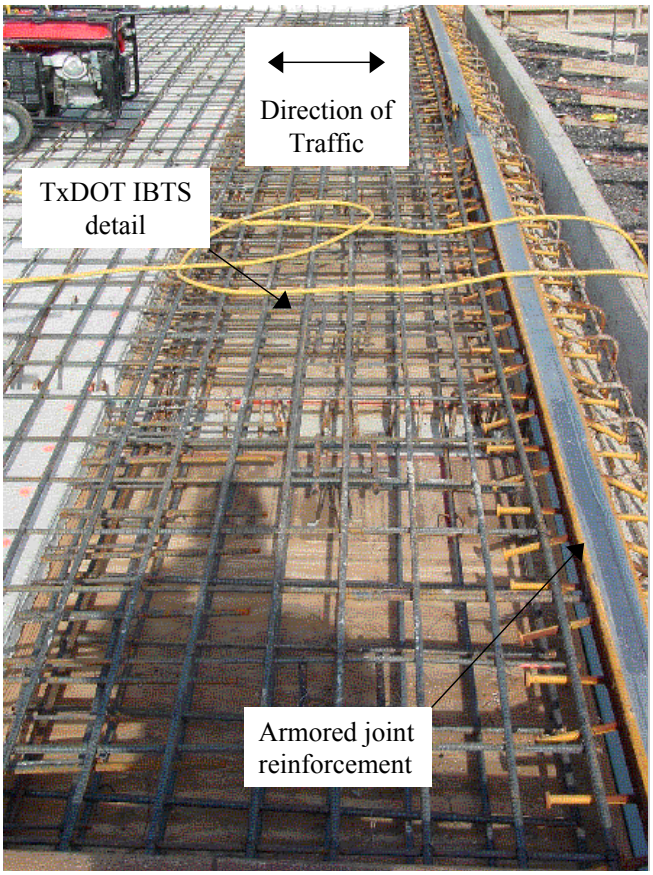

Figure 1-5: IBTS detail prior to concrete placement

The concrete was placed using a concrete pump with a boom that reached across the deck and vibrated to eliminate voids. A movable screed riding on temporary rails was used to finish the fresh concrete (Figure 1-6). Finally, construction workers bull floated the deck for a final finish. The process was continuous, allowing long lengths of deck to be placed efficiently.

Figure 1-6: Placing of concrete in the field

CHAPTER 2
Background Bridge Deck Research

2.1 INTRODUCTION

A literature review was performed to gain knowledge on the history and the current state-of-practice of bridge deck research. In addition, the literature review was carried out to determine if similar research has already been conducted. The research described in this thesis is then compared and contrasted with other researcher's work.

2.2 DETECTION OF ARCHING ACTION

In the 1950's, most research was focused on building slabs as opposed to deck slabs. Ockleston (3) tested the floor slabs of a three-story reinforced concrete building in South Africa to failure. The failure loads recorded were much higher than predicted by flexural theory. He later (4) determined the increase was due to compressive membrane action.

Also referred to as arching action, compressive membrane action is an in-plane force generated after cracking of laterally restrained slabs. Once cracking occurs, a compression field emanating from the load point spreads to the supports (Figure 2-1). Equilibrium is created by a tension hoop formed around the compression field as well as tension ties along the bottom of the slab (Graddy et al., 5). The bottom reinforcement serves as a tension tie. The amount of arching action generated depends on a number of factors including lateral restraint of the supports, material properties and slab thickness. Full lateral restraint of the supports is not necessary to develop in-plane forces, as continuous deck slabs on

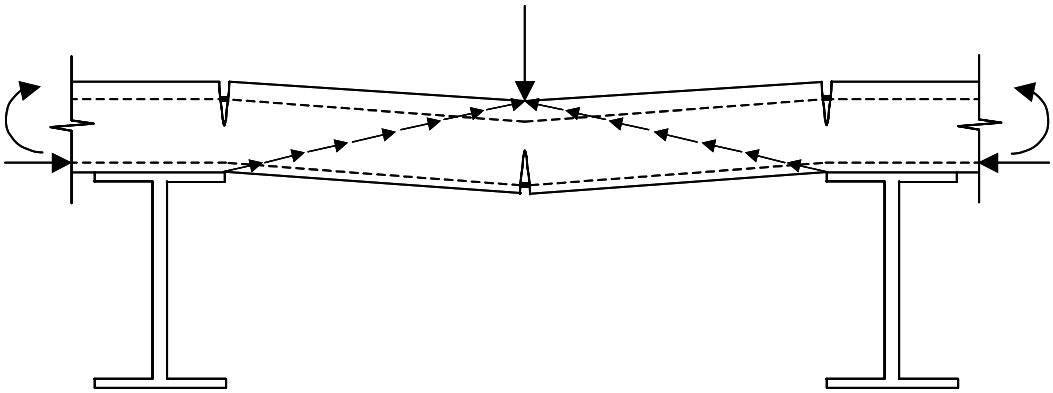

Figure 2-1: Arching action

girders can exhibit arching action. However, the deck's thickness must be sufficient to create the arching behavior.

Other researchers such as Liebenberg (6), Park and Gamble (7), and Christiansen (8) detected the increased capacity in building slabs due to arching action during research performed in the 1950's and 1960's.

2.3 BRIDGE DECK TESTS

Before long, the previous researchers' findings started to be applied to bridge decks. Batchelor and Hewitt (9) tested many scale models of bridge decks and published a number of papers on this subject. They found that bridge decks were significantly over-designed for service loads due to arching action increasing bridge deck capacity by as much as six times the design loading. Decks without reinforcement were able to carry more than twice the design load. In a paper published in the *ACI Journal* in 1976 (10), they recommended the use of 0.2% isotropic reinforcement per mat in a seven-inch deep deck. This amount was chosen because it satisfied the 11th edition of the AASHTO Standard Specification (11) requirements for temperature and shrinkage reinforcement. Batchelor and Hewitt found that this resulted in a decrease in reinforcement by as much as 66% compared to the code's requirements for strength. Based partly on

Batchelor and Hewitt's work at Queen's University in Kingston, Ontario, the Ontario Bridge Design Code (12) was published in 1979 and recommended 0.3% isotropic reinforcement in two mats.

Beal (13) tested two full-scale bridge decks, detailed in accordance with the Ontario Bridge Design Code, which had ultimate capacities of more than six times the design loading. However, the decks failed in punching shear, which is non-ductile. Punching as the primary failure mechanism has been verified by recent research for typical deck configurations.

2.4 RECENT RESEARCH, 1985 – PRESENT

In recent years, numerous bridge deck specimens have been tested. Azad et al. (14) constructed 12 bridge deck specimens with varying reinforcement percentages. The approximately 1/3-scale specimens had a 2.7in thick deck and a 28in deck span. The test specimens consisted of a two-span deck on three girders with shear studs spaced at 8in O.C. connecting them. A single load was applied monotonically at midspan of the deck both longitudinally and transversely within the span.

This research tested the effect of reinforcement percentage and load plate size on bridge deck performance. Azad et al. (14) compared the failure loads of their specimens to the ACI punching equation as well as some advanced analysis techniques, such as finite element modeling, which yielded more precise failure load predictions. They concluded that the ACI punching equation was very conservative and presented a variation, which increased the formula's accuracy for their test specimens.

Fang (15) constructed and tested a 20ft by 50ft, full-scale composite bridge specimen at the University of Texas at Austin. The deck contained two seven-foot spans and two 3.25ft overhangs (measured from girder centerlines).

Half the bridge deck was constructed using four-inch thick prestressed concrete panels with four-inches of cast-in-place topping while the other half was eight-inch thick, cast-in-place concrete. The load application protocol consisted of an initial static load of 60kips per tire (an overload of approximately three times the design loading) on an eight-inch by 20-inch steel plate. Then, various fatigue loadings were applied with static tests interspersed at intervals of approximately one million load cycles. The HS-20 truck loading configuration was used to test the specimens at locations in the interior of the bridge deck.

This research was undertaken to assess the behavior of a full-scale bridge deck, detailed using the Ontario Bridge Design Code (12) provisions, under AASHTO design loading configurations. Fang (15) determined that bridge decks with 0.3% isotropic reinforcement in two mats, a design prescribed in the Ontario Bridge Design Code, perform satisfactorily under monotonic design loads and overloads as well as fatigue loadings. The bridge deck was not loaded to failure, and therefore, compressive membrane action, ultimate capacity and the failure mechanism of the bridge deck were not researched or discussed. However, compressive membrane action was found to affect the bridge deck capacity after cracking occurred. Fang's PhD research, discussed above, is summarized in Fang et al. (16).

Fang continued to research bridge deck behavior at the National Cheng Kung University in Taiwan, China. Fang, Lee and Chen (17) monotonically loaded 18 reinforced slab test specimens with varying geometries and material properties. The specimens contained a deck slab spanning 39.4-inches between two edge beams, which were tied down in order to the floor to create partial lateral restraint. Research variables included slab thickness (4.5in and 3.0in), steel yield strength (45ksi and 68ksi), concrete compressive strength and reinforcement ratio. All specimens failed in flexural punching shear with the

concrete strength and slab thickness primarily controlling the ultimate capacities. Fang, Lee and Chen (17) recommended further reasearch on compressive membrane action in bridge decks.

Graddy et al. (5) tested 12 full-scale, simply supported specimens, which represent a piece of deck slab in the interior of the bridge. Most of the specimens were fatigue loaded, however, two were statically loaded at their geometric center with a 14in by 24in loading footprint. Graddy et al. (5) determined that the punching shear capacity at the interior of bridge decks is significantly higher than that predicted by the ACI equations. In addition, even though the test specimens were simply supported on the test frame, arching action was evident.

Youn and Chang (1) tested five, 1/3-scale composite bridge specimens in order to determine the effect of load location on bridge deck performance. The specimens consisted of a 2.4in thick deck cast on steel girders, with shear studs to provide composite action. The bridge specimens had a single 27.6in deck span with 7.9in overhangs on either side. Both monotonic and fatigue loads were applied to the test specimens.

Although the main variable in this research was loading location, the specimens were not tested near their edges. The five specimens all failed in punching shear. Youn and Chang (1) compared the ultimate capacity of the test specimens to the prediction from the ACI punching equation. The researchers found that the ACI equation was conservative compared to the test results.

Fiber-reinforced bridge decks were studied by Mufti and Newhook (18). Three 1/2-scale bridge deck specimens were tested to determine their ultimate capacity. The bridge decks contained no steel reinforcing, however, the concrete contains polypropylene fibers in order to reduce plastic shrinkage cracking. Mufti and Newhook (18) developed a model to predict punching shear capacity of the test specimens. In addition, they compared the punching shear model to results

reported by other researchers, including Fang (15), and obtained reasonably accurate ultimate load predictions.

In recent years, with the advent of the personal computer, detailed analysis methods such as finite element models and truss models have come into being. Researchers have begun applying these analysis methods to bridge decks. Most of the papers discussed herein contain an analysis method that agrees with test data.

Attempts to accurately model the punching shear failure mechanism as a snap-through instability have been made by Petrou and Perdikaris (19). They modeled the concrete compression struts, formed due to the application of a concentrated load, as truss elements in a two-dimensional, shallow arch. Stiff springs representing the reinforcing steel were used to model the horizontal support of the arch. The analysis method yielded results that were reasonable when compared to the ultimate capacity of monotonically loaded decks.

Previous researchers have subjected bridge deck specimens to static loading to determine ultimate capacity as well as fatigue loading to determine the effect of repeated loads on bridge deck performance. Variables tested in the research discussed above include load plate size and location, material properties, reinforcing ratio and lateral restraint. All of these researchers identified arching action in their specimens; however, its effect on capacity is still not understood.

2.5 RESEARCH SIGNIFICANCE

Although there have been a significant number of scale model experiments, few full-scale bridges have been tested. The effects of scaling can be complicated for shear-related effects. Full-scale tests must be performed to determine whether the scale models accurately represent real bridge decks.

The majority of research on punching shear in bridge decks has focused on interior locations of the deck. The effect of loads applied at the edge of the deck has not been researched thoroughly. This is a critical location because the free edge cannot be assisted in carrying the load by surrounding concrete. There is a smaller shear perimeter and the load is carried similar to a beam, in one-way action; as opposed to the interior of the deck, which has two-way action.

None of the previous research has tested the TxDOT IBTS detail. With the increased truck traffic and loads on Texas bridges, the capacity of the detail is of interest. Additionally, no alternative edge beam details, where strength increase is achieved through an increased percentage of steel as opposed to an increased thickness, have been tested as of yet.

CHAPTER 3
Design of Test Specimen

3.1 INTRODUCTION

The test specimen was designed to accurately represent the edge conditions of a typical bridge deck. The selection of the overall dimensions of the test specimen was of prime concern. The transverse dimension was based on both the number and length of the spans between girders required to reflect continuity in typical bridges. The length of the bridge between the edge to be tested had to be sufficient to prevent interaction between test areas when the edges were loaded. Laboratory space limitations were also taken into account when deciding how large to make the deck. SAP 2000 was used to analyze the effect of these variables such that a realistically sized specimen could be designed and built. The effect of the girder type on bridge deck behavior and the shear connection between the deck and the girders were investigated.

3.2 TEST MODEL

An objective of this research is to evaluate the performance of the TxDOT IBTS detail under service load conditions (HS-20 and HS-25), under overload conditions (1.2xHS-25, 1.75xHS-25 and 3xHS-25), and at ultimate capacity. To realistically model actual bridge decks at expansion joints, it was decided to build a full-scale specimen.

The thickness of the typical TxDOT bridge deck (eight-inch) and the IBTS detail (10inch) were maintained. Rebar sizes and quantities used in design and construction were not altered. In addition, realistic girder spacings had to be determined from TxDOT designers and the TxDOT Bridge Design Manual (20).

However, the length of the specimen as well as the number of girders needed to be decided, such that the experimental results would reflect reality with very little or no influence from dimensioning considerations.

3.3 SPAN

The TxDOT Bridge Standards website (http://www.dot.state.tx.us/business/standardplanfiles.htm) contains information on typical spans used in the field. Hence, the information contained in this website was analyzed carefully. In the following two sections, common TxDOT bridge designs as well as SAP 2000 analysis were used to determine the test specimen's final dimension are briefly discussed.

3.3.1 Transverse

Transverse refers to the direction perpendicular to the vehicle traffic on an actual bridge; therefore, transverse indicates the direction that the deck spans. The decision on the transverse dimension of the specimen was also based on the amount of space available in the laboratory. In the future, skewed specimens will be constructed, which require significantly more space than a zero-skew deck. Since comparisons must be made between the specimens, a design that could be imitated for skew decks was essential.

3.3.1.1 Transverse Span Lengths

TxDOT plans were studied to determine typical spans to use in the test specimen. Common spans range between 6.67 feet and 8.67 feet as shown in Table 3-1, with 8 feet being the most common. Information obtained from the project director and TxDOT designers showed that deck spans may reach upwards of 10 feet due to curved girder layouts in some extreme cases. In addition, when the deck edge is skewed, the transverse span increases, which can have a large

Table 3-1: Typical TxDOT bridge designs

Roadway Width	24 ft	28 ft	30 ft	38 ft	44 ft
Number of girders	4	4	4	5	6
Girder spacing	6.67 ft	8 ft	8.67 ft	8.5 ft	8 ft

effect when skew angles as high as 60^0 are used in special bridge configurations. Figure 3-1 shows graphically that a 60^0 skew doubles the span. It was decided to test both an eight-foot and a 10-foot span, spans typically used in the field. The incorporation of two different spans allows comparison of the behavior of the IBTS detail for different girder spacings with other parameters held constant.

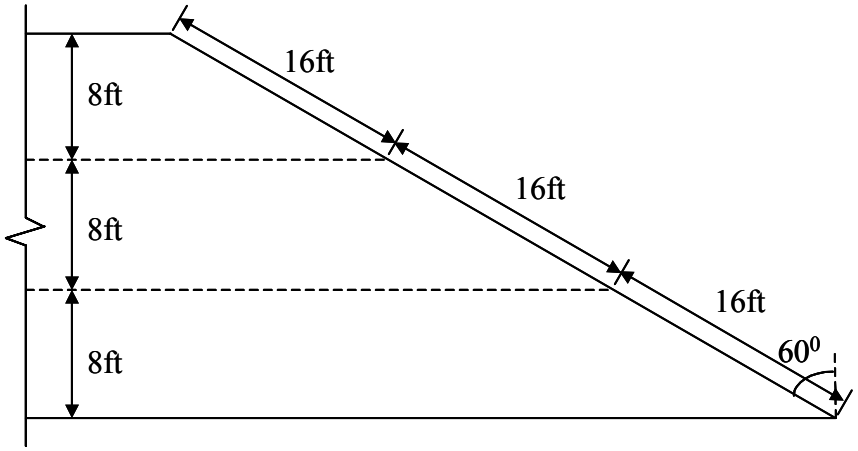

Figure 3-1: Effect of 60^0 skew on span length

3.3.1.2 Number of Spans

The TxDOT plans were again reviewed to determine common girder layouts (Table 3-1). The maximum number of girders used is six (five deck spans), which would not be feasible to build in the laboratory due to size

constraints. Therefore, models of the four and five-girder bridges in Table 3-1 as well as two, three-girder bridges were created in SAP 2000 to determine the minimum number of transverse spans necessary to accurately model a bridge deck. The SAP 2000 models shown in Figure 3-2 are cross-sections of the bridge deck, transverse to the direction of traffic. Frame elements were used to model the bridge deck since in-plane effects are not of concern for this analysis. While the roller supports used in the SAP 2000 model for the supporting girders do not imitate the conditions in an actual bridge deck, the moments generated can be compared. The span lengths of all the models were kept the same. Figure 3-3 is a plot of the models' respective moment diagrams.

Referring to Figure 3-3, the load was applied at midspan between girders A and B. All the models are lined up in relation to the edge of the overhang, x=0ft. A model of the 6-girder bridge is not shown because the results are very similar to those obtained from the 5-girder bridge, Model #2.

Models #2 and #3 are actual girder layouts used by TxDOT and the other models were compared with them. As can be observed in Figure 3-3, Model #4 does not provide a realistic estimation for moment at point C since a typical bridge that may have four or more girders would have a negative moment developing at this location when a concentrated load is applied in the first span.

Model #1 was included to alleviate the deficiency of moment in Model #4 at point C. However, it creates too large a moment at that location due to the rotational restraint imposed by the fixed support. In addition, it is difficult and costly to create a fully-fixed support. Model #3 matches Model #2 between points A and C almost exactly. The moment at all other locations along the deck is not critical.

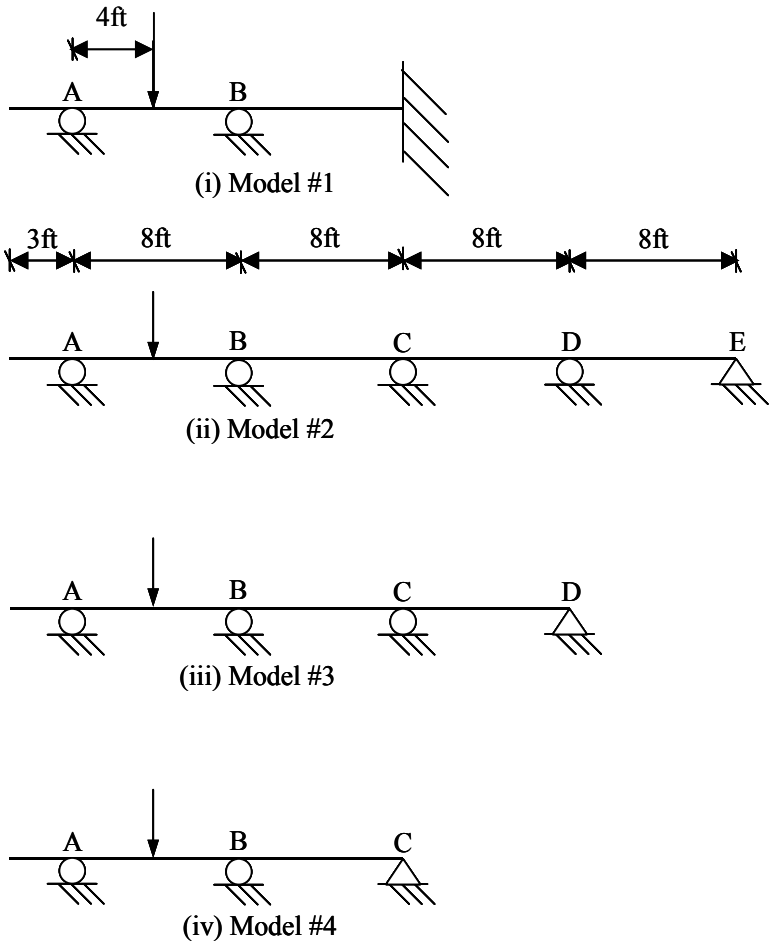

Figure 3-2: Models used to determine number of transverse spans

Since both Models #2 and #3 reflect the behavior of actual bridge configurations, Model #3 is preferable in order to reduce the size and cost of the specimen. Another benefit to using the 3-span model is that two tests can be performed at each edge of the test specimen. Tests can be conducted in the first span and then the third span. The second span should remain relatively undamaged because the moments are low in this region.

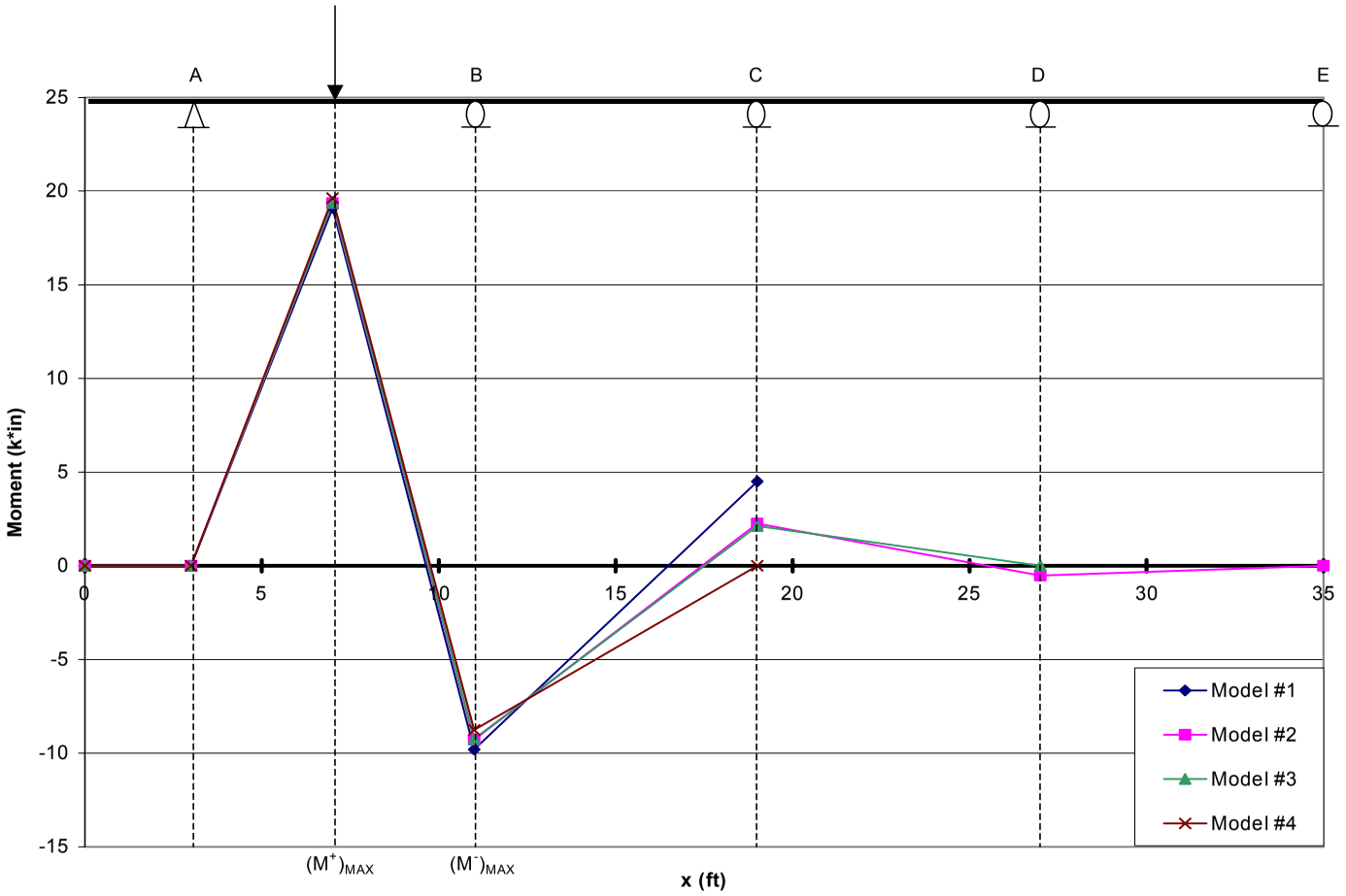

Figure 3-3: Moment diagram for model alternatives

3.3.2 Longitudinal Dimension of the Test Model

Since tests are conducted on the edges of the specimen, the critical decision for longitudinal span involves providing enough separation between the two edges of a laboratory deck model to avoid damaging the unloaded side. In other words, containing the damage associated with one test within that zone and leaving the rest of the deck undamaged for other tests. As the IBTS detail is stiffer than the rest of the deck, it would be expected to carry most of the applied load along the edge of the deck.

To determine the critical length, a finite element model of a bridge 25 feet long was created, assuming this was an upper limit on the area available in the lab (Figure 3-4). Loads were applied (at midspan of both the eight-foot and 10-foot spans) at the edge of the deck and four feet from the edge. The four foot wide IBTS detail was modeled with 10in thick shell elements whereas the rest of the model had eight-inch shell elements. Then, the transverse moment across a section through the load points in the eight-foot and 10-foot span load points was plotted. Figure 3-5 shows that the moment drops drastically after the four foot thickened edge. At nine feet into the deck, the moment is less than ten percent of the maximum moment value at the edge. Therefore, an 18-foot long bridge should allow testing of each edge without significantly affecting the other edge.

In addition to the FEM results, the AASHTO LRFD code recommended design strip widths were studied. Section 4.6.2.1.4c contains a method to determine an equivalent edge strip that would contribute in carrying the loads applied at the edge. This method is a simplified design procedure, reducing the deck to a wide beam. AASHTO LRFD does not suggest that beyond the contributing strip, there is no effect from the loading; however, it does state that most of the load should remain in the design strip. Two different equations are

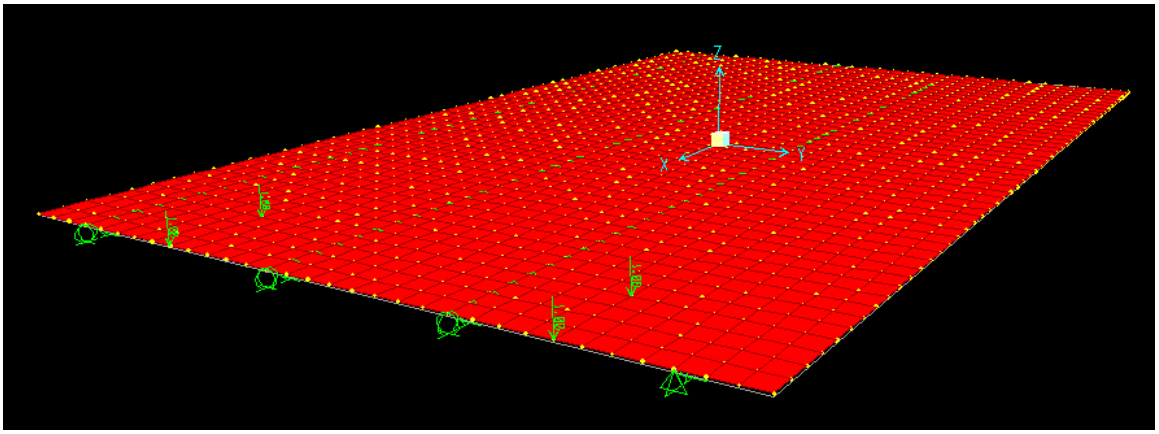

Figure 3-4: SAP 2000 finite element model

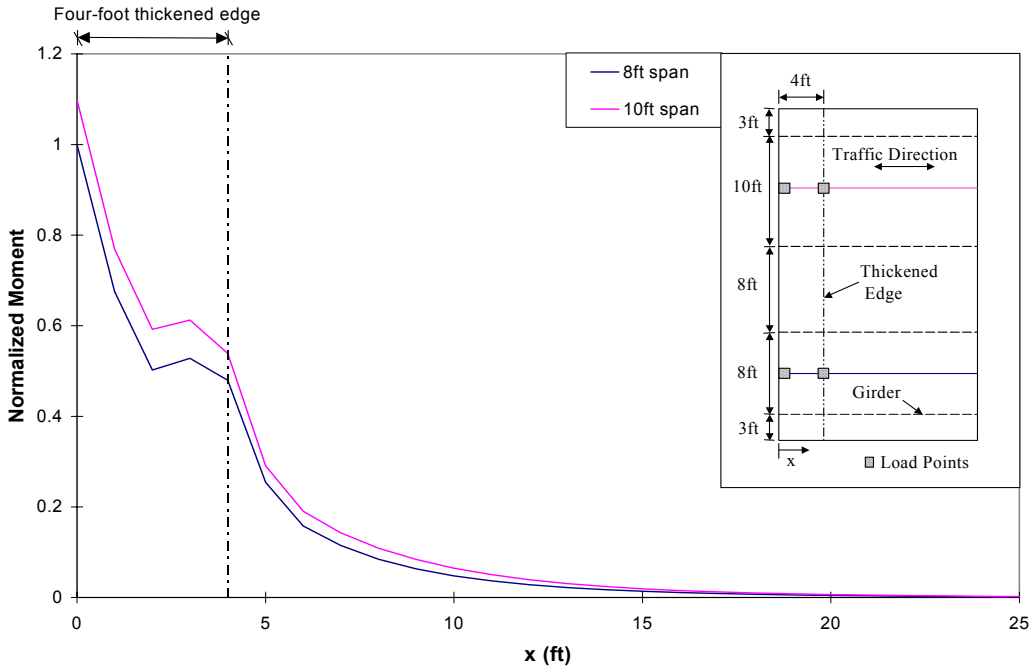

Figure 3-5: Spread of moment longitudinally into the specimen

given for the positive (+M) and negative (-M) moment section. Table 3-2 shows the resulting strip widths and the amount of moment the strip contains based on the SAP 2000 analysis shown in Figure 3-5. The 18-foot test specimen should be sufficient to separate the test areas.

Table 3-2: AASHTO LRFD equivalent strip formulas and comparison to alternatives

Location in strip	*AAHSTO LRFD Equation	8ft Span		10ft Span	
		Equation result	**from Figure 3-5	Equation result	**from Figure 3-5
+M	$W_G + \frac{1}{2}[26 + 6.6 * S]$	63.4in	77%	70in	79%
-M	$W_G + \frac{1}{2}[48 + 3 * S]$	60in	75%	63in	74%

*W_G =girder height (inches), S= Girder spacing (feet)
** Percentage of moment contained in strip width defined by the equation.

3.4 ZERO SKEW BRIDGE DECK

An objective of this research is to determine the effect of skew on bridge deck behavior at expansion joints. However, the behavior of bridge decks at expansion joints with zero degree skew needs to be clearly understood in order to evaluate the effect of skew on deck behavior. In addition, a zero degree skew bridge acts as a baseline for comparison with future skewed decks. Further, no experimental data on zero degree skew deck end details is available in the literature. For these reasons, it was decided that the first specimen built for this research would be a zero degree skew bridge deck at both edges. Subsequent bridge decks, not covered in this thesis, will be skewed at various angles.

3.5 ALTERNATIVE DETAIL FOR BRIDGE DECKS AT EXPANSION JOINTS

In the interest of maximizing the information gathered from this specimen, an alternative detail was designed for the edge opposite the IBTS detail. The IBTS detail may not be easy to construct because of the additional formwork required for the two-inch drop down. Four-inch thick prestressed panels, topped with four inches of cast-in-place concrete are often used in lieu of constructing formwork for the length of the bridge. However, the panels must be stopped at

the IBTS edge detail, requiring formwork, to allow the thickening of the edge. An eight-inch deep edge detail would be expected to improve construction economy.

The alternative section, named the Uniform Thickness Slab End (UTSE) detail, contains the same size rebar as the interior of the bridge and the IBTS detail in order to simplify construction. The quantity of bars in the alternative detail is increased to 24 as opposed to 16 in the IBTS detail (Figure 3-6). Even though the UTSE detail is only eight inches deep, it has a slightly higher flexural capacity than the IBTS detail. Figure 3-7 shows the moment curvature behavior of the two details. Figure 3-8 uses the same analysis as Figure 3-7, however, it focuses on cracking and yielding of the sections. The UTSE detail has a lower stiffness, both before and after cracking due to the reduced section depth. The reinforcing steel in the UTSE detail yields at an 11% and 6% higher moment than the IBTS detail in positive bending and negative bending, respectively.

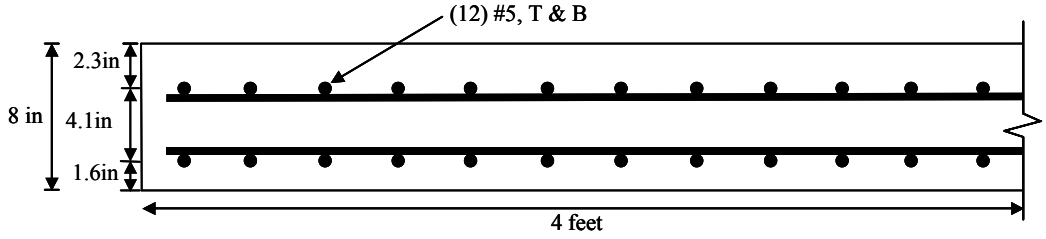

Figure 3-6: UTSE detail

3.6 PRESTRESSED PANELS

Prestressed panels are typically used in the field because of the reduced amount of forming required. For this test specimen, it was decided not to use prestressed panels because they are not used in the thickened edges in the field and it was expected that they would have little effect on the behavior of decks at expansion joints. In the specimen tested, in the first phase of the ongoing

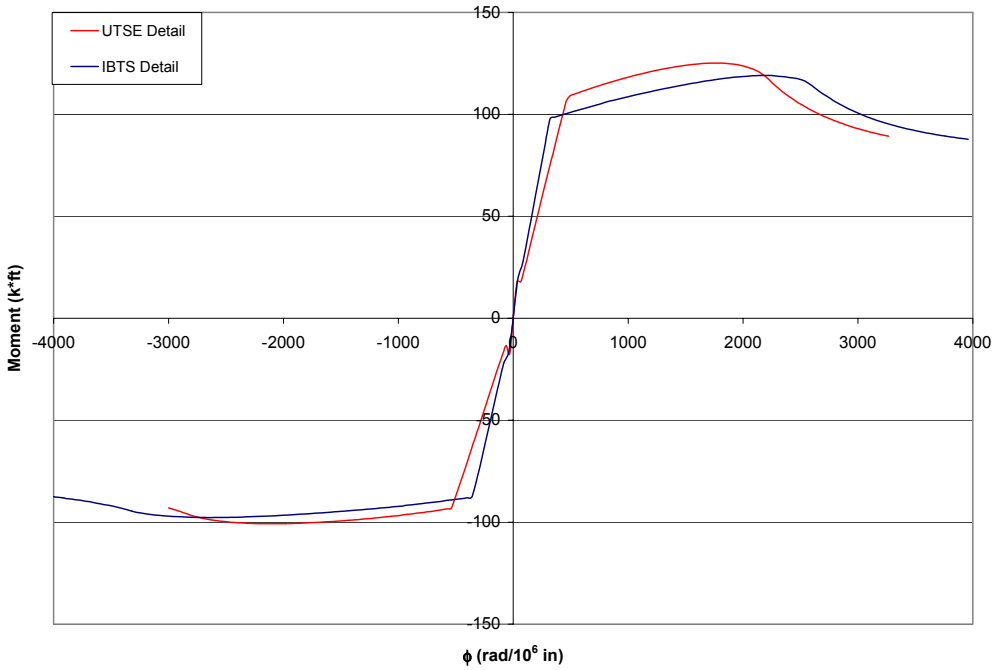

Figure 3-7: Overall moment-curvature

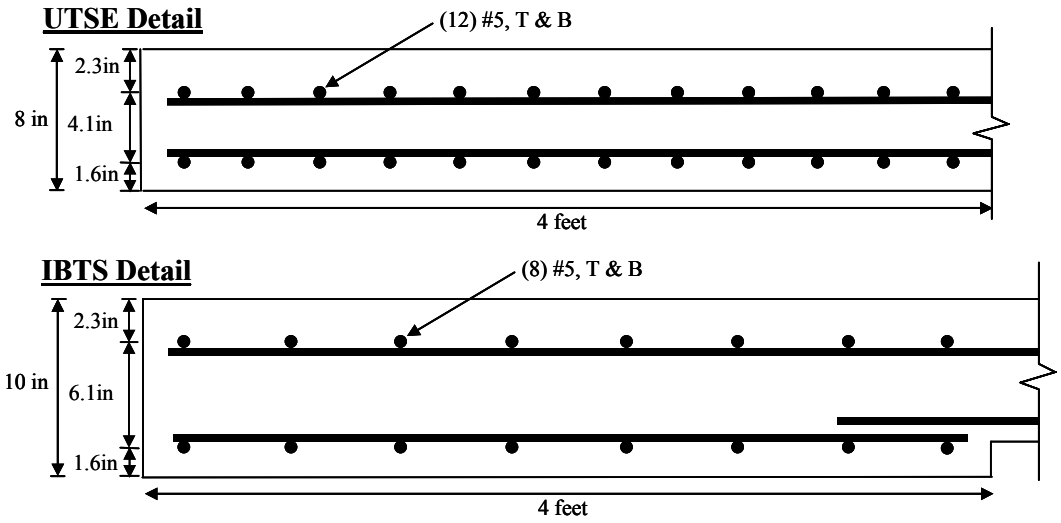

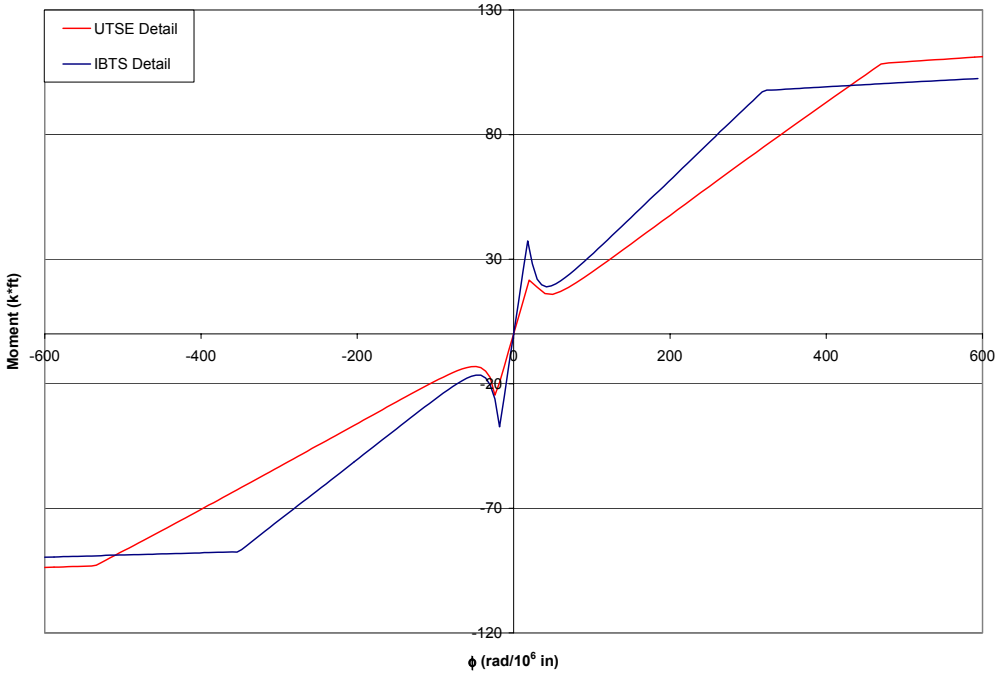

Figure 3-8: Moment-curvature focused on cracking and yield

experimental program, two main variables, the span length (eight foot vs. 10-foot) and the slab end detail (IBTS vs. UTSE) were considered.

3.7 GIRDERS

Bridges in Texas typically are built using precast, prestressed concrete girders. However, for this experimental work, they were not feasible as they were expensive, difficult to transport and not reusable. Since the girders will have very little effect on the behavior of the deck along the edge it was decided to use steel girders (W24 X 104) in the experimental program, as they could be reused for the different tests anticipated for the planned research.

3.7.1 Shear Studs

In order to obtain full composite action between the deck and the girders, as in an actual concrete girder bridge, shear studs were fabricated using double nutted bolts (Figure 3-9). This allows the girders to be reused by removing the bottom nut and lifting the slab off the girders. This shear stud detail proved to be a very efficient method to produce composite action. Figure 3-10 shows the actual method for creating composite action used by TxDOT as well as the equivalent design used in the test specimen. The shear stud diameter and spacing was designed to match the cross-sectional area of the rebar stirrups that are used with precast, prestressed girders (Table 3-3).

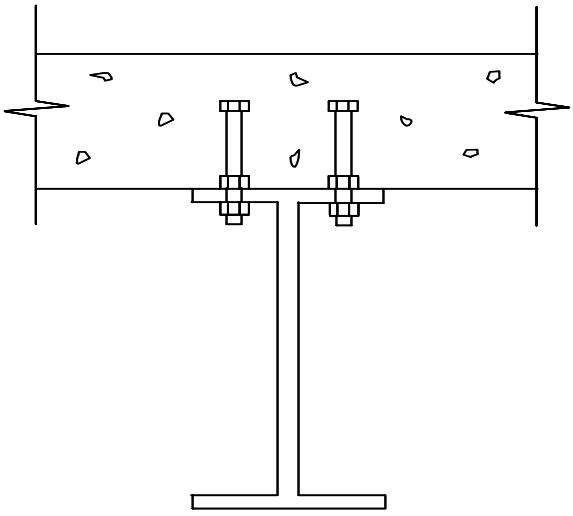

Figure 3-9: Shear stud detail

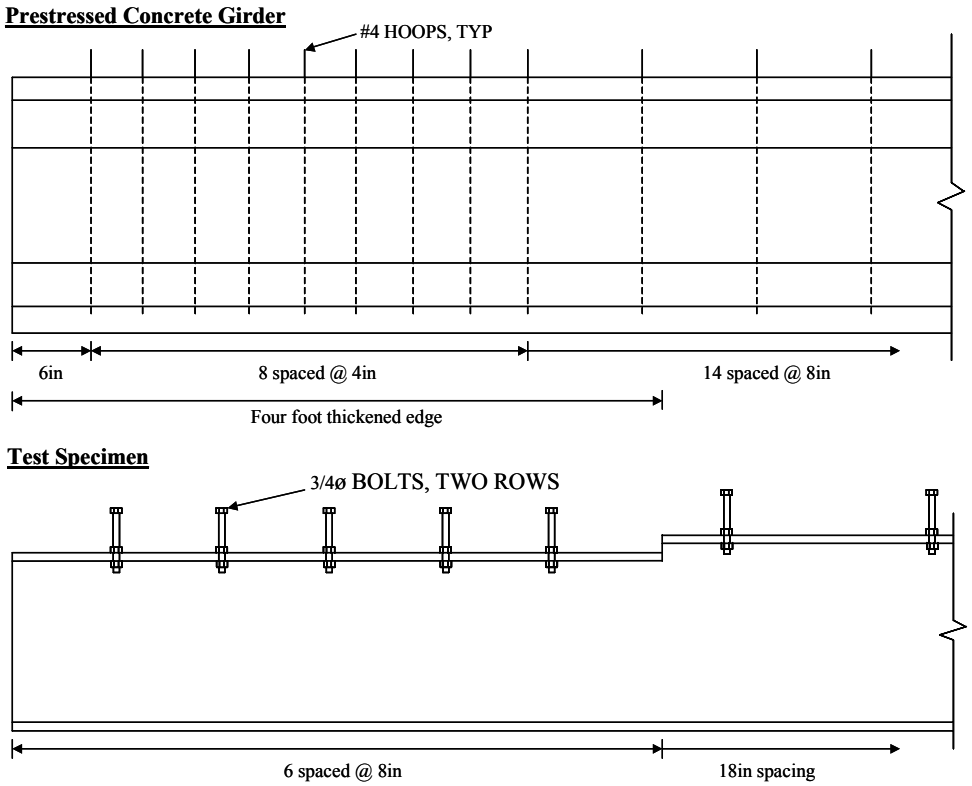

Figure 3-10: Composite shear reinforcement

Table 3-3: Comparison of composite shear reinforcement

Girder type	Shear connection method	Area of composite reinforcement (per 4ft)	
		IBTS Detail	Typical Deck
Prestressed Concrete	CIP #4 rebar, hoops	$4in^2$	$0.6in^2$
Steel	CIP 3/4⌀ bolts, two rows	$4.4in^2$	$0.59in^2$

3.8 SUMMARY

The final dimensions of the test specimen were 18 feet (longitudinally) by 32 feet (transversely) and contained four test areas (Figure 3-11). It had three

transverse spans, two at eight-feet and one at 10-feet, and overhangs on both longitudinal sides.

The IBTS detail (Figure 1-3) was used for the two test areas on the south side of the bridge deck, while the UTSE detail (Figure 3-6) was used for the north edge. The entire deck was cast-in-place as opposed to using the four-inch thick prestressed panels and a four-inch topping. This was done to simplify comparisons between test areas on this specimen as well as other skewed deck specimens by eliminating a variable from the research. The supporting girders were steel wide-flange beams with two rows of temporary shear studs used for creating composite action with the bridge deck.

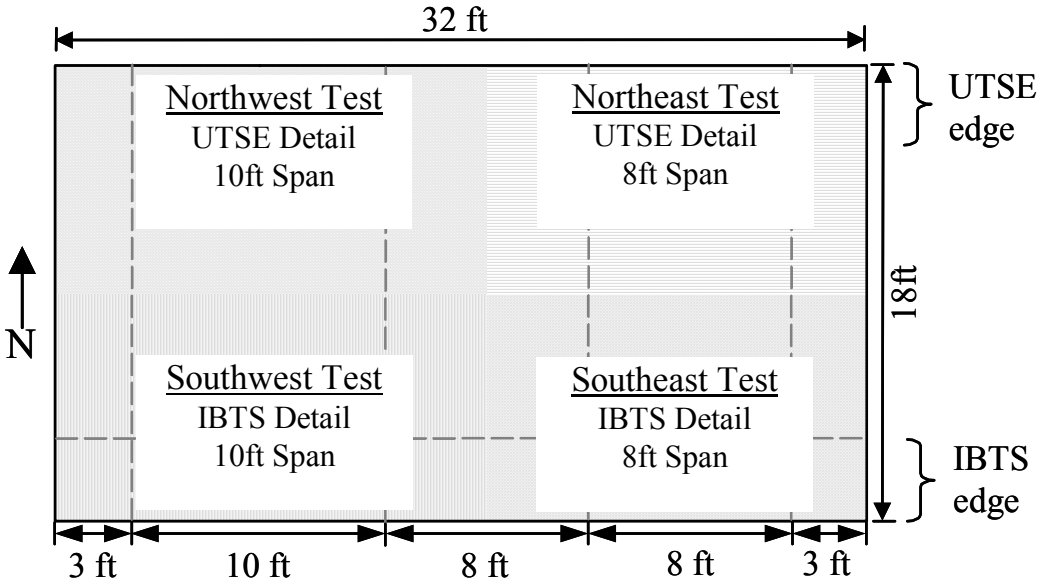

Figure 3-11: Test areas and variables

CHAPTER 4
Experimental Program

4.1 INTRODUCTION

Construction began once the final dimensions and the girder arrangement for the test specimen were determined. This chapter describes the construction of the test specimen and the load frame. The design vehicles and load magnitudes given in the TxDOT Bridge Design Manual (20) and AASHTO LRFD (1) are discussed as they apply to this research project. In addition, the method used to determine the transverse load locations in order to maximize moments induced in the section is described in section 4.3.2.

Instrumentation type and location is illustrated as well as the material testing performed to determine the actual material properties of the test specimen. Finally, the steps followed in applying the three vehicle configurations in the two loading locations are explained.

4.2 CONSTRUCTION OF TEST SPECIMEN

It was necessary to elevate the bridge deck in order to inspect the bottom of the specimen for cracking during load tests. Four-foot tall by two-foot diameter concrete columns were cast to support the girders. The girders had to be specially fabricated to permit the IBTS detail's two-inch deep thickened edge. A four-foot length of the top flange was cut off, and then a two-inch deep piece of web was removed. Lastly, the top flange was reconnected to the girder with a full-penetration weld (Figure 4-1). Full-depth web stiffeners were welded at the centerline of the supports and the top flange was punched to fit the shear studs.

Figure 4-1: Girder flange drop down

Once the girders were erected on the columns and laterally braced for stability, elevated formwork was built using four-foot by eight-foot panels. The panels were made up of ¾-inch thick plywood supported by 2x6 stringers at 16-inches on center. The panels were propped up by 4x4 posts as well as 2x4's wedged between the bottom flange of the girder and the 2x6 stringers.

In order to provide a shear connection between the girders and the formwork (necessary for the overhang forms), metal clips were fabricated that linked the shear studs to the panels. Edge boards, which formed the sides of the deck, were diagonally braced to the lower formwork. Gaps in the forms were sealed with caulking and the forms were oiled to allow easier removal from the hardened concrete after casting (Figure 4-2). The reinforcing steel, both instrumented and bare, was then placed, chaired and tied. Block-outs, made of PVC pipe, were located in the bridge deck to allow loading rods to pass through the specimen. Prior to placing the concrete, the exact location of all strain gauges was recorded and their wires were routed out of the specimen.

Approximately sixteen cubic yards of concrete was placed on July 25, 2002 at Ferguson Structural Engineering Laboratory with help from fellow graduate students and lab technicians (Figure 4-3). The wet concrete was transported within the lab with a bottom-drop bucket hoisted by a crane. Then the

Figure 4-2: Finished formwork

Figure 4-3: Placing concrete

concrete was vibrated to eliminate voids in the specimen. A vibrating, aluminum screed was used to level the top surface of the bridge deck. Finally, the bridge deck was bull-floated and hand-finished to create a smooth, flat surface. The specimen was cured for seven days by placing saturated strips of burlap, covered by plastic sheeting to reduce evaporation, over the entire surface of the deck. After 28 days, the forms were stripped and block-outs removed.

4.3 LOAD FRAME

The test specimen was built on the Ferguson strong floor in order to allow application of the vehicle loads. Loading the bridge deck from above, with a reaction frame, was not feasible because of the large area of the test specimen and the need to move the load frame often. A compact, reconfigurable load frame was designed and built which could fit underneath the test specimen and be moved with hand trucks (Figure 4-4).

For the load arms, C10 X 20 channels were connected back-to-back with plate spacers to allow loading through their center-of-gravity. The lower load arm flanges were drilled to match the strong floor bolt pattern and stiffened adjacent to the holes. The upper load arm was connected to two lower load arms by a threaded rod, which was prestressed prior to performing a test in order to eliminate rotation of the arm due to minor imperfections. The load rod was routed through the loading assembly on top of the bridge deck and attached to the upper load arm underneath the deck (Figure 4-5, i and ii). Six lower load arms and four upper load arms were built, enabling the application of up to four tire loads at any location under the deck.

4.3.1 Load magnitude

One of the main objectives of this research was to determine the behavior of the TxDOT IBTS edge detail at AASHTO LRFD design loadings, namely HS-

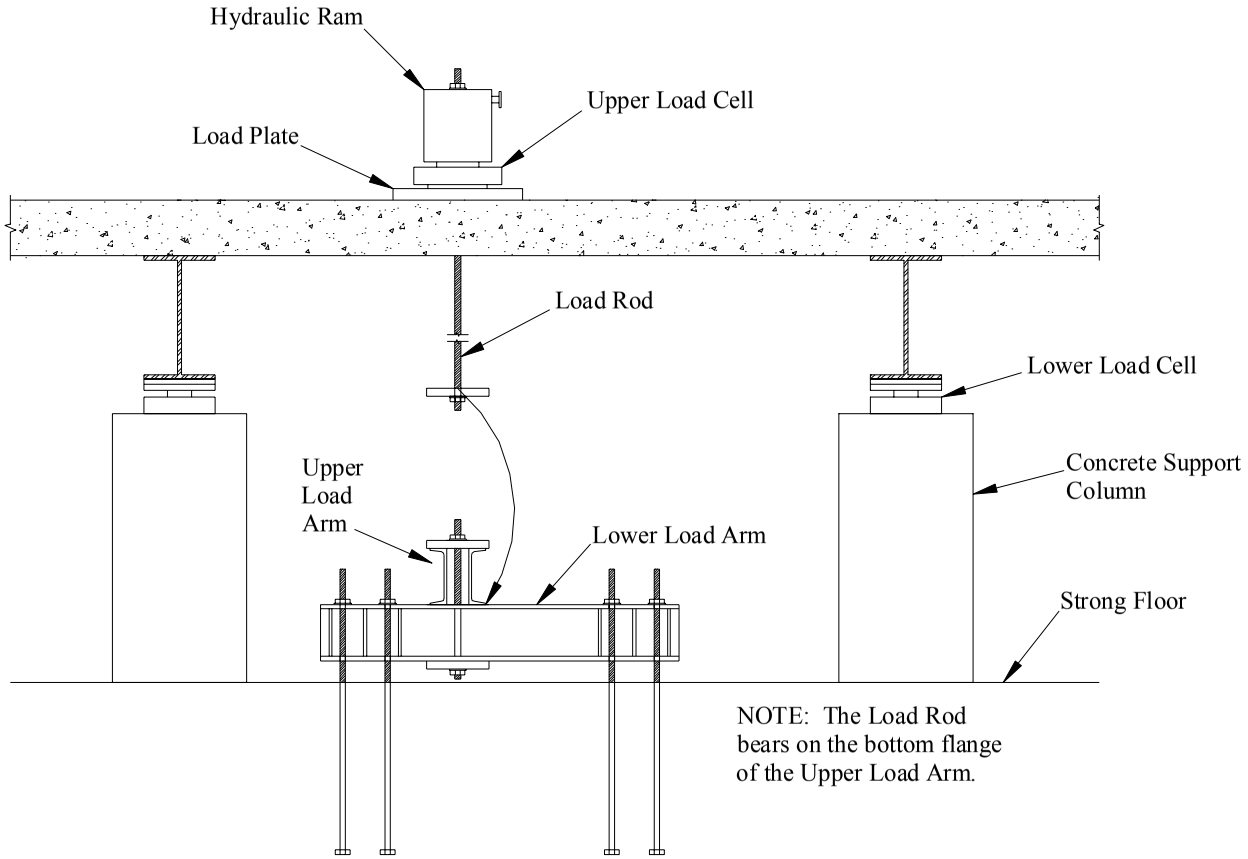

Figure 4-4: AutoCAD drawing of load frame

(i)Facing south (same view as Figure 4-4)

(ii)Facing east (perpendicular to view in Figure 4-4)

Figure 4-5: Pictures of load frame

20 and HS-25. There were two primary types of vehicle considered for each design loading (Figure 4-6). The TxDOT Bridge Design Manual (20) uses the same truck vehicle, however, instead of the tandem vehicle there is an alternate military vehicle with 24kip axles but the same loading configuration. The tandem loading from AASHTO LRFD will be applied to the test specimen although the alternate military vehicle is almost identical. HS-25 loading utilizes the same vehicle arrangements, however, the load magnitudes are increased by 25%. The loadings shown in Figure 4-6 are axle loads. Half of the axle load goes to each tire and the tires are spaced six feet apart.

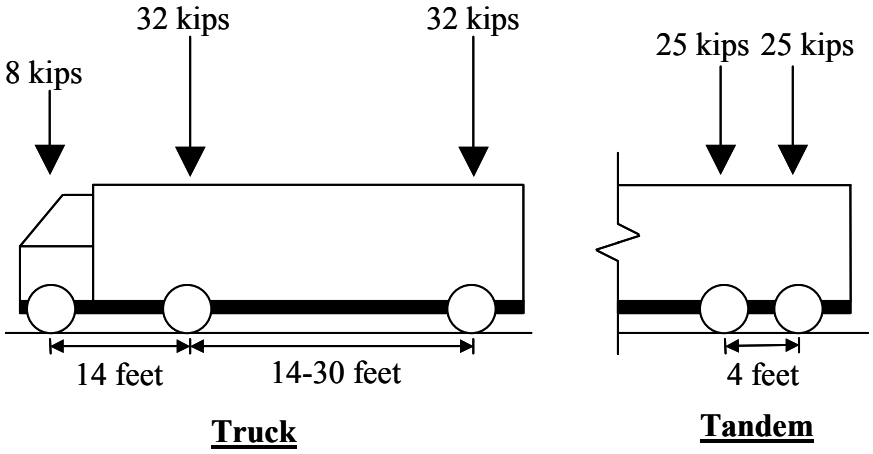

Figure 4-6: HS-20 design vehicles

Since the truck's axles are far apart in relation to the four-foot edge detail, only one of the axles was applied to the bridge deck test specimen at any one time. Therefore, one of the 32kip axles was applied at the edge of the deck, named truck axle-front, and at four feet from the edge, called truck axle-back. The tandem vehicle's axles both affect the edge detail since they are spaced four feet apart. In summary, tandem loading refers to four tire loads while the truck axle loadings indicates two tire loads.

AASHTO LRFD also requires a lane load of 64psf to be applied simultaneously with the vehicle loads. Since this small uniform load is difficult to create in the laboratory and it is not likely to have much effect at the edge of the bridge deck, the lane load has been omitted.

Section 3.6.2 in the AASHTO LRFD code establishes a dynamic load allowance. This increases the static vehicle loads by 75% in order to account for dynamic effects in the bridge at expansion joints. The allowance applies to expansion joints because they often have a bump, which causes a hammering effect in the deck structure.

The AASHTO LRFD Bridge Design Specification, 1999 Supplement also specifies a tire contact area to be used in design in section 3.6.1.2.5. The code stipulates a 20-inch width (transverse direction) and a 10-inch length (longitudinal direction), therefore, a 20-inch by 10-inch by 2½-inch thick steel plate was used for the tire contact areas in the southeast and northeast areas.

When a punching failure occurred in the southeast test, the plate size was increased based on the 1998 AASHTO LRFD Bridge Design Specification. In section 3.6.1.2.5 of this code, a constant tire width of 20-inches is given as well as a formula to determine the length based on the load factor, dynamic load allowance and load magnitude. The formula results in a length of 15-inches for the tandem vehicle and 20-inches for the truck. Therefore, 15-inch by 20-inch by 2½-inch steel load plates with neoprene bearing pads between the plate and the bridge deck were used for the southwest and northwest tests.

4.3.2 Load location

The vehicle loads must be applied at the transverse location on the bridge deck where they cause the maximum moment effects. To determine the transverse location to apply loads, influence lines were developed. SAP2000's

moving load capabilities allowed quick generation of influence lines. The bridge deck was simplified as a two-dimensional frame element model since the longitudinal dimension of the deck would not effect the transverse location of the loads. Point supports and loads were used due to limitations in the analysis program. This simplification will not significantly affect the desired outcome of this analysis, which is to determine the transverse location at which the design loadings should be applied in order to cause the maximum effect in the bridge deck.

Two loads, six feet apart to imitate the AASHTO LRFD design axle length, were applied to each influence line. Then the influence line location and load location which maximized positive and negative moments were identified (Figure 4-7). For each test area, in order to run the load rod through the bridge deck, blockouts were located at the center of the four tire load plates for maximum negative moment loading, prior to placement of concrete. For the southeast and northeast test areas, the positive moment loading was applied by an axle loaded through its mid-length, requiring a blockout for the load rod at x=9ft. For the southwest and northwest tests, the load plate size was changed after casting the bridge deck specimen, which required coring new holes for the load rods.

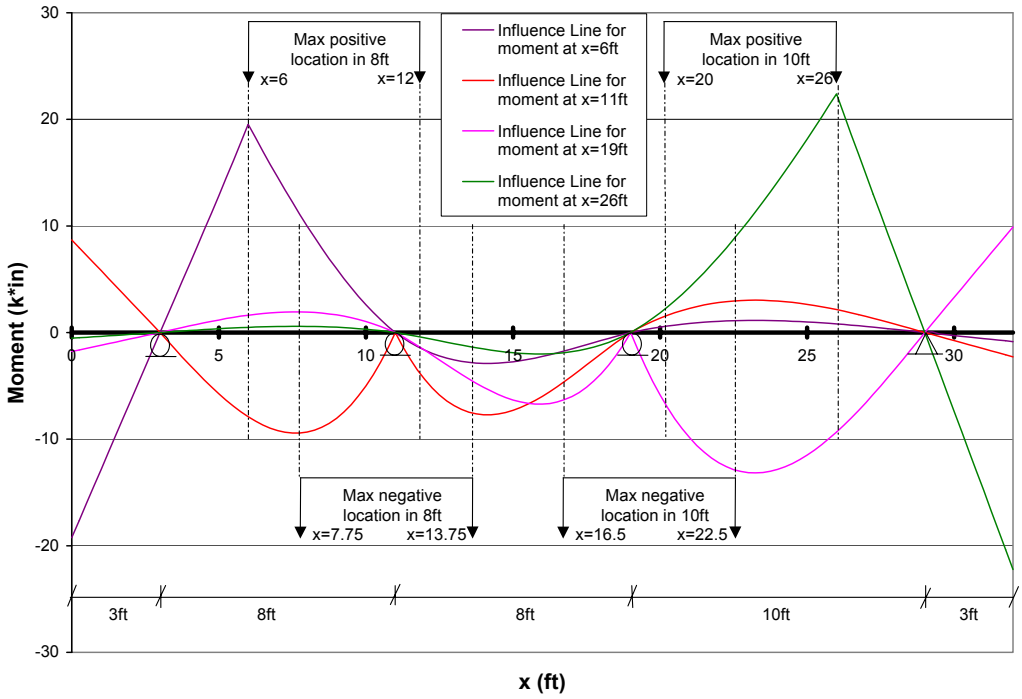

Figure 4-7: Location of maximum influence due to AASHTO vehicle

4.4 INSTRUMENTATION

Since this was the first bridge deck tested, and the results will be compared with data from future bridge deck tests, great care was taken in locating the instrumentation. It was essential to anticipate locations critical for understanding the bridge deck behavior. The bridge deck was heavily instrumented internally with strain gauges on the reinforcing steel and externally with load cells and linear potentiometers.

4.4.1 Strain measurements

Strain gauges were the primary instrumentation used in the bridge deck test specimen. Since the strain gauges were placed before the concrete was cast,

they were located carefully and protected to avoid damage during concreting operations.

4.4.1.1 Location of strain gauges

Each rebar in the IBTS and UTSE details was instrumented in order to evaluate reinforcing bar strains at various load levels and show the variation in strain longitudinally across the section. The strain gauges were also used to determine the strain profile within the deck slab, by assuming a linear strain profile from readings at both the top and bottom mat of reinforcing steel. They were situated at locations of maximum positive and negative moment, based on the influence line analysis, in order to monitor failure of the deck. These locations were at x=6ft and 26ft for positive moment and at x=11ft and 19ft for negative moment (Figure 4-7). Backup gauges were used on roughly half of the bars. Approximately 270 strain gauges were applied to the reinforcing steel in the test specimen.

Figure 4-8 and Figure 4-9 show plan views of the locations of strain gauges in the specimen. In the eight-foot span, gauges were also attached to bars in the interior of the specimen. In the transverse direction, they were placed at the locations of maximum positive and negative moment, as in the edge beams. Named middle strip gauges, these were used to determine the amount of applied load being carried by the edge beams. All strain gauges were applied to the transverse bars, as they are the primary reinforcement.

A labeling system was created to identify the strain gauges (Figure 4-10). For example, the NT105+ strain gauge was located in the north edge detail (UTSE detail) on the top mat of steel in the 10-foot span. It was on the fifth rebar from the edge-most bar and was in the location of maximum transverse positive moment.

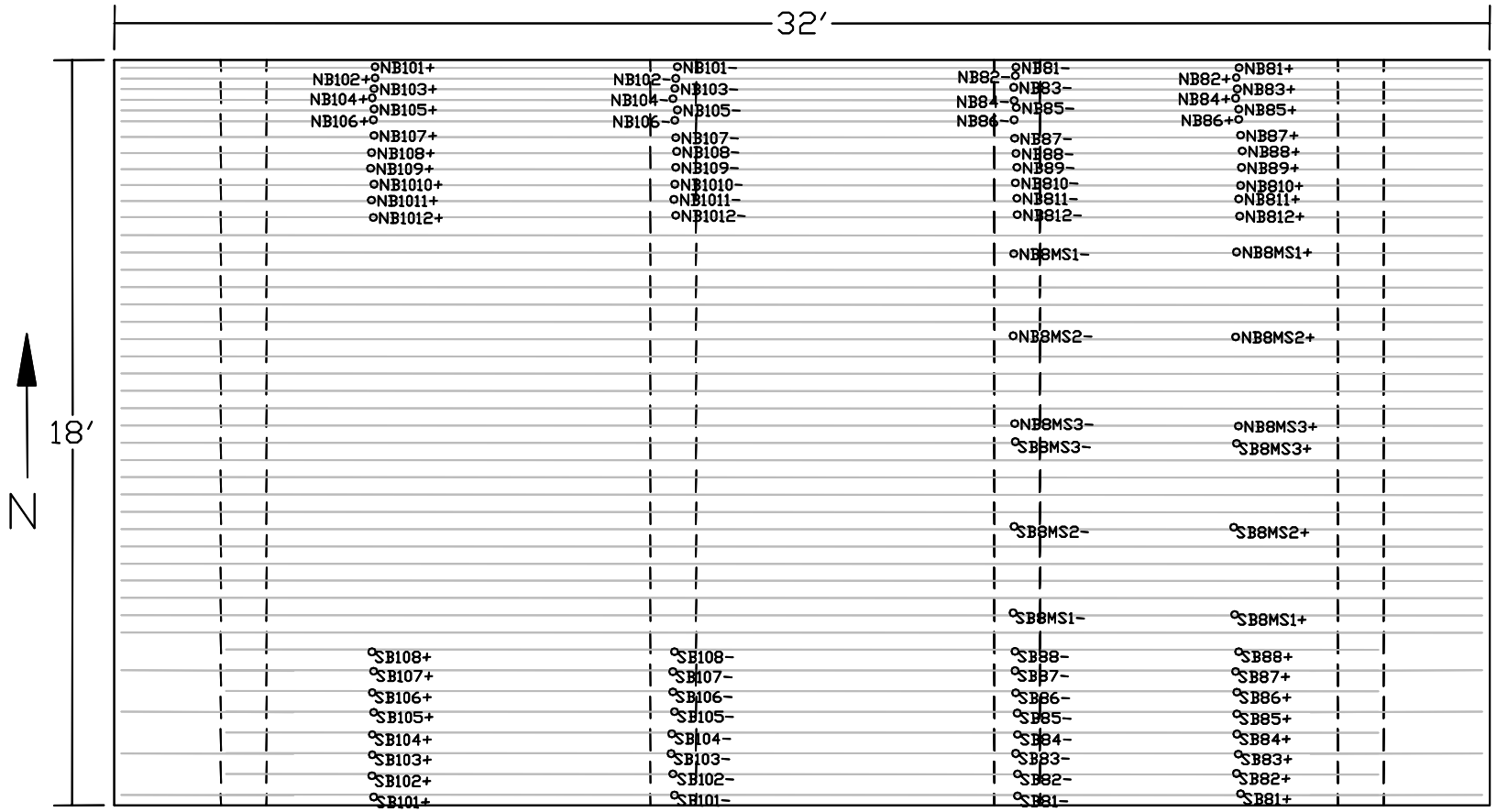

Figure 4-8: Strain gauge locations on the bottom mat of reinforcing steel

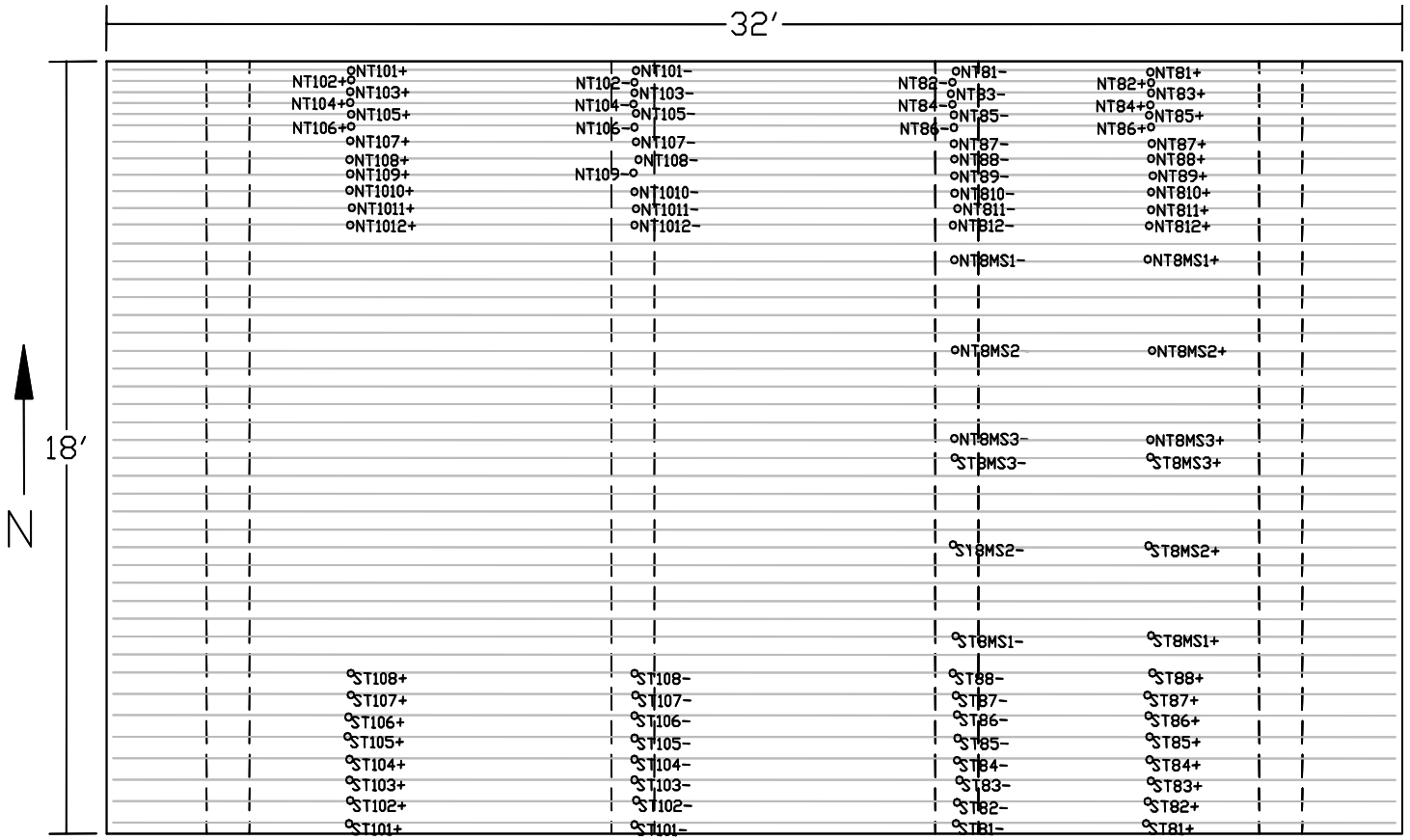

Figure 4-9: Strain gauge locations on the top mat of reinforcing steel

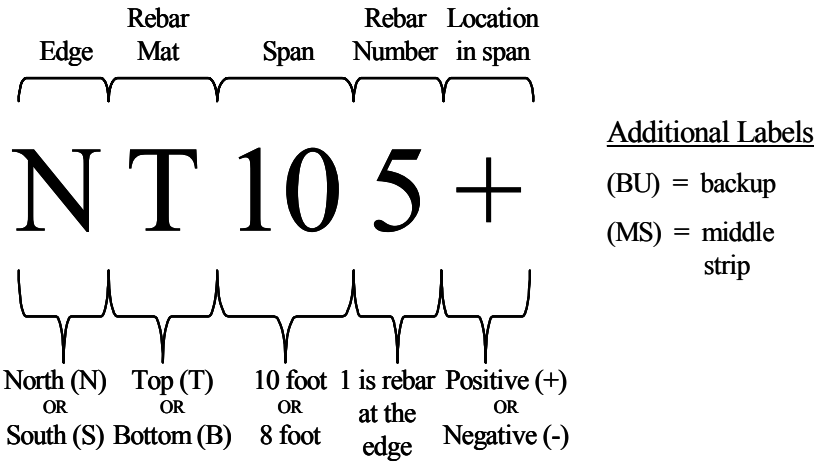

Figure 4-10: Strain gauge labeling system

4.4.1.2 Installation of strain gauges

The strain gauges used were FLA-5-11-3LT. They had a five-millimeter gauge length, three-meter pre-attached leads and were temperature compensating (three-wire gauges). The rebar was prepped for strain gauge application by grinding off one rib to create a flat surface on the bar. After which, the application area was cleaned with conditioner and neutralizer. Cyanoacrylate (CN) adhesive was used to bond the strain gauges to the rebar. Then, the gauges were waterproofed with M-coat D, an acrylic coating. Next, a neoprene rubber pad was placed over the gauge for padding and then the installation area was covered with foil tape. Finally, the edges of the foil tape were wrapped with electrical tape to seal out concrete and water.

A pilot test to determine the effectiveness of strain gauge protection methods was performed separately from the bridge deck specimen research. Strain gauges were protected in various ways, including some with only the acrylic coating, and then set in a water bath for a week. Upon testing, all provided reasonable strain readings, showing they are possibly less sensitive than

originally thought. However, the intensive protection method described previously was followed in order to assure the procurement of sufficient useful data. Figure 4-11 shows a picture of the specimen just prior to placing of concrete, with the strain gauges (silver foil tape) and block outs (white PVC pipe) in-place.

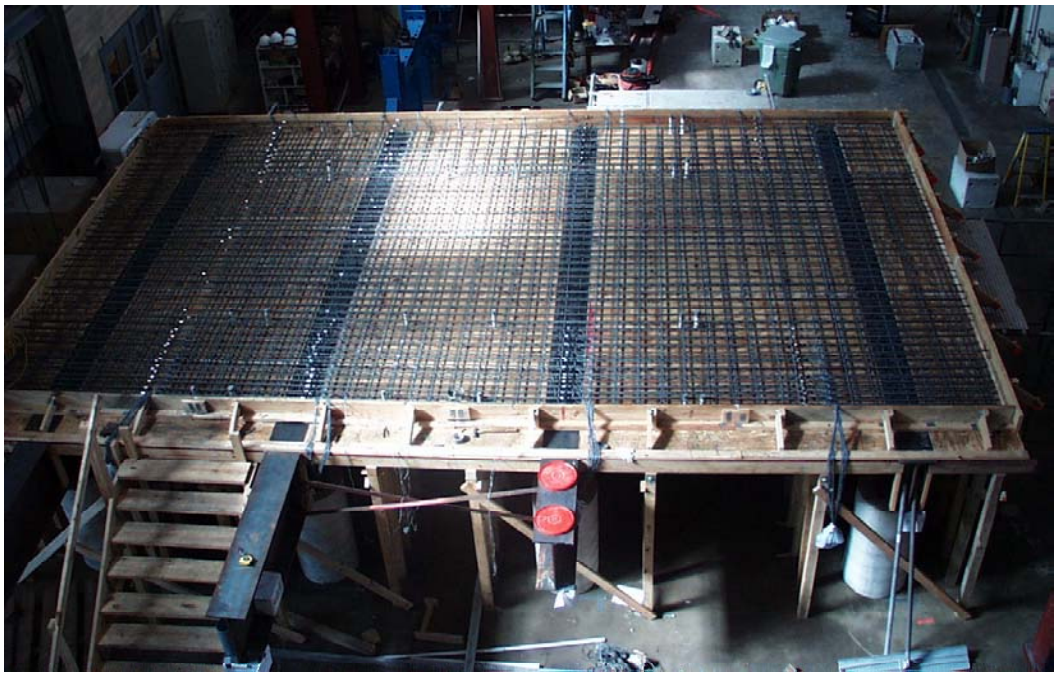

Figure 4-11: Test specimen just prior to placing of concrete

4.4.2 Load measurements

Loads were measured by load cells, located underneath the girders (lower load cells) and at the hydraulic rams (upper load cells) (Figure 4-4). The lower load cells were only used under the edge of the bridge deck being tested, since the majority of the applied load is going directly into those supports. The upper, center-hole load cells were the primary measurement of applied load. In addition, a pressure transducer was connected at the hydraulic pump. Pressure transducers are typically less accurate than load cells, therefore, the pressure transducer was

used to verify the load cell readings. In addition, when applied load exceeded the upper load cell capacity, near failure of the test area, the load was determined exclusively with the pressure transducer.

4.4.3 Deflection measurements

Deflection measurements were taken under the girders, midspan, and the overhang, using both linear and string potentiometers. At midspan, deflections were taken at the edge of the deck and at four feet from the edge in the longitudinal direction of the deck. String potentiometers were used in highly congested locations where there wasn't room for a linear potentiometer's stand. Figure 4-12 shows a plan view of the measurement locations.

Due to concerns about the flexibility of the web of the steel girders, during the first test (southeast test), linear potentiometers were used to measure rotation of the girders (Figure 4-13). Deflection readings from the southeast test area were converted to rotations, resulting in a maximum rotation of 0.37 degrees as well as a rotation of 0.04 degrees (one eighth of the maximum) at the HS-25 load step. Therefore, it was decided that the rotations were minute, even at failure loadings, and not of concern for other test areas.

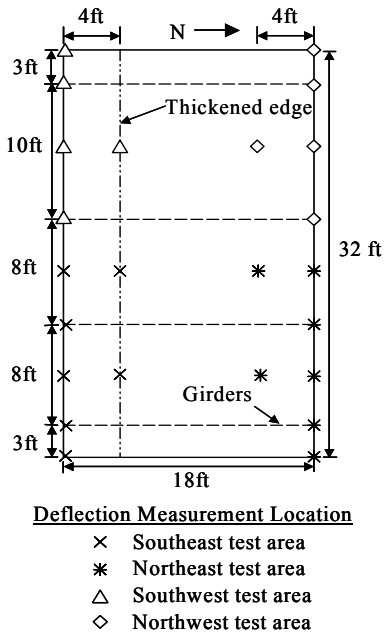

Figure 4-12: Location of deflection measurements

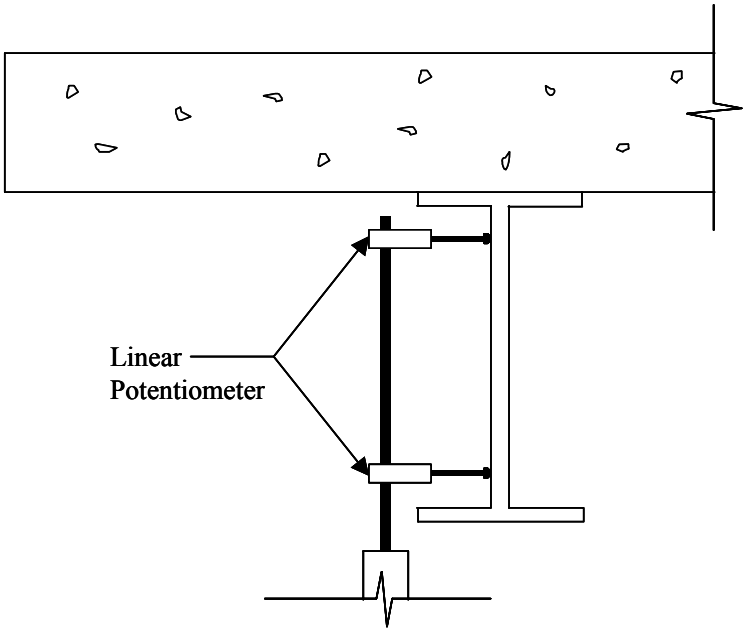

Figure 4-13: Girder rotation measurement

4.4.4 Data acquisition system

The output of the instrumentation was voltage (analog signal). The instrumentation was connected to bridge boxes, which converted the alternating current from the instrumentation to a steady current that the scanner read. The scanner converted the voltages to a digital format. This digital output was readable by the data acquisition software installed on a personal computer and set up near the test.

The data acquisition software used in the Ferguson Laboratory was National Instrument's Win/NT Measure, which records the data in EXCEL files for easy analysis. It also plots real-time test data, allowing the specimen's behavior to be monitored while loading.

4.5 PROPERTIES OF MATERIALS

Actual material properties were determined in order to facilitate accurate analysis of the bridge deck's behavior when loaded with the design vehicles and overloads. In addition, the material testing was used to verify the minimum strengths specified by the manufacturer.

4.5.1 Reinforcing steel

The reinforcing steel used in the specimen came from two different heats. Two specimens from each heat were tested in tension. An extensometer was used to determine strains (Figure 4-14) and the applied load was measured by the built-in load cells in the test machine. After converting the load measurements to stresses, stress versus strain plots were created. Figure 4-15 and Figure 4-16 each show a close agreement between the two tests and a yield plateau above 60ksi for all tests. The average modulus of elasticity for heats 1 and 2 were 30600ksi and 31300ksi, respectively.

Figure 4-14: Rebar tension test

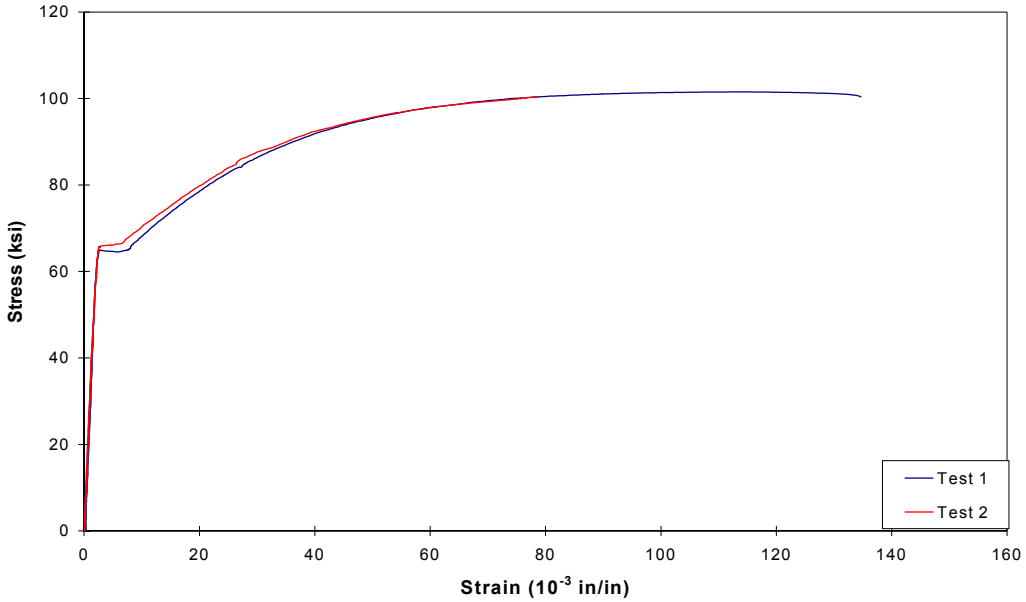

Figure 4-15: Stress vs. strain plot of rebar tension test, heat 1

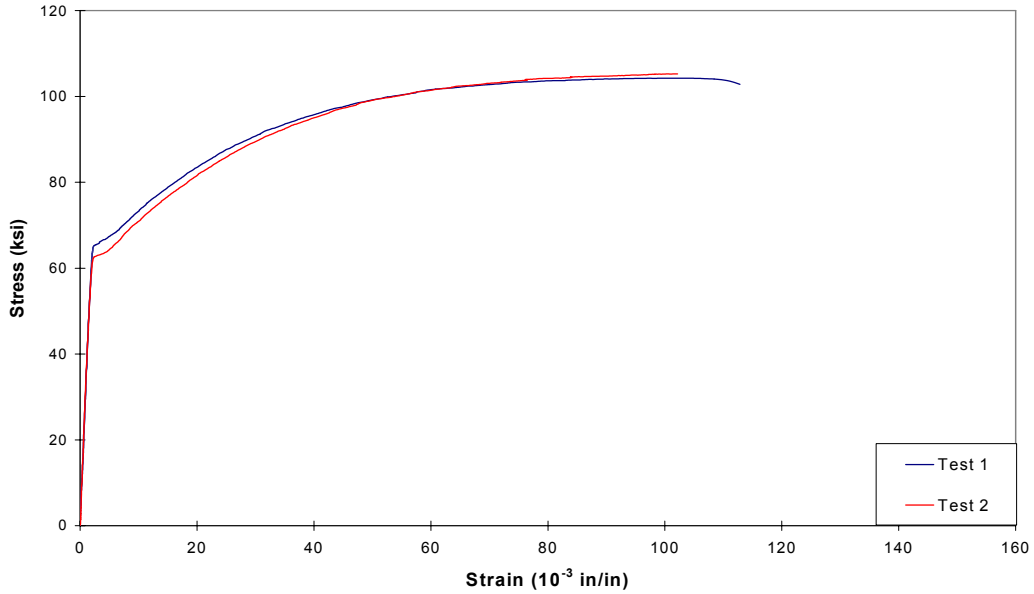

Figure 4-16: Stress vs. strain plot of rebar tension test, heat 2

4.5.2 Concrete

The TXDOT Bridge Design Manual (20) currently requires a compressive strength of 4000psi or above for concrete used in bridge decks. Therefore, a mix design with a range of compressive strength from 4000psi to 6000psi was ordered (Table 4-1).

Table 4-1: Bridge deck concrete mix design, one-yard weights

Mix #	Description	f'_c (psi)	Cement	Fly Ash	Course Agg.	Fine Agg.	Water	Ad-mixture
227	UT5000A 3/8in minus	4000 to 6000	564	0	1625	1469	280	16.8

*All quantities are in units of pounds (lbs).

Capitol Aggregates provided three trucks of concrete, approximately 16 cubic yards total. During placing of concrete, a slump test was done on concrete

from each of the trucks, resulting in slumps of 5.5 in, 5.5 in and 9.5 in, respectively. In addition, six by twelve test cylinders from the three trucks were prepared with standard ASTM procedures.

4.5.2.1 Compression tests

Compression tests only were performed on trucks one and two as concrete from truck three was placed solely in the east overhang, an area that was not tested in this study. Therefore, its strength was not important. For each point plotted on the strength versus time curve in Figure 4-17, a minimum of two cylinders were tested. If their strengths did not show good correlation, a third test was done for verification. Truck one's cylinder test results appear reasonable, with strength increasing quickly during the first couple of days, then, gradually increasing afterward. Results of the cylinder strength tests for truck two are approximately identical for the 14-day strength and 28-day strength, when a strength increase would be expected. Therefore, a 56-day test was done to verify the concrete strength, which resulted in an f'_c of 6500psi. In any case, the 28-day strengths of both trucks were around 5000psi, well above the minimum required by TxDOT.

4.5.2.2 Split cylinder tests

Split cylinder tests were performed after 28-day strength occurred. Two cylinders from both trucks one and two were tested. The tensile strength, f_{ct}, was determined by the formula $f_{ct} = \frac{2P}{\pi l d}$, with P equal to the failure load. Truck one and two test results were 620psi, 502psi, 568psi and 576psi, respectively. The split cylinder test results show good correlation.

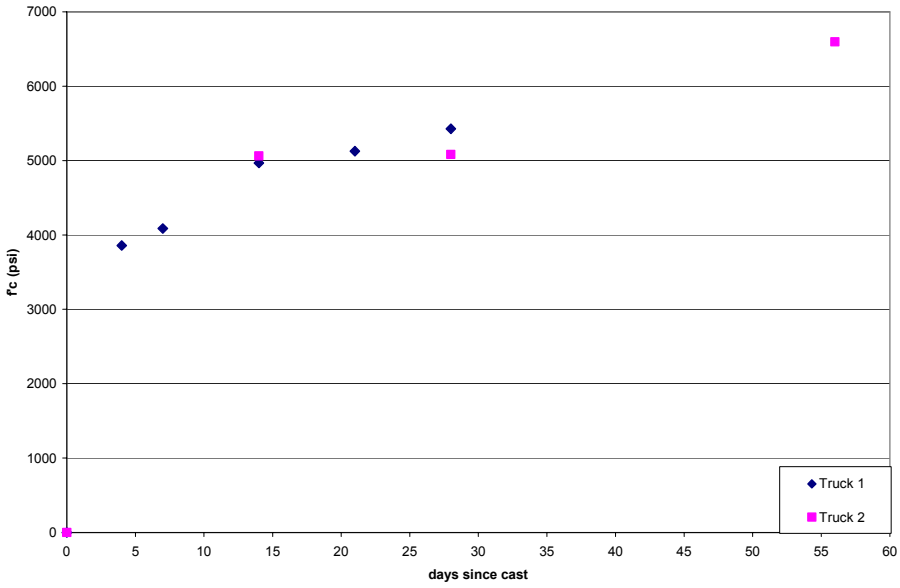

Figure 4-17: Bridge deck concrete compressive strength

The average of these tensile strengths gives a factor of 7.33 times the root of f'_c. Engineering design assumes a tensile strength of six times the root of f'_c, therefore, these results show the conservative nature of design values. The average tensile strength calculated from the split cylinder test was used in the moment calculations, when tension in concrete is included.

4.6 TEST PROTOCOL

Load was applied to the test specimen with 60-ton hydraulic rams connected to a tee from a pneumatic, hydraulic pump to assure equal load application to all tires. After verifying that the instrumentation was working properly, the load was increased gradually. Since the scanner took nine seconds to record readings from 90 channels, load was increased in small increments. During testing, a load vs. strain plot of the most critically strained gauge was generated in real-time in order to monitor the response of the deck to applied

loadings. Intermittently, loading was paused and cracks, if any, were traced and recorded.

The southeast and northeast test areas were loaded to HS-25 load levels in tandem, truck axle-front and truck axle-back vehicle arrangements at the location to maximize positive moment. Then, the load frame was moved to the location to maximize negative moment for the rest of the load applications in these two test areas. At the location to maximize negative moment, the design loadings, HS-20 and HS-25, along with typical overloads, 1.2, 1.75, and 3 times HS-25, were applied for the three vehicle arrangements. After looking at the test data for these load levels, the most critical loading arrangement was determined to be the tandem vehicle loading. Therefore, the test area was taken to failure in tandem loading with intermediate stops to map cracks.

The overload load steps mentioned above were chosen because they are commonly used by bridge designers and researchers. A factor of 1.2 times HS-25 loading is a typical design load increase to account for overloaded trucks. 1.75xHS-25 was chosen as a load step because 1.75 is the value of the live load, load factor for the load combination, Strength I from the AASHTO LRFD code (section 3.4.1 in AASHTO LRFD). In addition, the dynamic load allowance in section 3.6.2 of the AASHTO LRFD code requires the design loading to be increased by 1.75 for expansion joints. An overload level of 3xHS-25 was also applied to all test areas because the product of the load factor and the dynamic load allowance is approximately three. When designing the expansion joint of a bridge deck, the actual design load required by the AASHTO LRFD code is three times the typical design load.

The southwest and northwest test areas were loaded at midspan only, because failure occurred in the middle span during testing of the southeast test area. In order to avoid the damaged area of the specimen and since the two

loading locations (maximizing positive or negative moment) produce almost the same effects, vehicle loadings were applied at midspan. In addition, only one tire per axle had to be applied because the other tire lay directly above the girder flange. The same load steps and vehicle arrangements were used.

CHAPTER 5
Behavior of Bridge Deck Specimen

5.1 INTRODUCTION

The test specimen contained four test areas, designated southeast, southwest, northwest and northeast, in reference to the arrangement of the bridge in the laboratory. Figure 3-11 shows the variables tested in each area of the bridge deck. The four test areas were loaded to HS-20 and HS-25 levels, typical overload levels (1.2, 1.75 and 3xHS-25) and ultimately to failure. Strains, deflections, applied loads and crack widths and lengths were recorded for all tests performed. Interpretation of the acquired data and discussions on the bridge slab end behavior are included in this chapter. The performance of the slab end in each test area will be described and critically examined.

Figure 5-1 shows an example of the legend used in figures herein to explain the test being performed on the bridge deck. The black-filled circles represent tires that are loaded in a particular loading configuration. The loading location is distinguished by a + or – sign to indicate a positive or negative moment test, respectively (Figure 4-8). For example, the legend shown in Figure 5-1 is for the truck axle-front loading configuration at the location to maximize negative moment in the southeast test area. The load values plotted in all figures in this chapter are the average of all upper load cells used in the test, except at failure loadings, when the pressure transducer readings were used exclusively. The term load step refers to loading and unloading of the test specimen.

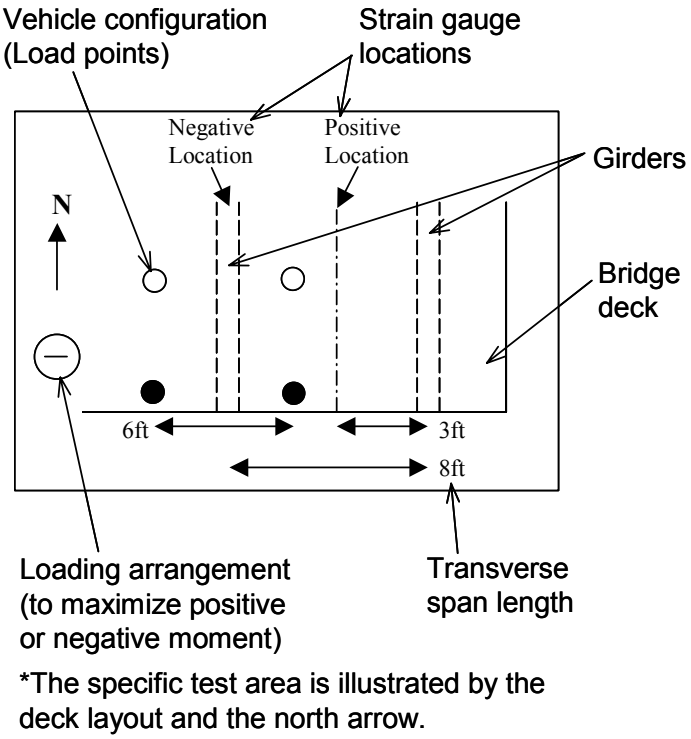

Figure 5-1: Typical plot legend

5.2 SOUTHEAST TEST AREA

This was the first area tested because it models a typical TxDOT slab end detail. In this test zone, the performance of the IBTS detail was evaluated using an eight-foot transverse girder span. 10in by 20in load plates, bearing on a layer of hydrostone, were used to apply loads in this test area. Loads were applied first in the location to maximize the positive moment, and then the load frame was shifted to maximize the negative moment for the rest of the tests. Table 5-1 shows a list of the load tests performed on the southeast test area.

A plot of load versus strain in rebar SB81+, by intuition the most critically strained rebar, was monitored during testing. Cracking, as well as imminent failure was identified in this plot, by noting when there was a pronounced

Table 5-1: Order of testing in southeast test area

Test No.	Loading Location	Load Type Tandem/Truck	Which axle?	Load per tire (kips)	Load per tire (xHS-25)
1	Positive	Tandem	Both	15.6	1
2	Positive	Truck	Front	20.0	1
3	Positive	Truck	Back	20.0	1
4	Negative	Tandem	Both	15.6	1
5	Negative	Truck	Front	20.0	1
6	Negative	Truck	Back	20.0	1
7	Negative	Tandem	Both	18.8	1.2
8	Negative	Truck	Front	24.0	1.2
9	Negative	Truck	Back	24.0	1.2
10	Negative	Tandem	Both	27.3	1.75
11	Negative	Truck	Front	35.0	1.75
12	Negative	Truck	Back	35.0	1.75
13	Negative	Tandem	Both	45.3	2.9
14	Negative	Tandem	Both	67.2	4.3
15	Negative	Tandem	Both	82.8	5.3
16*	Negative	Tandem	Both	93.8	6
17**	Negative	Tandem	Both	90.6	5.8

*Punching of edge tire in interior span; **Punching of edge tire in exterior span

reduction in the stiffness and damage in the bridge deck. The applied loads were maintained and visual inspections of the test specimen were performed at several load stages (1.0, 1.2, 1.75, 2.9, 4.3, 5.3 and 6xHS-25). All crack lengths, widths and locations were mapped as part of the testing protocol.

5.2.1 Loading to maximize positive moment

In order to maximize the positive moment, an axle made of back-to-back C12X25 channels was loaded through its mid-length by a hydraulic ram connected to the load rod (Figure 5-2). Roller supports were placed between the axle and the load plates to ensure uniform loading of the plates, simulating tire loads. Tandem, truck axle-front and truck axle-back loading configurations were applied at the HS-25 load level (Table 5-1).

Figure 5-2: Axle loading used to maximize positive moment

5.2.1.1 Load vs. deflection response

Load versus deflection plots were created using the readings of the linear and string potentiometers measuring vertical deflection of the bridge deck. The deflection readings from the potentiometer located in the interior of the deck (four-feet from the edge longitudinally, at midspan of the exterior span transversely) were very small, essentially indistinguishable from the noise produced by the instrumentation. Therefore, transverse deflection of the edge is used in the subsequent discussions. The relative deflection at the edge was calculated by averaging the two girder deflection readings and then subtracting this from the deflection reading at midspan (Figure 5-3). In this way, rigid body movement of the bridge deck was filtered out and deformations that cause stresses and strains are reported.

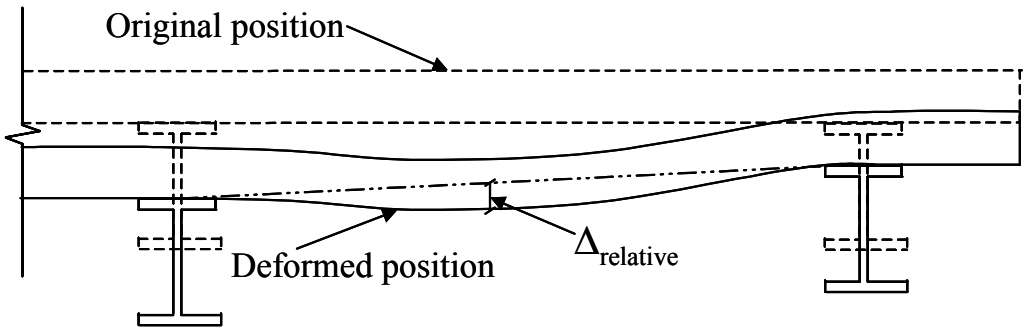

Figure 5-3: Relative deflection

Figure 5-4 shows load versus deflection plots for load tests performed in the location to maximize positive moment at the HS-20 and HS-25 load steps. The slab end behavior was elastic for all loading configurations at the HS-25 load level. The tandem vehicle caused the largest relative deflection of 0.07in and its plot (Figure 5-4, i) showed a slight change in stiffness during loading, indicating some minor deterioration within the deck, probably microcracking of the concrete around the reinforcing steel. The truck axle-front loading configuration caused nearly the same deflection as the tandem configuration, however, no stiffness change occurred during the load test. In addition, the plot for truck axle-front loading configuration (Figure 5-4, ii) is essentially a single line for loading and unloading, indicating linear behavior of the bridge deck. The truck axle-back loading configuration caused very small deflections in relation to the other loading configurations (Figure 5-4, iii).

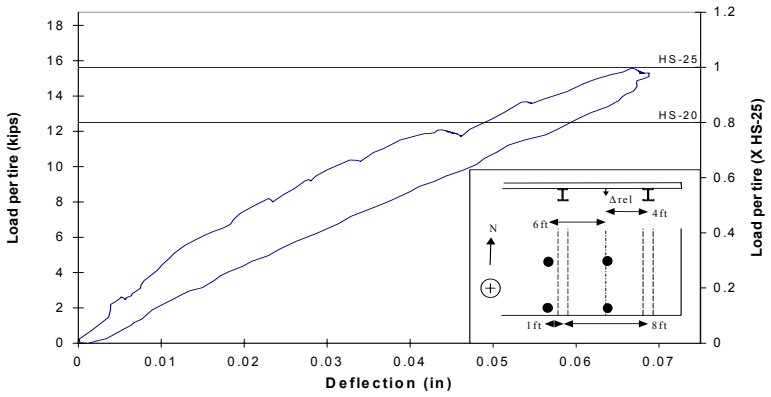

(i) Tandem

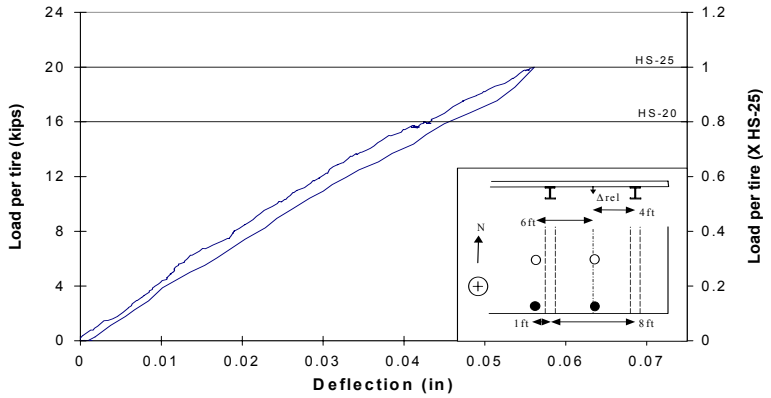

(ii) Truck axle-front

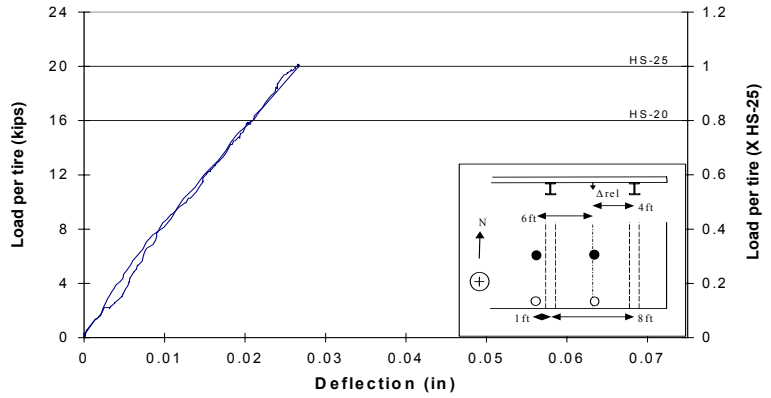

(iii) Truck axle-back

Figure 5-4: Load vs. deflection HS-25 load step, positive moment loading, southeast test area

5.2.1.2 Load vs. strain response

Load versus strain plots were used to study cracking of the concrete, yielding of the steel, strain gradients in the thickened edge, and other events occurring in the section. Representative strain gauges on reinforcing steel in tension (bottom mat of rebar at the maximum positive moment section and top mat at the maximum negative moment section) are discussed. Figure 5-5 shows plots of load versus strain for the three loading configurations tested at the HS-25 load step. Readings obtained from three representative gauges in the section are shown.

The first load test performed in this test area was tandem HS-25 to maximize positive moment. The applied loading induced small strains both at the positive and negative moment section (Figure 5-5). The tandem loading configuration caused a maximum strain of 265με (about 13% of the yield strain of the reinforcing bars). The truck axle-front loading configuration (Figure 5-5, iii) strained the edge reinforcing bar of the IBTS detail more than the SB84+ and SB88+ gauges. In contrast, the truck axle-back loading configuration strained the SB88+ gauge more than any other gauge in the section, however, this strain (60με) was very small relative to the yield strain of steel.

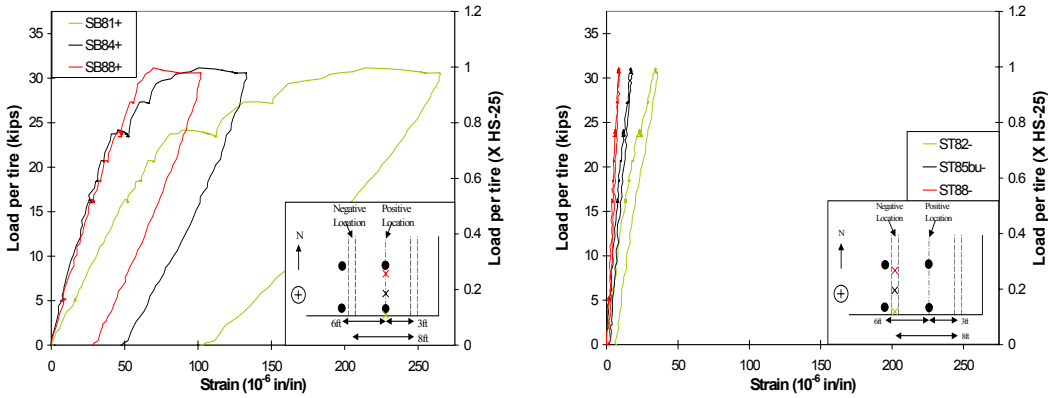

(i) Tandem

(ii) Tandem

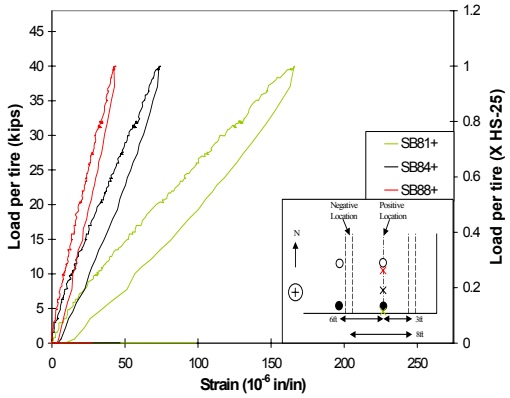

(iii) Truck axle-front

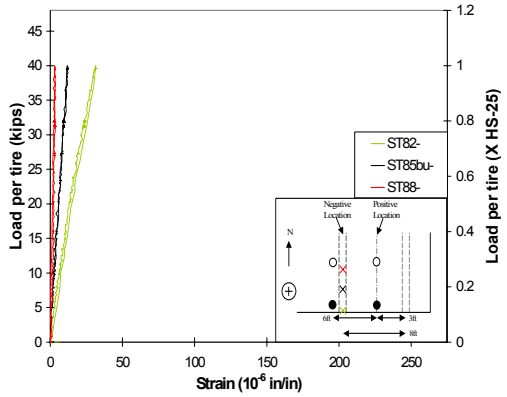

(iv) Truck axle-front

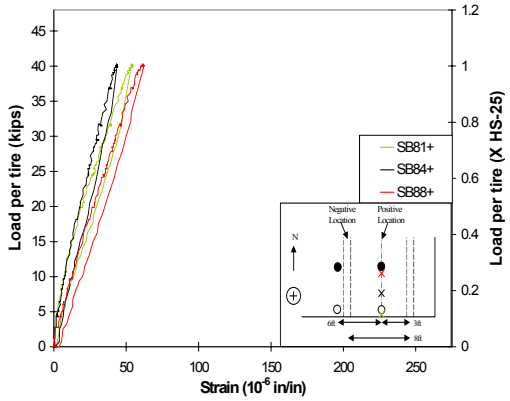

(v) Truck axle-back

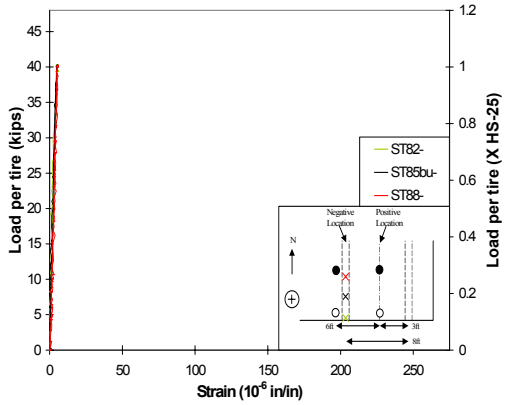

(vi) Truck axle-back

Figure 5-5: Load vs. strain, HS-25 load step, positive moment loading, southeast test area; (i), (iii) and (v): bottom mat at positive location; (ii), (iv) and (vi): top mat at negative location

The strains induced by the applied load at the maximum negative moment section (Figure 5-5, ii, iv and vi) are much lower in magnitude than at the positive location. This is to be expected because positive moment was being maximized in this loading configuration. The maximum strain of 40με (approximately 2% of yield strain of the rebar) was caused by the tandem loading configuration. The plot for the truck axle-front loading configuration (Figure 5-5, iv) again shows strains focused at the edge of the bridge deck. The truck axle-back vehicle essentially created zero strain at the maximum negative moment section (Figure 5-5, vi).

As can be observed in Figure 5-5 (i), at the maximum positive moment section, insignificant plastic strains (about 100με for the SB81+ gauge) remained after unloading. In addition, there was a reduction in stiffness at about 70με indicating some inelastic deformation or possible microcracking at the edge. This was likely due to the concrete deteriorating (i.e. microcracking) around the first rebar. However, it is important to note that there were no visible cracks at the edge of the IBTS detail. Both the truck loading configurations applied to the bridge deck (Figure 5-5, iii, iv, v and vi) created elastic behavior during the load test.

The plots in Figure 5-5 show a succession of decreasing strain from the edge of the deck to the interior, except for the truck axle-back vehicle loading. For the tandem and truck axle-front loading configurations, the strains created in the maximum negative moment section are very small, amounting to 15-20% of the strains induced at the positive location. This confirms the analysis reported in CHAPTER 4 where influence lines were used to determine the critical loading locations.

5.2.1.3 Strain profiles

Strain profiles were used to compare strain readings from reinforcing steel in the test area at a specific location (positive or negative moment sections). Figures in this section show the strain in the rebar at explicit load steps. This is equivalent to looking at a plan view of the strain measurements from reinforcing steel in the edge detail. The strain profiles were used to compare strains induced within the bridge deck for the three loading configurations and the two sections. Since the edge deflection was much greater than the deflection four feet into the deck, the expected strain profile would give a maximum strain at the edge rebar, gradually decreasing for rebars further into the section. However, the specific shape of the strain profile varies depending on the loading configuration and the section.

Figure 5-6 shows the strain profiles for the three loading configurations loading to maximize positive moment at the HS-25 load step. The tandem loading configuration created the largest strains across the section, at both the positive and negative moment sections (Figure 5-6, i and ii). The strains induced at the maximum negative moment section were significantly smaller than those at the positive location. The strain profiles confirm expected behavior based on first principles of mechanics for the tandem and truck axle-front loading configurations, with strains declining from the edge moving into the deck.

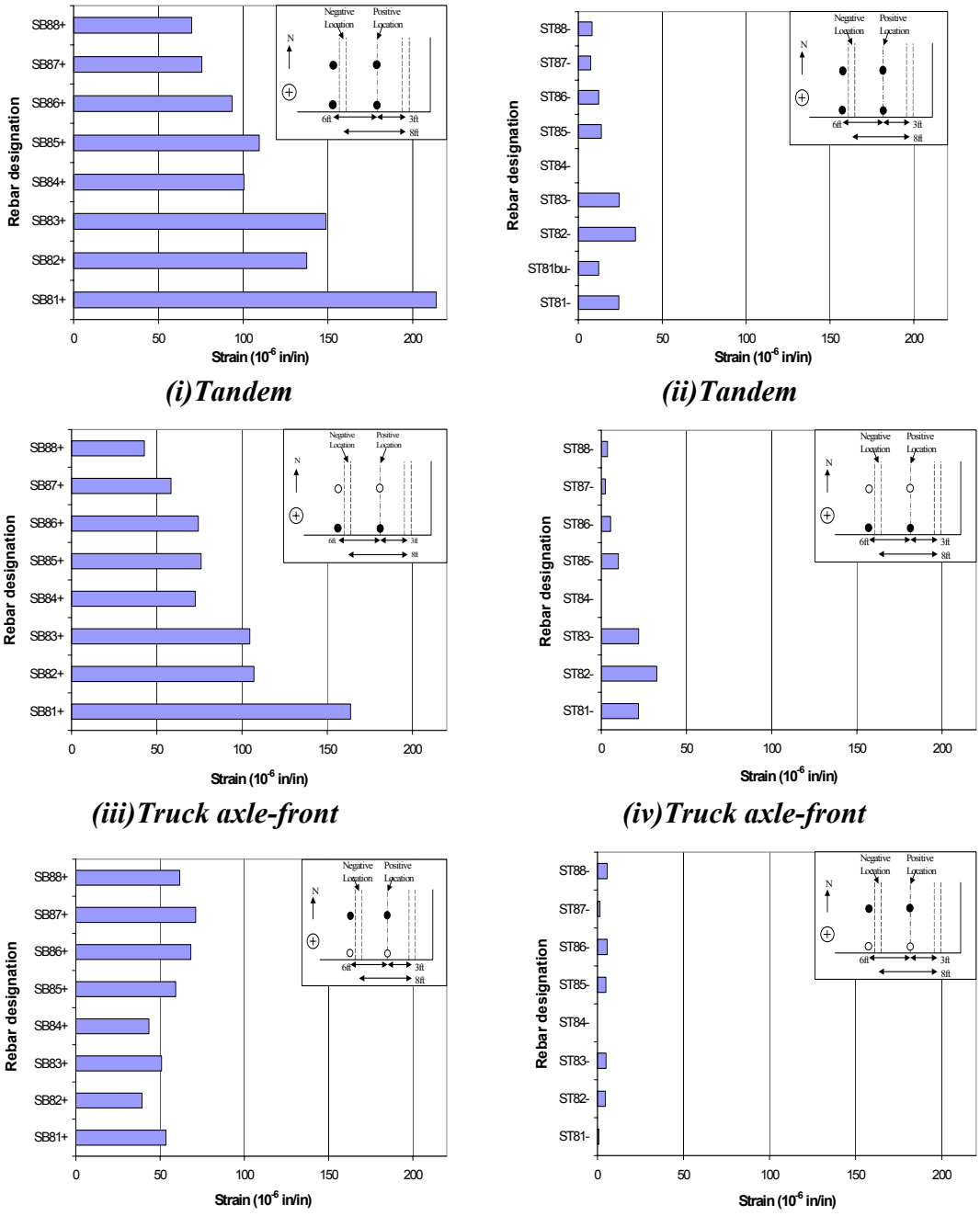

(i) Tandem *(ii) Tandem*

(iii) Truck axle-front *(iv) Truck axle-front*

(v) Truck axle-back *(vi) Truck axle-back*

Figure 5-6: Strain profiles, HS-25 load step, positive moment loading, southeast test area; (i), (iii) and (v): bottom mat at positive location; (ii), (iv) and (vi): top mat at negative location

At the maximum positive moment section, the truck axle-front loading configuration caused smaller strains than the tandem vehicle. In addition, the truck axle-front loading configuration resulted in strains primarily at the edge reinforcing steel in both gauge locations (Figure 5-6, iii and iv). During the truck axle-back loading application, larger strains were measured in the reinforcing steel located in the interior of the thickened edge than in the rebars near edge (Figure 5-6, v and vi). The loads were applied at four feet from the edge of the deck for this loading configuration, creating the larger strains adjacent to the tire loads. However, the tensile rebar strains caused by the application of truck axle-back loading configuration are considerably smaller than the other loading configurations.

5.2.2 Loading to maximize negative moment

After the HS-25 load step to maximize positive moment was completed, the load frame was shifted to maximize the negative moment at the first interior girder for the rest of the load tests. For the eight-foot girder spacing, the two loading locations were reasonably close to each other. One inch separated the edges of the load plates for the positive and negative locations (i.e. a distance of 21 inches measured from center to center).

Tandem, truck axle-front, and truck axle-back loading configurations were applied at HS-25, 1.2xHS-25, and 1.75xHS-25 load steps. Then, strain readings from gauges at the first interior girder and extent of cracking were compared for the three loading configurations partly to determine which created the most severe effect on the bridge deck. First cracking occurred due to the tandem loading configuration and the cracks did not elongate when truck axle-front and back loads were applied. Figure 5-7 shows typical strain profiles comparing the effects of the three loading configurations, with the tandem vehicle inducing the largest

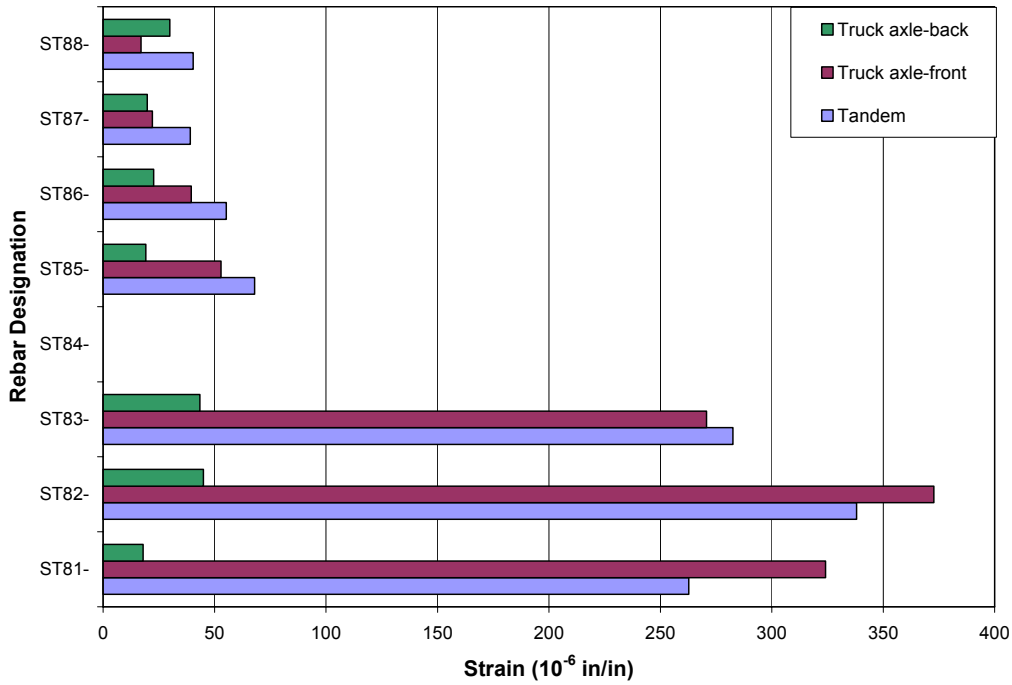

Figure 5-7: Strain profile for top gauges at the girder, 1.75xHS-25 load step

strains across the section. The truck axle-front loading configuration also caused large strains at the edge of the IBTS detail; however, the tandem loading configuration created somewhat larger strains across the entire thickened edge.

Based on this comparison, it was concluded that (i) the tandem loading causes the largest cumulative tensile strain in all the bars on top of the girder and (ii) maximization of the negative moment was more critical than the positive moment for this test area. Therefore, the slab end was loaded up to failure in the tandem loading configuration while maximizing the negative moment, with three intermediate load steps. Failure occurred at a load of 93.75kips per tire (6xHS-25 or 7.5xHS-20) by a punching failure at the edge loading plate in the interior span.

5.2.2.1 Load vs. deflection response

As in section 5.2.1.1, the relative midspan deflection at the edge of the bridge deck was plotted versus applied load for all load tests performed. Plots for the three loading configurations applied for a single load step make up one figure.

5.2.2.1.1 HS-25 load step

The maximum relative deflection of 0.02in was caused by the tandem loading configuration (Figure 5-8, i). The deck returned to zero deflection after unloading, exhibiting a purely elastic response to the load application. The truck axle-front loading configuration created an almost identical load versus deflection plot (Figure 5-8, ii) to the tandem vehicle, both in magnitude and slope. The truck axle-back loading configuration caused very small relative deflections at the edge of the deck.

The behavior of the bridge deck was elastic and linear at the HS-25 load step for the three loading configurations. In addition, the deflections induced were very small in relation to the span length.

5.2.2.1.2 1.2xHS-25 load step

Figure 5-9 shows plots of load versus relative deflection for the 20% overload test. The applied loading in the tandem loading configuration produced a linear, elastic response in the bridge deck. The increase in relative deflection between the HS-25 load step and the 1.2xHS-25 load step was proportional to the

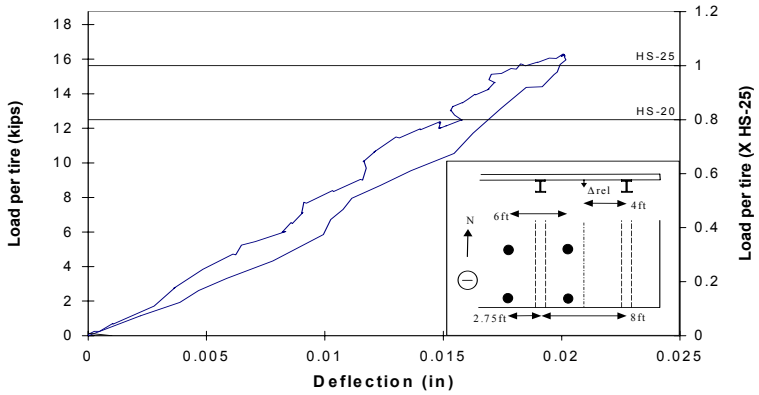

(i) Tandem

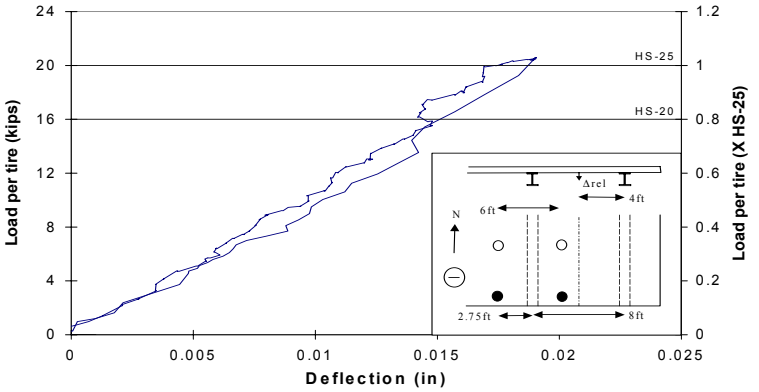

(ii) Truck axle-front

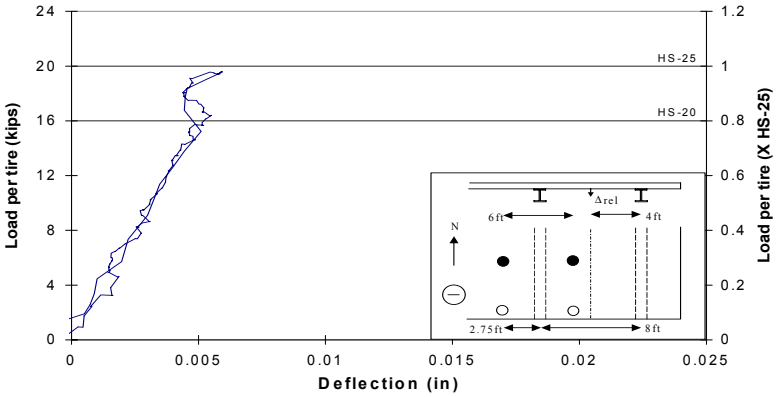

(iii) Truck axle-back

Figure 5-8: Load vs. deflection, HS-25 load step, negative moment loading, southeast test area

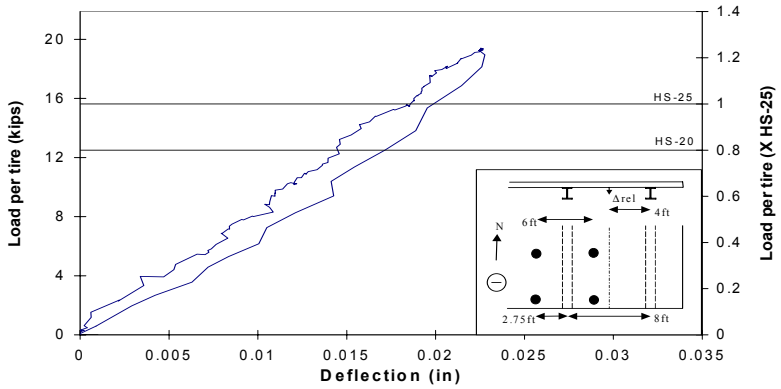

(i) Tandem

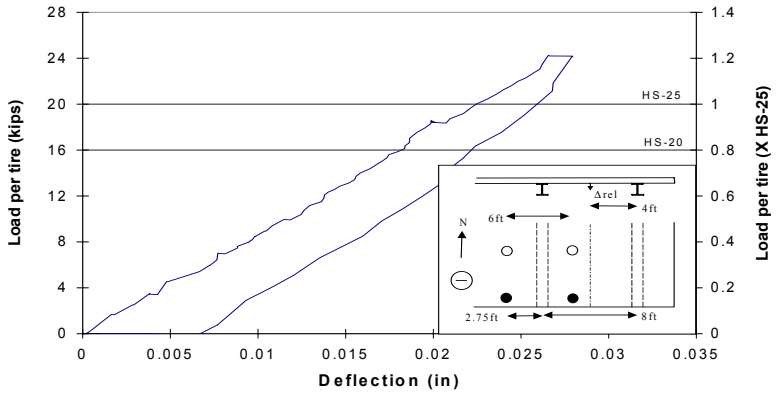

(ii) Truck axle-front

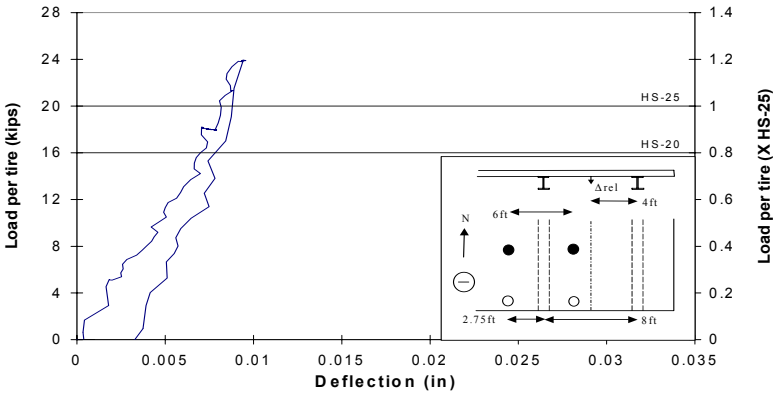

(iii) Truck axle-back

Figure 5-9: Load vs. deflection, 1.2xHS-25 load step, negative moment loading, southeast test area

increase in applied load. The truck axle-front loading configuration caused the maximum relative edge deflection of 0.03in for this load step.

5.2.2.1.3 1.75xHS-25 load step

The 75% increase in the applied design loading produced a proportionate increase in the relative midspan deflection (Figure 5-10). The tandem loading configuration created the largest relative midspan deflection at the edge of the bridge deck (0.04in) for this load step. The truck axle-front loading configuration produced nearly the same relative deflection as the tandem vehicle. The truck axle-back loading configuration produced a maximum relative deflection of 0.01in at the edge of the deck. When loaded in the truck axle-back loading configuration, the stiffness displayed by the bridge deck was significantly larger than when loaded in the truck axle-front configuration. This is because the deck was much stiffer four feet longitudinally into the deck, where the truck axle-back tire loads were applied, than at the edge.

5.2.2.1.4 Loading to failure

Figure 5-11 shows the load versus deflection response of the bridge deck as it was loaded to failure. After the design loading and typical overloads, the bridge deck was loaded to failure in the tandem loading configuration, as it typically created the most critical strain condition in the test specimen. The plot for loading to failure includes the load versus deflection response of the bridge deck for all tandem configuration loadings applied. There was essentially no deterioration caused by the HS-25, 1.2xHS-25 and 1.75xHS-25 load steps.

Several different load cycles were applied during loading to failure because testing had to be stopped when problems with the load frame occurred. The composite of these loading and reloading cycles are shown in Figure 5-11. The initial failure load cycle was stopped at a load of 45.3kips, without gradually

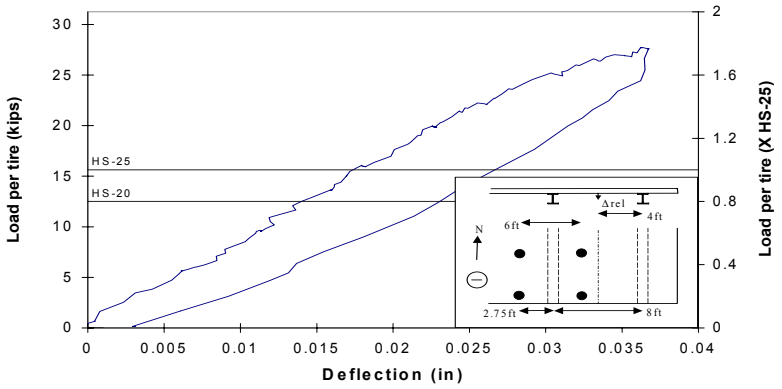

(i) Tandem

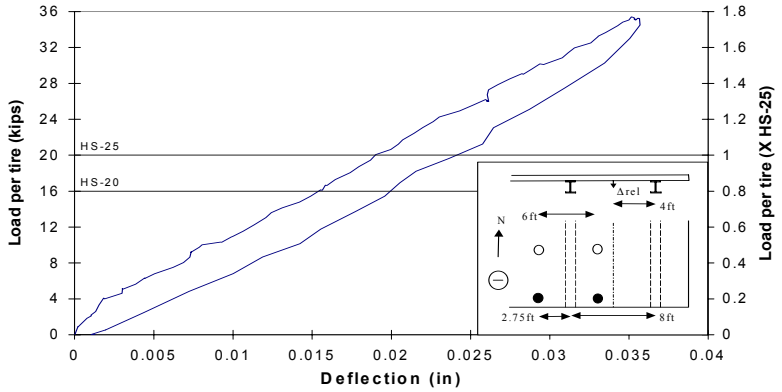

(ii) Truck axle-front

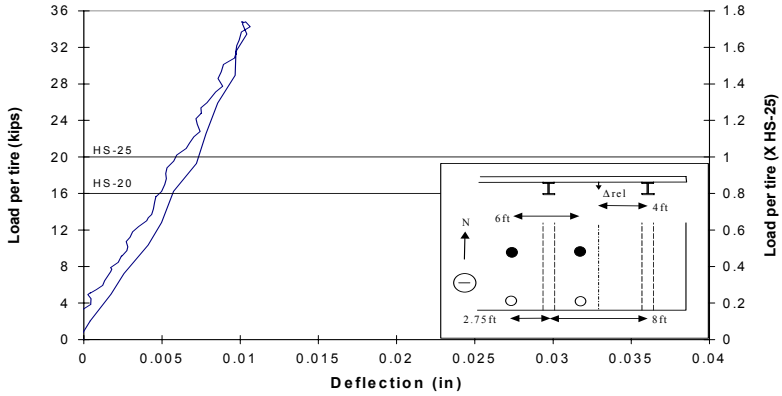

(iii) Truck axle-back

Figure 5-10: Load vs. deflection, 1.75xHS-25 load step, negative moment loading, southeast test area

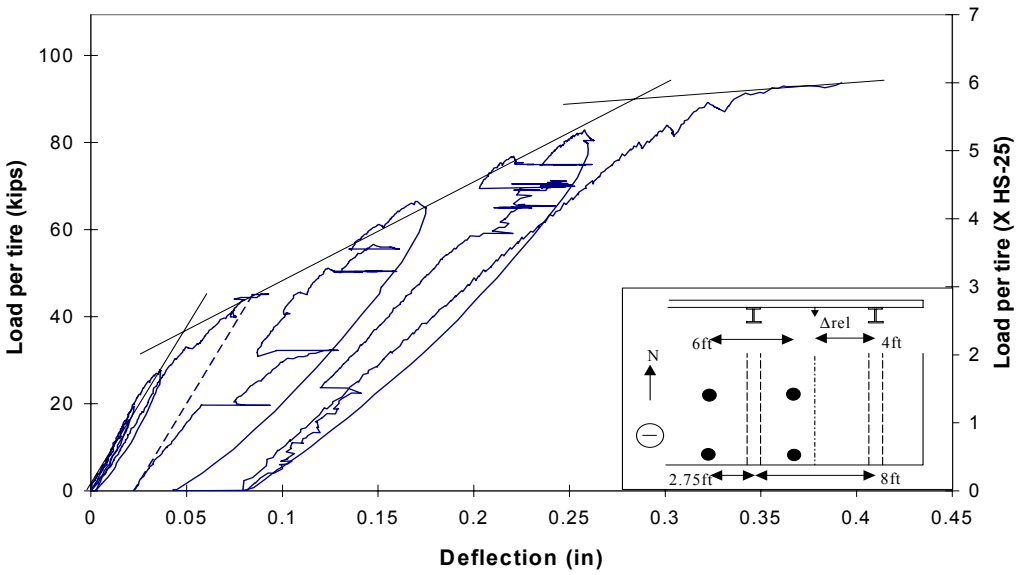

Figure 5-11: Load vs. deflection, loading to failure, negative moment loading, southeast test area

reducing the applied load, because the load frame was rotating hazardously. Therefore, the unloading portion of the initial failure load cycle plot was constructed by matching its stiffness to that of the loading portion of the plot (dashed lines in Figure 5-11).

The envelope of the load steps shows three distinct stiffnesses (Figure 5-11). There is a change in stiffness at a load of about 32kips (2.0xHS-25) per tire that corresponds well with the crack maps in section 5.2.2.2 and the load versus strain plots for loading to failure in Figure 5-21, which indicate cracking in the section near this load level. Just prior to punching of the interior span, at an applied load of about 91kips (5.8xHS-25) per tire, the stiffness of the bridge deck reduces to nearly zero. The maximum relative deflection at the edge of deck was 0.39in.

5.2.2.2 Crack maps

Numerous photographs were taken of the cracks occurring on the surface of the bridge deck during testing. At specific load levels, the length and maximum width of the cracks were determined using a crack width comparator. Using these two sources, the location and orientation of the cracks, as well as their dimensions have been accurately represented on the crack maps in Figure 5-12 through Figure 5-14. The crack maps included here are for the 2.1xHS-25 (first cracking), 2.9xHS-25 and 6xHS-25 (failure) load levels at the bottom, top and side of the bridge deck specimen. Each figure contains three crack maps and a key that gives the widths and lengths of the cracks.

The crack maps were selected to display the crack propagation from first cracking to ultimate capacity. They are useful to show the degradation of the test specimen under applied loads. In addition, the crack maps show when and where serviceability becomes an issue. They can also be used to identify potential failure mechanisms, such as in Figure 5-13 (iii), which shows cracks T3-T10, T19 and T20 curved around the load plates. These cracks indicate initiation of a punching failure mechanism.

At the bottom of the bridge deck, first visible cracking occurred at a load of 33kips (2.1xHS-25) in the exterior span (Figure 5-12, i). The 2.9xHS-25 load step caused increased cracking, however, still in the exterior span only (Figure 5-12, ii). At failure of the test area, just before the edge-most tire in the interior span punched, extensive bottom cracks had formed in both the interior and exterior spans (Figure 5-12, iii). The crack widths were very small at the 2.1x and 2.9xHS-25 load steps. The crack widths remained very small until the loading to failure, at which point they widened significantly. In addition, the loading to failure caused the bottom cracks to lengthen considerably, with the longest crack,

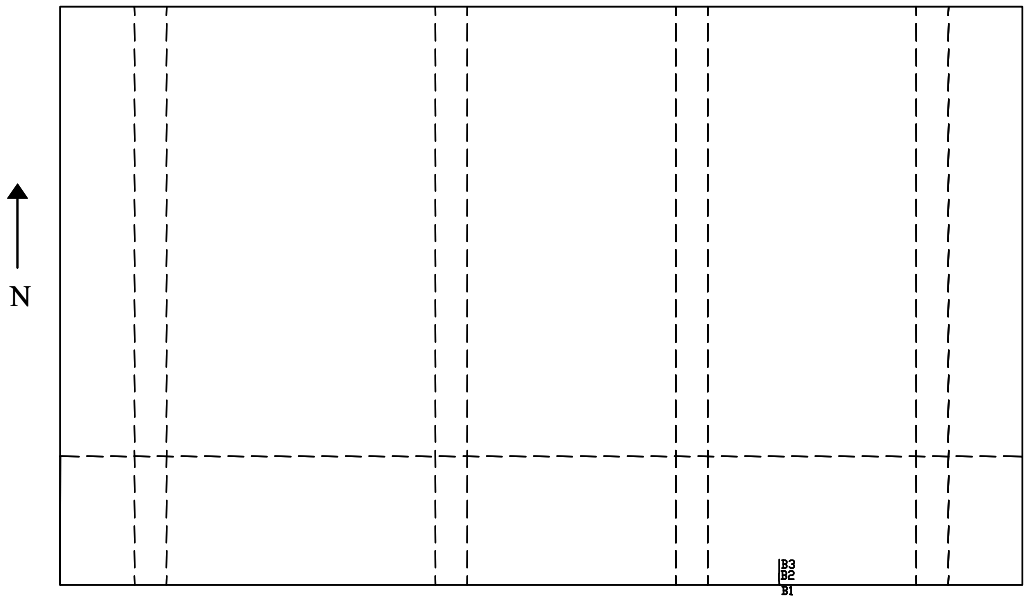

(i)2.1xHS-25 applied load (first cracking)

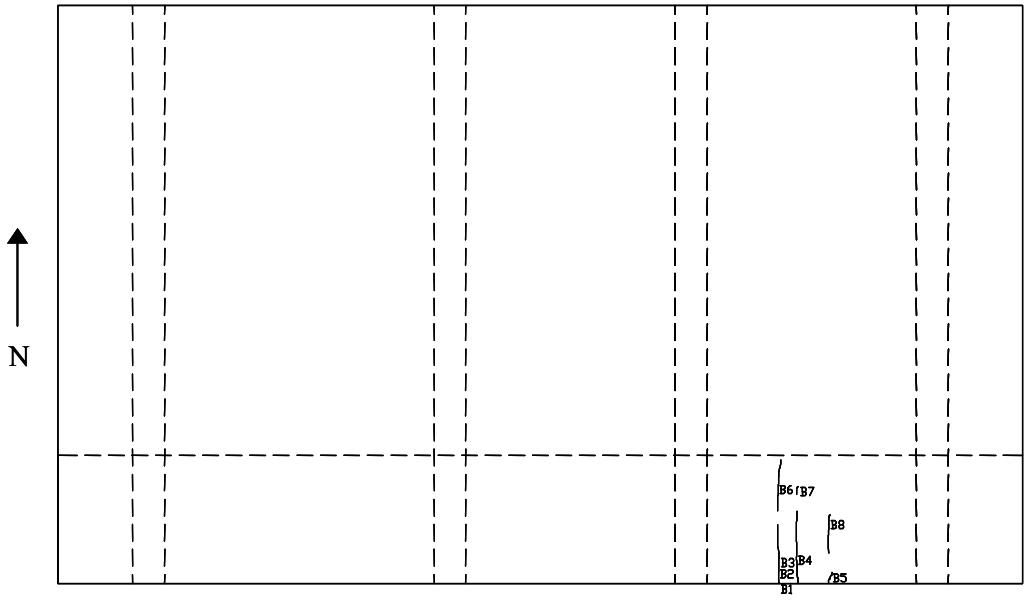

(ii)2.9xHS-25 load step
**Reference (iv) for crack widths and lengths*

Figure 5-12: Crack maps for the bottom of the bridge deck

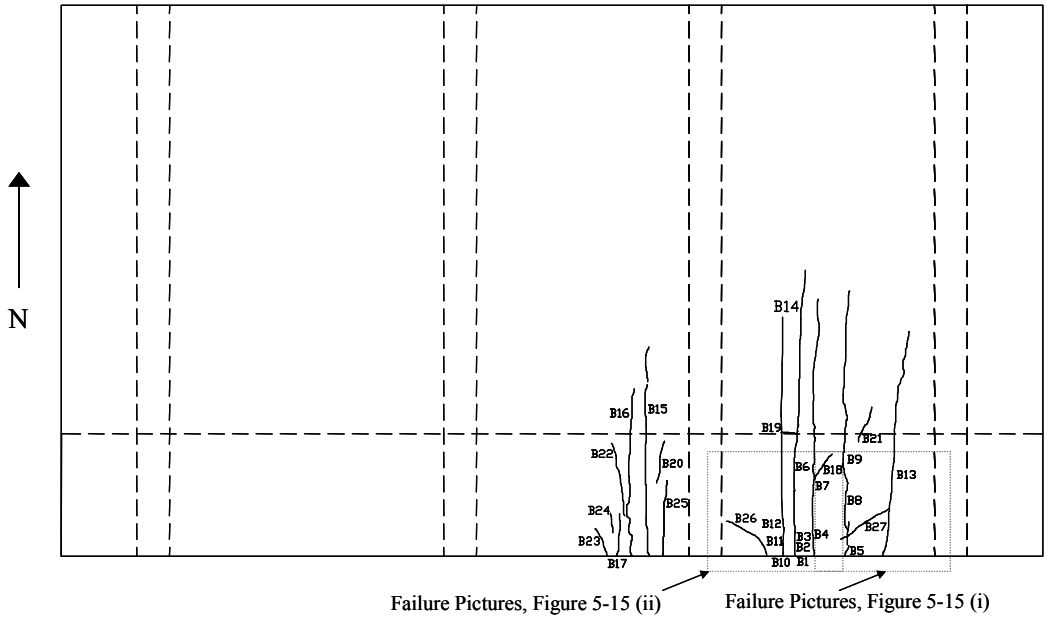

(iii)6xHS-25 load step (failure)

Load=2.11XHS-25			Load=2.92XHS-25			Load=6XHS-25		
Crack Name	Width (in)	Length (in)	Crack Name	Width (in)	Length (in)	Crack Name	Width (in)	Length (in)
B1-B2-B3	0.002	9.25	B1-B2-B3	0.002	22	B1-B2-B3-B6-B14	0.0016	112
			B4	0.002	27	B4-B7	0.014	100
			B5	0.002	4	B5-B8-B9	0.01	103
			B6	0.003	20	B10-B11-B12	0.02	93
			B7	0.0025	3	B13	0.007	87
			B8	0.002	14	B15	0.009	81
						B16	0.009	65
						B17	0.002	16
						B18	0.002	13
						B19	0.002	6
						B20	0.002	17
						B21	0.002	15
						B22	H	27
						B23	H	14
						B24	H	9
						B25	H	28
						B26	0.009	21
						B27	0.013	20

(iv)Key of crack widths and lengths for i, ii and iii

*H = hairline crack

Figure 5-12, cont'd: Crack map and key for the bottom of the bridge deck

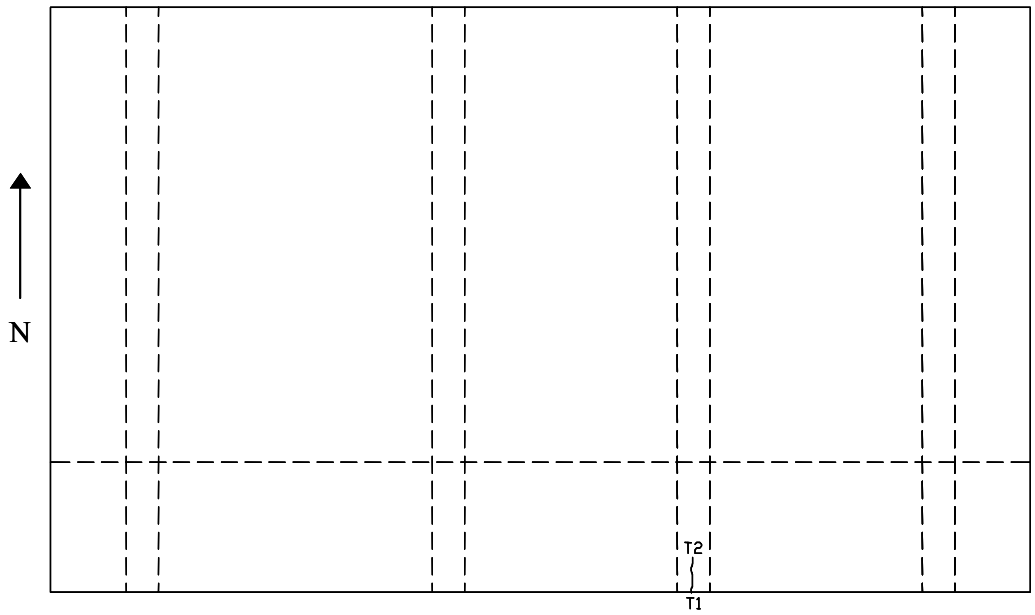

(i)2.1xHS-25 applied load (first cracking)

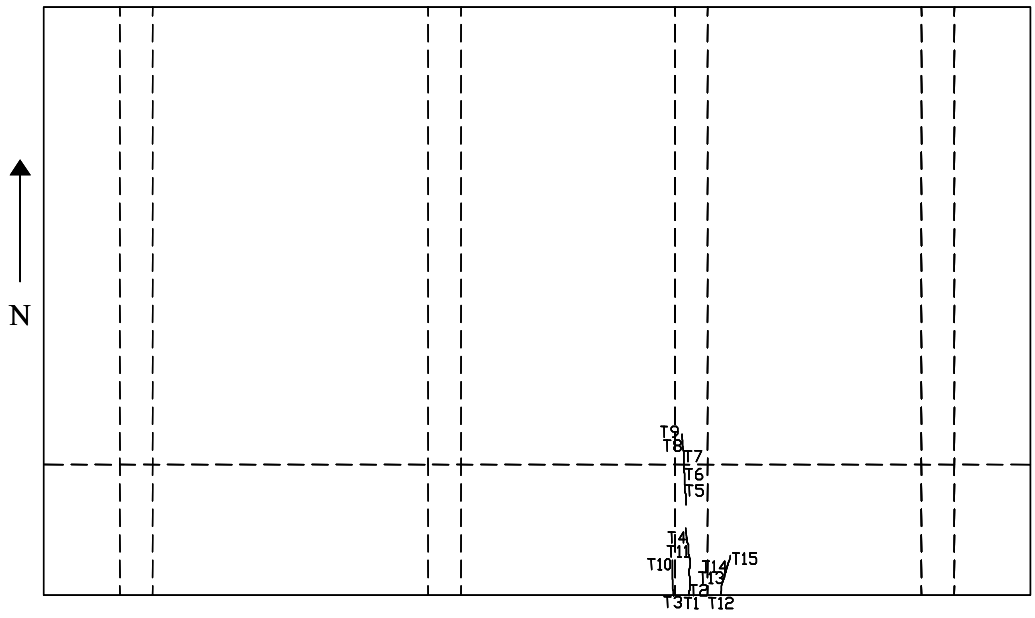

(ii)2.9xHS-25 load step
**Reference (iv) for crack widths and lengths*

Figure 5-13: Crack maps for the top of the bridge deck

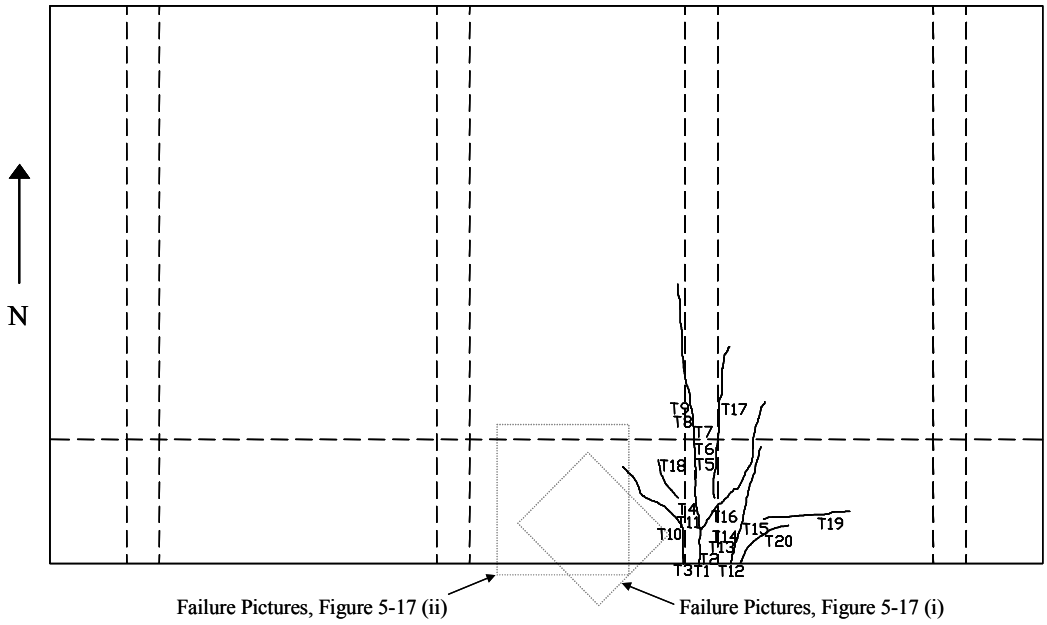

(iii)6xHS-25 load step (failure)

Load=2.11XHS-25			Load=2.92XHS-25			Load=6XHS-25		
Crack Name	Width (in)	Length (in)	Crack Name	Width (in)	Length (in)	Crack Name	Width (in)	Length (in)
T1-T2	H	12	T1-T2-T4-T11	H	24	T1-T2-T4-T11-T16	0.014	35 (55)
			T3-T10	H	13	T3-T10	0.016	43
			T5-T6-T7-T8-T9	0.002	25	T5-T6-T7-T8-T9	0.012	84
			T12-T13-T14-T15	H	17	T12-T13-T14-T15	0.018	46
						T17	0.006	56
						T18	0.003	15
						T19	H	28
						T20	H	25

(iv)Key of widths and lengths for i, ii and iii

*H = hairline crack, parenthesis measurement refers to the branch named B16

Figure 5-13, cont'd: Crack map and key for the top of the bridge deck

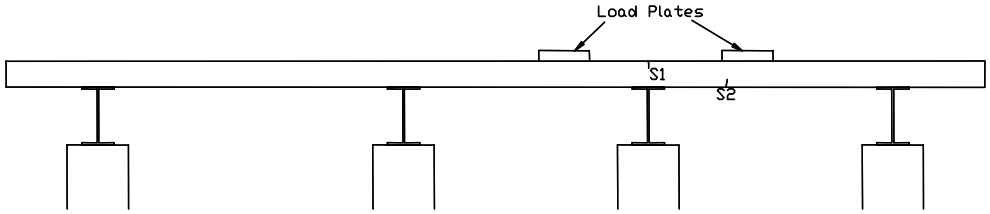

(i)2.1xHS-25 applied load (first cracking)

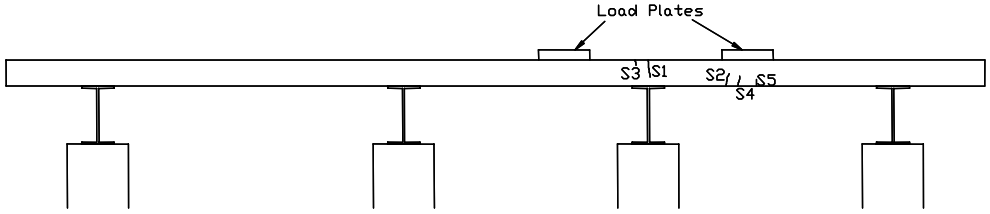

(ii)2.9xHS-25 load step

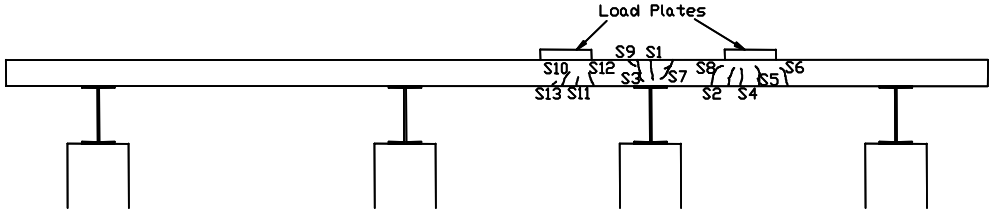

(iii)6xHS-25 load step (failure)

Load=2.1xHS-25			Load=2.9xHS-25			Load=6xHS-25		
Crack Name	Width (in)	Length (in)	Crack Name	Width (in)	Length (in)	Crack Name	Width (in)	Length (in)
S1	0.002	3	S1	0.002	6.5	S1	0.008	8
S2	0.003	3	S2	0.004	5	S2	0.012	7.5
			S3	H	2.5	S3	0.01	9
			S4	0.002	4	S4	0.01	7.5
			S5	H	2.5	S5	0.009	8
						S6	0.007	8
						S7	0.01	9
						S8	0.13	10
						S9	0.004	4
						S10	0.005	6
						S11	0.005	3.5
						S12	0.002	5
						S13	H	2

(iv)Key of crack widths and lengths of for i, ii and iii

*H = hairline crack

Figure 5-14: Crack map and key for the side of the bridge deck

B1-B2-B3-B6-B14, extending slightly more than half the longitudinal dimension of the bridge deck.

Figure 5-13 shows the crack maps for the top surface of the bridge deck when it was loaded in the location to maximize negative moment. The initial crack at the top of the deck formed approximately at the centerline of the girder. The formation of this crack was also shown by the strain profiles in Figure 5-24, which display large strains created in the three bars near the edge of the deck at the 1.75xHS-25 load step. The cracks induced in the top of the bridge deck initially followed the longitudinal dimension of the girder, however, by the loading to failure, they had branched into the deck spans on either side of the girder.

The crack maps for the side of the deck show cracking occurring at both the critical moment locations as well as the failure location (Figure 5-14). The crack map for the 2.9xHS-25 load step (Figure 5-14, ii) shows that the loading to maximize negative moment creates similar deterioration in the positive and negative moment locations of the bridge deck. At the 6xHS-25 load step, the crack widths under the load plate in the exterior span were larger than those in the interior span, however, the interior span tire punched first.

5.2.2.3 Failure pictures

Failure of the test area was due to punching at the tire closest to the edge in the interior span of the bridge deck. After failure occurred, pictures of the failure surface were taken (Figure 5-15 through Figure 5-17). The bottom failure involved a large area of the bridge deck (Figure 5-15). The inside edge of the failure crack ran parallel to the deck edge, about 2 ½ feet into the deck, except at the west girder where it curved toward the edge of the deck.

(i) East side of interior span, facing south

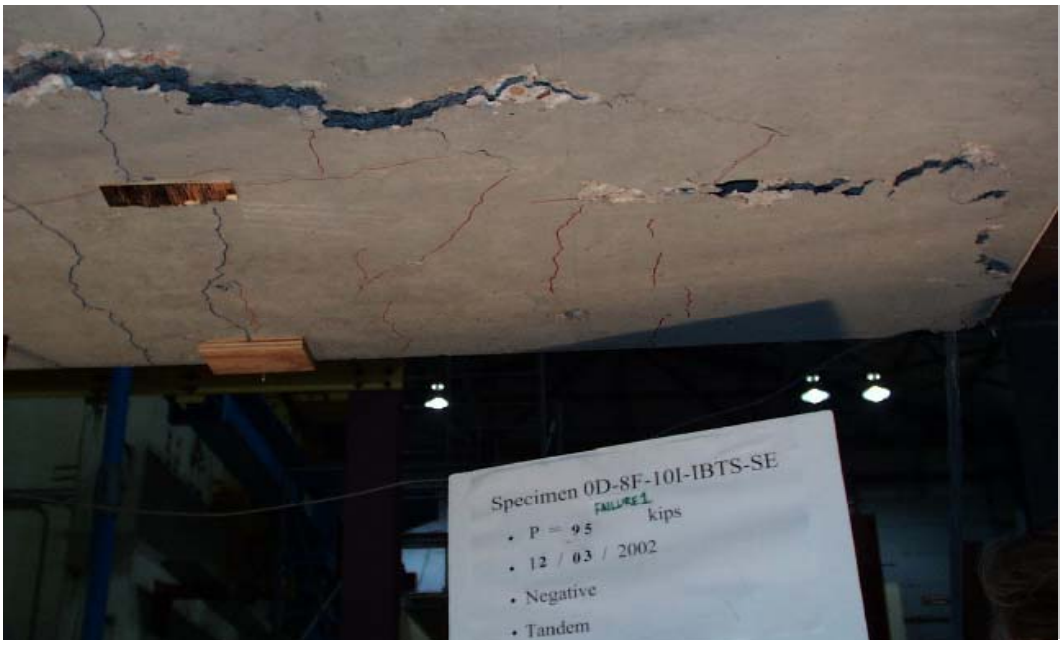

(ii) West side of interior span, facing south

Figure 5-15: Interior span failure at bottom of deck

Figure 5-16: Interior span failure at side of deck, interior span, facing north

Figure 5-16 shows the failure surface on the side of the deck. Major failure cracks extended from the edges of the load plate to the girder flanges. The failure surface on each side of the load plate formed at different angles in order to reach the girders. The major failure crack on the west side of the load plate branched near the top of the deck, resulting in two main cracks.

(i) Facing southwest

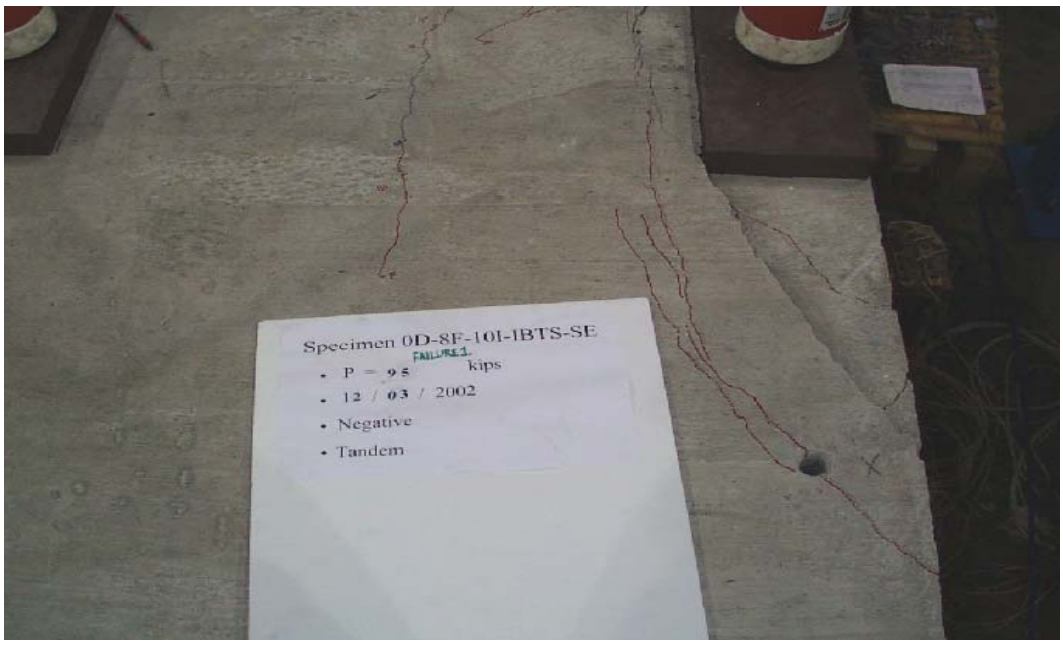

(ii) Facing east

Figure 5-17: Interior span failure at top of deck

5.2.2.4 Load vs. strain response

Load versus strain plots were prepared for all loading configurations at all load steps. Again, a representative selection of strain gauges in tension (bottom mat of rebar at the positive moment location and the top mat at the negative moment location) have been included in Figure 5-18 through Figure 5-21.

5.2.2.4.1 HS-25 load step

Figure 5-18 shows load versus strain plots for the three loading configurations at the HS-25 load step. The strain gauges located in the bottom mat of steel at the positive moment location (Figure 5-18, i, iii and v) all behaved linearly and remained elastic during the HS-25 load application. The maximum strain measured at the positive moment section was 80με (4% of yield strain of the steel), caused by the tandem loading configuration. The truck axle-front loading configuration created a maximum strain of roughly 66% of the maximum tensile strain caused by the tandem loading at the positive location.

The largest strain reached at the negative moment section was 87με (4% of yield strain of the steel), due to the truck axle-front loading configuration (Figure 5-18, iv). The truck axle-back loading configuration (Figure 5-18, vi) resulted in the gauge farthest into the thickened edge being strained more than the other gauges, however, all strains induced by the truck axle-back loading configuration were small.

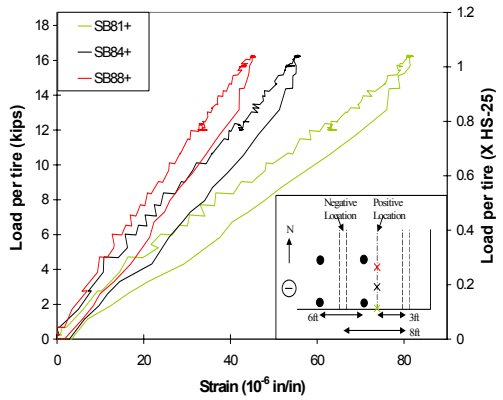

(i) Tandem

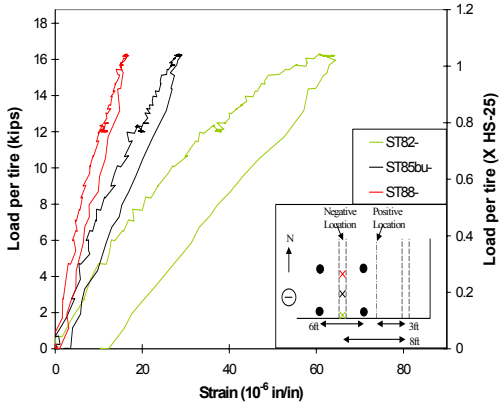

(ii) Tandem

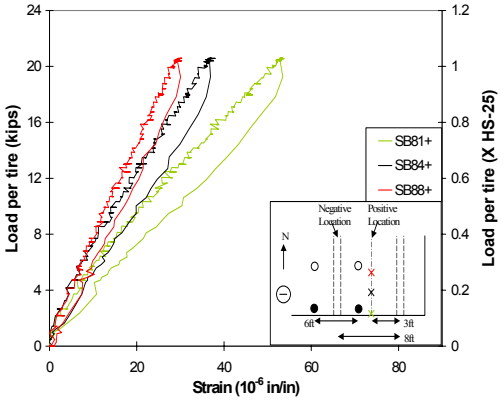

(iii) Truck axle-front

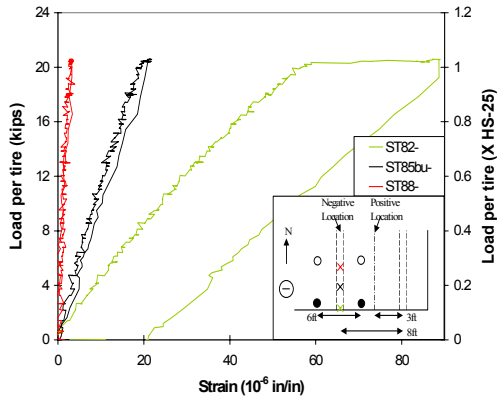

(iv) Truck axle-front

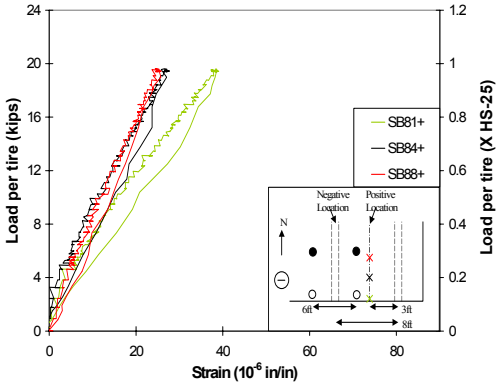

(v) Truck axle-back

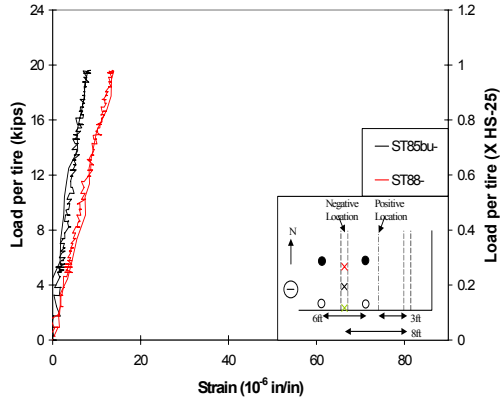

(vi) Truck axle-back

Figure 5-18: Load vs. strain, HS-25 load step, negative moment loading, southeast test area; (i), (iii) and (v): bottom mat at positive location; (ii), (iv) and (vi): top mat at negative location

All of the load versus strain plots for the HS-25 load step show gradually decreasing strain readings from the edge gauge into the section, except the truck axle-back loading configuration at the negative moment section (Figure 5-18, vi). The strains caused by the applied loads were well below yield strain of the reinforcing steel, with a maximum strain of 90με (4% of yield strain of the steel). The residual strains measured at the negative moment section were insignificant. In short, the behavior of the IBTS detail in negative bending at HS-25 loading can be considered elastic. Reinforcing bar strains measured at this load level were very low and the slab end detail remained undamaged during the load tests. Naturally, at the HS-20 load level the strains were even smaller.

5.2.2.4.2 1.2xHS-25 load step

In Figure 5-19, the load versus strain plots for the 1.2xHS-25 load step begin at the origin, since only small residual strains, if any, were created in the reinforcing steel at the HS-25 loading. The general shape of the plots for the 1.2xHS-25 load step were similar to the HS-25 load step. The magnitude of the loads and strains increased proportionally. The strain gauges located in the bottom mat of reinforcing steel at the positive moment location (Figure 5-19, i, iii and v) indicate essentially linear reloading behavior. The 20% increase in loading magnitude increased the strain readings roughly the same amount.

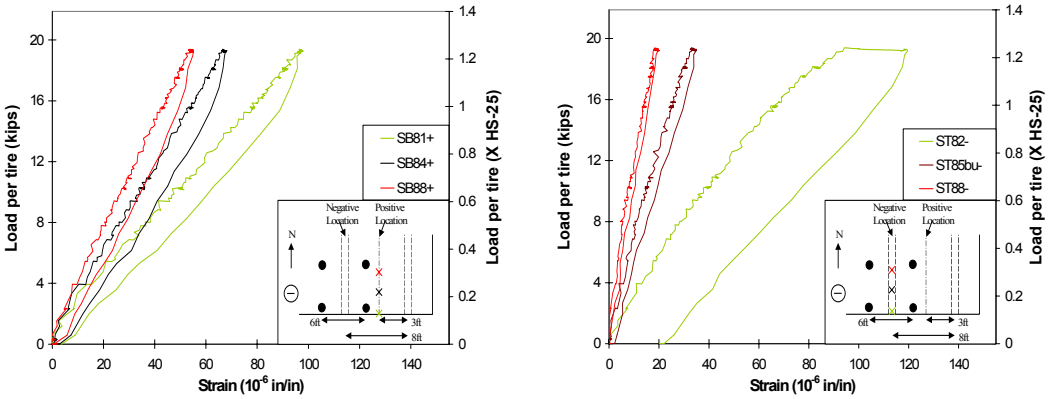

(i) Tandem

(ii) Tandem

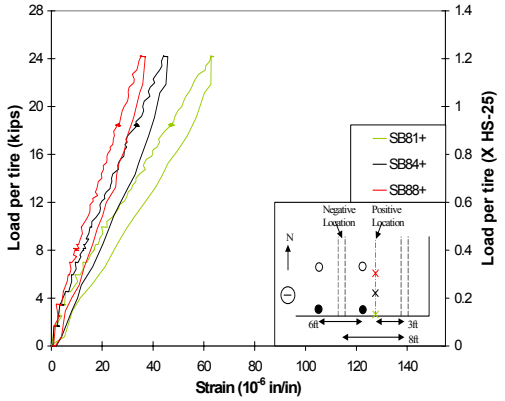

(iii) Truck axle-front

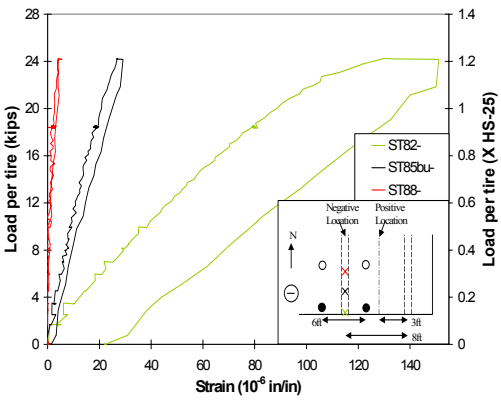

(iv) Truck axle-front

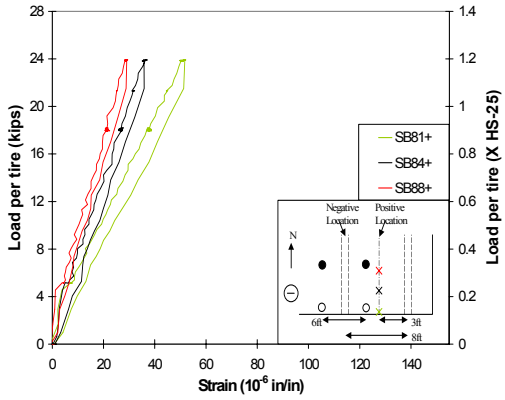

(v) Truck axle-back

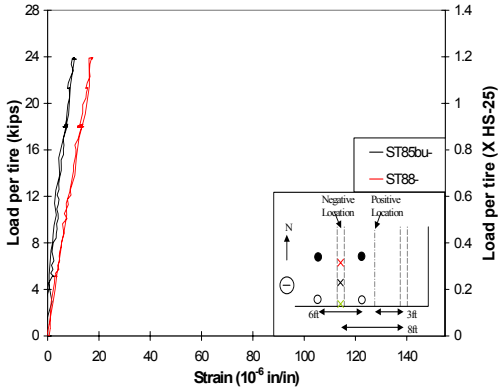

(vi) Truck axle-back

Figure 5-19: Load vs. strain, 1.2xHS-25 load step, negative moment loading, southeast test area; (i), (iii) and (v): bottom mat at positive location; (ii), (iv) and (vi): top mat at negative location

The gauges in the top mat of steel at the negative moment location (Figure 5-19, ii, iv, and vi) showed some non-linearity for the tandem and truck axle-front loading configurations. At this location, the strains increased more than 50% compared to the 20% increase in load magnitude. However, the magnitude of the strains remained reasonably small in comparison to the yield strain of reinforcing bars. It is important to appreciate that most of the "nonlinear" increases in strain readings occurred when the tests were stopped to measure crack widths and lengths. Loads applied in the truck axle-back loading configuration again created small strains.

The response of the IBTS detail to the 20% overload test was elastic. The largest strain induced by this loading was 150με, about 7% of yield strain of the rebars, caused by the truck axle-front loading configuration. As in the HS-25 load step, the strain magnitude decreased from the edge of the deck into the section, except when loaded by the truck axle-back loading configuration.

5.2.2.4.3 1.75xHS-25 load step

Figure 5-20 contains plots of load versus strain for an applied loading of 1.75xHS-25. The gauges on the bottom mat of steel at the positive moment section (i, iii and v) showed linear behavior throughout the load test. The maximum tensile strain reading from the SB81+ gauge was 124με, caused by the tandem loading configuration.

The tandem and truck axle-front loading configurations strained the reinforcing bars close to the edge at the negative moment section up to 348με and 380με, respectively (Figure 5-20, ii and iv). In addition, the load versus strain plot for the tandem loading configuration shows a noticeable slope change at about 19kips (1.2xHS-25). This change in stiffness indicates cracking in the vicinity of the gauge.

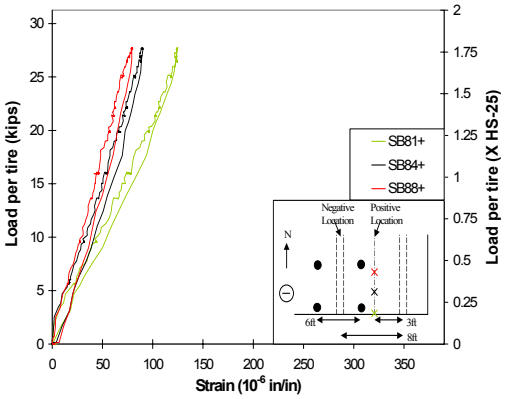

(i) Tandem

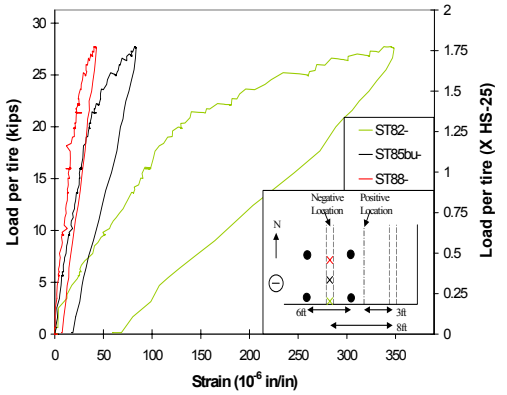

(ii) Tandem

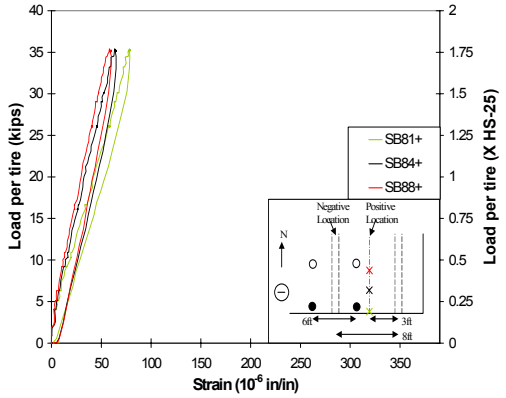

(iii) Truck axle-front

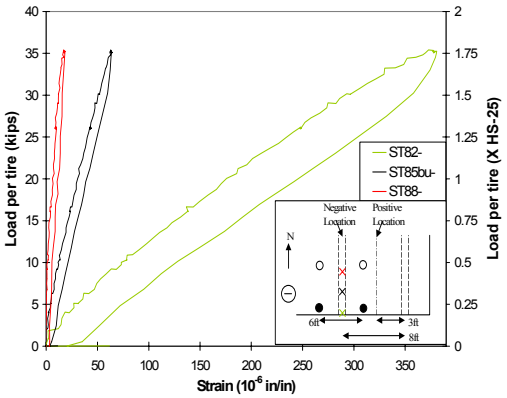

(iv) Truck axle-front

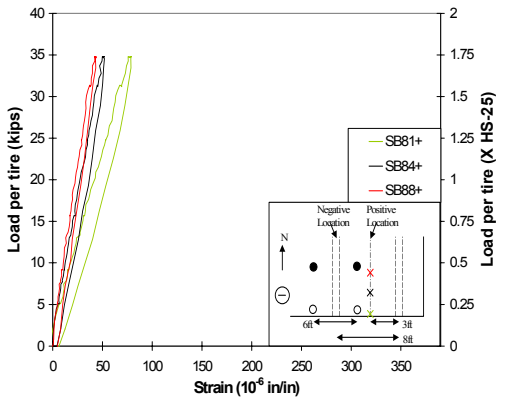

(v) Truck axle-back

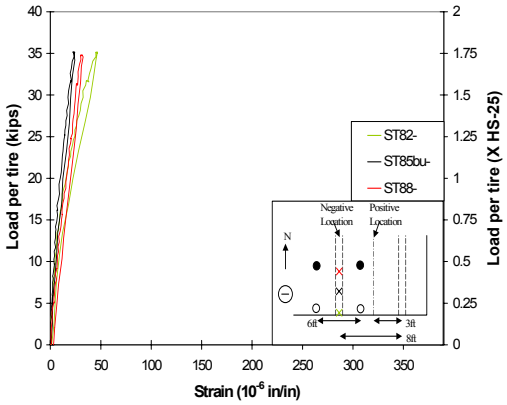

(vi) Truck axle-back

Figure 5-20: Load vs. strain, 1.75xHS-25 load step, negative moment loading, southeast test area; (i), (iii) and (v): bottom mat at positive location; (ii), (iv) and (vi): top mat at negative location

The truck axle-front loading configuration (Figure 5-20, iv) caused a higher strain in the ST82- gauge than the tandem configuration. However, the truck axle-front vehicle did not induce further cracking as the plot does not show a sudden change in stiffness. This plot shows the edge bars were strained significantly whereas the interior bars were very lightly strained due to the fact that the large axle load was located at the edge of the bridge deck. The truck axle-back loading configuration produced very small strains in relation to the other loading arrangements, especially at the negative bending moment location (Figure 5-20, vi).

The load versus strain plots for this load step show small residual strains as well as initiation of cracking at the negative moment section. The strains at the positive location were small compared to the negative location since the load was applied to maximize negative moment. Overall, the section appears to be relatively undamaged at the 1.75xHS-25 load level.

5.2.2.4.4 Loading to failure

Figure 5-21 (i) illustrates the strain history of the SB81+ strain gauge, the gauge closest to the edge of the bridge deck, located in the bottom mat of reinforcing steel at the positive moment section. The plot includes residual strains caused by inelastic loading cycles during previous load tests. The residual strains induced by the HS-25, 1.2xHS-25, and 1.75xHS-25 load steps were very small, and therefore, were not included in the plots in Figure 5-21.

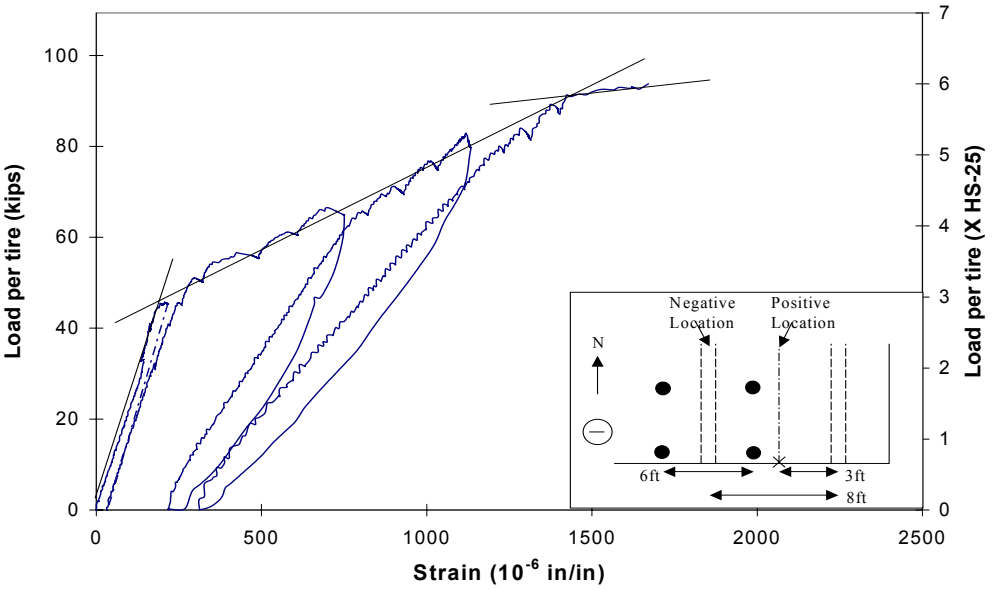

(i)SB81+ strain gauge, tandem loading configuration

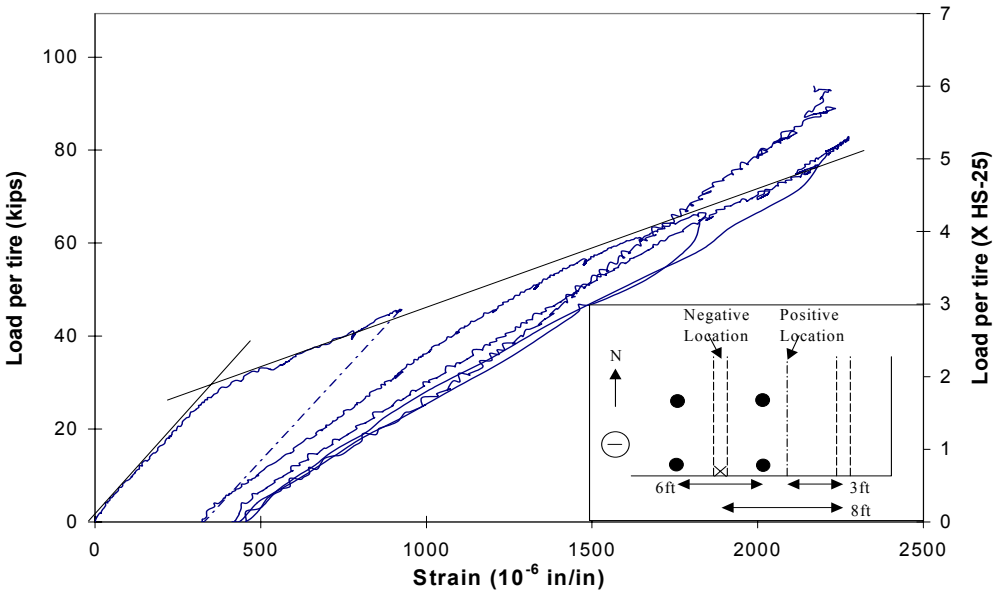

(ii)ST82- strain gauge, tandem loading configuration

Figure 5-21: Load vs. strain, loading to failure, negative moment loading, southeast test area

The maximum strain in the SB81+ gauge was 1670με, approximately 81% of yield strain in the steel, at failure of the test area. Based on the strain readings, the reinforcing steel was close to, but not exactly at the yield point when the specimen failed. This is reasonable since the bridge deck failed due to a punching failure, not a flexural failure. The stiffness displayed by the SB81+ strain gauge gradually reduced as the loading cycles became larger.

As in the load versus deflection plot for loading to failure (Figure 5-11), at the envelope of the load versus strain plots, three different slopes can be observed by fitting lines as shown in Figure 5-21 (i). The first stiffness change occurred at a load of approximately 45kips per tire (2.9xHS-25) and indicated substantial cracking of the slab end detail. The other abrupt stiffness change occurred just prior to failure, at a load of approximately 91kips per tire (5.8xHS-25), when the slope reduced almost to zero indicating yielding of the flexural reinforcement. Soon afterwards, a punching shear failure occurred at an ultimate load of 94kips, six times the HS-25 tandem design loading.

Figure 5-21 (ii) shows the load versus strain plot for the ST82- gauge, a critical strain gauge at the negative moment section. The plot shows a change in stiffness at a load of approximately 30kips (2xHS-25), due to initiation of cracking. This matches a slight stiffness change shown on the initial failure loading cycle plot for the SB81+ strain gauge (Figure 5-21, i) at a load of 31kips. The crack maps in section 5.2.2.2 identify first visible cracking occurring at an applied load of 2.1xHS-25, which substantiates the stiffness change visible in the load versus strain plots for loading to failure. The stiffness displayed by the ST82- strain gauge at large failure loading cycles remained relatively constant to a strain of 1300με.

Beyond 1300με in the ST82- strain gauge, the experimental results indicated some minor increase in stiffness. However, the test section cannot

stiffen under increasing load; therefore, the strain gauge readings were verified by plotting the load versus strain results for other strain gauges at this location. The other gauges verified the occurrence of this slight amount of stiffening. The strain gauges in this location were situated over the centerline of the girder; however, the location of maximum strain was at the edge of the beam flanges based on recorded crack widths. The development length of the reinforcing steel (#5 rebar) in the section is 14.5inches based on ACI 318-02, section 12.2.3. Therefore, in the distance from the edge of the girder flange to its centerline (6.4in), the strain could change by as much as 44%. Since the measured strains were large in relation to yield strain at the centerline of the girder, near the edge of the flanges the rebar was most likely yielding when this apparent stiffening took place. The girder flanges together with the shear studs provide rotational restraint to the bridge deck, creating a region that is controlled by complicated mechanics. The ST82- gauge appears to reach the reinforcing steel's yield strain of 2070με at an applied load of 82kips; however, there is no distinct effect on the section's stiffness. In short, the complicated nature of the mechanics in the joint region may be the cause of this otherwise insignificant stiffening. In addition, the strain readings from the centerline of the girder are not greater than those measured over the flange, however, they are useful in showing trends and overall ideas about strain levels.

The bridge deck failed at the edge tire on the interior span at a load of 93.75kips per tire (6xHS-25 or 7.5xHS-20). After failure, the punched tire continued to carry an applied load of 45kips per tire, approximately 300% of the design load. Then, the two tires located in the bridge deck's exterior span were loaded in order to determine the capacity for this section. Under this loading, a punching failure occurred at the edge tire at an applied load of 90.47kips (5.8xHS-25 or 7.25xHS-20) (Test No.17, Table 5-1)

5.2.2.5 Strain profiles

Strain profiles were created for all load steps applied at the location to maximize negative moment. As stated in section 5.2.1.3, the strain profiles were used to compare the effect of the loading configurations on the strain distribution across the edge detail.

5.2.2.5.1 HS-25 load step

The strain magnitudes created by the tandem loading configuration at the HS-25 load step, applied in the location to maximize negative moment, are more critical for the maximum positive moment section than the negative location (Figure 5-22, i and ii). The largest strain of 90με (SB85bu+) was caused by the tandem loading configuration and occurred at the positive moment section. However, the strains measured in the HS-25 load step were small at both locations. With increased applied load, larger strains were measured at the negative moment section.

In addition, the strain gauges at the negative moment section are located at the centerline of the girder. As discussed previously, the maximum strain over the girder was at the edge of the flange. The maximum strain at the edge of the flange could be 44% higher than the readings obtained from the strain gauges located at the centerline of the girder, based on the development length of the reinforcing steel.

The truck axle-front loading configuration imposed larger strains at the negative moment section (Figure 5-22, iii and iv). These two figures show a different variation in the strain across the section. The profile for the positive moment section (Figure 5-22, iii) is close to uniform across the thickened edge whereas the strain profile at the negative moment section (Figure 5-22, iv) shows a significant decline in strain readings from the edge of bridge deck to the interior.

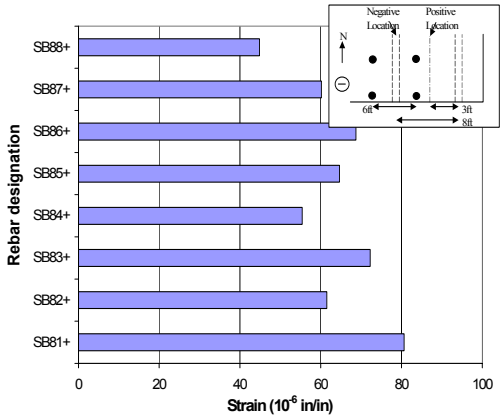

(i) Tandem

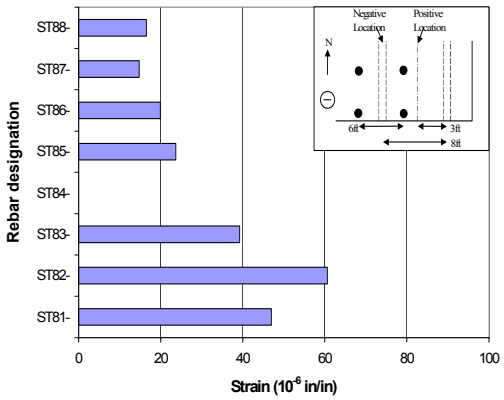

(ii) Tandem

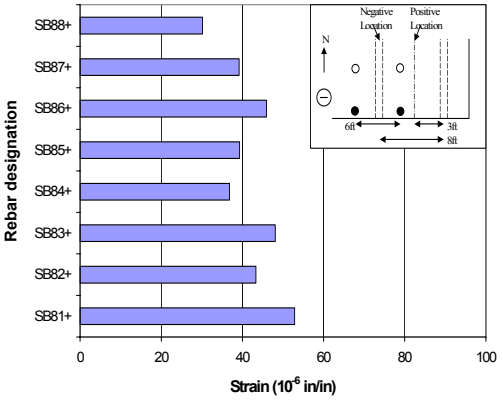

(iii) Truck axle-front

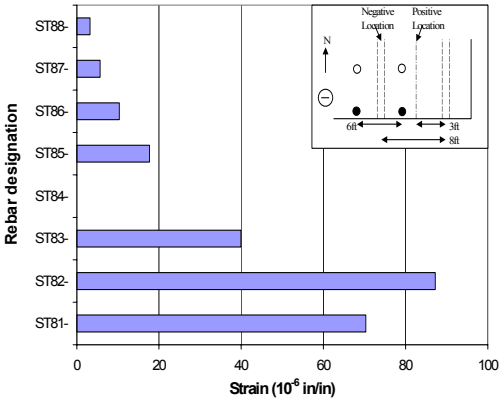

(iv) Truck axle-front

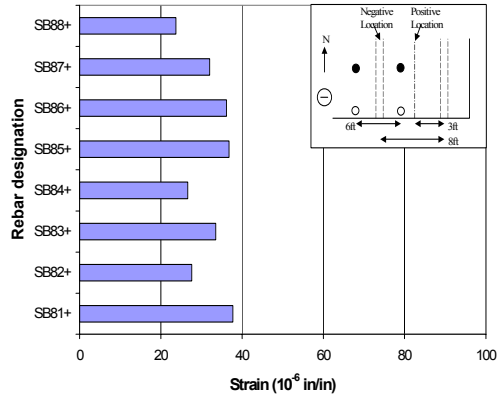

(v) Truck axle-back

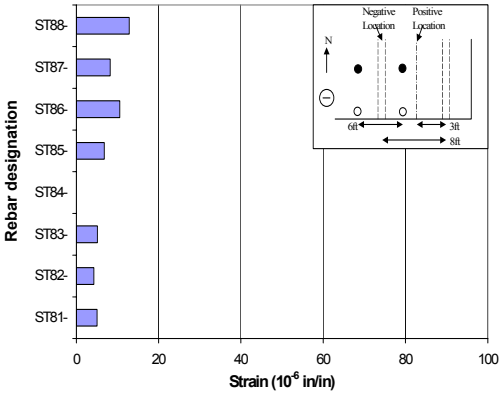

(vi) Truck axle-back

Figure 5-22: Strain profiles, HS-25 load step, negative moment loading, southeast test area; (i), (iii) and (v): bottom mat at positive location; (ii), (iv) and (vi): top mat at negative location

This behavior is also evident in the tandem loading configuration strain profiles. The strains induced by the truck axle-back loading configuration (Figure 5-22, v) are the smallest of the three loading configurations.

5.2.2.5.2 1.2xHS-25 load step

The maximum strain induced by the tandem loading configuration again occurred at the positive moment section (Figure 5-23, i and ii). However, the strain readings from the two sections were much closer in magnitude than at the HS-25 load step.

The maximum strain at this load step was caused by the truck axle-front loading configuration in the SB81bu+ strain gauge (Figure 5-23, iv). The strain magnitudes in the edge bars at the maximum positive moment section (Figure 5-23, iii) are now much smaller in magnitude than in the negative location. The truck axle-back loading configuration again induced insignificant strains at the maximum negative moment section (Figure 5-23, vi) and larger strains at the positive location (Figure 5-23, v).

5.2.2.5.3 1.75xHS-25 load step

Figure 5-24 shows the strain profiles obtained at the 75% overload level. At this load step, strains measured on top of the girder are higher than those measured at the positive moment section. The largest strain of 370με (18% of yield strain of the steel) was caused by the truck axle-front loading configuration in the ST82- gauge; however, the average of the strain readings in the thickened edge are larger for the tandem loading configuration. The truck axle-back loading configuration again resulted in insignificant strains at both the positive and negative moment sections (Figure 5-24, v and vi).

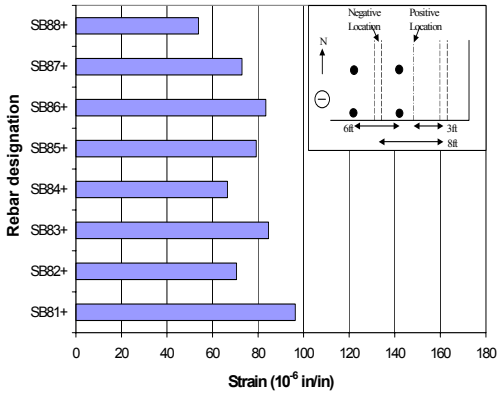

(i) Tandem

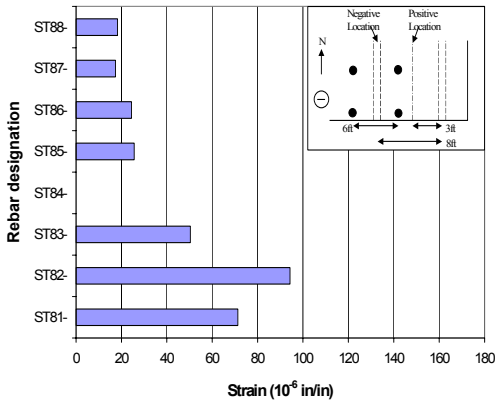

(ii) Tandem

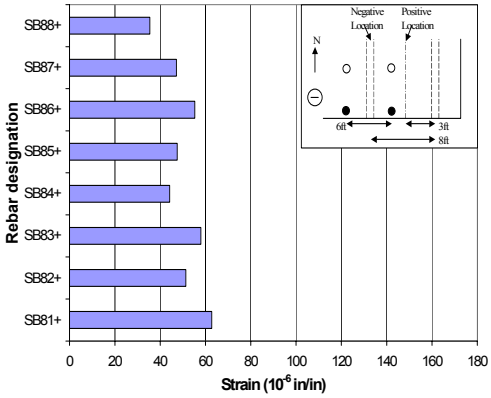

(iii) Truck axle-front

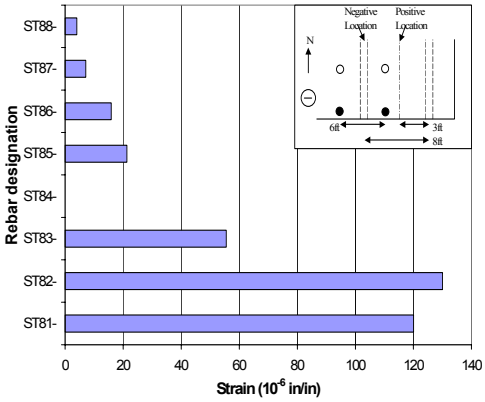

(iv) Truck axle-front

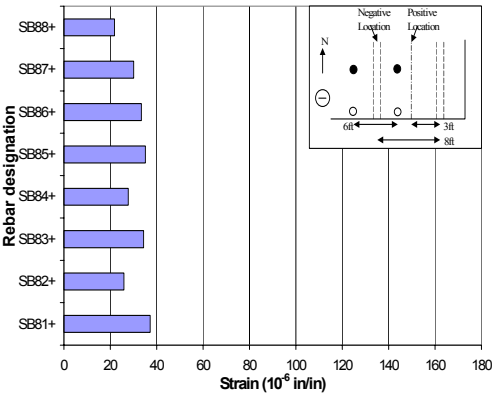

(v) Truck axle-back

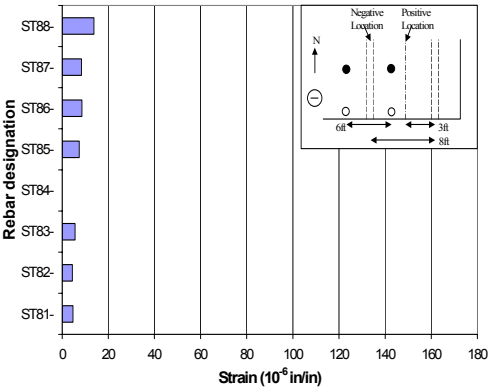

(vi) Truck axle-back

Figure 5-23: Strain profiles, 1.2xHS-25 load step, negative moment loading, southeast test area; (i), (iii) and (v): bottom mat at positive location; (ii), (iv) and (vi): top mat at negative location

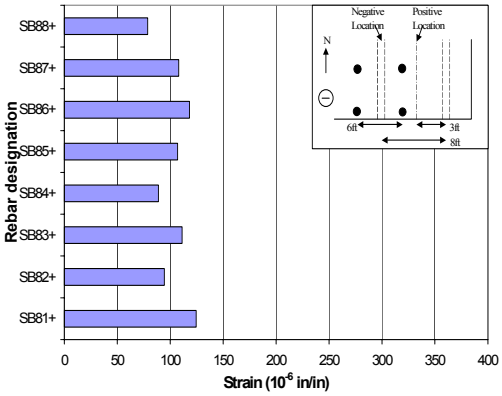

(i) Tandem

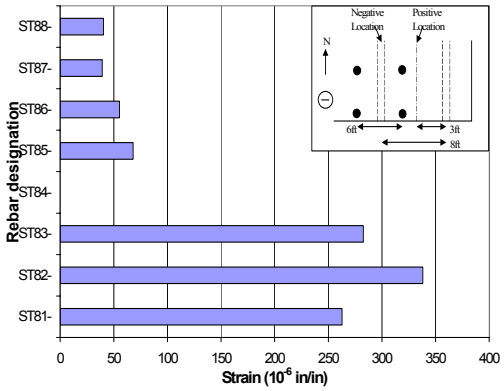

(ii) Tandem

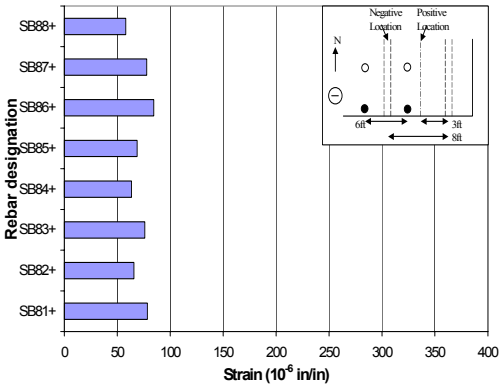

(iii) Truck axle-front

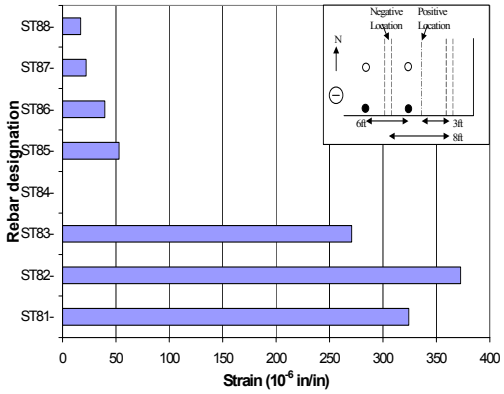

(iv) Truck axle-front

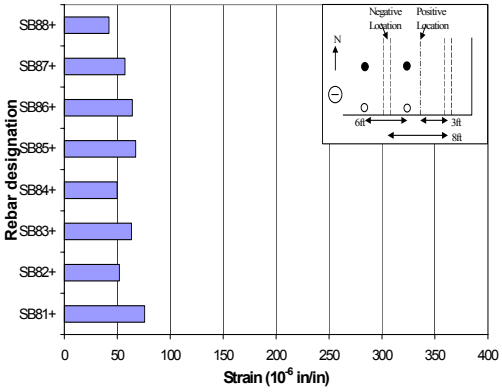

(v) Truck axle-back

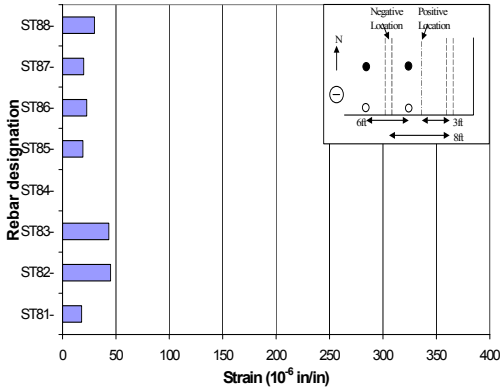

(vi) Truck axle-back

Figure 5-24: Strain profiles, 1.75xHS-25 load step, negative moment loading, southeast test area; (i), (iii) and (v): bottom mat at positive location; (ii), (iv) and (vi): top mat at negative location

For the tandem and truck axle-front loading configurations (Figure 5-24, ii and iv), the strains in the reinforcing steel near the edge of the bridge deck (bars 1, 2 and 3) substantially increased at this load step. In addition, the strain in these three bars was much greater than the strain in the other bars in the thickened edge. Considering the strain level of the reinforcing steel (250-350με), the increased strain measurements in the three edge bars indicate crack formation in the vicinity of these bars. This can be verified by the crack maps in section 5.2.2.2 which show a 12-inch long crack forming at this location soon after the 1.75xHS-25 load step, at 2.11xHS-25 (Figure 5-13, i).

5.2.2.5.4 Loading to failure

Figure 5-25 shows strain profiles for loading to failure. The bridge deck was loaded to failure in the tandem loading configuration as it created the largest cumulative strains across the thickened edge. The strain profiles for the loading to failure (6xHS-25) (Figure 5-25, vii and viii) are from strain readings obtained just prior to the punching shear failure.

At the 2.92xHS-25 load step, the strains in the three bars closest to the edge at the negative moment section (Figure 5-25, ii) were significantly larger than the strains in the rest of the reinforcing steel in the thickened edge. However, tracking the strain profiles for the maximum negative moment section at increasing load steps (Figure 5-25, iv, vi and viii) shows the strains across the IBTS detail becoming more uniform. This is due to cracks propagating into the deck longitudinally in the vicinity of the gauged negative moment section.

At the 2.92xHS-25 load step, the strains across the thickened edge at the positive moment section are significantly lower than those at the negative moment section (Figure 5-25, i and ii). However, just prior to failure of the test area, strains across the IBTS detail are comparable at these two sections. In fact, the

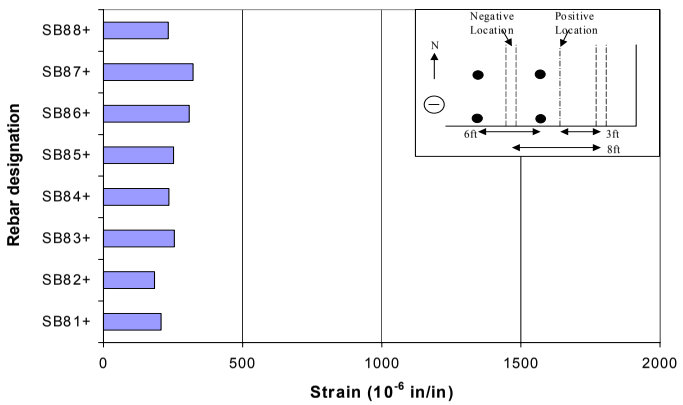

(i)2.92xHS-25, bottom mat, positive location

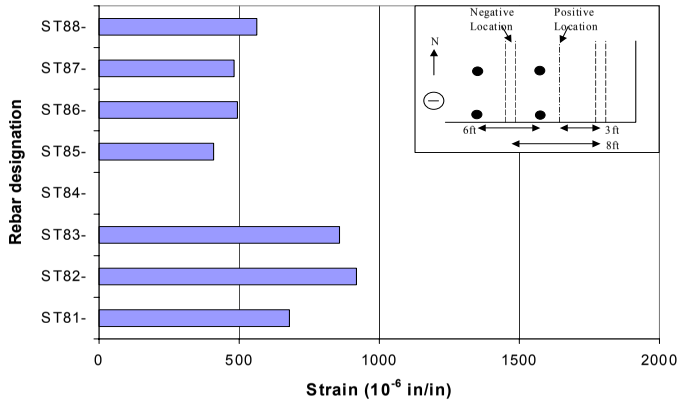

(ii)2.92xHS-25, top mat, negative location

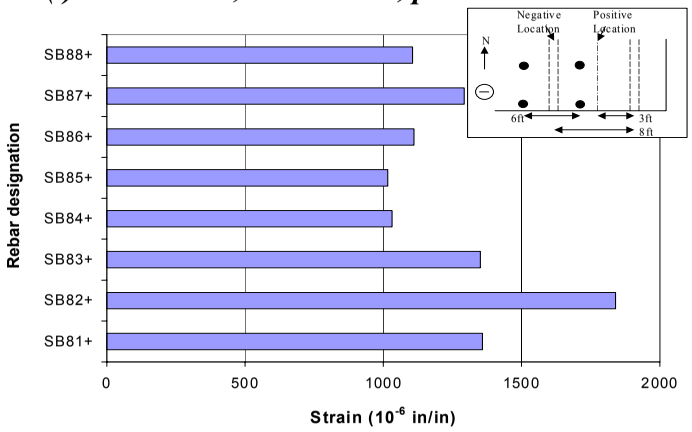

(iii)6xHS-25, bottom mat, positive location

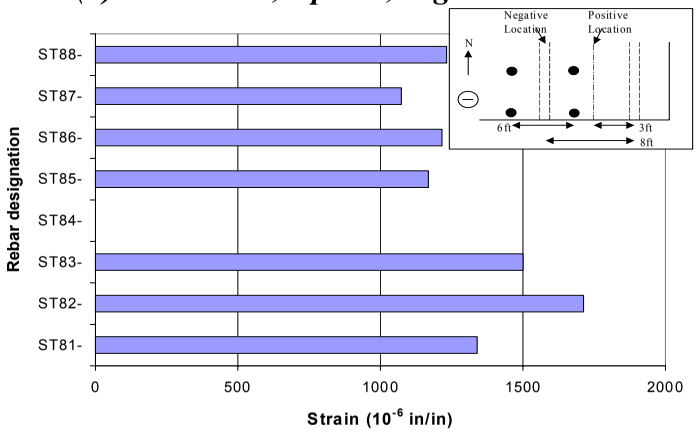

(iv)6xHS-25, top mat, negative location

Figure 5-25: Strain profiles, loading to failure, negative moment loading, southeast test area

largest strain induced at the loading to failure (6xHS-25) was in the SB82+ strain gauge, located in the positive moment section (Figure 5-25, vii). This is likely attributable to redistribution of stresses between the positive and negative moment sections prior to failure.

5.2.2.6 Moment calculations

The strain gauge readings were used to calculate moments induced in the four-foot thickened edge at the applied load steps. At the positive and negative moment sections, the average strain from the top and bottom gauges was used in conjunction with the "plane sections remain plane" principle to establish linear strain profiles through the depth of the sections. Figure 5-26 shows two examples of the constructed linear strain diagram for the tandem loading configuration at the HS-25 load step.

The average strain readings were converted to stresses in the concrete and rebar. The in-plane forces and moments were calculated. Since the shape of the concrete stress diagram is parabolic, a method to convert the diagram to a rectangle was used to simplify the calculation. The compression force in the concrete was calculated by stress block factors α_1 and β_1 (Figure 5-27).

The moment calculations were performed both with and without tension in concrete. The concrete tension force was determined by assuming a triangular stress distribution (Figure 5-27). The concrete tensile strength, σ_{cr}, of 570psi was determined from the split cylinder tests performed on the deck concrete. y_t, the depth of the concrete tension block, was adjusted as cracking stress was reached in the section.

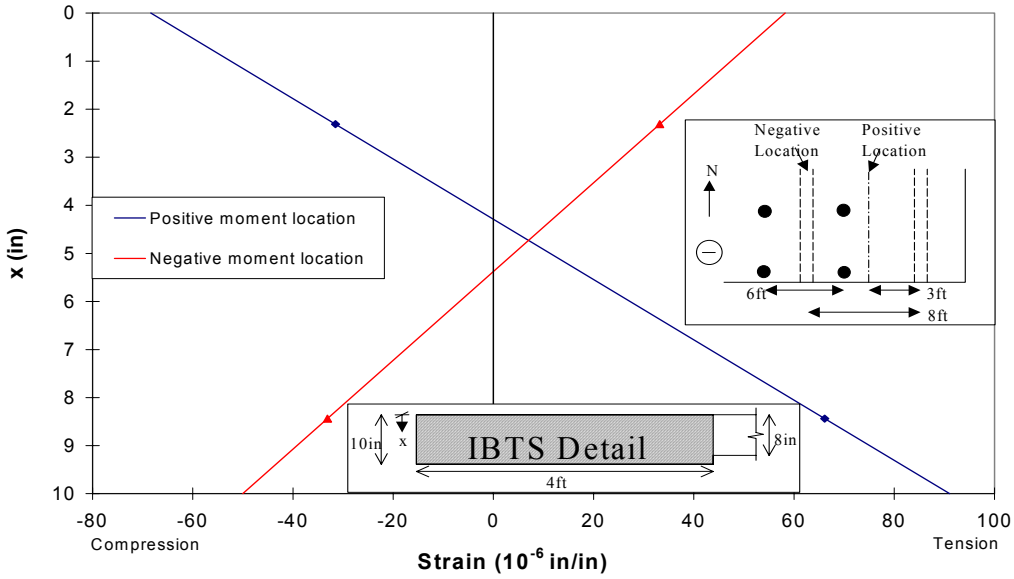

Figure 5-26: Strain diagram, HS-25 load step, tandem loading configuration

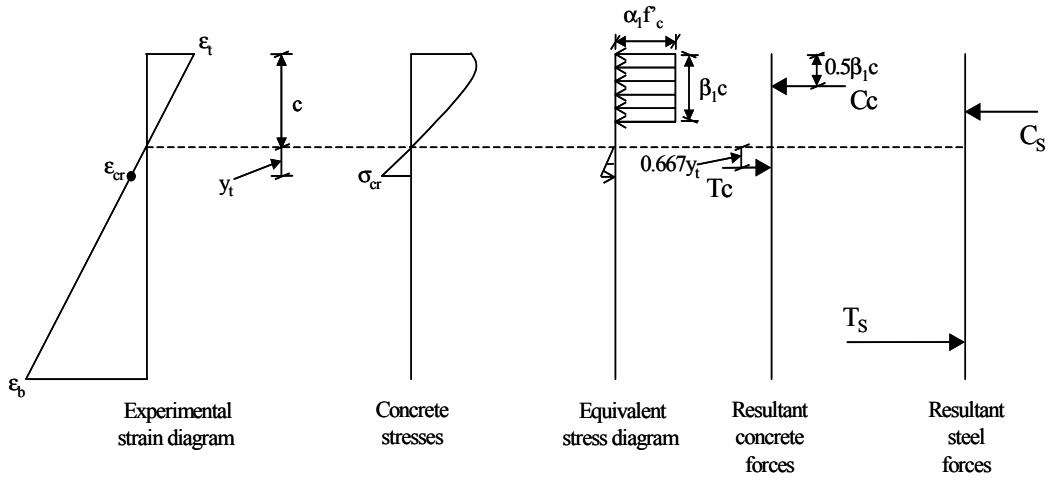

$$E_c = 40000\sqrt{f'_c} + 1000000 \qquad n = 0.8 + \frac{f'_c}{2500} \qquad \varepsilon'_c = \frac{f'_c}{E_c}\frac{n}{n-1}$$

$$\beta_1 = \frac{4 - \dfrac{\varepsilon_t}{\varepsilon'_c}}{6 - \dfrac{2\varepsilon_t}{\varepsilon'_c}} \qquad \alpha_1\beta_1 = \frac{\varepsilon_t}{\varepsilon'_c} - \frac{1}{3}\left(\frac{\varepsilon_t}{\varepsilon'_c}\right)^2$$

Figure 5-27: Internal stresses and resultant forces

Figure 5-28 shows a sample of the spreadsheet calculation used to determine the force and moment in the section. The moments and in-plane forces at the positive and negative moment sections were plotted versus applied load (Figure 5-29 and Figure 5-30). The moment calculations were prepared for the tandem loading configurations only since they typically create the most critical behavior in the bridge deck as well as being the loading configuration used to fail the specimen.

Figure 5-29 (i) shows the moment calculated from the strain gauges at the positive moment section in the deck for all tandem vehicle loadings performed (the 0.8xHS-25 data point is HS-20 loading). When tension in concrete, Tc, is ignored, the relationship of moment to applied load is approximately linear. When Tc is included, for the same applied load, the moment is larger prior to cracking. However, once the extreme tensile fiber cracks, both analyses yield very similar results. By the 2.92xHS-25 load step, tension in concrete does not effect the moment.

At the negative moment section (Figure 5-29, ii), the plot without tension in concrete is very close to linear. The difference caused by Tc is smaller in magnitude than at the positive moment section. The negative section cracks earlier than the positive moment section. The moment created at the two sections was very close when the bridge deck punched.

Moment Calculation from Strain Gauge Data

Negative Tandem HS-25 Loading
10 inch, IBTS detail
8 foot span
4 foot wide strip
Positive moment location

Tire load (k)	15.625

E_s (ksi)	29000
top surface-to-top bar (in)	2.3
top bar-to-bottom bar (in)	6.1
bot. bar to bot. surface (in)	1.6
A_{bar} (in^2)	0.31
f'_c (ksi)	6
E_c (ksi)	4098
n	3.2
e'_c (in/in)	0.0021
b (in)	48
number of bars	8
σ_{CR} (ksi)	0.57

Bottom Bars (Tension)

Rebar Name	Strain from S.G.
SB81+	81
SB82+	61
SB83+	72
SB83bu+	74
SB84+	56
SB85+	66
SB85bu+	90
SB86+	69
SB86bu+	81
SB87+	60
SB87bu+	58
SB88+	45
SB88bu+	45
Average	66

Top Bars (Compression)

Rebar Name	Strain from S.G.
ST81+	-32
ST82+	-28
ST82bu+	-42
ST83+	-42
ST85+	-24
ST86bu+	-28
ST87+	-31
ST88bu+	-26
Average	-32

Concrete stress at bottom bar level (ksi)	0.270964
Concrete stress at top bar level (ksi)	-0.129166
Bottom rebar stress (ksi)	1.917327
Top rebar stress (ksi)	-0.913976

ε_{CR}	0.0001
y_t (in)	5.71
σ_{TEN} (ksi)	0.37

y_{NA}' (in)	1.98
c (in)	4.29
σ_{COMP} (ksi)	-0.28
ε_t	-6.84E-05
ε_t/e'_c	0.03
β_1	0.67
α_1	0.05

T_C (k)	51.1
T_S (k)	4.8
C_S (k)	-2.3
C_C (k)	-39.2

ΣF (k)	14.4
M (k*in)	320.7

* Moment summed about middepth

Figure 5-28: Sample moment calculation spreadsheet

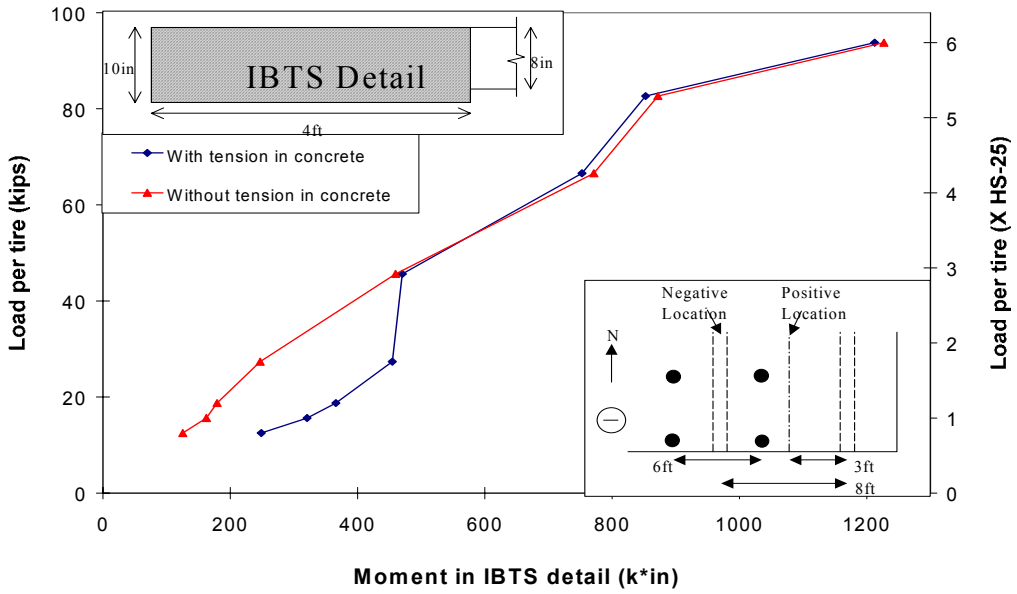

(i)Positive moment section

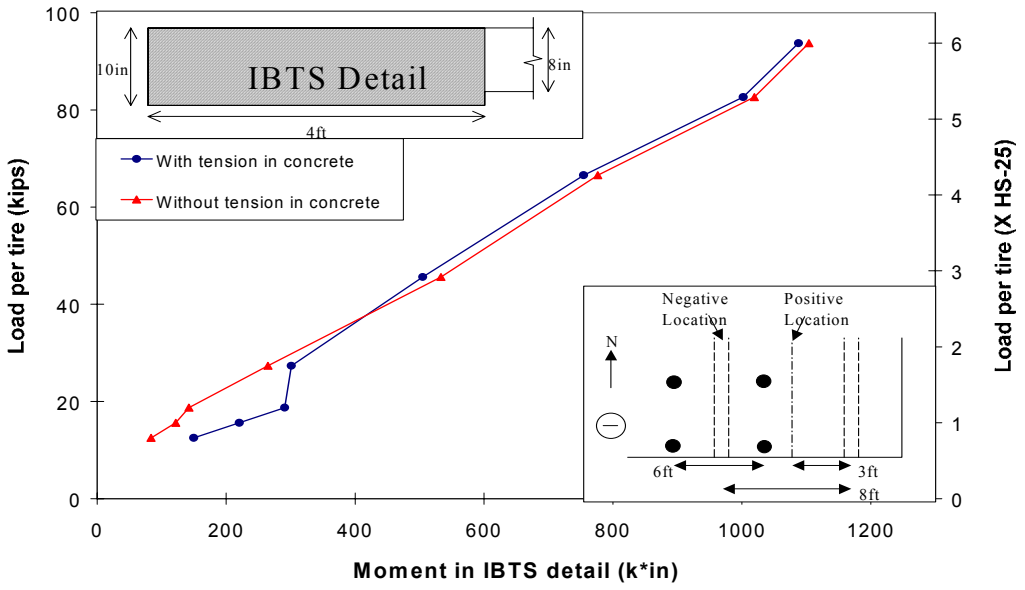

(ii)Negative moment section

Figure 5-29: Moment calculated from strain gauge readings, tandem loading configuration only

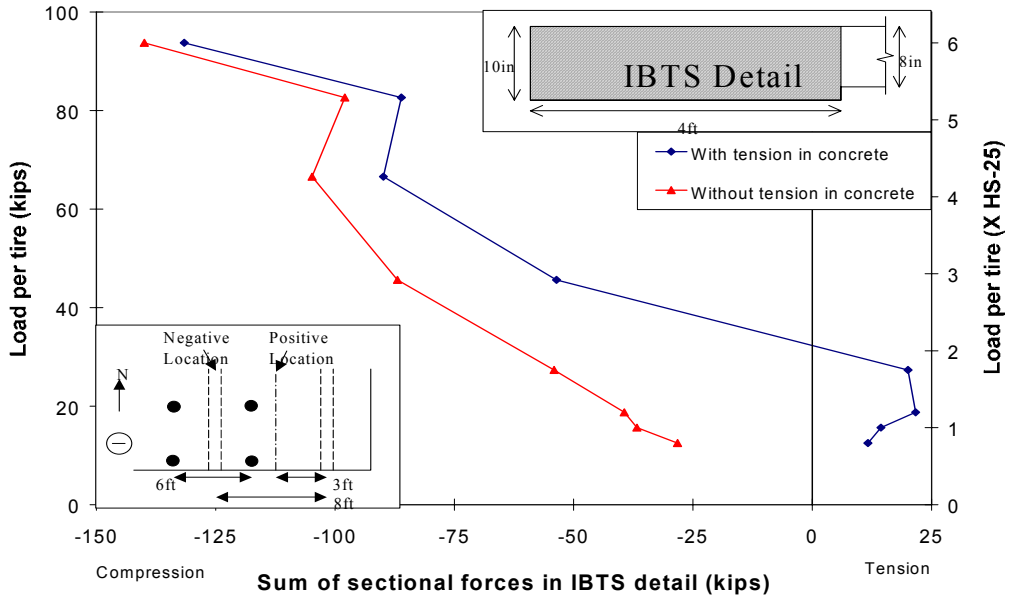

(i)Positive moment section

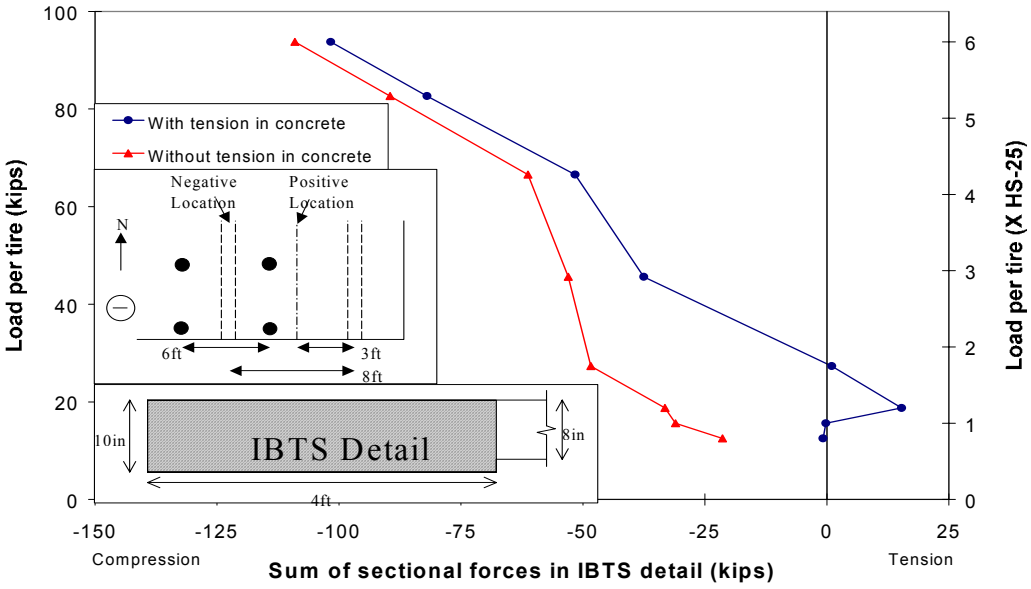

(ii)Negative moment section

Figure 5-30: In-plane force calculated from strain gauge readings, tandem loading configuration only

The calculated in-plane force for the positive section is shown in Figure 5-30 (i). The in-plane force is in tension when Tc is included in the sectional force calculation, prior to cracking in the thickened edge. This is because the deck had a large area of uncracked concrete in tension. However, this tension force is small in relation to the in-plane compression force created at failure of the bridge deck. Once the section cracks, the in-plane force goes into compression. At failure, the maximum in-plane compression is 140kips. This is due to lateral restraint of the bridge deck, caused by arching action and the lateral rigidity of the steel girders. The two plots (with and without Tc) gradually approach each other as the section becomes cracked more extensively, until failure, when there is only nine kips between them.

Figure 5-30 (ii) shows the in-plane force at the negative moment section. The plot including Tc is similar to the in-plane force plot for the positive moment section, initially going into tension, then switching to compression after initial cracking. The two plots again approached each other as load was increased and cracking became more extensive. The maximum in-plane force in the negative moment section is 110kips.

5.2.2.7 Elastic moment comparison

Elastic moment diagrams were created for a three-span continuous beam, using point loads and point supports for the HS-25 and 1.75xHS-25 load steps. These load steps were chosen because the section had not cracked, and therefore, the elastic assumption still held. Two loads were applied to the model, each representing two tires. The moments from the strain gauge readings are plotted for comparison. For the continuous beam analysis, the negative moment at the girder reaches a high value because of the point support. The elastic moment at

the edge of the flange was used across the full width of the flange, as the actual variation of moment over the girder is not known.

The moment from the strain gauges is slightly larger than the elastic analysis for the HS-25 load step at the positive moment section (Figure 5-31, i). This is likely due to the large variability in the strain gauge readings at low strains. At the 1.75xHS-25 load step, the experimentally calculated moment matches the elastic analysis at the positive moment section (Figure 5-31, ii).

The moments from the strain gauges match the elastic analysis very well at the positive moment section. At the girder, however, the experimentally calculated moments are roughly half of the continuous beam analysis moments. This is due to the specific location of the strain gauges, which are at the centerline of the girder. The cast-in-place concrete bridge deck is restrained at the girder by the shear studs and the girder itself, reducing the strains measured at the centerline of the girder. The maximum strains over the girder flange were located at its edge as shown by the crack maps in Figure 5-13.

The #5 rebar used for primary reinforcement in the bridge deck can develop large strains in a very short length. A calculation using ACI 318-02, section 12.2.3 gives a development length of 14.5in for a #5 rebar. Algebraically modifying the development length equation to determine the stress change in 6.4 inches, the distance from the centerline of the girder to the edge of the flange, results in a stress change of 26.3ksi. This change can alter the forces in the tension reinforcement in the IBTS detail by 65kips, which would drastically increase the moments calculated in the section. There is a clear uniformity between the elastic analysis and the experimental results before cracking of the bridge deck.

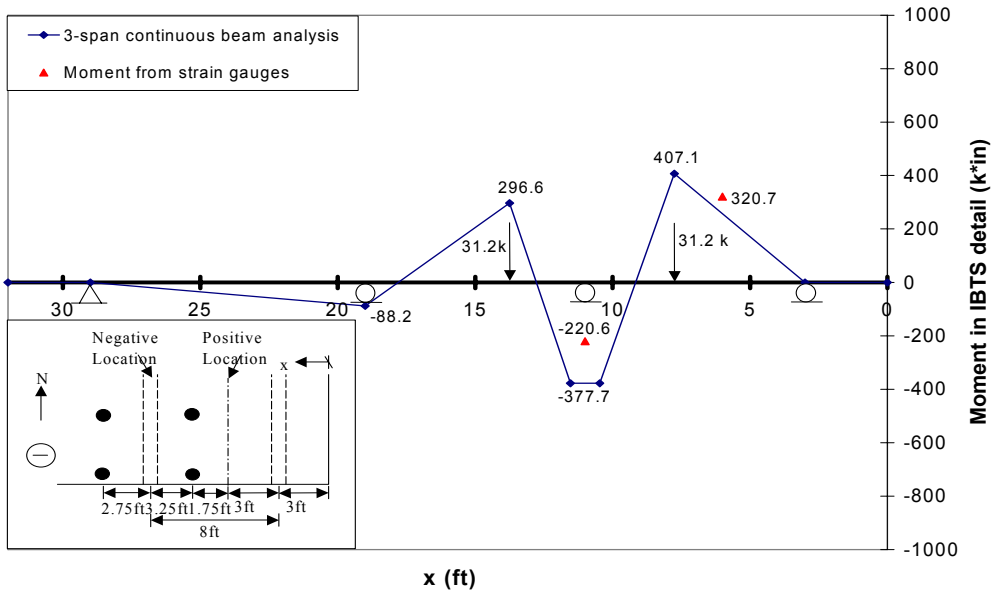

(i) HS-25 load step

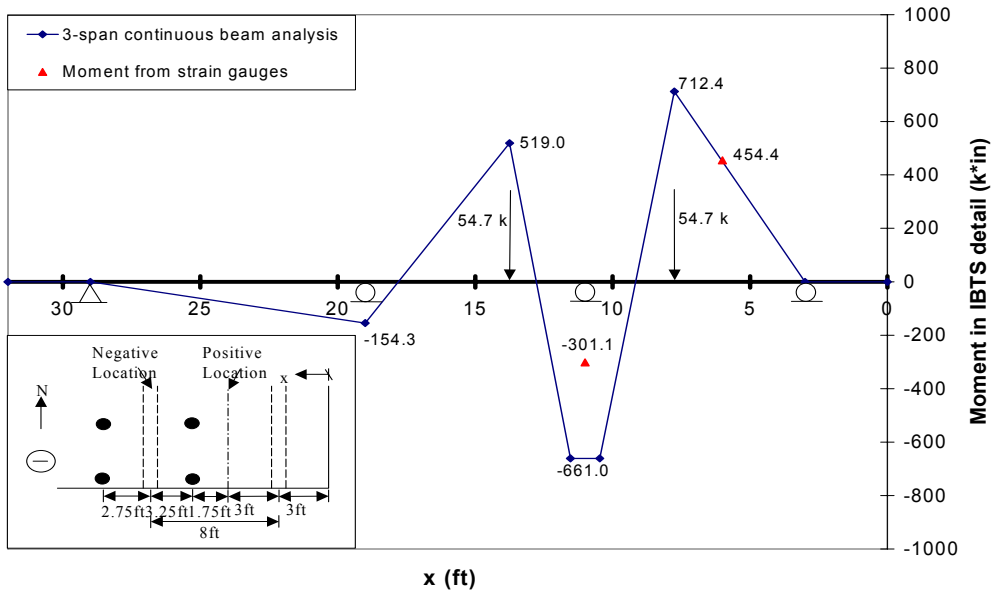

(ii) 1.75xHS-25 load step

Figure 5-31: Elastic moment compared to moment from strain gauges

5.2.2.8 Failure of the exterior span

Since only the interior span of the southeast test area initially failed, the two tires located in the exterior span of the test area were subsequently loaded to failure. This span also failed by punching of the edge-most tire at a load of 90.5kips (5.8xHS-25 or 7.2xHS-20) per tire. Pictures of the failure in the exterior span are shown in Figure 5-32 through Figure 5-34.

The bottom failure surface was closer to elliptical around the load plate than the interior span failure (Figure 5-32). The side cracks once again extended from the load plate to the girders (Figure 5-33). The top failure surface was different from the interior span failure, with the major failure cracks occurring further from the edge of the load plate (Figure 5-34).

Figure 5-32: Exterior span failure at bottom of deck, facing south

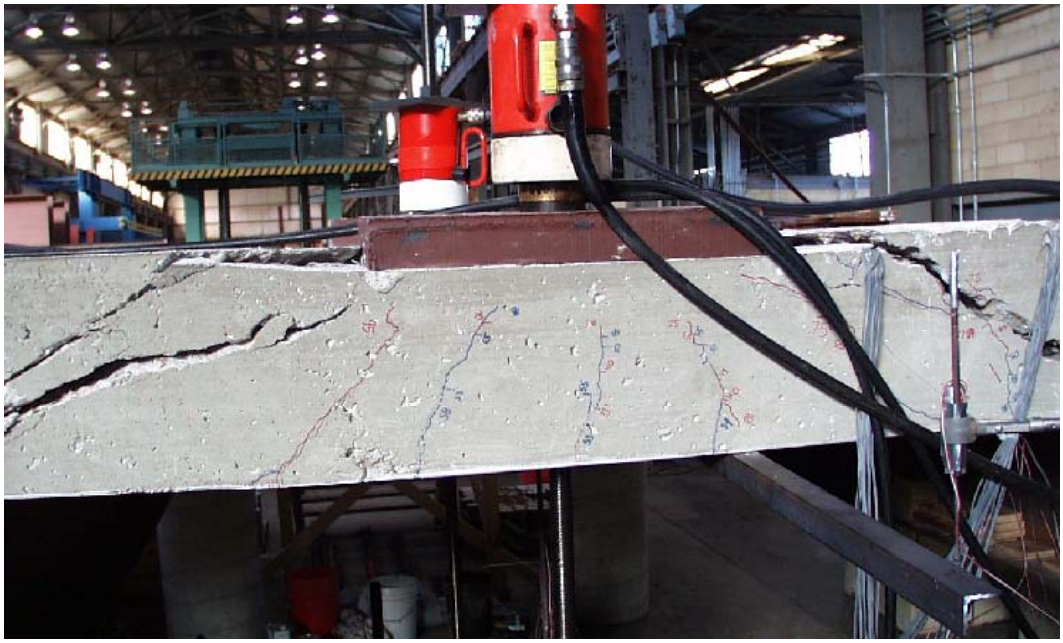

Figure 5-33: Exterior span failure at side of deck, facing north

(i) Facing south

(ii) Facing east

Figure 5-34: Exterior span failure at top of deck

5.2.3 Southeast test area summary

The southeast area of the bridge deck specimen tested the IBTS detail and an eight-foot deck span. It was loaded in the tandem, truck axle-front and truck axle-back loading configurations for typical design loads and overload levels. The test area was then taken to failure in the tandem loading configuration. The test area behaved superbly from a serviceability standpoint. Measured deflections were very small at all design loads as well as overload levels. In addition, first cracking occurred at an applied load of 33kips (2.1xHS-25) per tire. This is a substantial reserve strength for serviceability concerns.

The bridge deck was very stiff based on the small relative deflections that were measured at various load steps. The relative midspan deflection increased at a rate proportional to the load increase. The strain profiles showed that the distribution of strain across the thickened edge was different for the positive and negative locations, regardless of the loading configuration applied. The strains dropped quickly moving from the edge of the IBTS detail to the interior at the negative moment location. However, the strain magnitudes were almost uniform across the section at the maximum positive moment section. This is caused by the difference in support conditions of the two locations. The girder at the negative moment section did not allow the deck to deflect significantly, which also reduced the measured strains in the interior of the bridge deck.

The deck sustained large loads and extensive cracking prior to failing by punching of the edge-most tire in the interior span. Near failure, the bridge deck was deflecting with almost no increase in applied load. This behavior typically indicates an impending flexural failure. However, prior to a ductile flexural failure, the inclined cracks opened significantly and a punching shear failure was experienced by the bridge deck.

The test area has a factor of safety of six times the HS-25 design loading. However, the punching failure was non-ductile, which is typically avoided as the critical failure mechanism in structural design. The large factor of safety and the residual capacity after the punching failure (300% of the design load) show this is a very conservative design. Overall, the southeast test area of the bridge deck performed very well under the applied loadings and also displayed the benefits of arching action.

5.3 SOUTHWEST TEST AREA

The southwest test area contained the IBTS detail, spanning 10ft. As reported in section 5.2, the interior span of the IBTS side of the test specimen had been loaded to failure before this area was tested (southeast test area). This changed the boundary conditions at the interior girder of the southwest test area. The punching shear failure in the middle span of the deck necessitated a change in the test protocol. As opposed to using loading locations determined using influence lines, which were based on linear elastic analyses and continuity at supports, the test area was loaded at its midspan.

The positive moment section strain gauges were located three-feet from the centerline of the exterior girder, based on the linear elastic influence line analysis described in section 4.3.2. For positive bending, the critical section in the bridge deck is at the load point. Figure 5-35 shows an elastic analysis for a three-span continuous beam on point supports. This simplified analysis shows the strain gauges were at approximately 60% of the strain magnitude at the critical section in the linear elastic range. In addition, the negative moment section strain gauges are not at the critical location for negative bending, as they are not placed at the face of the support. Therefore, the load versus strain plots, strain profiles, moment calculations and elastic moment comparisons have not been included herein. However, they are presented and discussed in Appendix A.

The loading to maximize negative moment could not be applied since the interior span of the south edge was damaged. Based on influence lines presented in Figure 4.7, the loading to maximize positive moment places a tire one-foot from the centerline of the interior girder. This tire's load will go directly into the supporting girder and not significantly affect the bridge deck behavior. Therefore, it was only necessary to apply one tire load per axle. Since the

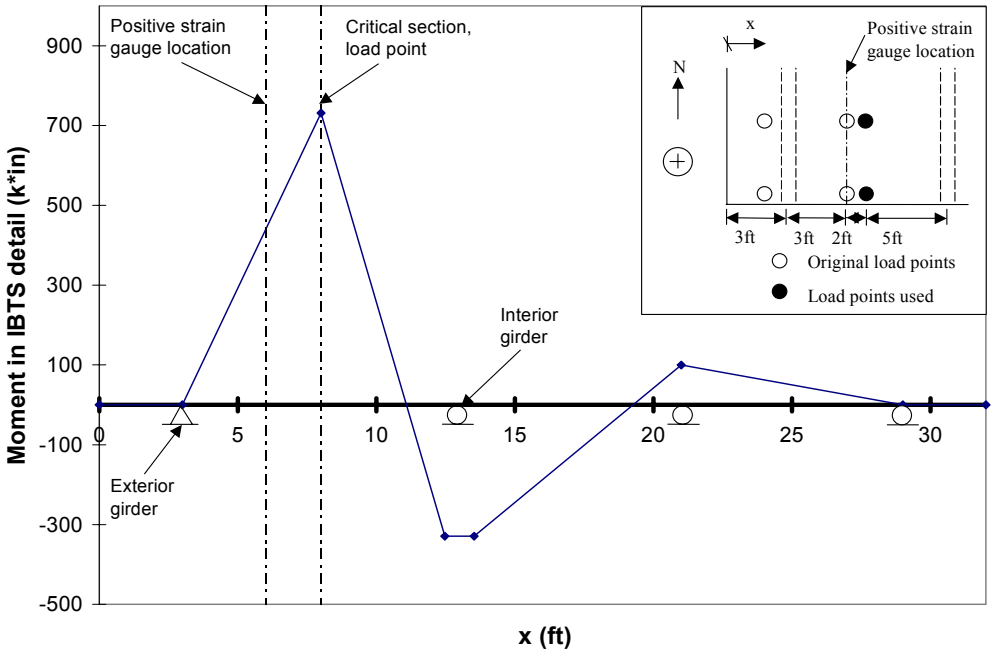

Figure 5-35: Critical section shift due to loading location change

rotational restraint of the bridge deck had been reduced by the punching failure in the southeast test area, the southwest test area behaved similar to a single-span deck, which shifted the critical section towards midspan. In addition, the tire location was near midspan and the loading holes needed to be repositioned due to the larger load plates so it was decided to load this test area at midspan. Table 5-2 shows a list of the load tests performed on the southwest test area.

Loads were applied by hydraulic rams bearing on 15in by 20in load plates on top of neoprene bearing pads placed on the bridge deck. After obtaining a punching failure in the southeast test area, the load plate area was increased using the provisions of section 3.6.1.2.5 in the 1998 AASHTO LRFD Bridge Design Specification. The larger load plate required coring new holes in the span of the southwest test area. The concrete was scanned prior to coring in order to locate the reinforcing steel.

Table 5-2: Order of testing in the southwest test area

Test No.	Location Pos/Neg	Load Type Tan/Truck	Which axle?	Load per tire (kips)	Load per tire (xHS-25)
1	Positive	Tandem	Both	31.2	2
2	Positive	Truck	Front	40	2
3	Positive	Truck	Back	40	2
4	Positive	Tandem	Both	37.5	2.4
5	Positive	Truck	Front	48	2.4
6	Positive	Truck	Back	48	2.4
7	Positive	Tandem	Both	54.7	3.5
8	Positive	Truck	Front	70	3.5
9	Positive	Truck	Back	70	3.5
10*	Positive	Tandem	Both	95.6	6.1

*Punching of edge tire

The SB101+ strain gauge was monitored during testing. Due to a conversion error, the intermediate applied load steps were twice as large as the load steps used in other test areas (i.e. 2xHS-25, 2.4xHS-25 and 3.5xHS-25). The plots of load versus deflection are reported at the doubled load steps. However, readings from all instruments have been collected continuously at the typical load steps (HS-25, 1.2xHS-25 and 1.75xHS-25), which allowed comparisons between test areas. The crack widths and lengths are presented for first cracking (HS-25), regular load steps and failure (6.1xHS-25).

5.3.1 Load vs. deflection response

The relative midspan deflection was calculated in the same manner used in the southeast test area (section 5.2.1.1). The plots are jagged because string potentiometers, which give lower resolution than linear potentiometers, were used to measure deflection at midspan. It is important to note that the bridge deck deflects continuously with increasing loads and the noise in the data is associated

to the instrumentation. In addition, the noise level appears very high, as the deformations being measured are very small.

5.3.1.1 2xHS-25 load step

Figure 5-36 shows plots of load versus deflection for the three loading configurations applied at the 2xHS-25 load step. The HS-20 and HS-25 load levels are also shown in the figure. The maximum relative edge deflection measured at this load step was 0.11in, caused by the tandem loading configuration (Figure 5-36, i). The truck axle-front loading configuration induced a maximum relative deflection of 0.09in, about 80% of the tandem deflection. Figure 5-36 (iii) shows the small relative deflection (0.02in) caused by the truck axle-back loading configuration.

The deflections created at this load step are small and compare to the noise in the readings from the string pot. The behavior of the bridge deck at the 2xHS-25 load step appears to be linear for all loading configurations. However, first cracks were visually observed at the bottom side of the deck when HS-25 loads were applied. It is important to note that the lengths and widths of these cracks were small and did not cause a noticeable slope change in the overall load versus deformation response (Figure 5-36). The tandem loading configuration resulted in a residual relative deflection of 0.04in after unloading, indicating some inelasticity that is likely due to microcracking around the reinforcing steel.

5.3.1.2 2.4xHS-25 load step

Figure 5-37 shows the relative midspan deflections recorded at the 2.4xHS-25 load step, which were not significantly larger than those of the 2xHS-25 load step. The maximum edge deflection again occurred under the tandem loading configuration (0.12in), however, the increase was only about 9% compared to the edge deflection measured at the 2xHS-25 load step. The truck

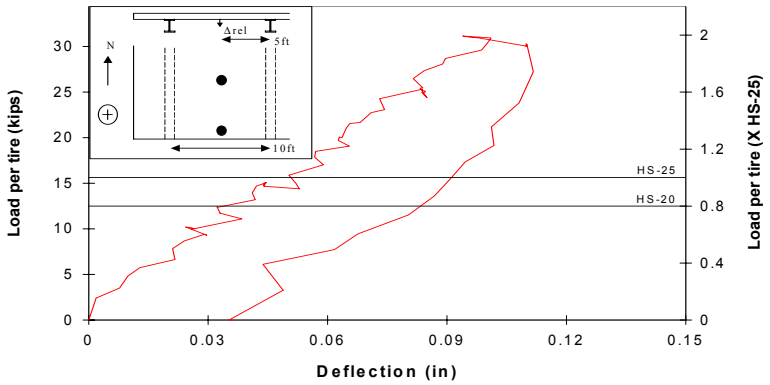

(i) Tandem

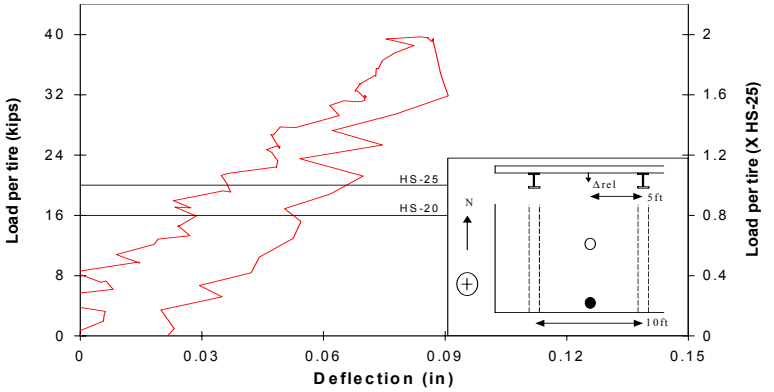

(ii) Truck axle-front

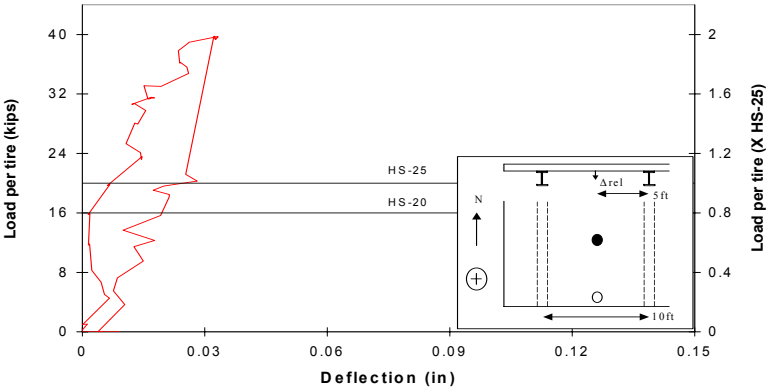

(iii) Truck axle-back

Figure 5-36: Load vs. deflection, 2xHS-25 load step, midspan loading location, southwest test area

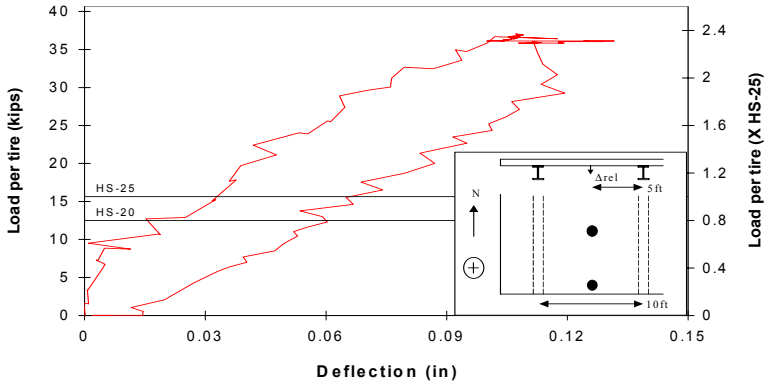

(i) Tandem

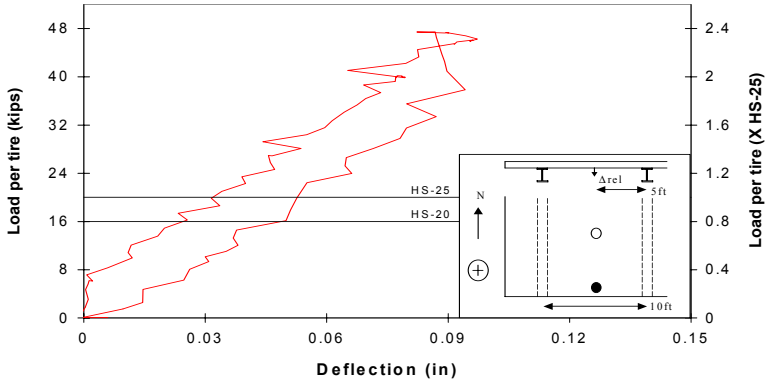

(ii) Truck axle-front

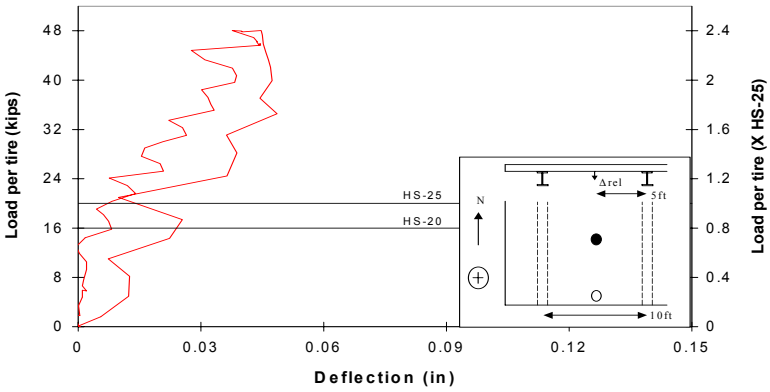

(iii) Truck axle-back

Figure 5-37: Load vs. deflection, 2.4xHS-25 load step, midspan loading location, southwest test area

axle-front loading configuration created a maximum deflection comparable to the tandem configuration while the truck axle-back loading configuration deflected the edge of the deck insignificantly. The bridge deck's response to all loads applied at the 2.4xHS-25 load level was essentially linear.

5.3.1.3 3.5xHS-25 load step

The tandem loading configuration created the largest relative midspan deflection of 0.25in. Figure 5-38 (i) also shows a slight amount of non-linearity in the behavior of the bridge deck at a load of approximately 41kips (2.6xHS-25). The unloading portion of the plot has roughly the same slope as the reloading portion.

The relative deflection response of the bridge deck was the stiffest for the truck axle-back loading configuration and the most flexible for the tandem loading configuration. This indicates the stiffness of the deck where the loadings were applied and vulnerability of the deck to various loading configurations. The maximum relative deflections at the 3.5xHS-25 load step increased over 200% compared to the 2xHS-25 load step, a load increase of 175%.

5.3.1.4 Loading to failure

The loading to failure plot in Figure 5-39 includes the load versus deflection response of the test area at the 2xHS-25, 2.4xHS-25 and 3.5xHS-25 load steps in the tandem loading configuration. At the envelope of the plots, four distinct slopes are evident as shown by the fitted lines. The first stiffness change was slight and occurs at a load of approximately 31kips (2xHS-25) per tire. This corresponds with the crack map for the bottom of the bridge deck (Figure 5-41). First cracking of the bridge deck occurred at the HS-25 load level, however, the cracks did not cross the slab end detail until the 2xHS-25 load level. The cracks that formed at the HS-25 load level were not significant enough to change the

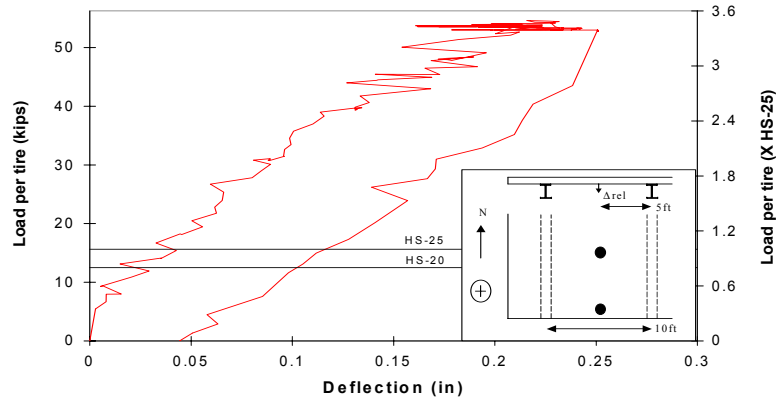

(i) Tandem

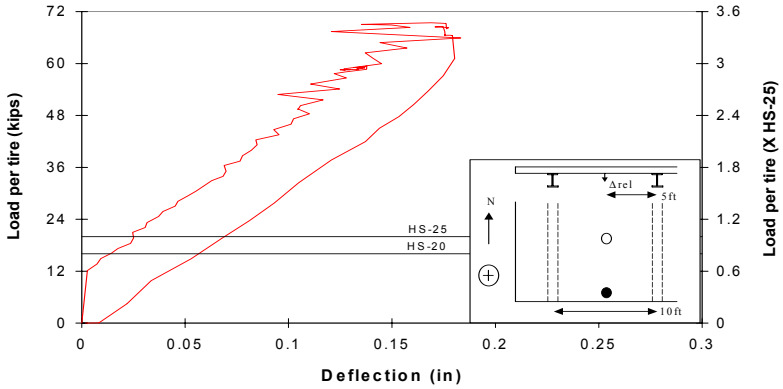

(ii) Truck axle-front

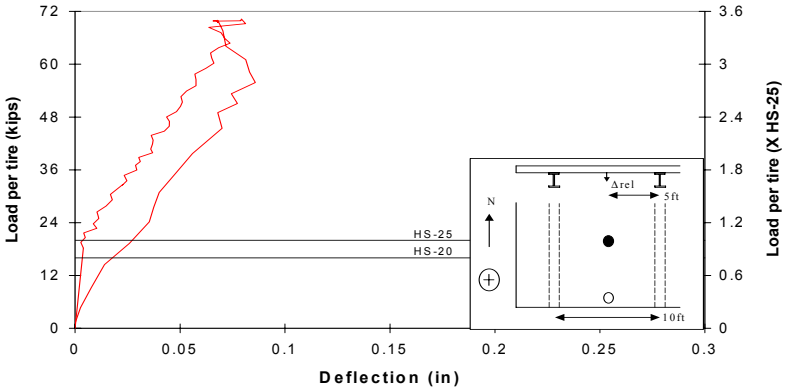

(iii) Truck axle-back

Figure 5-38: Load vs. deflection, 3.5xHS-25 load step, midspan loading location, southwest test area

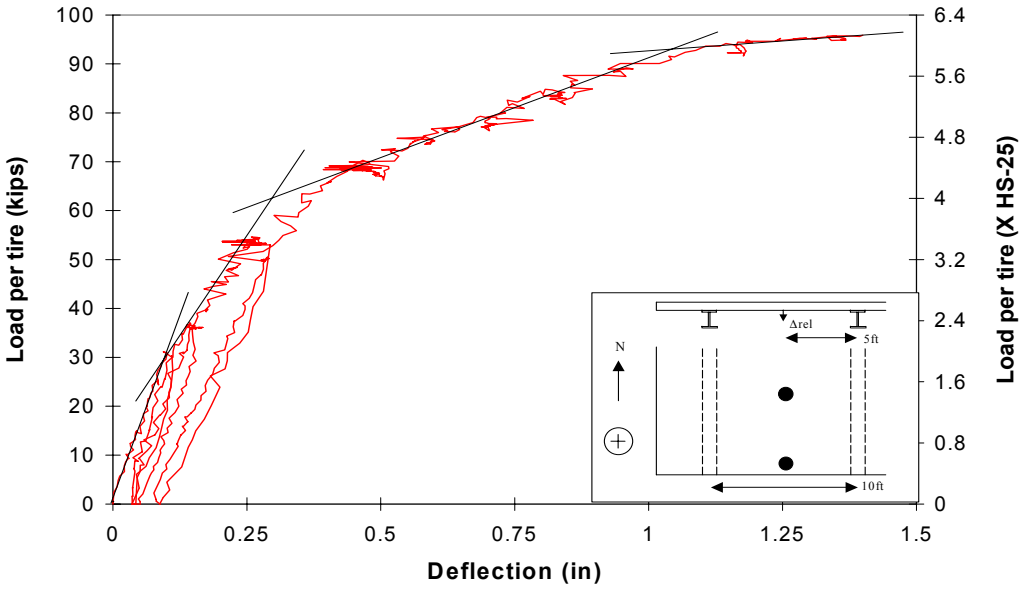

Figure 5-39: Load vs. deflection, loading to failure, midspan loading location, southwest test area

stiffness of the slab end detail. The second stiffness change occurs at a load of approximately 62kips (4xHS-25) per tire, indicating significant deterioration within the thickened edge as the slope change is large. The final slope of the plot, just prior to failure, is nearly horizontal, indicating yielding of the flexural steel.

The relative deflection measured at a load of 2xHS-25, during the loading to failure (Figure 5-39), is nearly the same as that at the 2xHS-25 load application (Figure 5-36). Therefore, the section had not been significantly deteriorated after being loaded to the 2xHS-25, 2.4xHS-25 and 3.5xHS-25 load steps. Overall, the slab end detail behavior was relatively stiff up to failure carried large applied loadings prior to punching.

5.3.2 Crack maps

Section 5.2.2.2 describes the process used to produce the crack maps presented herein. The crack maps in Figure 5-40 through Figure 5-42 were created for first cracking and all load steps after that including failure. First cracking at the bottom and side of the bridge deck occurred at the HS-25 load level in the southwest test area. However, the cracks did not propagate significantly until the 2xHS-25 load step. The top of the deck cracked much later, at a load of 3.5xHS-25. The three cracks present on the bottom of the deck extended across the thickened edge at this load step (Figure 5-40, ii).

The load versus deflection plots show a change in stiffness at a load of about 41kips (2.6xHS-25) per tire, however, the stiffness change due to first cracking is not clear (Figure 5-38, i). This is because the crack widths remained small until the 3.5xHS-25 load step, at which point they began to increase significantly. The deck must be significantly cracked in order to identify the stiffness change it causes on the load versus deflection plots.

At failure, the bottom of the deck was extensively cracked (Figure 5-40, v). The cracks initially propagated perpendicular to the edge of the bridge deck. Close to failure, they began to branch toward the flanges of the supporting girders in the interior of the deck. This cracking pattern shows the preliminary formation of a yield-line pattern, extending from midspan near the edge of the deck, and then, branching toward the girders in the interior of the deck. This behavior is verified by the crack maps for the top of the bridge deck (Figure 5-41), which show negative moment yield lines forming at the girders. It is important to note that failure occurred due to punching of the edge tire rather than formation of a collapse mechanism through fully developed yield lines.

The top of the deck cracked at a larger load level than the bottom and side. The crack widths remained very small until failure. The cracks on the top of the

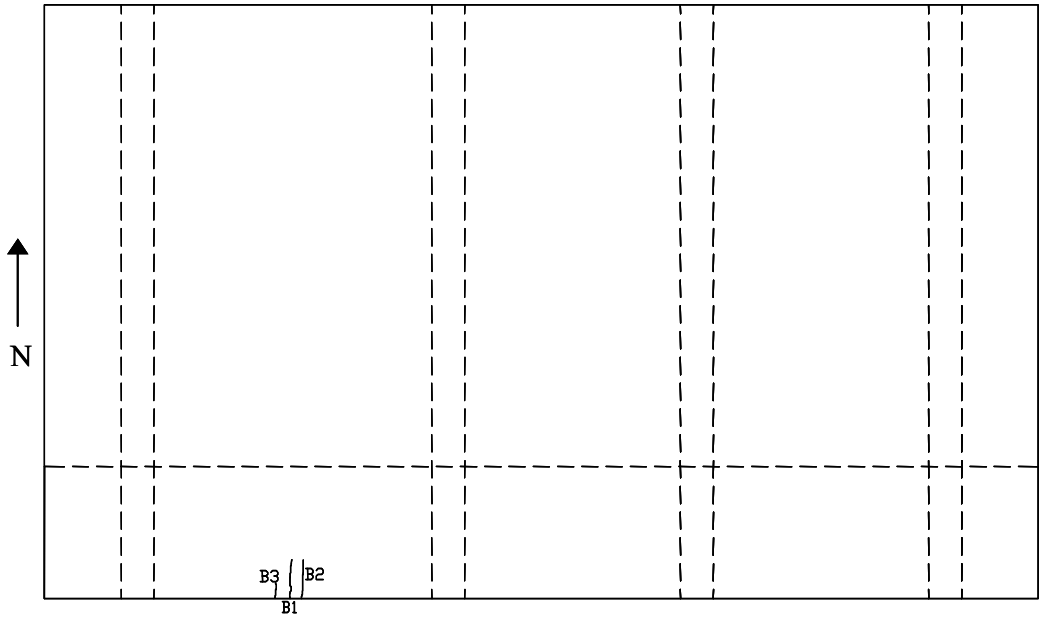

(i)HS-25 applied load (first cracking)

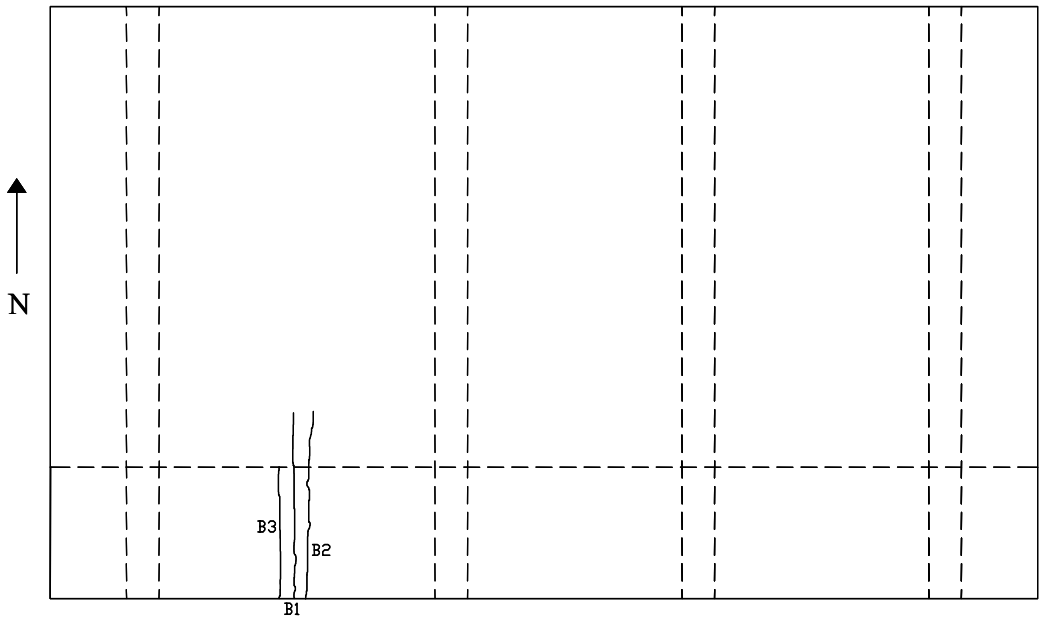

(ii)2xHS-25 load step
**Reference (vi) for crack widths and lengths*

Figure 5-40: Crack maps for the bottom of the bridge deck

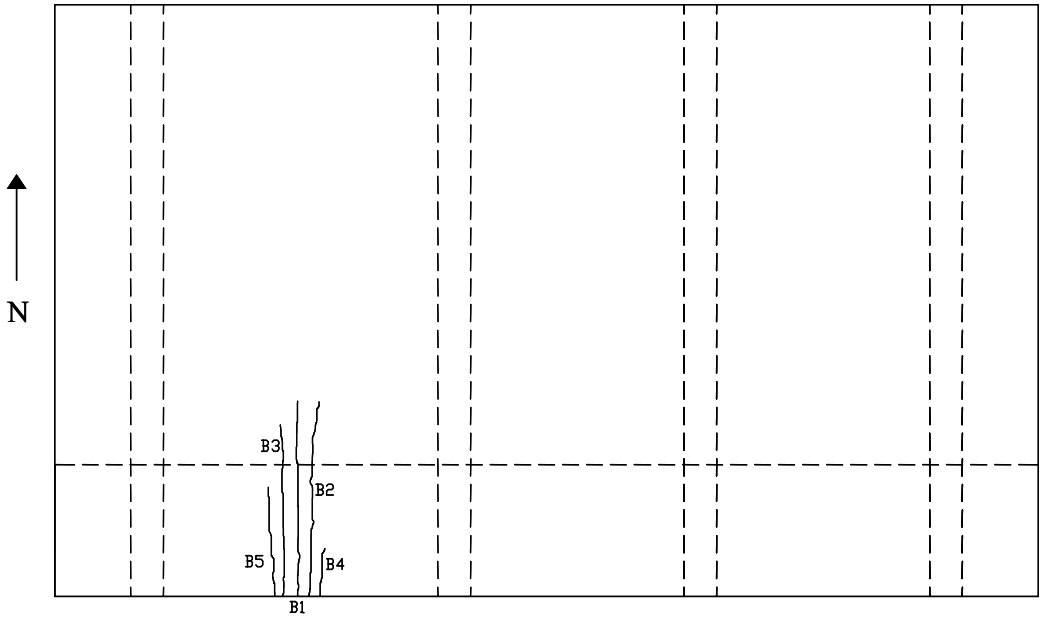

(iii)2.4xHS-25 load step

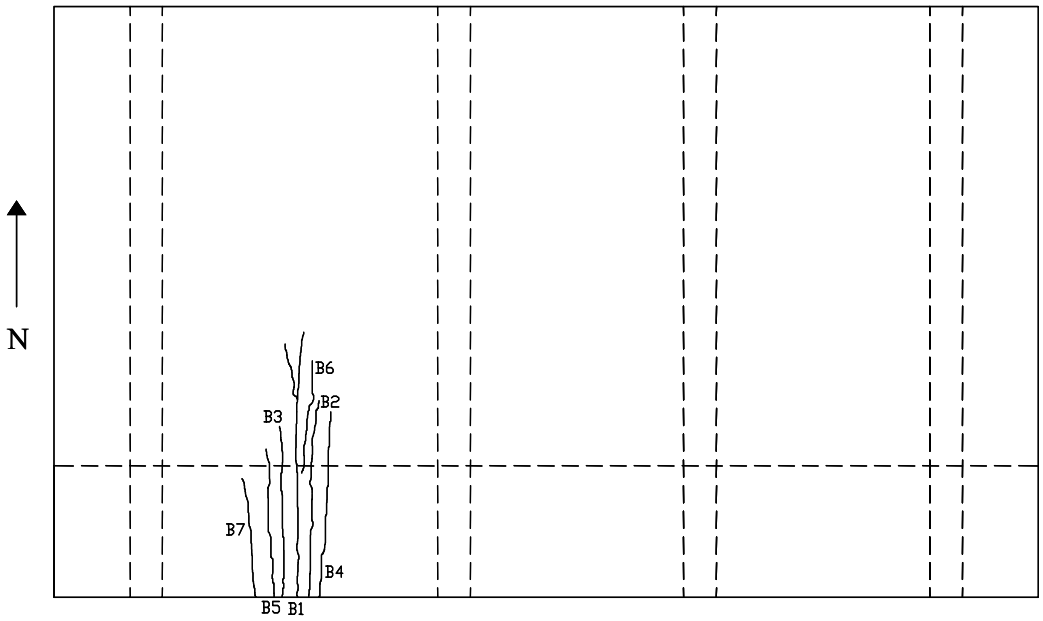

(iv)3.5xHS-25 load step
**Reference (vi) for crack widths and lengths*

Figure 5-40, cont'd: Crack maps for the bottom of the bridge deck

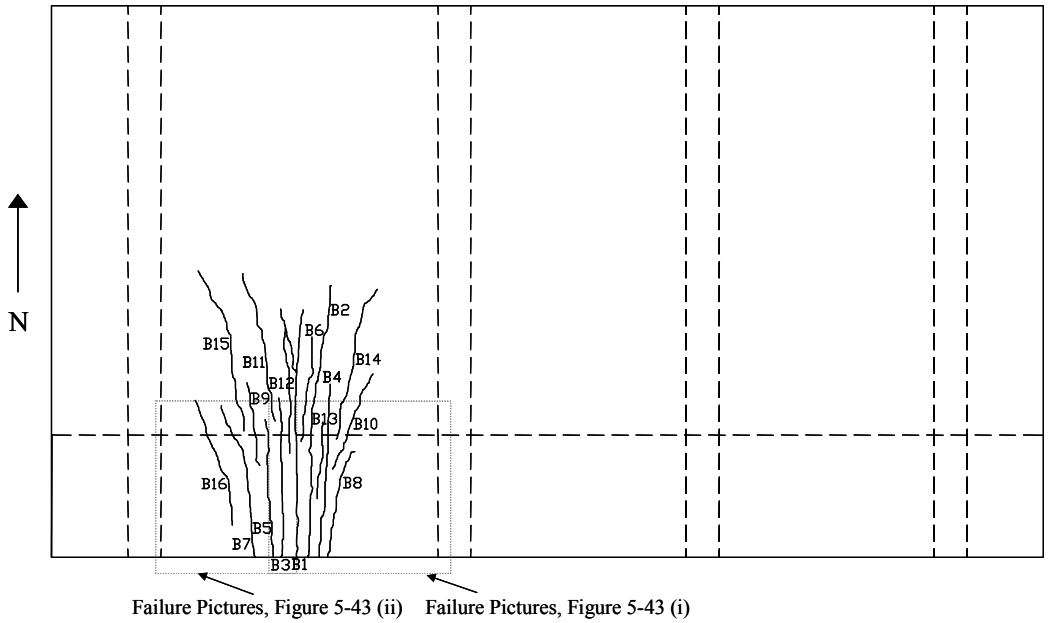

(v)6.1xHS-25 load step (failure)

Load=HS-25			Load=2xHS-25			Load=2.4xHS-25			Load=3.5xHS-25			Load=6.1xHS-25		
Crack Name	Width (in)	Length (in)	Crack Name	Width (in)	Length (in)	Crack Name	Width (in)	Length (in)	Crack Name	Width (in)	Length (in)	Crack Name	Width (in)	Length (in)
B1	H	14	B1	0.003	68	B1	0.005	71	B1	0.008	92 (21)	B1	0.033	92 (25)
B2	H	14	B2	0.002	62	B2	0.005	65	B2	0.008	66	B2	0.01	102
B3	H	6	B3	0.002	48	B3	0.004	62	B3	0.006	62	B3	0.014	62
						B4	H	17	B4	0.004	68	B4	0.003	60
						B5	H	40	B5	0.003	53	B5	0.008	53
									B6	H	43	B6	0.016	13
									B7	H	45	B7	0.009	65
												B8	0.009	43
												B9	0.005	33
												B10	H	40
												B11	H	58
												B12	H	41
												B13	H	30
												B14	H	59
												B15	H	65
												B16	H	46

(vi)Key of widths and lengths of cracks for i, ii, iii, iv and v

*H = hairline crack, parenthesis measurement refers to the branch of crack B1

Figure 5-40, cont'd: Crack map and key for the bottom of the bridge deck

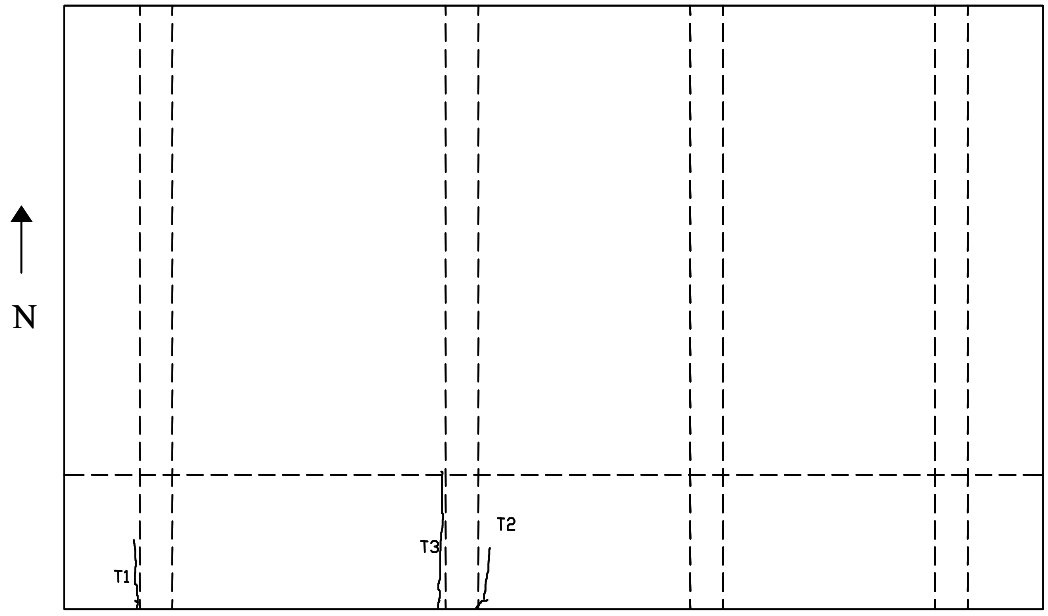

(i)3.5xHS-25 load step (first cracking)

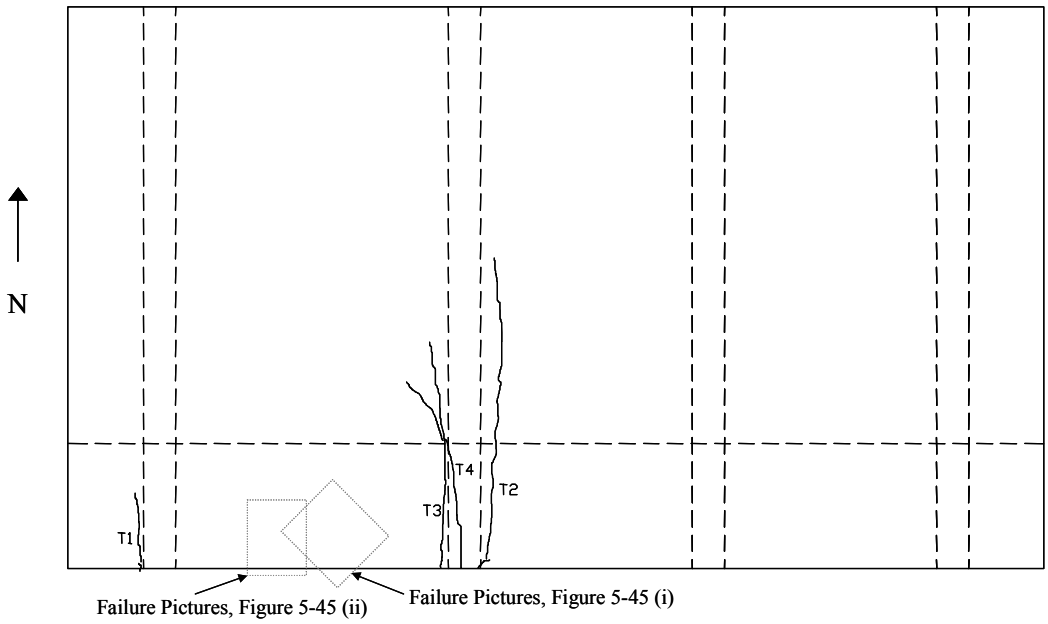

(ii)6.1xHS-25 applied load (failure)
**Reference (iii) for crack widths and lengths*

Figure 5-41: Crack maps for the top of the bridge deck

Load=3.5xHS-25			Load=4.5xHS-25		
Crack Name	Width (in)	Length (in)	Crack Name	Width (in)	Length (in)
T1	H	26	T1	0.002	30
T2	H	23	T2	H	118
T3	H	48	T3	0.004	73
			T4	0.004	87

(iii)Key of crack widths and lengths for i and ii
*H = hairline crack

Figure 5-41, cont'd: Crack map and key for the top of the bridge deck

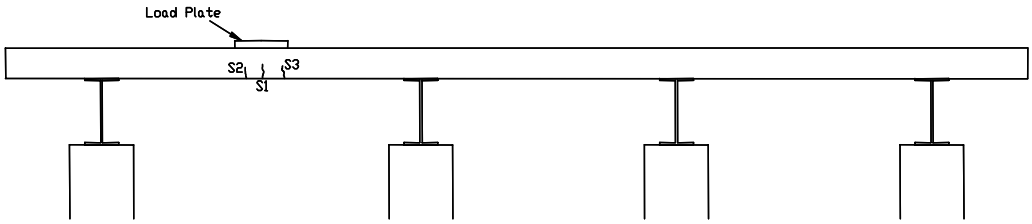

(i)HS-25 applied load (first cracking)

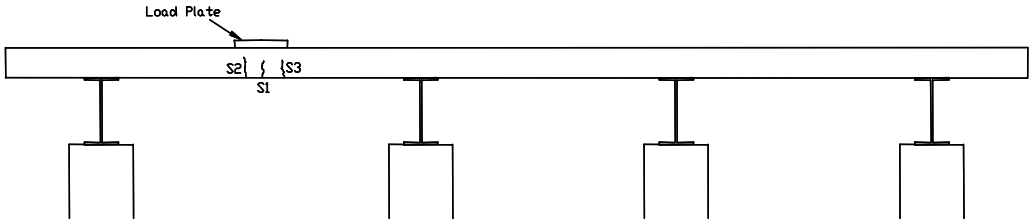

(ii)2xHS-25 load step

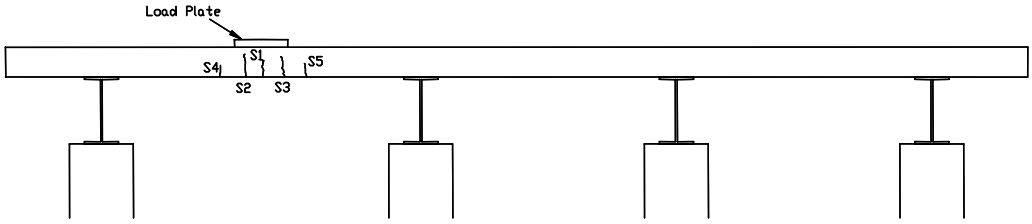

(iii)2.4xHS-25 load step
****Reference (vi) for crack widths and lengths***

Figure 5-42: Crack maps for the side of the bridge deck

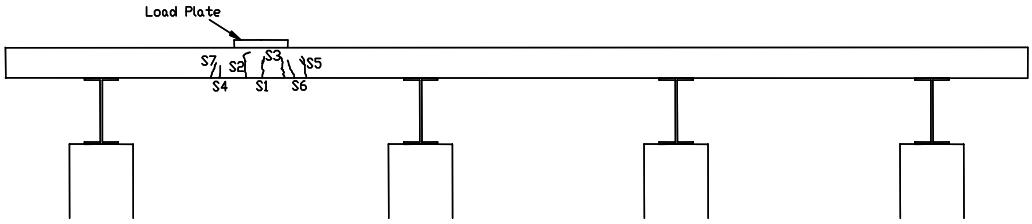

(iv)3.5xHS-25 load step

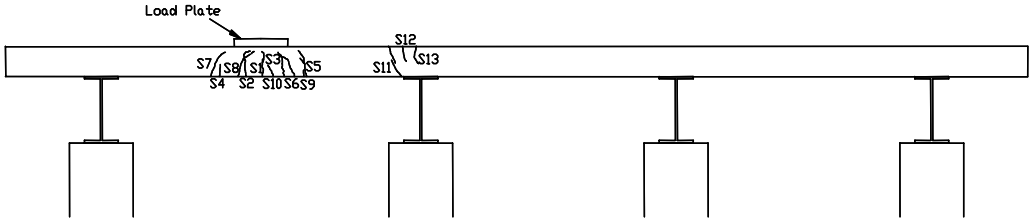

(v)6.1xHS-25 load step (failure)

Load=HS-25			Load=2xHS-25			Load=2.4xHS-25			Load=3.5xHS-25			Load=6.1xHS-25		
Crack Name	Width (in)	Length (in)	Crack Name	Width (in)	Length (in)	Crack Name	Width (in)	Length (in)	Crack Name	Width (in)	Length (in)	Crack Name	Width (in)	Length (in)
S1	H	5	S1	0.003	6	S1	0.005	6	S1	0.009	8	S1	0.05	8.5
S2	H	3.5	S2	0.003	6	S2	0.004	7.5	S2	0.008	8	S2	0.007	8
S3	H	4	S3	0.003	5.5	S3	0.004	6.5	S3	0.008	7	S3	0.009	7
						S4	H	4.5	S4	0.004	4.5	S4	0.005	4.5
						S5	H	4	S5	0.004	7.5	S5	0.01	9
									S6	H	6	S6	0.03	9.5
									S7	H	5.5	S7	0.004	9
												S8	0.029	8
												S9	H	1
												S10	H	4.5
												S11	0.002	13
												S12	H	6
												S13	H	8

(vi) Key of crack widths and lengths for i, ii, iii, iv and v
*H = hairline crack

Figure 5-42, cont'd: Crack map and key for the side of the deck

deck initially formed at the edge of the girder flanges, verifying that the flange and shear studs restrain the concrete over the girder. The midspan loading created more extensive cracking in the bottom of the deck near midspan than in the top of the deck over the girder. As mentioned previously, the cracks began to open

significantly at the 3.5xHS-25 load step. At failure, the cracks in the deck span are centered under the load plate (Figure 5-42). In addition, they are very concentrated at midspan showing the initiation of a yield-line.

5.3.3 Failure Pictures

Failure of the southwest test area occurred due to punching of the edge tire at a load of 96kips (6.1xHS-25 or 7.6xHS-25). The failure surface was documented with failure pictures discussed herein. Figure 5-43 shows the failure surface at the bottom of the deck. The failure surface was very similar to the interior span failure in the southeast test area, which formed roughly 2.5ft into the deck, parallel to the edge of the deck. In addition, both test area's major failure cracks curved toward the edge of the deck at the girder on the west side of the test span.

The side of the bridge deck after failure is shown in Figure 5-44. The shear cracks formed at different angles on each side of the load plate, with a steeper inclination on the west side (i.e. the shear crack on the left side of the loading plate in Figure 5-44). The failure crack on the west side of the loading plate did not extend to the girder flange, but reached the bottom surface of the deck a few inches from the edge of the flange. Whereas, the shear crack on the east side of the plate extended to the girder flange. By comparing the failure pictures to the crack maps, it can be seen that the shear cracks defining the punching core formed in a location where there was no previous visible flexural or shear cracks.

The failure surface extended diagonally from the north side of the load plate to deck edge (Figure 5-45). The failure surface was again flush along the north side of the load plate.

(i) East side of test span, facing south

(ii) West side of test span, facing south

Figure 5-43: Southwest test area failure pictures at bottom of deck

Figure 5-44: Southwest test area failure picture at side of deck, facing north

(i) East side of interior span, facing south

(ii) West side of test span, facing east

Figure 5-45: Southwest test area failure pictures at top of deck

5.3.4 Southwest test area summary

The performance of the IBTS detail on a deck span of 10ft was tested in the southwest test area of the bridge deck specimen. It was loaded at midspan with 15in by 20in load plates. One tire load per axle was applied to the deck because the loads from the other two tires were directly on top of the supporting girder. Three loading configurations were applied at load steps of 2xHS-25, 2.4xHS-25 and 3.5xHS-25. Then, the test area was taken to failure in the tandem loading configuration.

The deflections for the southwest test area were small in relation to the span of the deck. At failure, the slope of the load versus deflection plot was nearly horizontal; indicating steel in the thickened edge was yielding. The southwest test area reached an ultimate relative midspan deflection of 1.4in.

The IBTS detail cracked at the bottom and side of the deck at the HS-25 load level. If minor cracks at service loads are to be avoided, the performance of the IBTS detail spanning 10ft could be unacceptable. Early cracking (HS-25 load level) occurred on the bottom of the deck, which is a less critical location for corrosion issues than the top of the bridge deck. Top cracks did not form until an applied load of 3.5xHS-25. In addition, the bottom cracks did not become significant, both in number and in width, until the 200% overload as evidenced by the stiffness change shown in the load versus deformation plots. The relative edge deflections were small at the service load levels.

The southwest test area failed by punching of the edge tire at a load of 96kips (6.1xHS-25 or 7.6xHS-20). The shear cracks extended to the girder on one side of the load plate and within inches of the girder on the other side. The deck deflected a small amount compared to the span length while sustaining large overloads. Significant flexural cracking occurred prior to the punching failure.

5.4 NORTHWEST TEST AREA

The first test on the UTSE detail was performed in the northwest test area. In this test area, the girder spacing was 10ft. In order to provide a basis for comparison with the southwest test area, the deck was loaded at the midspan. In this way, the performance of the UTSE detail was tested for positive bending. Table 5-3 shows a summary of the load steps performed in the northwest test area. The typical load steps (HS-25, 1.2xHS-25, 1.75xHS-25 and 3xHS-25) were applied to be consistent with other test areas, prior to loading the specimen to failure.

During the first test, conducted at the southeast test area, a punching shear failure occurred in the interior span of the test specimen. Damage associated with this failure had an impact on the loading configuration of the second test, in the southwest test area. As discussed earlier, the load points were moved to midspan (i.e. five-feet from the centerline of the girders) in the southwest test area. Due to the change in loading location, the strain gauges in the southwest and northwest test areas were not at the locations of maximum positive and negative moment. In other words, strains at critical locations were not measured in this test area. Therefore, the load versus strain plots, strain profiles, moment calculations and elastic moment comparisons are presented in Appendix A. As can be observed in Table 5-3, after carrying out design load and overload tests, the slab end was loaded to failure in the tandem loading configuration. As in the southwest test area, 15in by 20in load plates were used to apply loads to the deck. The strain gauge on the rebar at the edge of the deck in the positive moment section (NB101+) was monitored during the load testing.

Table 5-3: Order of testing in northwest test area

Test No.	Loading Location	Load Type Tandem/Truck	Which axle?	Load per tire (kips)	Load per tire (xHS-25)
1	Positive	Tandem	Both	15.6	1
2	Positive	Truck	Front	20.0	1
3	Positive	Truck	Back	20.0	1
4	Positive	Tandem	Both	18.8	1.2
5	Positive	Truck	Front	24.0	1.2
6	Positive	Truck	Back	24.0	1.2
7	Positive	Tandem	Both	27.3	1.75
8	Positive	Truck	Front	35.0	1.75
9	Positive	Truck	Back	35.0	1.75
10	Positive	Tandem	Both	46.9	3
11	Positive	Truck	Front	60.0	3
12	Positive	Truck	Back	60.0	3
13	Positive	Tandem	Both	81.3	5.2

*Punching of edge tire

5.4.1 Load vs. deflection response

In this section, load versus deflection behavior of the test specimen is discussed. Since the strain measurement locations were not at the critical locations, the strain readings were not especially useful and are presented in Appendix A. Therefore, the load versus deflection plots, crack maps and failure pictures were used as the primary evaluation of the test area performance at service loads and overloads. The relative deflection measurement and calculation is discussed in section 5.2.1.1.

5.4.1.1 HS-25 load step

The deflection readings obtained at the HS-25 load step were small compared to the resolution of the displacement transducers. Hence, the plots of the load versus deflection response of the bridge deck are jagged and they show

considerable noise at the HS-25, 1.2xHS-25 and 1.75xHS-25 load steps. However, it is important to appreciate that such small deformations are indications of very stiff deck behavior and superior structural performance under service load and overload conditions. The behavior of the bridge deck at the HS-25 load level was linear elastic. The tandem loading configuration created the largest relative deflection (approximately 0.07in) at this load step (Figure 5-46, i). The relative deflection caused by the truck axle-front loading configuration was about 0.045in while the deflection caused by the truck axle-back loading configuration was within the noise in the data (less than 0.005in). For this reason, the load versus deformation plot for the truck axle-back loading configuration is not presented.

5.4.1.2 1.2xHS-25 load step

The tandem and truck axle-front loading configurations caused roughly the same maximum relative deflection of 0.07in. The applications of tandem loading configuration resulted in a slightly larger maximum midspan deflection at the 1.2xHS-25 load step compared to the HS-25 load step. However, the maximum relative deflection due to the truck axle-front configuration increased by 40% compared to the 20% increase in load. This seemingly large difference stems from small deflections and noise levels that were comparable to measured deflections. The truck axle-back loading configuration again caused insignificant deflections (Figure 5-47, iii). The behavior of the bridge deck was linear elastic at the 1.2xHS-25 load step. The residual deformations measured at the HS-25 and 1.2xHS-25 load steps were comparable to the resolution of the displacement measurements and hence can be assumed to be zero for all practical purposes.

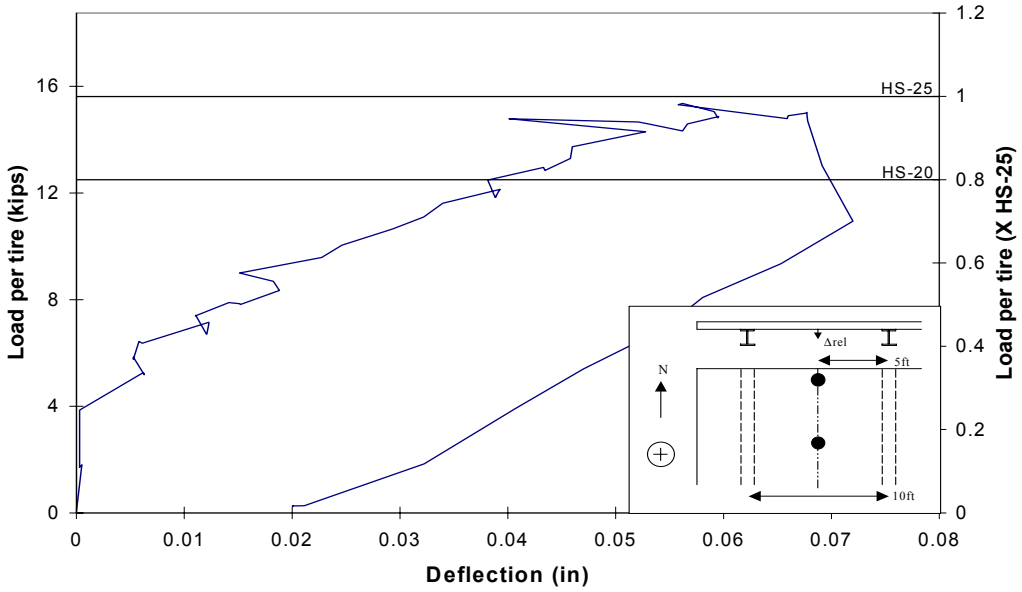

(i) Tandem

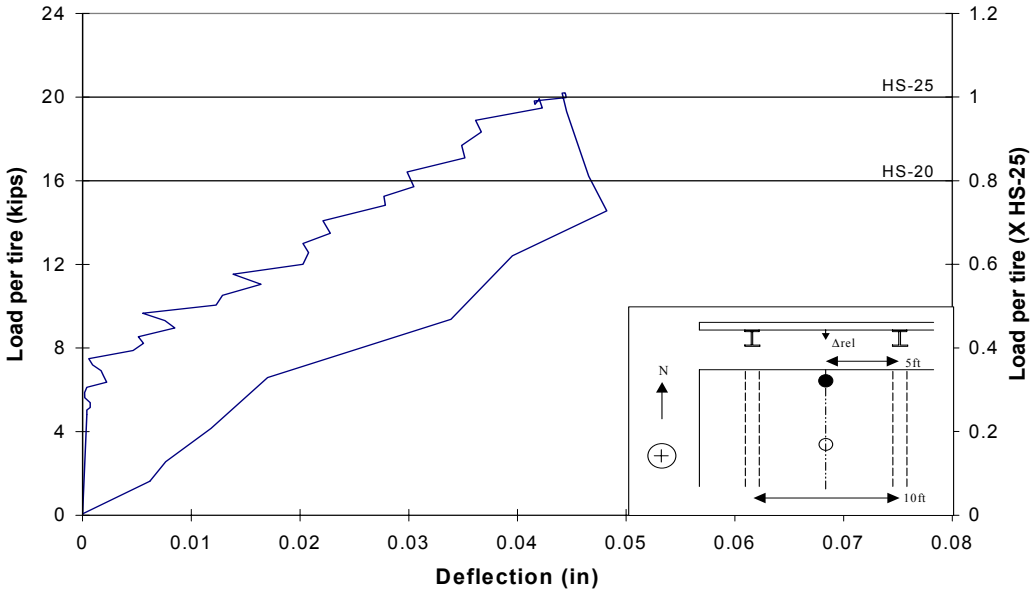

(ii) Truck axle-front

Figure 5-46: Load vs. deflection, HS-25 load step, midspan loading location, northwest test area

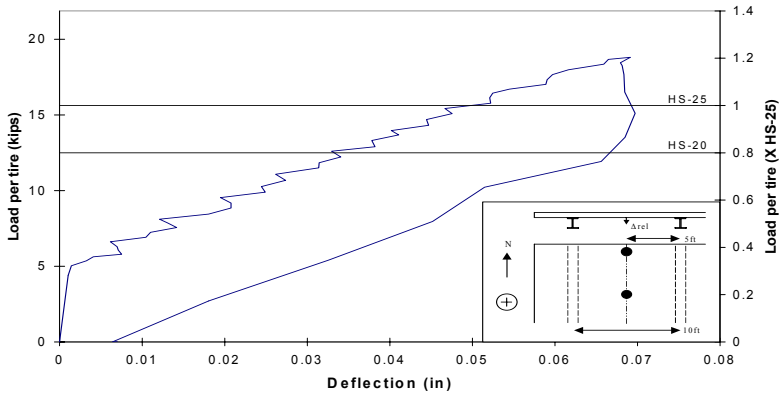

(i) Tandem

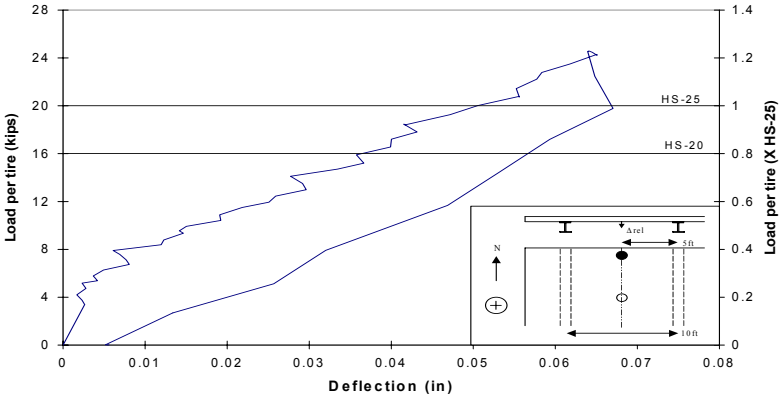

(ii) Truck axle-front

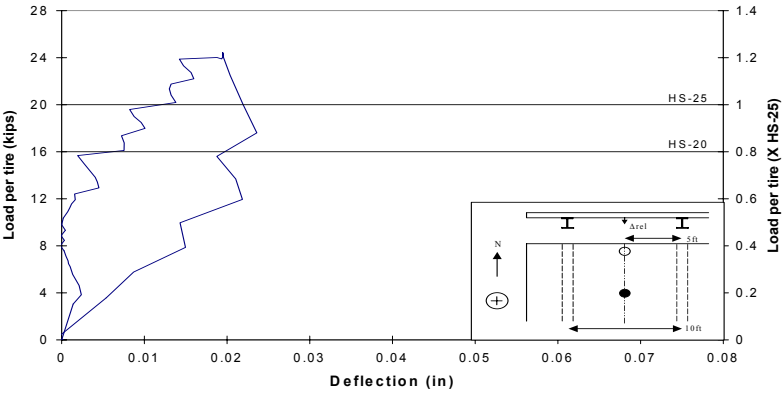

(iii) Truck axle-back

Figure 5-47: Load vs. deflection, 1.2xHS-25 load step, midspan loading location, northwest test area

5.4.1.3 1.75xHS-25 load step

Figure 5-48 shows the load versus deflection plots for the 1.75xHS-25 load step. The relative deflections measured at this load step are significantly larger than those recorded in the previous load steps. The maximum relative deflection caused by the tandem and truck axle-front loading configurations at this load step is over twice as large as those measured at the HS-25 load step. This indicates a reduction in stiffness within the section and it can be attributed to cracking in the slab end detail. The crack maps in Figure 5-51 through Figure 5-53 show the initiation of cracking near midspan and over the girders at 1.2xHS-25 and 1.5xHS-25, respectively. The maximum relative deflection measured at this load step was 0.14in (Figure 5-48).

5.4.1.4 3xHS-25 load step

The bridge deck performed well at the 300% overload. Its response was linear except for a slight non-linearity caused by the tandem loading configuration. The slope of the loading portion of the tandem plot gradually decreases and there is a residual deflection of 0.07in after unloading (Figure 5-49, i). The change in slope begins at a load of approximately 27kips (1.75xHS-25), the largest load applied at the previous load step.

During this load application, at the HS-25 load level, the relative deflection at midspan was 0.07in. It is interesting to note that the bridge deck had a relative midspan deflection of 0.07in due to the tandem loading configuration at the HS-25 load step as well (Figure 5-46). This indicates that the previously applied loads did not significantly damage the thickened edge. Once again, the truck axle-front loading configuration created a maximum relative deflection comparable to that caused by the tandem loading configuration. The truck axle-

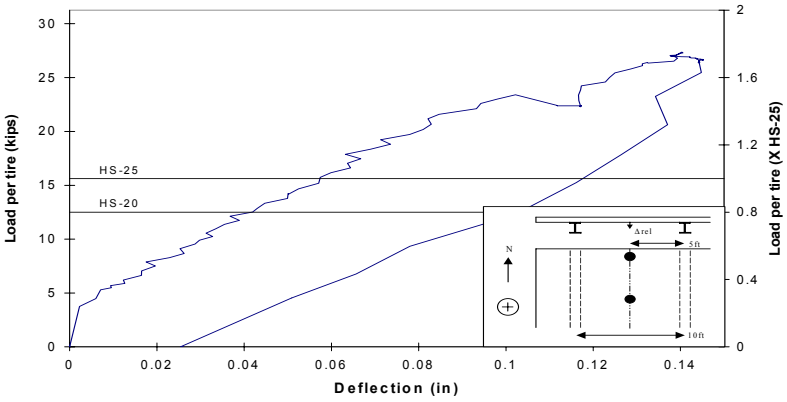

(i) Tandem

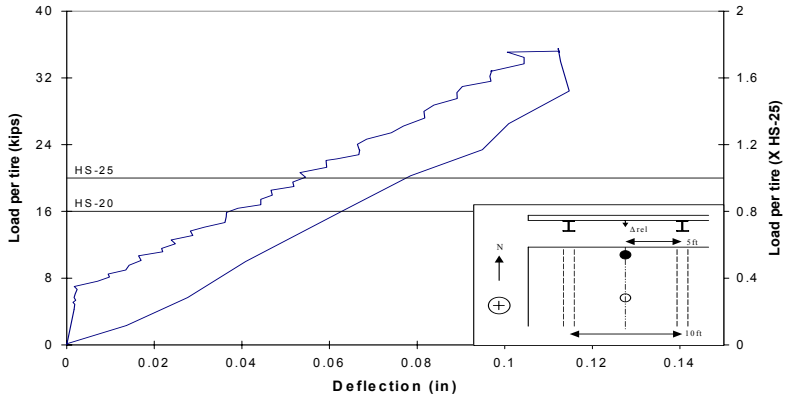

(ii) Truck axle-front

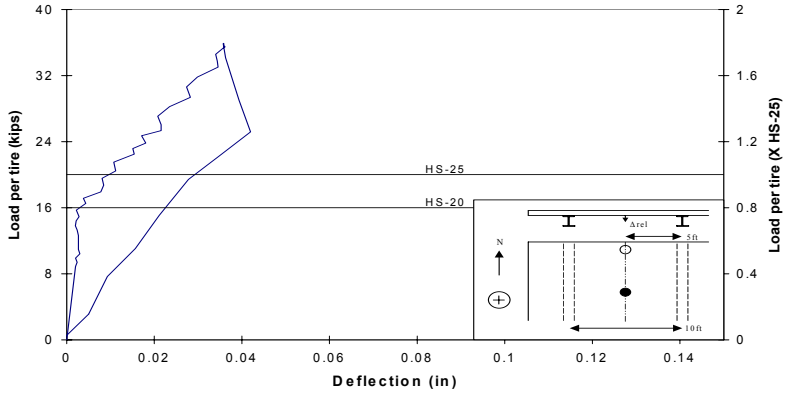

(iii) Truck axle-back

Figure 5-48: Load vs. deflection, 1.75xHS-25 load step, midspan loading location, northwest test area

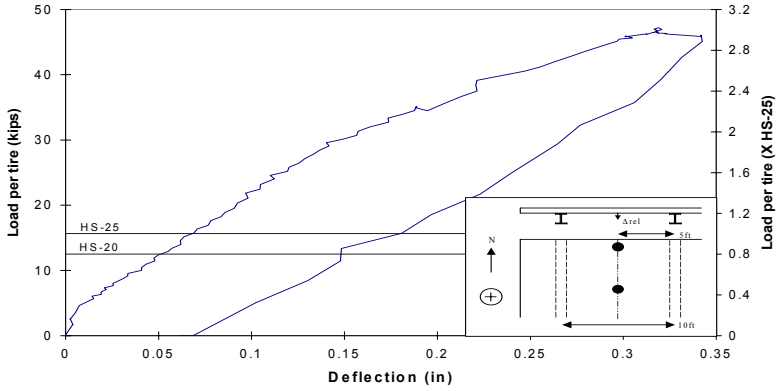

(i) Tandem

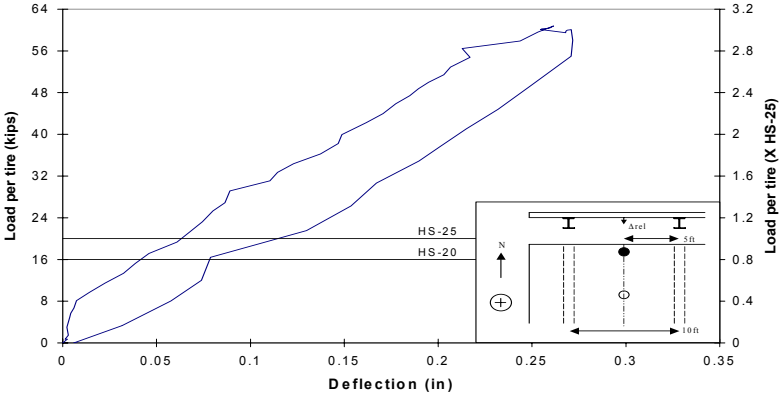

(ii) Truck axle-front

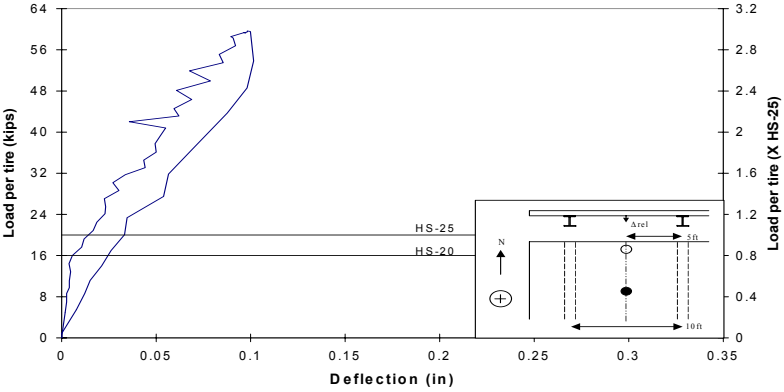

(iii) Truck axle-back

Figure 5-49: Load vs. deflection, 3xHS-25 load step, midspan loading location, northwest test area

back loading configuration created a maximum midspan deflection of approximately 0.1in (Figure 5-49).

5.4.1.5 Loading to failure

Figure 5-50 shows the load versus deflection response of the bridge deck in the northwest test area. The load versus deflection plots for the tandem loading configuration at the design and overload load steps have been included in order to show the full behavior of the slab end detail. On the reloading curve, the bridge deck reached a relative midspan deflection of 0.08in at the HS-25 load level during the loading to failure. This is greater than the relative edge deflection caused by the initial loading to the HS-25 load level, indicating a slight amount of damage was created by the overloads.

The stiffness changes caused by the design loadings and overloads are reflected in the loading to failure plot (Figure 5-50). The envelope of the load versus deflection plots shows a gradual deterioration of the thickened edge, however, four distinct slopes can be discerned shown by the fitted lines. The first stiffness change is small and occurred at an applied load of approximately 11kips (0.7xHS-25) per tire, which is not reflected in the crack maps. However, the second stiffness change is more substantial and occurs at a load of 45kips (2.9xHS-25) per tire. This is verified by the crack map in Figure 5-51 (ii), which show extensive cracking occurred before the 3xHS-25 load step. The stiffness of the bridge deck when the edge tire punched was substantial. The deck reached a maximum relative deflection of 1.17in just prior to failure.

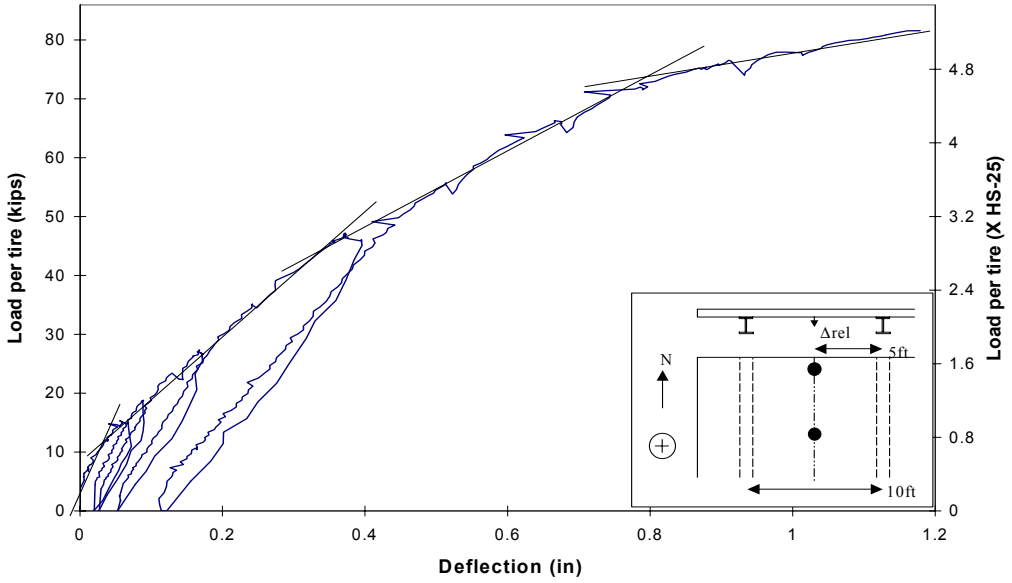

Figure 5-50: Load vs. deflection, loading to failure, midspan loading location, northwest test area

5.4.2 Crack maps

Crack maps for the bottom and side of the bridge deck are included for first cracking (1.2xHS-25), just prior to failure (5.2xHS-25) and an intermediate load step (3xHS-25). First cracking on the top of the deck occurred at a slightly higher load, 1.5xHS-25.

The northwest test area cracked relatively early. At a load of 19kips (1.2xHS-25) per tire, crack B1 had already propagated nearly across the width of the UTSE detail (Figure 5-51, i). However, the crack widths did remain small (0.002in) and they are located on the bottom of the deck where there is less of a corrosion risk. As discussed in section 5.4.1.3, the load versus deflection plot for the tandem loading configuration at the 1.75xHS-25 load step (Figure 5-48) shows a slight stiffness change at a load of approximately 22kips (1.4xHS-25) per

tire. This agrees well with visual observations of cracks, which occurred near midspan at a load of 1.2xHS-25. At failure, there was widespread cracking in the span and the maximum crack width measured was 0.04in.

Figure 5-52 shows crack maps for the top of the bridge deck during the northwest load tests. First cracking occurred slightly later on the top of the deck (1.5xHS-25) than on the bottom (1.2xHS-25). The first crack on the top of the deck (T1) formed at the centerline of the girder and then branched to the edge of the flange. At failure, there were a total of six cracks, however, the cracks were small in width (maximum crack width was 0.005in). At a load of 19kips (1.2xHS-25), the cracks at the bottom of the deck could be observed at the side as well. The visual observations conducted at the side of the deck indicated that cracking was centered under the loading plate and curved towards the plate near failure (Figure 5-53, iii). Just prior to failure, the cracks at the bottom of the deck near midspan were relatively wide, whereas the cracks at the top of the deck were much smaller in width.

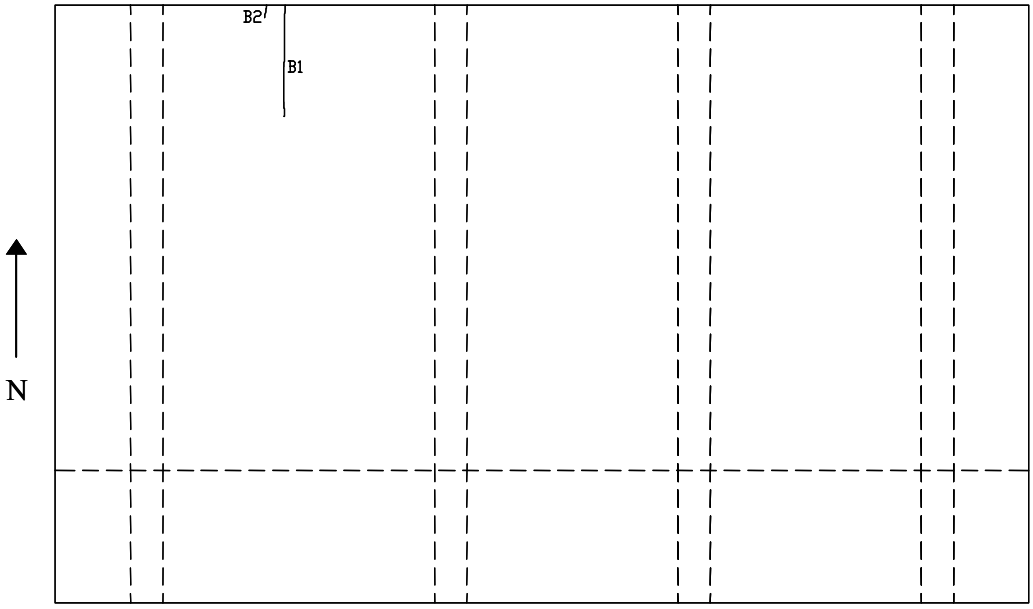

(i)1.2xHS-25 applied load (first cracking)

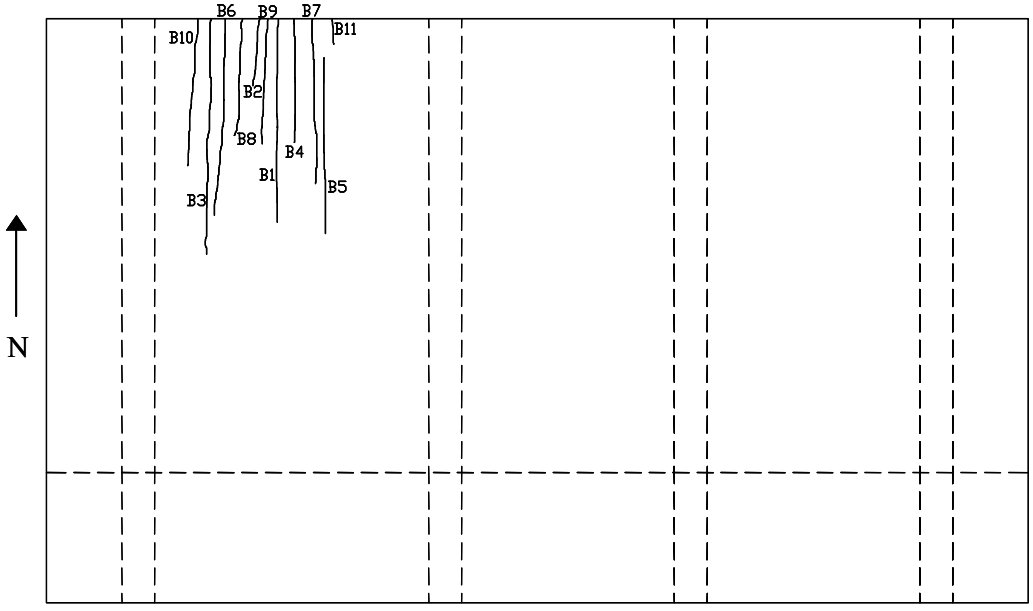

(ii)3xHS-25 load step
**Reference (iv) for crack widths and lengths*

Figure 5-51: Crack maps for the bottom of the bridge deck

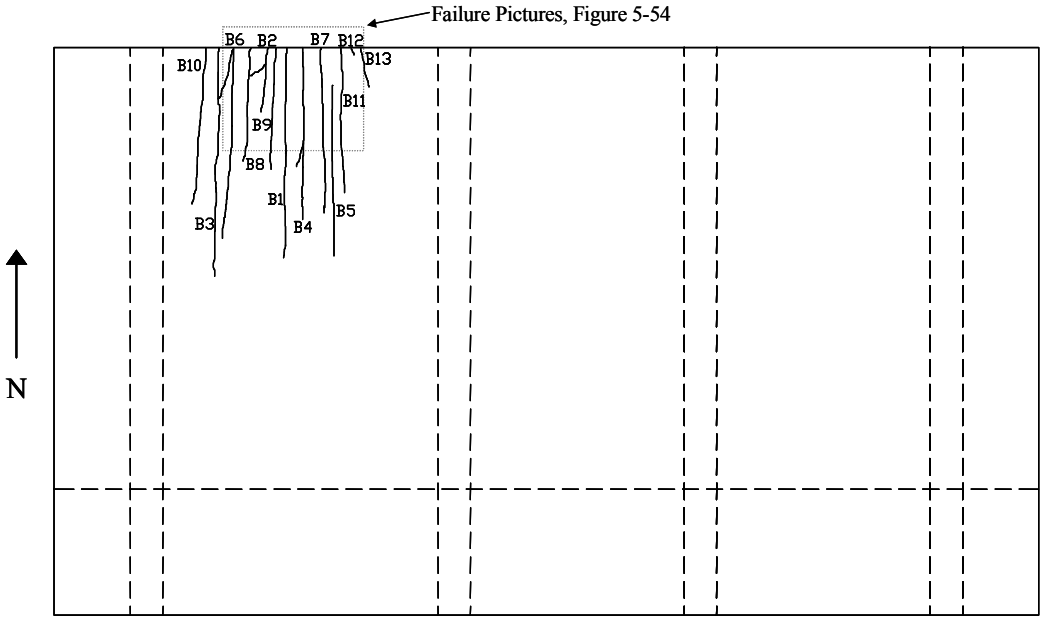

(iii)5.2xHS-25 load step (failure)

Load=1.2xHS-25			Load=3xHS-25			Load=5.2xHS-25		
Crack Name	Width (in)	Length (in)	Crack Name	Width (in)	Length (in)	Crack Name	Width (in)	Length (in)
B1	0.002	40	B1	0.007	85	B1	0.04	74
B2	H	5	B2	0.002	68	B2	0.005	68
			B3	H	87	B3	0.004	87
			B4	0.005	45	B4	0.015	65
			B5	0.004	64	B5	0.01	64
			B6	H	72	B6	0.004	72
			B7	0.004	60	B7	0.008	62
			B8	0.002	41	B8	0.005	41
			B9	0.003	46	B9	0.01	46
			B10	H	54	B10	0.005	59
			B11	0.003	9	B11	0.006	55
						B12	0.006	3
						B13	0.002	15

(iv)Key of widths and lengths of cracks for i, ii and iii

*H = hairline crack, parenthesis measurement refers to the branch of crack B1

Figure 5-51, cont'd: Crack map and key for the bottom of the bridge deck

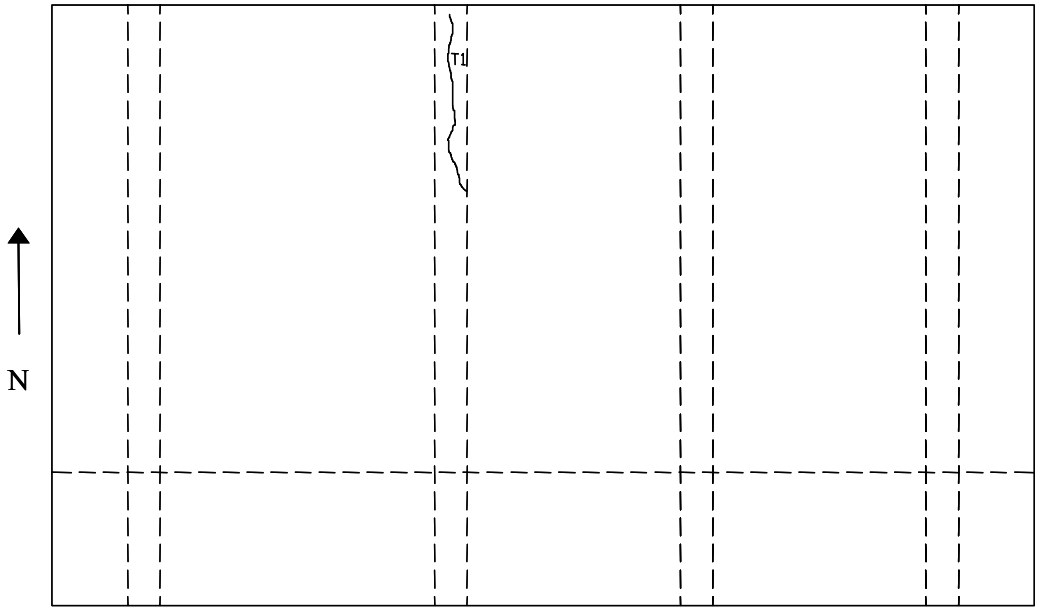

(i)1.5xHS-25 applied load (first cracking)

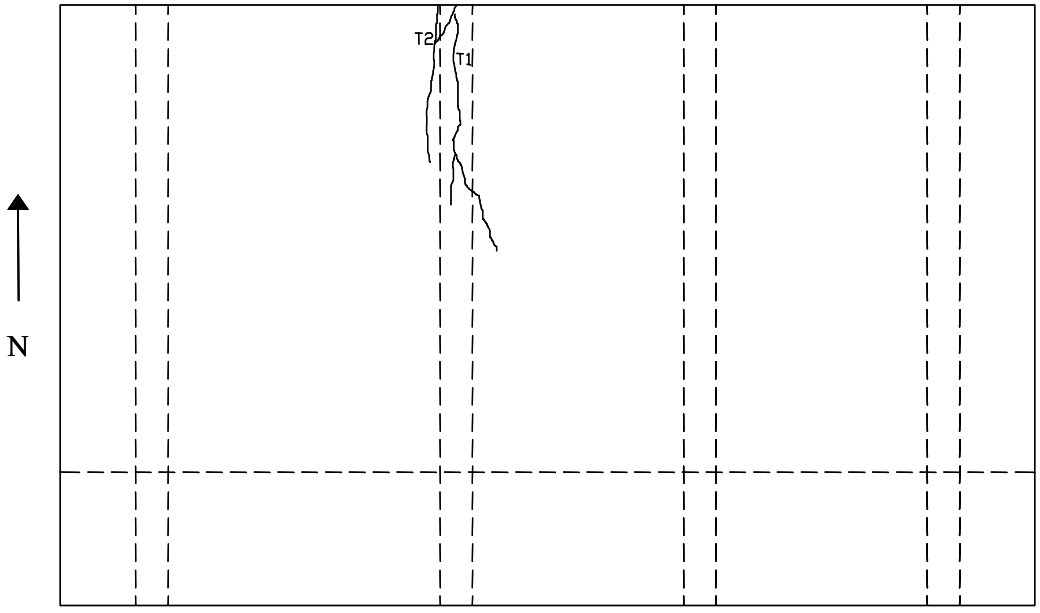

(ii)3xHS-25 load step
**Reference (iv) for crack widths and lengths*

Figure 5-52: Crack maps for the top of the bridge deck

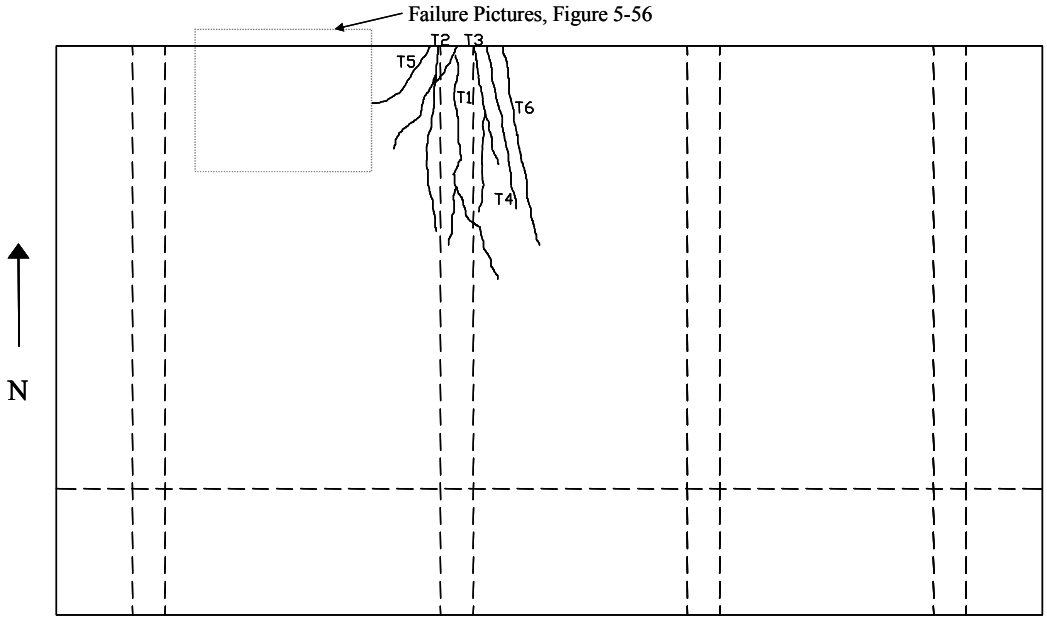

(iii)5.2xHS-25 load step (failure)

Load=1.5xHS-25			Load=3xHS-25			Load=5.2xHS-25		
Crack Name	Width (in)	Length (in)	Crack Name	Width (in)	Length (in)	Crack Name	Width (in)	Length (in)
T1	H	63	T1	0.003	87 (21)	T1	0.005	87 (24)
			T2	0.002	48	T2	0.004	58
						T3	0.004	36
						T4	0.004	62
						T5	0.004	32
						T6	0.004	77

(iv)Key of crack widths and lengths for i, ii and iii

*H = hairline crack, parenthesis measurement refers to the branch of T1

Figure 5-52, cont'd: Crack map and key for the top of the bridge deck

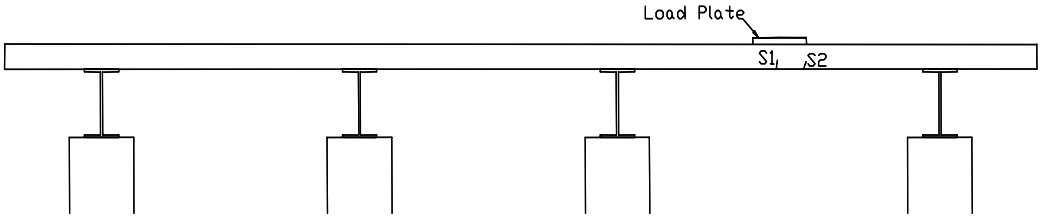

(i)1.2xHS-25 applied load (first cracking)

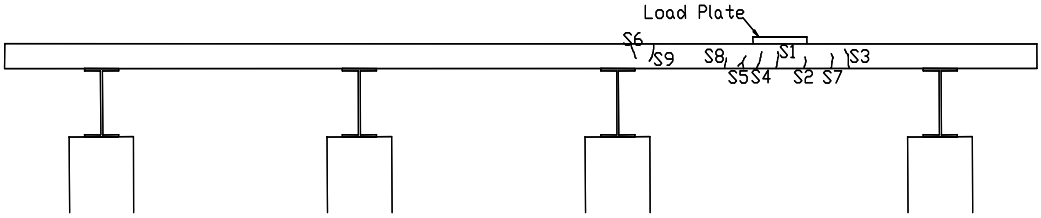

(ii)3xHS-25 load step

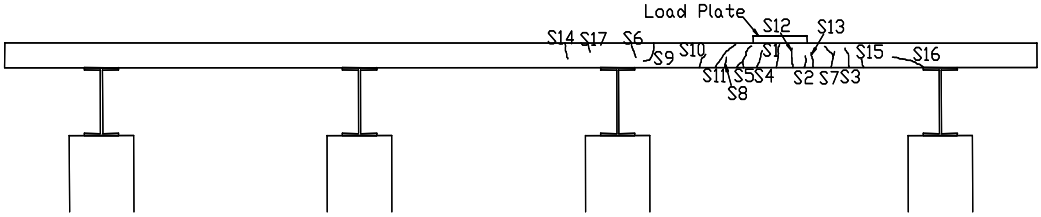

(iii)5.2xHS-25 load step (failure)

Load=1.2xHS-25			Load=3xHS-25			Load=5.2xHS-25		
Crack Name	Width (in)	Length (in)	Crack Name	Width (in)	Length (in)	Crack Name	Width (in)	Length (in)
S1	0.002	3	S1	0.006	5.5	S1	0.03	7.5
S2	H	2.5	S2	0.003	3.5	S2	0.005	3.5
			S3	0.003	4	S3	0.004	4
			S4	0.005	5.5	S4	0.006	5.5
			S5	0.006	2	S5	0.004	9
			S6	0.002	5	S6	0.006	5
			S7	0.003	5	S7	0.004	7
			S8	0.002	3	S8	0.005	3
			S9	H	5.5	S9	0.005	7.5
						S10	0.005	5
						S11	0.01	14
						S12	0.01	6
						S13	0.008	4
						S14	0.005	4
						S15	0.005	2
						S16	0.005	8
						S17	H	3

(iv) Key of crack widths and lengths for i, ii and iii

*H = hairline crack

Figure 5-53: Crack map and key for the side of the deck

5.4.3 Failure Pictures

The northwest test area failed due to punching of the edge tire at a load of 81kips (5.2xHS-25 or 6.5xHS-20) per tire. Figure 5-54 shows the underside of the bridge deck and the extent of the failure surface. The bottom surface of the punching cone was similar to the ones observed in other test areas in that it ran parallel to the edge of the deck near midspan and curved toward the deck edge at the girders. Inclined shear cracks on both sides of the loading plate can be seen in Figure 5-55. Some of the wide shear cracks on the west side of the load plate extended to the girder flange. On the east side, however, the shear cracks formed at a steeper angle and did not reach the girder. Some of the shear cracks that are mapped in Figure 5-53 (iii) widened and contributed to the formation of the punching cone at failure. The failure surface on the top of the deck followed the back of the loading plate on the south side and moved slightly away from the sides of the loading plate towards the edge (Figure 5-56). In addition, wide cracks encircling the load plate formed at failure.

Figure 5-54: Northwest test area failure at bottom of deck, facing north

Figure 5-55: Northwest test area failure picture at side of deck, facing south

Figure 5-56: Northwest test area failure at top of deck, facing north

5.4.4 Northwest test area summary

The positive bending behavior of the UTSE detail, spanning 10ft, was evaluated in the northwest test area. The bridge deck was loaded at midspan, as in the southwest test area. In addition, the 15in by 20in loading plates were used. The tandem, truck axle-front and truck axle-back loading configurations were applied at the HS-25, 1.2xHS-25, 1.75xHS-25 and 3xHS-25 load steps. The bridge deck was subsequently loaded to failure in the tandem loading configuration. Load versus deflection plots, crack maps and failure pictures for the northeast test area are discussed in this section.

First cracking in the northwest test area occurred at the bottom and side of the bridge deck at the 1.2xHS-25 load step. The top of the bridge deck cracked slightly later, at an applied load of 1.5xHS-25. This test area had a low cracking load in relation to the design loadings. The crack at the top of the deck may be of concern since corrosion of the reinforcing steel could potentially be more critical at the top. There was a significant amount of cracking at failure; however, the crack widths were small at the support.

The relative midspan deflection at failure of the northwest test area was 1.05in. The edge deflection for this test area was large because it contained the UTSE detail, which was 8in thick and spanned 10ft. Even though the deflections were noticeable and numerous flexural cracks formed, the bridge deck did not fail in flexure.

The northwest test area failed in punching shear at the edge tire under an applied load of 82kips (5.2xHS-25) per tire. The test area had a large reserve strength compared to the design loadings, however, the failure mechanism was non-ductile. The northwest test area performed well in relation to ultimate capacity, however, early cracking may not be desirable for serviceability requirements of the bridge deck.

5.5 NORTHEAST TEST AREA

The northeast test area containing the UTSE detail, spanning eight-feet, was the final area tested. As in the southeast test area, 10in by 20in load plates were used to apply loads to the bridge deck. The test area was first loaded to maximize positive moment at the HS-25 load level, and then, the load frame was shifted to maximize negative moment. In this way, behavior of this test area could be compared to that of the southeast test area (i.e. the performance of the IBTS detail can be compared to that of the UTSE detail). At the location to maximize negative moment, the deck was loaded to the same design loads and overloads as the southeast test area (HS-25, 1.2xHS-25 and 1.75xHS-25). In addition, the three loading configurations were applied at the 3xHS-25 load step. Then, the bridge deck was loaded to failure in the tandem loading configuration.

Table 5-4 shows a summary of the loadings applied to the northeast test area. The NB81bu+ strain gauge and the linear potentiometer at the edge were monitored during loading. Load versus relative deflection, crack maps, failure pictures, load versus strain and strain profiles are presented for this test area.

5.5.1 Loading to maximize positive moment

The performance of the IBTS and UTSE details in negative bending was the primary objective of all the tests performed in the southeast and northeast test areas. However, positive bending tests were also performed at the HS-25 load level in the southeast test area. Due to hydraulic pressure conversion problems, the loads to maximize positive moment were applied at the 0.5xHS-25 load level in this test area.

Table 5-4: Order of testing in northeast test area

Test No.	Loading Location	Load Type Tandem/Truck	Which axle?	Load per tire (kips)	Load per tire (xHS-25)
1	Positive	Tandem	Both	7.8	0.5
2	Positive	Truck	Front	10.0	0.5
3	Positive	Truck	Back	10.0	0.5
4	Negative	Tandem	Both	15.6	1
5	Negative	Truck	Front	20.0	1
6	Negative	Truck	Back	20.0	1
7	Negative	Tandem	Both	18.8	1.2
8	Negative	Truck	Front	24.0	1.2
9	Negative	Truck	Back	24.0	1.2
10	Negative	Tandem	Both	27.3	1.75
11	Negative	Truck	Front	35.0	1.75
12	Negative	Truck	Back	35.0	1.75
13	Negative	Tandem	Both	46.9	3
14	Negative	Tandem	Front	60.0	3
15	Negative	Tandem	Back	60.0	3
16*	Negative	Tandem	Both	76.6	4.9
17**	Negative	Tandem	Both	81.5	5.2

*Punching of edge tire in exterior span; **Punching of edge tire in interior span

5.5.1.1 Load vs. deflection response

The load versus deflection plots for the 0.5xHS-25 load step at the positive loading location are not presented herein as the deformation measurements compared to the noise levels. The largest relative deflection measured was 0.005in.

5.5.1.2 Load vs. strain response

All measured strains were small. The tandem loading configuration was the first loading applied to the deck. When the maximum load was held constant, very small (approximately 20με) creep deformations were recorded for one of the

gauges. This is due to microcracking in the concrete occurring around the rebar. The UTSE detail behaved linearly under all the truck loading configurations.

The maximum strain measured at this load step was 80με (4% of yield strain of the steel) at the positive moment section during application of the tandem loading configuration (Figure 5-57, i). The truck axle-front loading configuration caused strains that were comparable to strains from the tandem loading configuration. The strains caused by the truck axle-back loading configuration were about 40% of the strains created by the tandem loading configuration. At the negative moment section, the strain readings were less than 10με in all cases.

5.5.1.3 Strain profiles

Figure 5-58 shows strain profiles for the 0.5xHS-25 load step in the location to maximize positive moment. As shown in the load versus strain plots, the strain magnitudes at the negative moment section are very small relative to the positive section. The largest strain at the negative moment section is 10με, caused by the truck axle-front loading configuration (Figure 5-58, iv). All strains measured at this load step were very small compared to the yield strain of the rebar.

At the positive moment section, the location of the tire loads for the different loading configurations can be inferred from the strain gradient in the profiles. The tandem loading configuration created a uniform strain profile whereas the truck axle-back profile has a gradient with increasing strains going into the deck. Likewise, the truck axle-front loading configuration has a strain gradient that reduces going into the deck as it has tire loads at the edge of the deck.

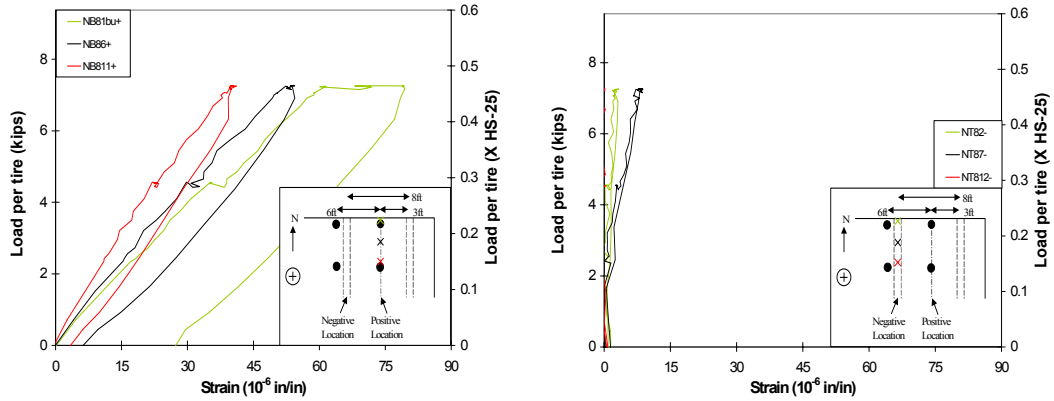

(i) Tandem

(ii) Tandem

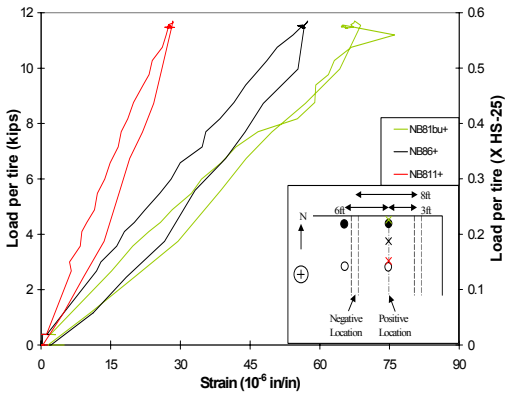

(iii) Truck axle-front

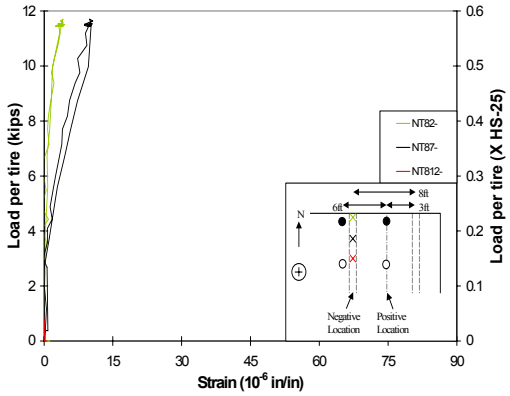

(iv) Truck axle-front

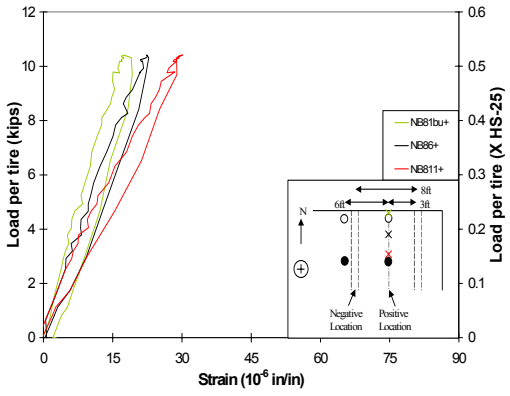

(v) Truck axle-back

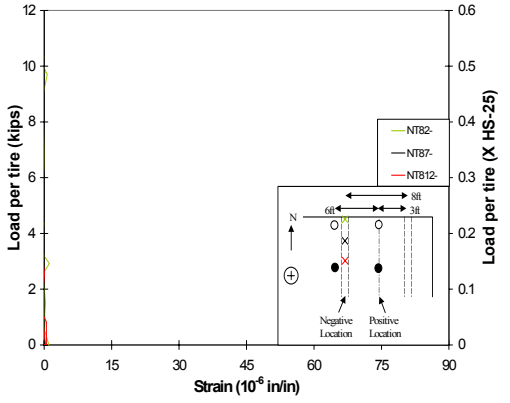

(vi) Truck axle-back

Figure 5-57: Load vs. strain, 0.5xHS-25 load step, positive moment loading, northeast test area; (i), (iii) and (v): bottom mat at positive location; (ii), (iv) and (vi): top mat at negative location

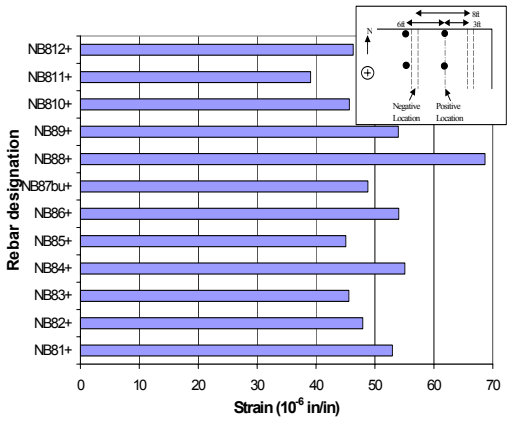

(i) Tandem

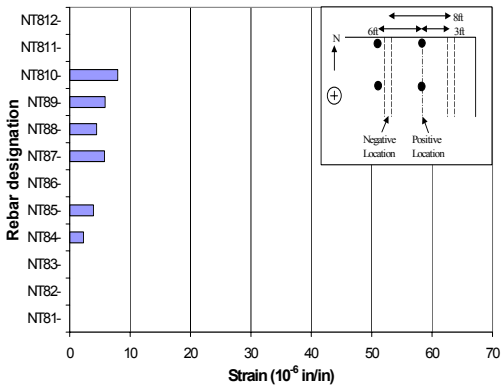

(ii) Tandem

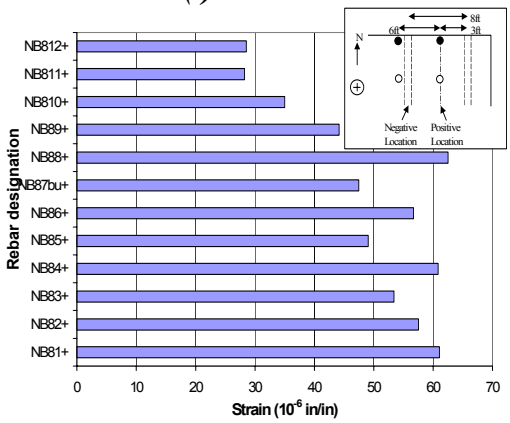

(iii) Truck axle-front

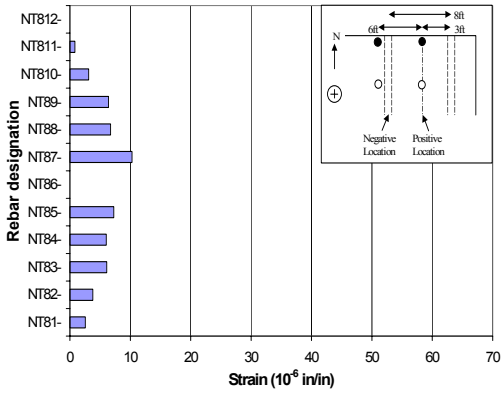

(iv) Truck axle-front

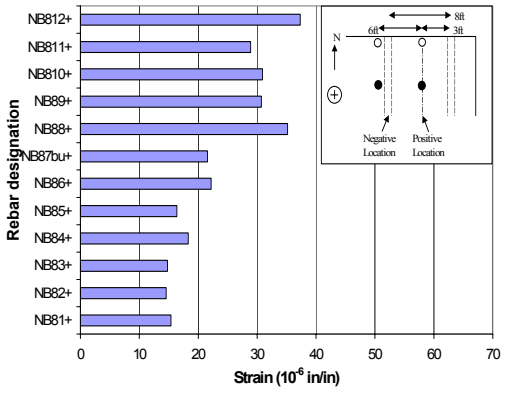

(v) Truck axle-back

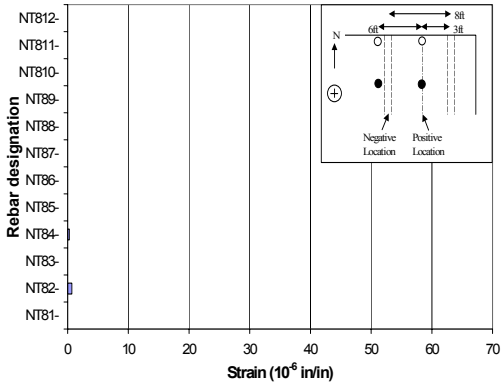

(vi) Truck axle-back

Figure 5-58: Strain profiles, 0.5xHS-25 load step, positive moment loading, northeast test area; (i), (iii) and (v): bottom mat at positive location; (ii), (iv) and (vi): top mat at negative location

5.5.2 Loading to maximize negative moment

The load frame was shifted to the location to maximize negative moment for the design loading, typical overloads and loading to failure. As stated in section 5.2.2, the two loading locations are separated by 21 inches. The loads were applied by hydraulic rams at each load plate. At the location to maximize negative moment, the northeast test area was loaded to design loads (HS-20 and HS-25) and typical overloads (1.2xHS-25, 1.75xHS-25 and 3xHS-25) in the three loading configurations. Then, the bridge was loaded to failure in the tandem loading configuration.

5.5.2.1 Load vs. deflection response

The HS-25 and 1.2xHS-25 load versus deflection plots have not been included herein, as the deflections were very small and compared to the accuracy level of the displacement transducer used.

5.5.2.1.1 1.75xHS-25 load step

The maximum edge deflection at the 1.75xHS-25 load step was 0.05in, created by the tandem loading configuration (Figure 5-59, i). The truck axle-front loading configuration created a very similar relative edge deflection. The truck axle-back loading configuration caused relative deflections that were indistinguishable from the noise in the data (approximately 0.005in) and are not presented herein.

The tandem loading configuration created a non-linearity at the 1.75xHS-25 load level and a residual deflection of 0.06in was recorded after unloading. The overall behavior of the bridge deck at the 1.75xHS-25 load step is essentially linear up until the application of the maximum load. Initiation of cracking was noted on top of the girder and at midspan at the maximum load applied in this

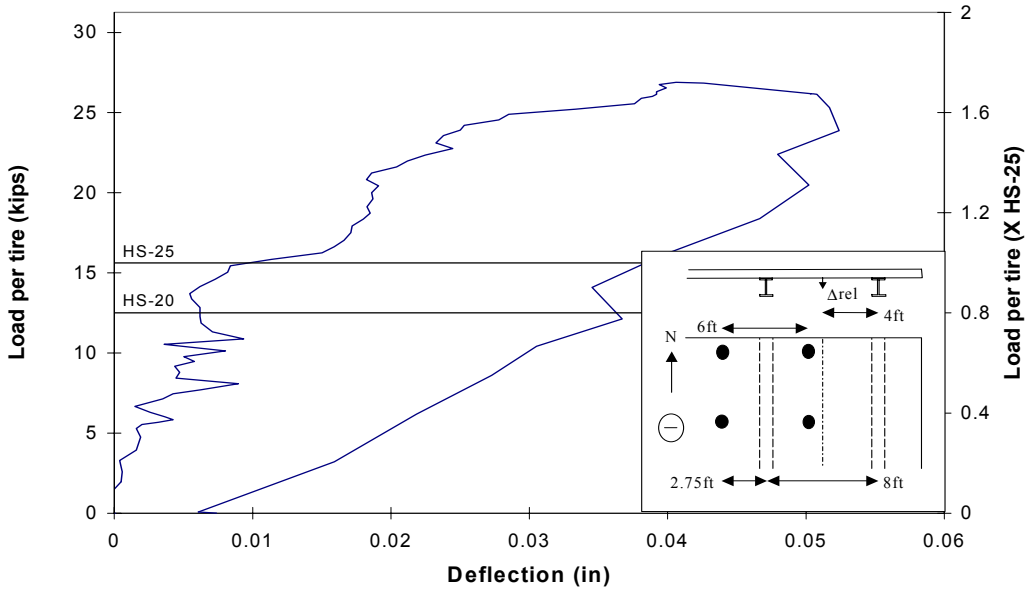

(i) Tandem

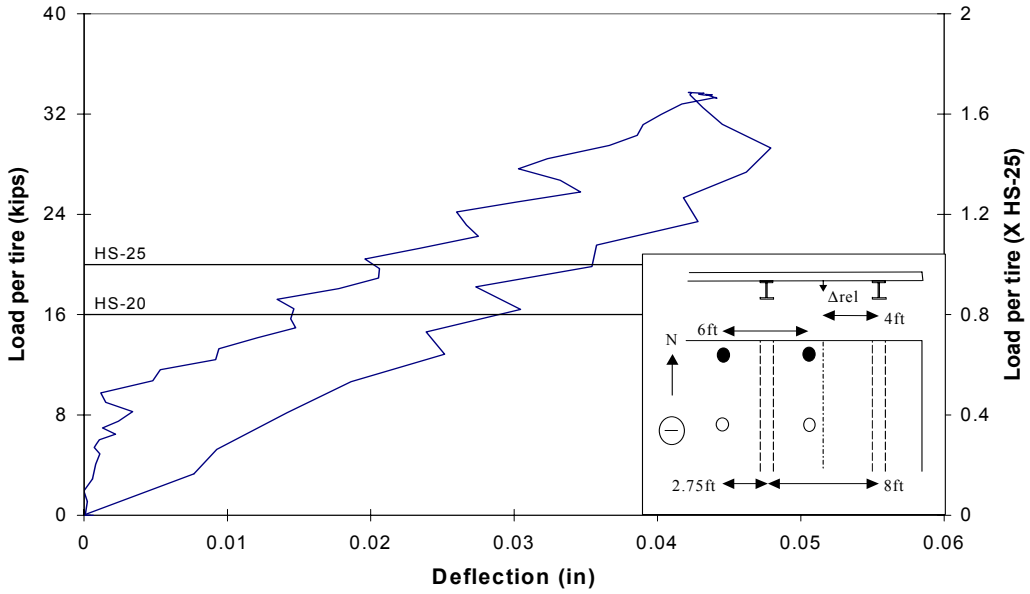

(ii) Truck axle-front

Figure 5-59: Load vs. deflection, 1.75xHS-25 load step, negative moment loading, northeast test area

load step. All relative deflections measured at the 1.75xHS-25 load step are small relative to the eight-foot span.

5.5.2.1.2 3xHS-25 load step

Figure 5-60 shows plots for the three loading configurations applied at the 300% overload level. The load versus deflection plot for the tandem loading configuration has two distinct slopes with an abrupt change in stiffness at approximately 30kips (1.9xHS-25) per tire. The residual deflection caused by this non-linearity was four times that of the residual deflection measured at the 1.75xHS-25 load step. The crack maps (i.e. visual observations) substantiate this stiffness change, as cracks near midspan initiate at the 1.75xHS-25 load step (a few hairline cracks) and extend across the UTSE detail by the 3xHS-25 load step.

At the 3xHS-25 load step, the maximum relative deflection of 0.13in was caused by the truck axle-front loading configuration. The maximum relative deflection caused by the tandem loading configuration (0.12in) was slightly less than this. The deflections measured at the 3xHS-25 load step increased approximately 100% compared to the 1.75xHS-25 load step while the load increased 70%. This indicates the test area deteriorated somewhat by the 3xHS-25 load application. However, the UTSE detail was still relatively undamaged after the 3xHS-25 load step.

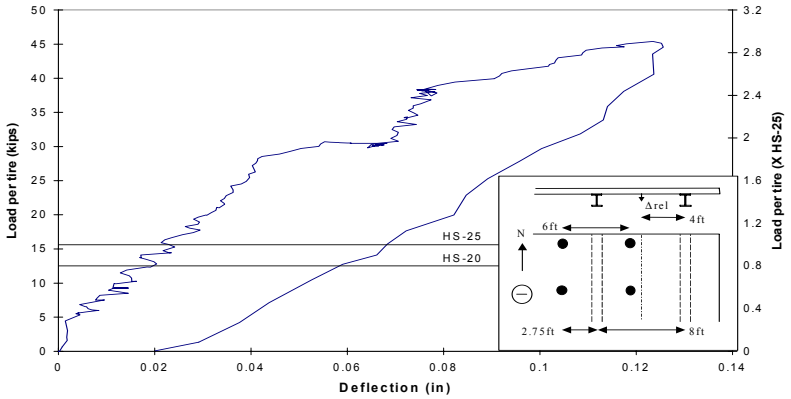

(i) Tandem

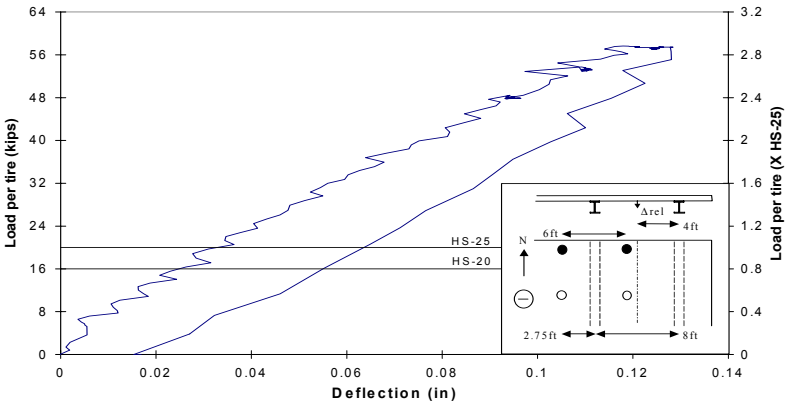

(ii) Truck axle-front

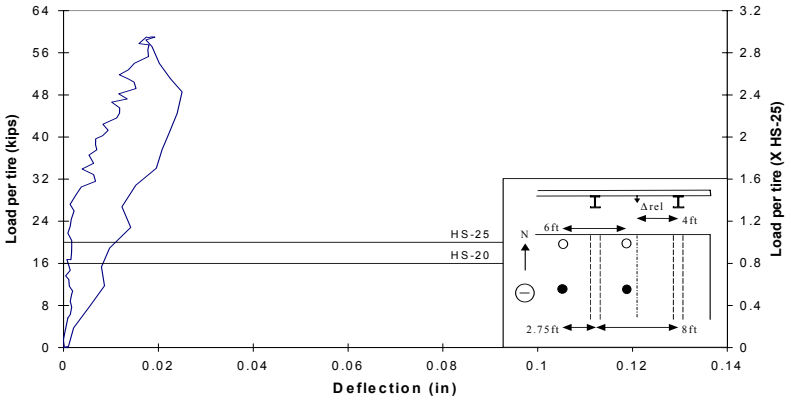

(iii) Truck axle-back

Figure 5-60: Load vs. deflection, 3xHS-25 load step, negative moment loading, northeast test area

5.5.2.1.3 Loading to failure

Figure 5-61 shows the load versus deflection response of the bridge deck when loading to failure as well as the response to the 1.75xHS-25 and 3xHS-25 load steps. During loading to failure, at the HS-25 load level, the relative deflection was approximately 0.03in if the residual deflections caused by the previous loadings are ignored. The relative deflection during the 3xHS-25 load step, at the HS-25 load level, was about 0.02in. This shows that some deterioration occurred within the UTSE detail during the 300% overload. In addition, small residual deflections were created by the 3xHS-25 load step.

On the reloading portion of the loading to failure curve the slab end detail behaved linearly up to a load of approximately 28kips (1.8xHS-25), then, its stiffness abruptly reduced. This agrees with the crack maps in Figure 5-62, which show cracks formed in the exterior span at the 1.75xHS-25 load step. The envelope curve in Figure 5-61 clearly indicates cracking and yielding points as well. Just prior to failure of the test area, the stiffness of the deck had reduced significantly. The ultimate relative deflection of the northeast test area was 0.36in.

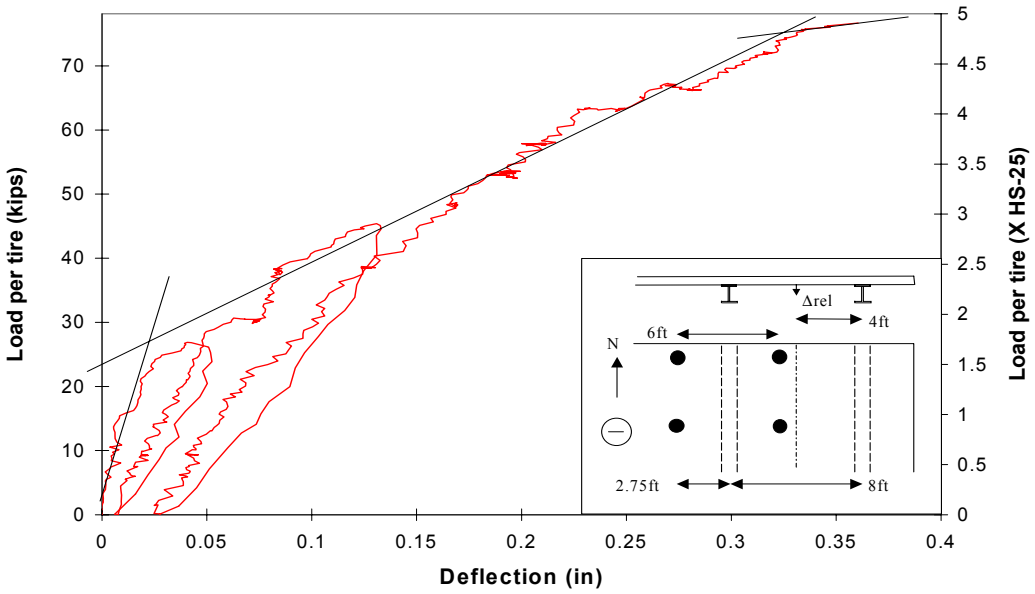

Figure 5-61: Load vs. deflection, loading to failure, negative moment loading, northeast test area

5.5.2.2 Crack maps

First cracking in the northeast test area occurred at a load of 1.75xHS-25. At this load step, the hairline cracks were 2-14in long (Figure 5-62, i). However, by the 3xHS-25 load step (Figure 5-62, ii), the cracks opened wider and extended across the slab end detail. The change of slope in the load versus deflection plots (Figure 5-61) for these load steps agrees with the crack maps. By the 3xHS-25 load step, cracks had formed in both the interior and exterior spans. Just prior to failure, the cracks on the bottom of the deck elongated substantially, reaching the midpoint of the bridge longitudinally (Figure 5-62, iii). The crack widths remained relatively small at failure of the test area.

First cracking on the top of the bridge deck occurred at the 1.75xHS-25 load step, as on the bottom of the deck (Figure 5-63, i). The top cracks initially

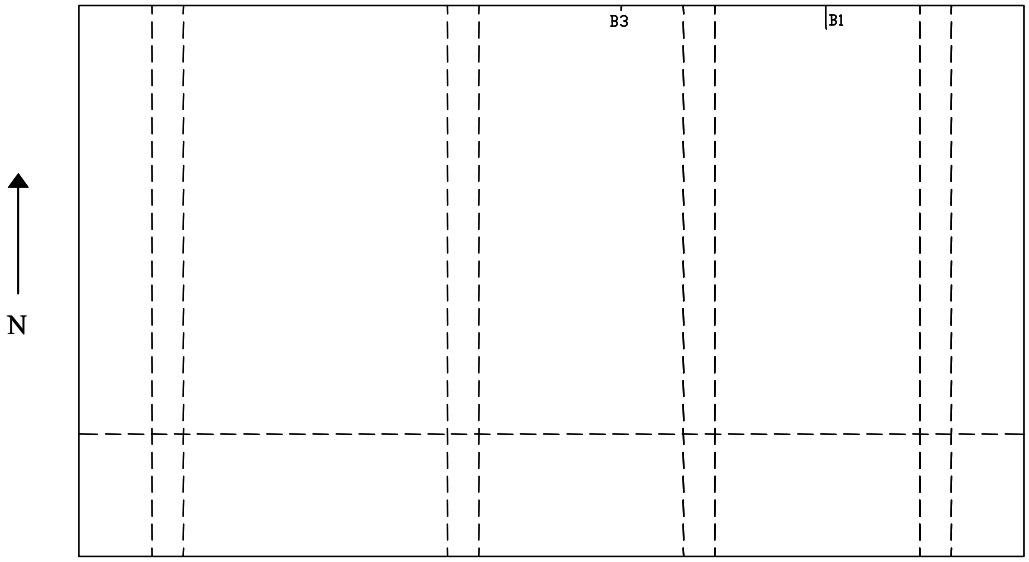

(i)1.75xHS-25 load step (first cracking)

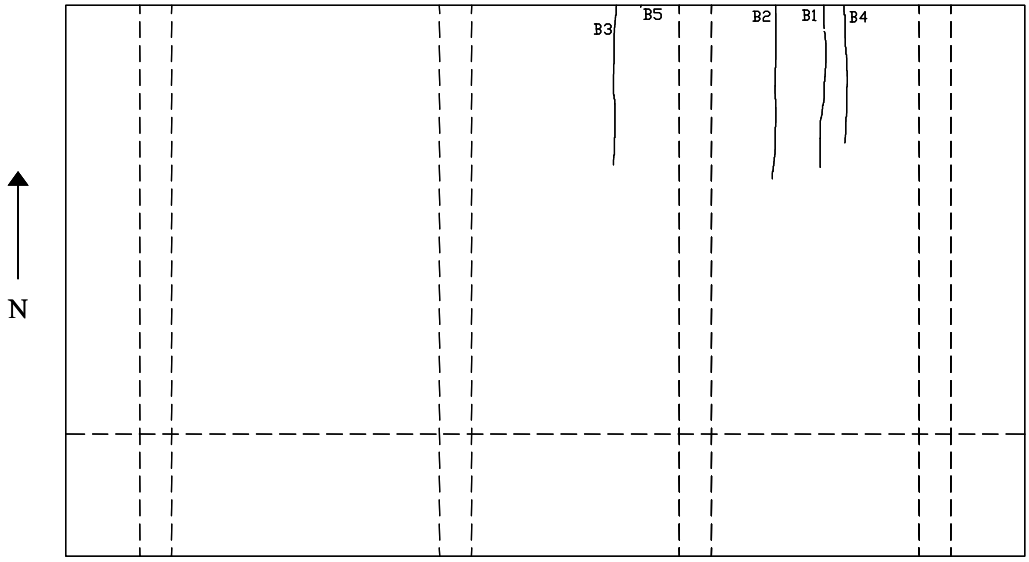

(ii)3xHS-25 load step
**Reference (iv) for crack widths and lengths*

Figure 5-62: Crack maps for the bottom of the bridge deck

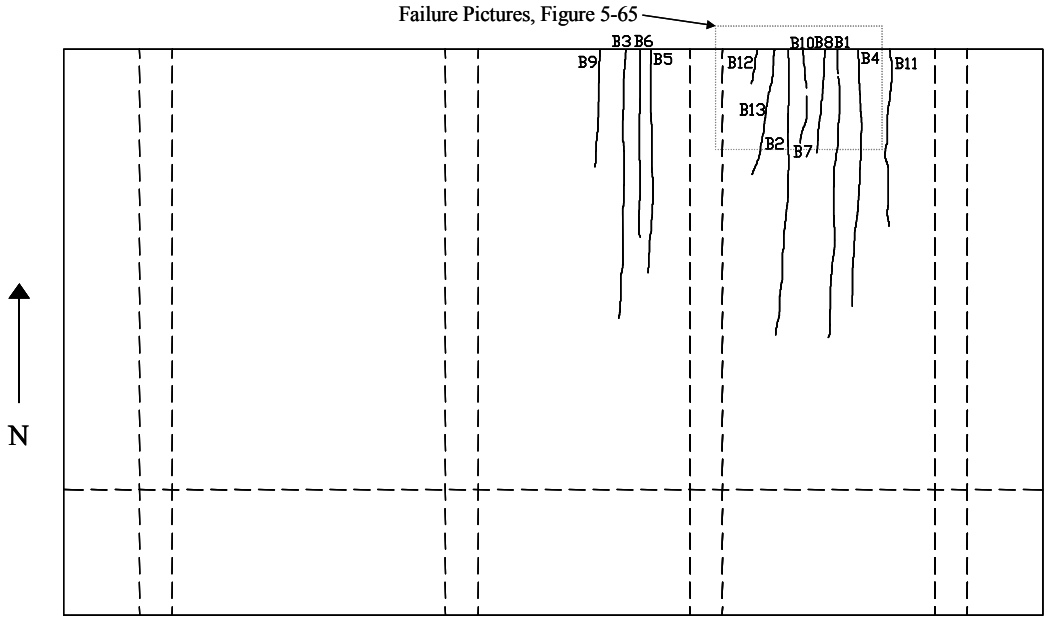

(iii)4.9xHS-25 load step (failure)

Load=1.75xHS-25			Load=3xHS-25			Load=4.9xHS-25		
Crack Name	Width (in)	Length (in)	Crack Name	Width (in)	Length (in)	Crack Name	Width (in)	Length (in)
B1	H	11	B1	0.004	63	B1	0.005	110
B3	H	2	B2	0.002	68	B2	0.003	108
			B3	0.003	62	B3	0.005	102
			B4	0.003	54	B4	0.004	98
			B5	H	1	B5	0.003	85
						B6	0.003	71
						B7	H	12
						B8	H	38
						B9	0.002	44
						B10	0.003	14
						B11	H	65
						B12	0.004	12
						B13	H	56

(iv)Key of crack widths and lengths for i, ii and iii
*H = hairline crack

Figure 5-62, cont'd: Crack map and key for the bottom of the bridge deck

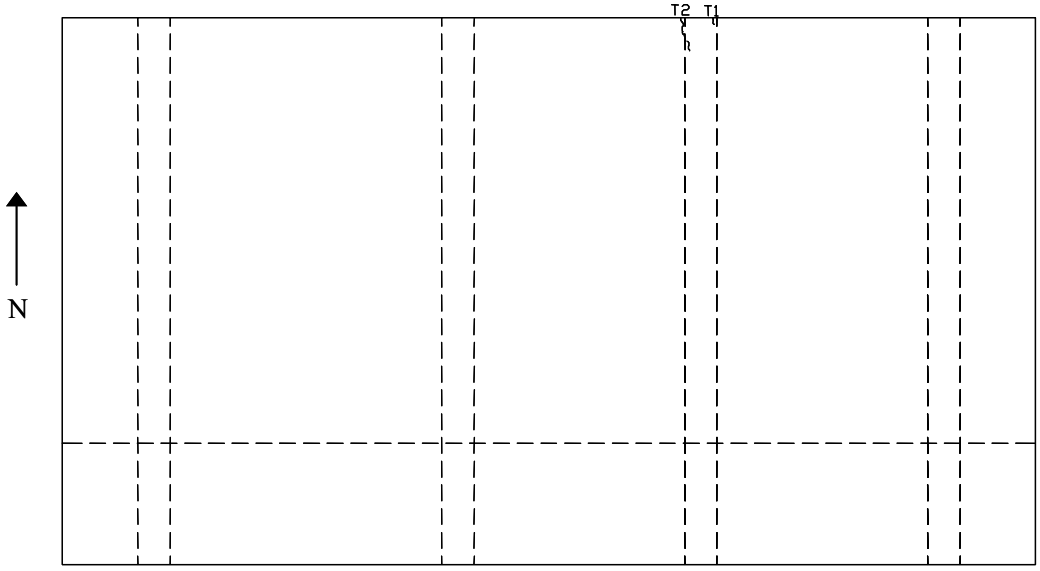

(i)1.75xHS-25 load step (first cracking)

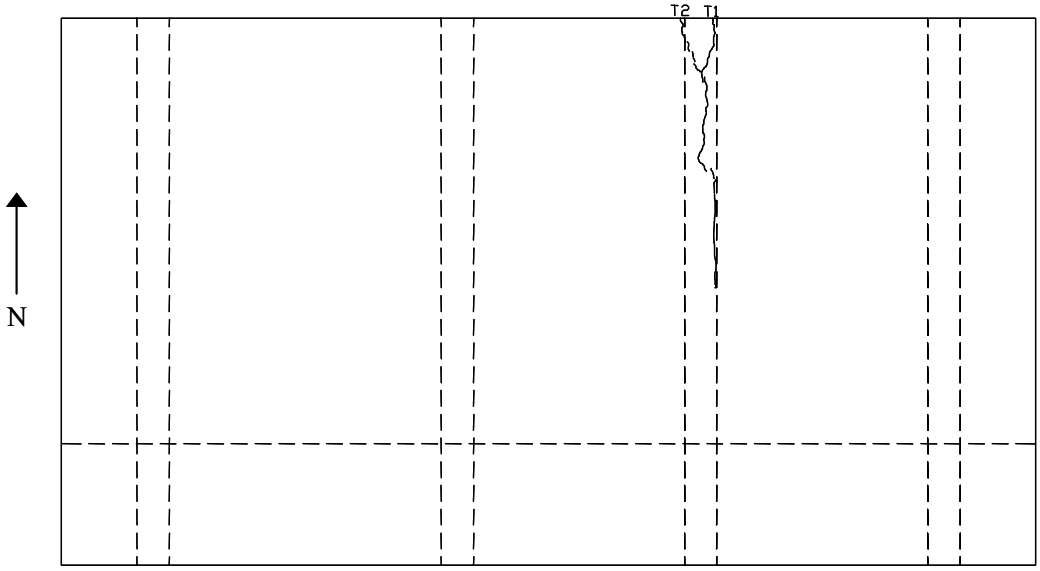

(ii)3xHS-25 load step
**Reference (iv) for crack widths and lengths*

Figure 5-63: Crack maps for the top of the bridge deck

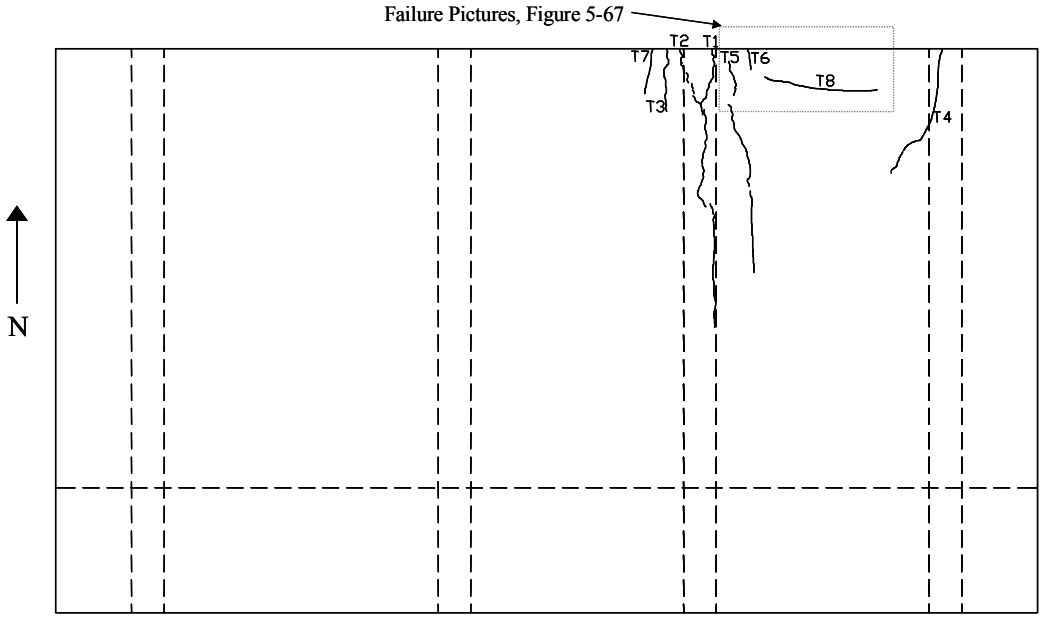

(iii)4.9xHS-25 load step (failure)

Load=1.75xHS-25			Load=3xHS-25			Load=4.9xHS-25		
Crack Name	Width (in)	Length (in)	Crack Name	Width (in)	Length (in)	Crack Name	Width (in)	Length (in)
T1	H	3	T1-T2	0.003	108 (21)	T1-T2	0.009	108 (21)
T2	H	13.5				T3	0.008	23
						T4	0.004	52
						T5	0.003	81
						T6	0.002	6
						T7	H	16
						T8	0.002	48

(iv)Key of widths and lengths for i, ii and iii

*H = hairline crack, parenthesis measurement refers to branch in crack T1-T2

Figure 5-63, cont'd: Crack map and key for the top of the bridge deck

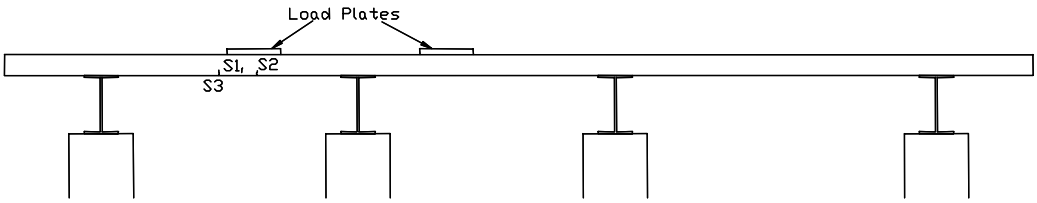

(i)1.75xHS-25 load step (first cracking)

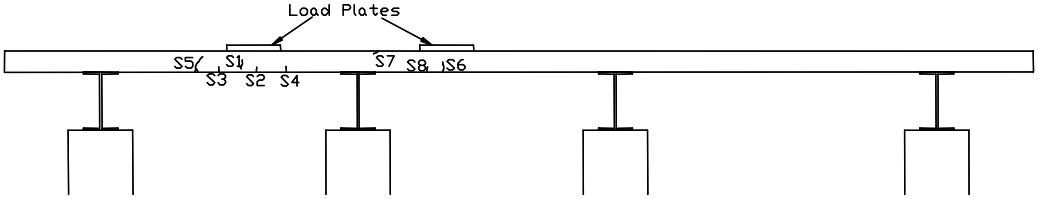

(ii)3xHS-25 load step

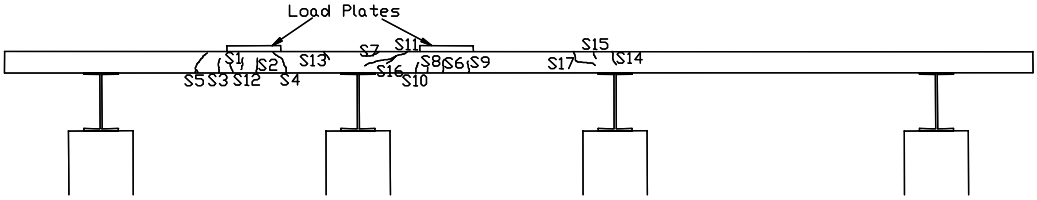

(iii)4.9xHS-25 load step (failure)

Load=1.75xHS-25			Load=3xHS-25			Load=4.9xHS-25		
Crack Name	Width (in)	Length (in)	Crack Name	Width (in)	Length (in)	Crack Name	Width (in)	Length (in)
S1	H	2	S1	0.005	4	S1	0.006	5
S2	H	1.5	S2	0.002	1.5	S2	0.005	5.5
S3	H	2	S3	0.004	2	S3	0.005	5
			S4	H	2	S4	0.009	9
			S5	0.003	7	S5	0.006	9
			S6	H	3	S6	0.004	4.5
			S7	H	2	S7	0.004	4
			S8	H	2	S8	0.004	2
						S9	0.004	3
						S10	0.003	3
						S11	0.003	5.5
						S12	0.003	3
						S13	H	4
						S14	H	2.5
						S15	H	1.5
						S16	0.01	11.5
						S17	0.002	6

(iv)Key of crack widths and lengths of for i, ii and iii

*H = hairline crack

Figure 5-64: Crack map and key for the side of the bridge deck

formed at the edges of the flange of the interior girder. Under increased load, they branched together and followed the girder. Top cracks also formed over the exterior girder near failure. Immediately before failure, crack T8 formed around the load plate, signaling imminent punching of this tire (Figure 5-63, iii). Cracks T1-T2 and T3 were the widest cracks on the bridge deck at failure.

The side of the deck showed cracking in the exterior span at the 1.75xHS-25 load step. Cracks were visible over the girder at the 3xHS-25 load step (Figure 5-64, ii). At failure of the test area, cracks (S14, S15 and S17) had formed over the third girder from the east side of the bridge as well (Figure 5-64, iii). The cracks observed on the side of the bridge deck, underneath the load plates, were similar in length at failure. However, the widths of the cracks under the load plate in the exterior span were larger.

5.5.2.3 Failure pictures

The northeast test area failed in punching shear at the edge-most tire in the exterior span at an applied load of 76kips (4.9xHS-25) per tire. The bridge deck specimen contained voids at the bottom of the deck in the exterior span due to insufficient vibration of the concrete during casting. Grout was injected into the voids as shown in Figure 5-65. The voids caused little difference in the flexural behavior of the specimen as they were in the tensile zone of the section. In addition, the voids did not affect the punching shear capacity significantly. However, it is believed that the concrete contribution to punching shear strength was slightly lower in the exterior span in comparison to that in the interior span. Hence, a punching shear failure was experienced in the exterior span. The failure surface again formed parallel to the edge of the deck and curved towards the deck edge near the girders.

Figure 5-65: Exterior span failure at the bottom of the deck

At the side of the deck, the major shear cracks on the west side of the load plate extended to the interior girder (Figure 5-66). The shear cracks on the east side of the load plate opened less and did not reach the exterior girder. The failure surface formed where no previous shear cracks had occurred. The failure surface at the top of the bridge deck formed flush along the interior edge of the load plate (Figure 5-67). Wedges of concrete at the sides of the load plate broke away.

Figure 5-66: Exterior span failure at the side of the deck, interior span, facing south

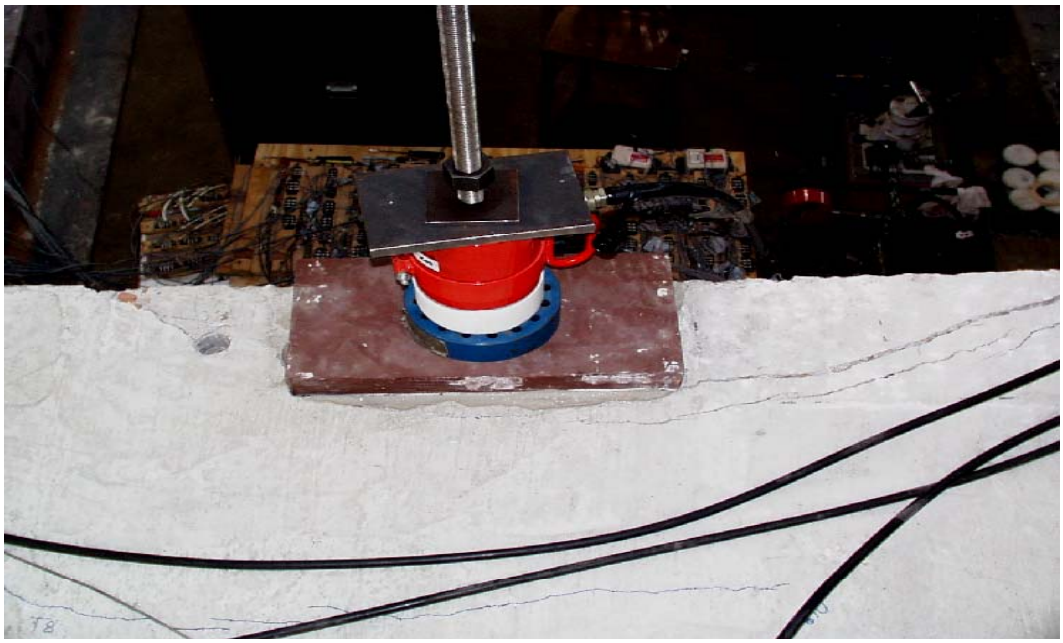

Figure 5-67: Exterior span failure at the top of the deck

5.5.2.4 Load vs. strain response

5.5.2.4.1 HS-25 load step

The plot of load versus strain for the tandem and truck axle-front loading configurations at the negative moment section (Figure 5-68, ii and iv) show a change in stiffness during loading to the HS-25 load step. The loading portion of the tandem loading configuration plot shows a slope change at approximately 6kips (0.4xHS-25) per tire, however, the unloading portion of the plot has a steeper slope and ends with virtually zero residual strain. Both the loading and unloading portions of the truck axle-front plot show a gradual stiffness change, recording zero residual strain after the load test. This type of behavior can be classified as nonlinear elastic behavior, likely influenced by the complicated load transfer mechanisms in the connection region.

The maximum strain of 94με (4% of yield strain of the steel) occurred at the negative moment section due to the tandem loading configuration (Figure 5-68, ii). The strain magnitudes caused by the truck axle-front loading configuration were comparable to those from the tandem configuration. The strain magnitudes at the negative moment section are larger than at the positive moment section for the tandem and truck axle-front loading configurations. However, the truck axle-back loading configuration created larger strains at the positive moment section. The largest strain measured during the application of the truck axle-back loading configuration was smaller than 40με.

Typical of load-controlled tests, minor creep deformations were experienced by the deck when the load was held constant at the HS-25 load level. However, all the plots returned to zero residual strain after the load application. The strains created by the HS-25 load step were small in relation to the yield strain of the reinforcing steel.

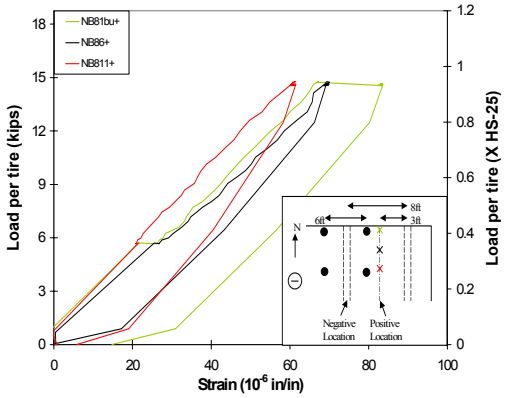

(i) Tandem

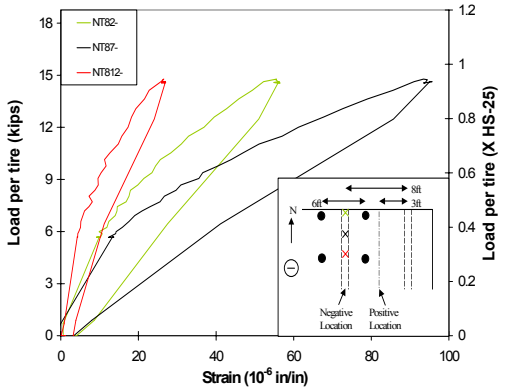

(ii) Tandem

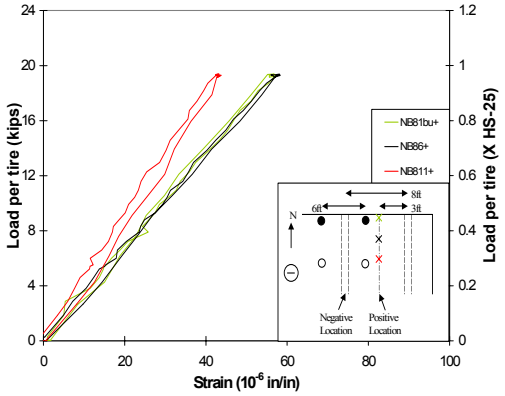

(iii) Truck axle-front

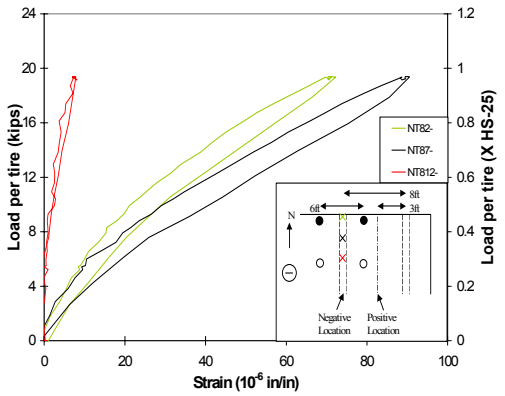

(iv) Truck axle-front

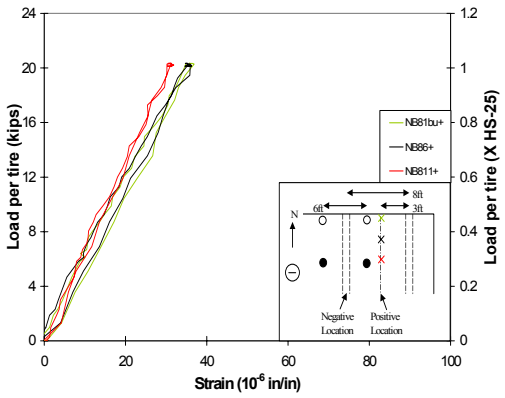

(v) Truck axle-back

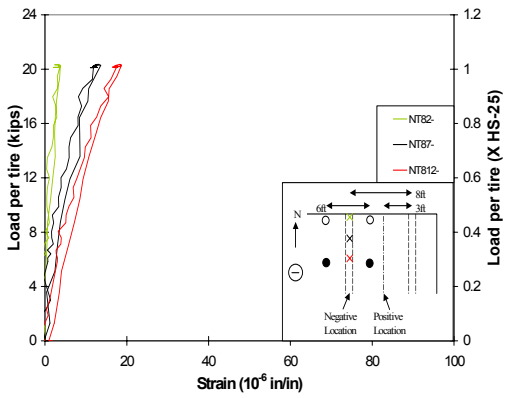

(vi) Truck axle-back

Figure 5-68: Load vs. strain, HS-25 load step, negative moment loading, northeast test area; (i), (iii) and (v): bottom mat at positive location; (ii), (iv) and (vi): top mat at negative location

5.5.2.4.2 1.2xHS-25 load step

At the negative moment section, the load versus strain plots for the tandem and truck axle-front loading configurations again show a change in stiffness during loading, which is also shown in the unloading portion of the plot (Figure 5-69, ii and iv). At the positive moment section, the strain magnitudes increased proportional to the 20% load increase. However, at the negative moment section, the strain magnitudes increased by more than 50%, indicating non-linear behavior in the bridge deck. No residual strains were recorded at this load step. The strains are again larger at the negative moment section than the positive section for the tandem and truck axle-front loading configurations. All load versus strain plots show elastic response to the 20% overload.

At the side of the deck, the major shear cracks on the west side of the load plate extended to the interior girder (Figure 5-66). The shear cracks on the east side of the load plate opened less and did not reach the exterior girder. The failure surface formed where no previous shear cracks had occurred. The failure surface at the top of the bridge deck formed flush along the interior edge of the load plate (Figure 5-67). Wedges of concrete at the sides of the load plate broke away.

5.5.2.4.3 1.75xHS-25 load step

Figure 5-70 shows the load versus strain plots for the three loading configurations applied at the 1.75xHS-25 load step. The strain magnitudes in the negative moment section are significantly larger than those in the positive section. However, at the HS-25 load step, the strains at the two moment sections were comparable.

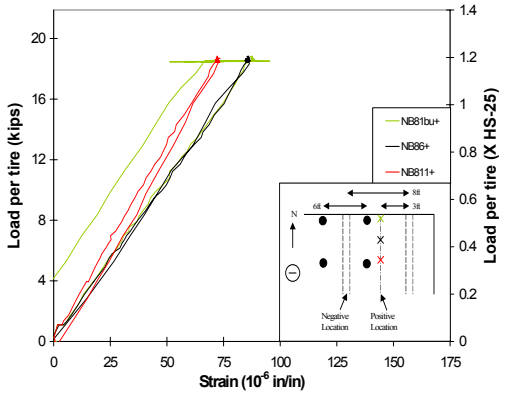

(i) Tandem

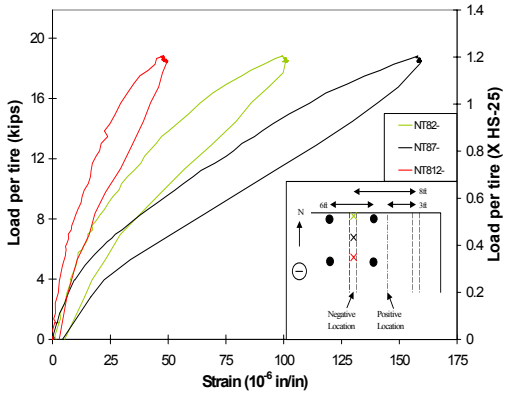

(ii) Tandem

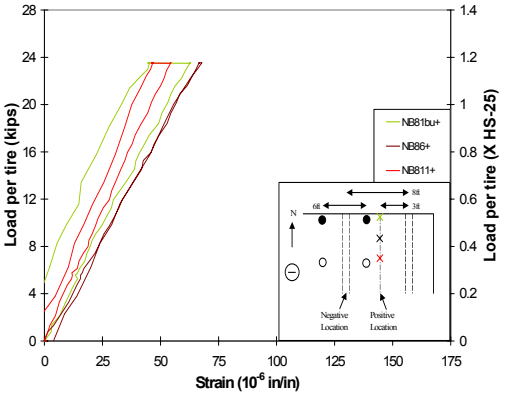

(iii) Truck axle-front

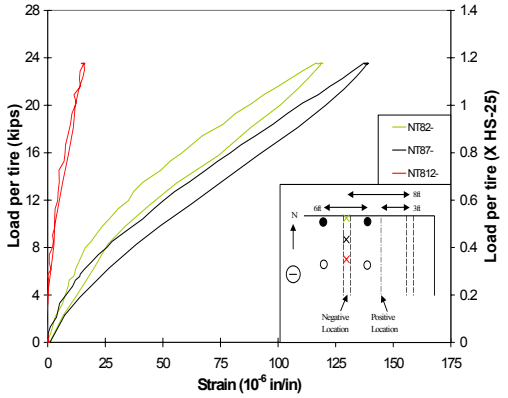

(iv) Truck axle-front

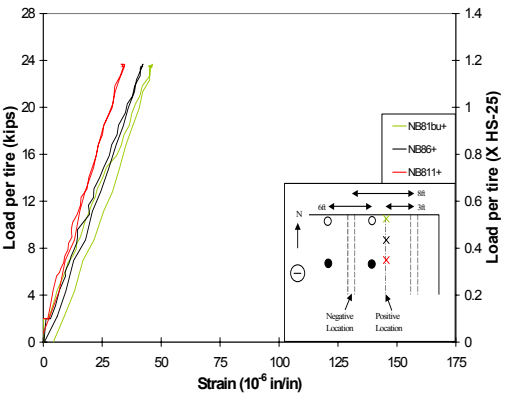

(v) Truck axle-back

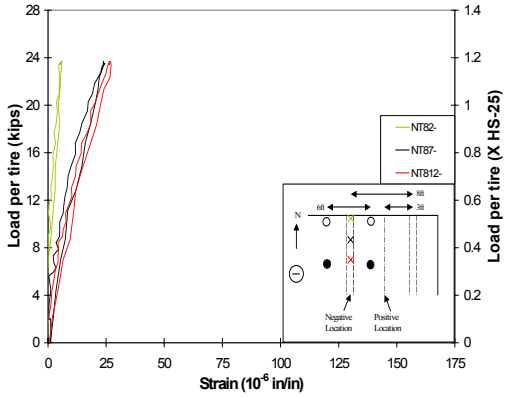

(vi) Truck axle-back

Figure 5-69: Load vs. strain, 1.2xHS-25 load step, negative moment loading, northeast test area; (i), (iii) and (v): bottom mat at positive location; (ii), (iv) and (vi): top mat at negative location

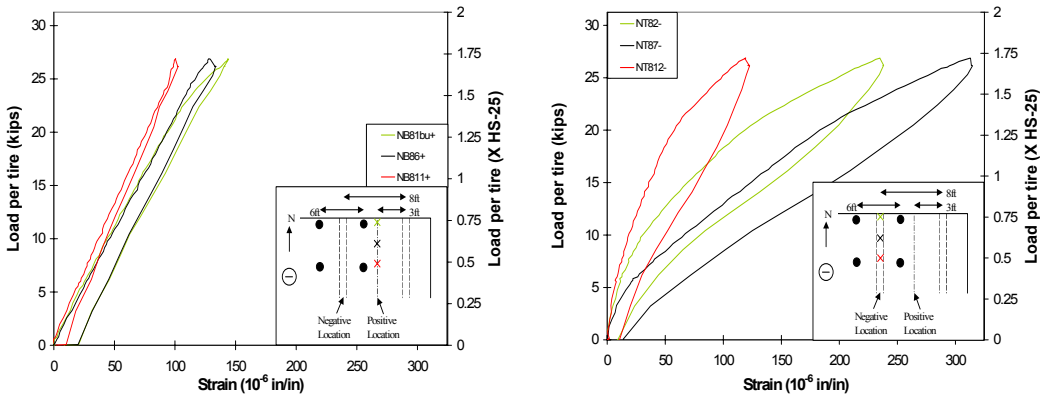

(i) Tandem

(ii) Tandem

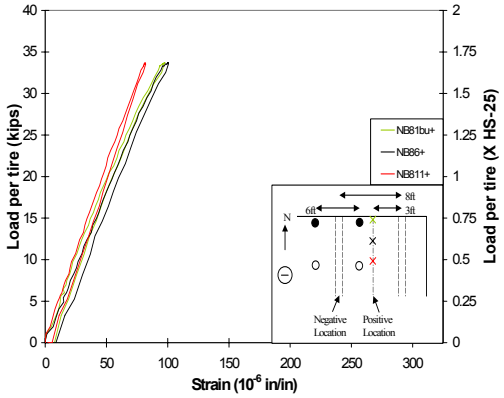

(iii) Truck axle-front

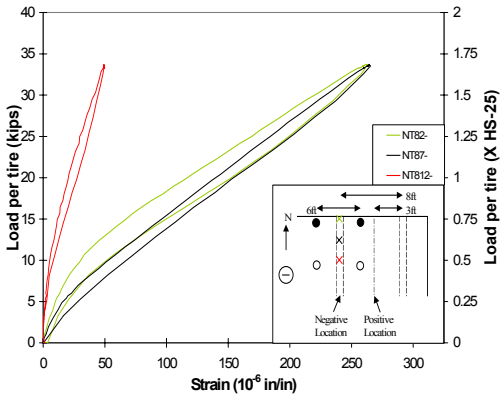

(iv) Truck axle-front

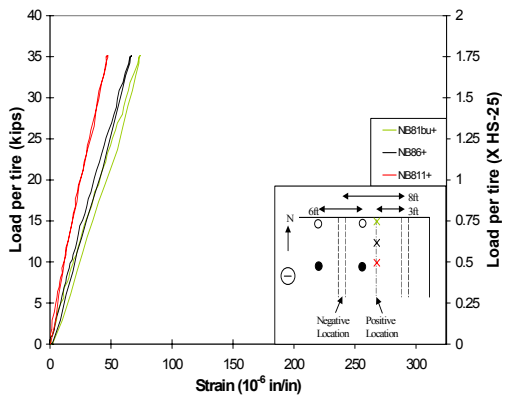

(v) Truck axle-back

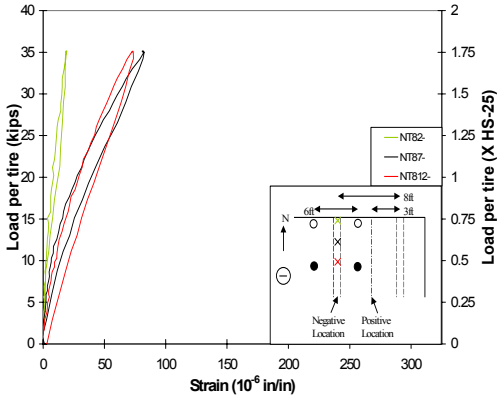

(vi) Truck axle-back

Figure 5-70: Load vs. strain, 1.75xHS-25 load step, negative moment loading, northeast test area; (i), (iii) and (v): bottom mat at positive location; (ii), (iv) and (vi): top mat at negative location

The maximum strain measured at the 1.75xHS-25 load step was 310με (15% of yield strain of the steel), due to the tandem loading configuration. The load versus strain plots in Figure 5-70 show linear elastic behavior with no significant residual strains at the 1.75xHS-25 load step. The strain magnitudes in the gauges at the positive moment section have increased proportional to the 75% load increase. However, the gauges at the negative moment section have increased about 300% during the same increase in loading, indicating non-linear behavior. This agrees with the crack maps, which show initiation of cracking over the girder initiating at the 1.75xHS-25 load step.

5.5.2.4.4 3xHS-25 load step

The 300% overload created a significant non-linearity at the positive moment section during application of the tandem loading configuration (Figure 5-71, i). At a load of approximately 31kips (2xHS-25) per tire, the stiffness of the slab end detail reduced noticeably. After unloading, a residual strain of 215με remained in the edge rebar. This rebar reached a maximum strain of 610με (29% of yield strain of the steel), the largest strain at this load step.

The tandem loading configuration created non-linear behavior at the negative moment section as well, where a residual strain of 55με was recorded after the 3xHS-25 load application (Figure 5-71, ii). The load versus deflection plot for the tandem loading configuration at the 3xHS-25 load step (Figure 5-60, i) confirms this response. The truck axle-front loading configuration also caused inelastic behavior in the bridge deck at the positive moment section (Figure 5-71, iii). The stiffness of the section began to reduce at an applied load of approximately 37kips (2.4xHS-25) per tire. The truck axle-back loading configuration created insignificant strains compared the other loading configurations.

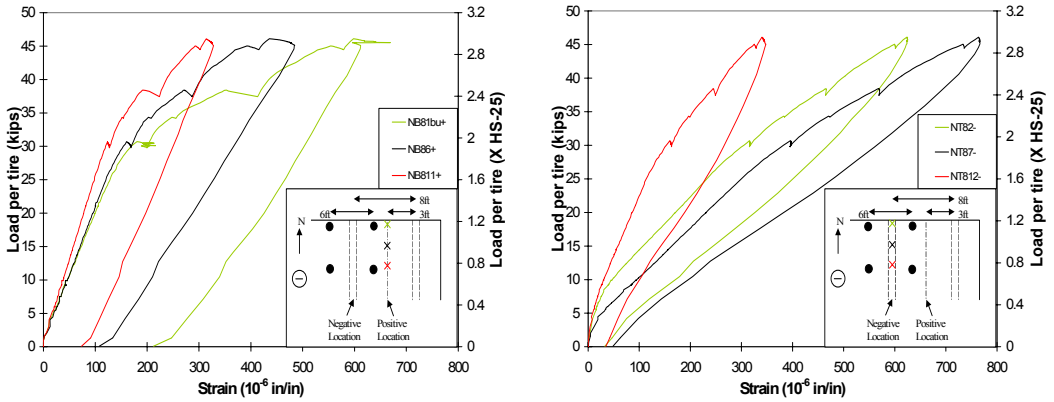

(i) Tandem *(ii) Tandem*

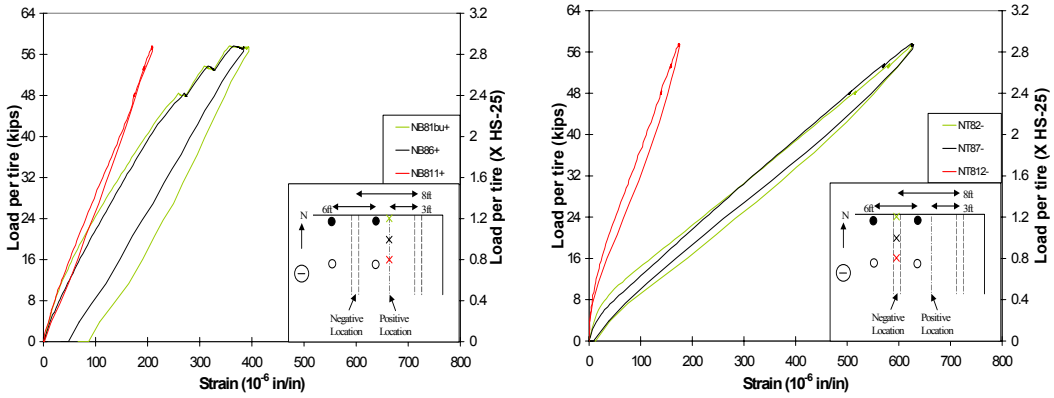

(iii) Truck axle-front *(iv) Truck axle-front*

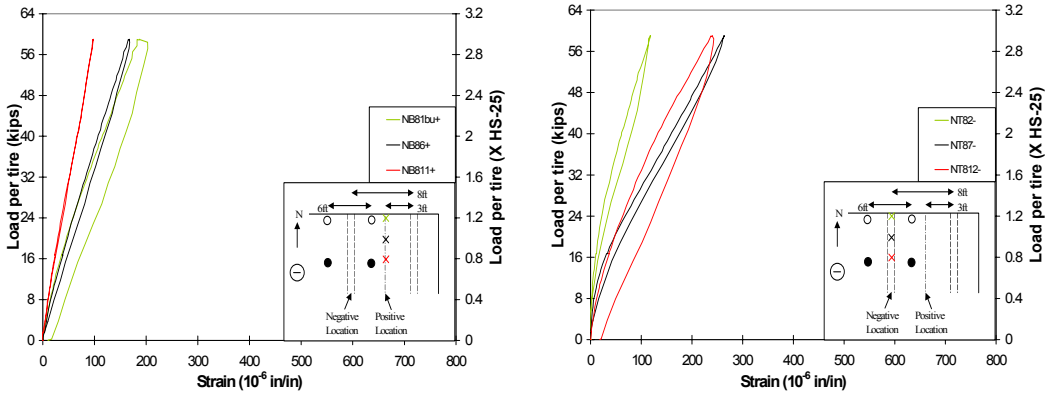

(v) Truck axle-back *(vi) Truck axle-back*

Figure 5-71: Load vs. strain, 3xHS-25 load step, negative moment loading, northeast test area; (i), (iii) and (v): bottom mat at positive location; (ii), (iv) and (vi): top mat at negative location

5.5.2.4.5 Loading to failure

Figure 5-72 shows the load versus strain plots for the NB81bu+ and NT82- strain gauges. The load versus strain response of the bridge deck during the 3xHS-25 load application is included in the plots as it created significant residual strains in the reinforcing steel. At the positive moment section, the load versus strain plot for the 3xHS-25 load step shows an abrupt stiffness reduction (Figure 5-72, i). The stiffness of the section remains relatively constant following this abrupt change at a load of approximately 30kips (1.9xHS-25) per tire. The ultimate strain reached at failure was 1600με (77% of yield strain of the steel), at the positive moment section (Figure 5-72, i).

The ultimate strain in the NT82- strain gauge was significantly less than in the NB81bu+ strain gauge. Even though the strains in the negative moment section were larger than those in the positive section at the 1.2xHS-25, 1.75xHS-25 and 3xHS-25 load steps. As explained earlier, the location of the strain gauges (at the centerline of the girder) and complicated mechanics involving the girder-shear stud-deck concrete interaction is responsible for the behavior illustrated in Figure 5-72. The widths of the cracks at the flange faces (Figure 5-63, iii) indicate that top reinforcing bars were likely yielding at failure. In fact, this is the main reason for the slight stiffening shown in the load versus strain plots.

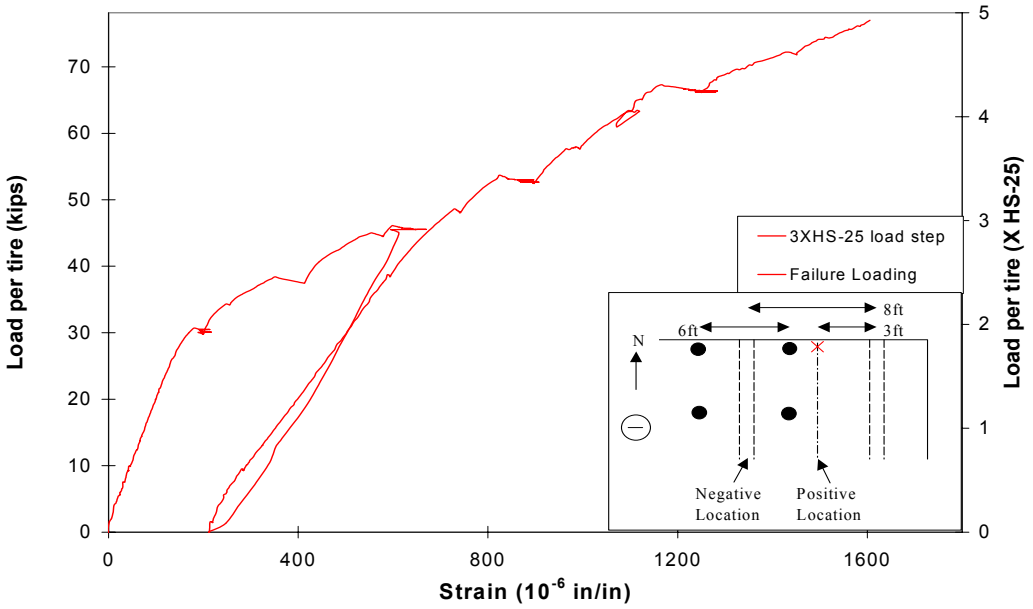

(i)NB81bu+ strain gauge

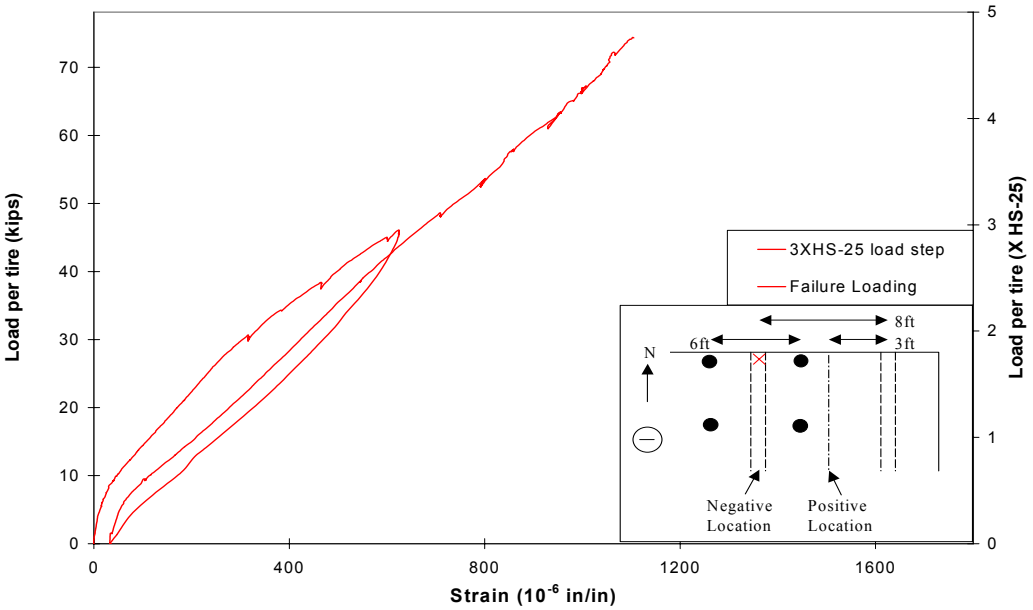

(ii)NT82- strain gauge

Figure 5-72: Load vs. strain, loading to failure, negative moment loading, northeast test area

5.5.2.5 Strain profiles

5.5.2.5.1 HS-25 load step

Figure 5-73 shows strain profiles for the three loading configurations applied at the HS-25 load step. The strain profiles for the positive moment section are relatively uniform across the slab end detail. At the negative moment section, the strain profiles show a gradient across the UTSE detail of varying shape. At both moment sections, the largest strains are created in the middle of the slab end detail, except at the negative moment section under the truck axle-back loading configuration (Figure 5-73, vi).

The maximum strain of 95με (4.6% of yield strain of the steel) occurred simultaneously at the two moment sections due to the tandem loading configuration. The NB88+ and NT87- strain gauges, located in the interior of the slab end detail at the positive and negative moment sections, respectively, reached identical maximum strains. The average strain across the slab end detail is roughly the same for the tandem and truck axle-front loading configurations. The truck axle-back loading configuration created strains at the positive moment section that were smaller than those measured at the other loading configurations.

5.5.2.5.2 1.2xHS-25 load step

The shape of the strain profiles for the 1.2xHS-25 load step are very similar to the profiles for the HS-25 load step. The largest strain magnitudes are again located in the middle of the slab end detail. At this load step, the tandem loading created larger strains across the UTSE detail than the truck axle-front configuration. The largest strain in the slab end detail at this load step was 160με (8% of yield strain of the steel) at the negative moment section, due to the tandem loading configuration (Figure 5-74, ii).

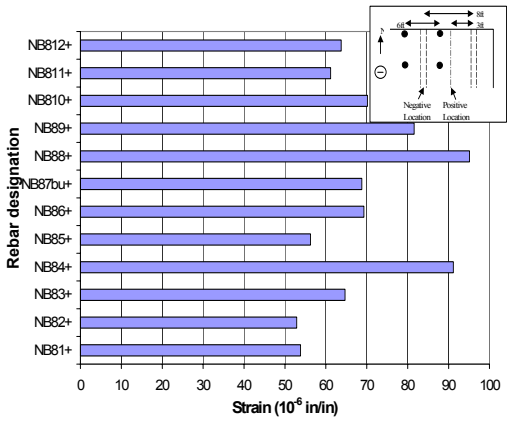

(i) Tandem

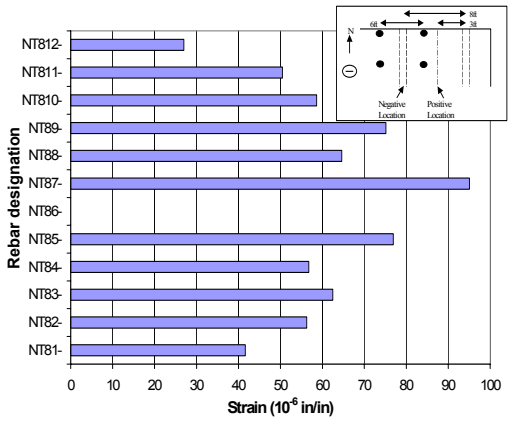

(ii) Tandem

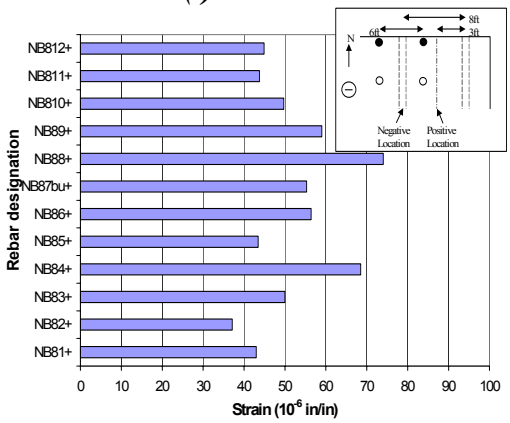

(iii) Truck axle-front

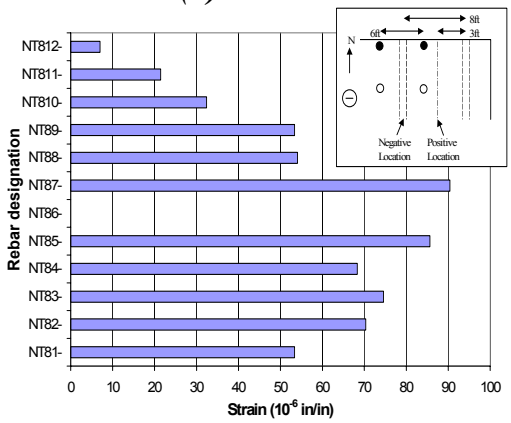

(iv) Truck axle-front

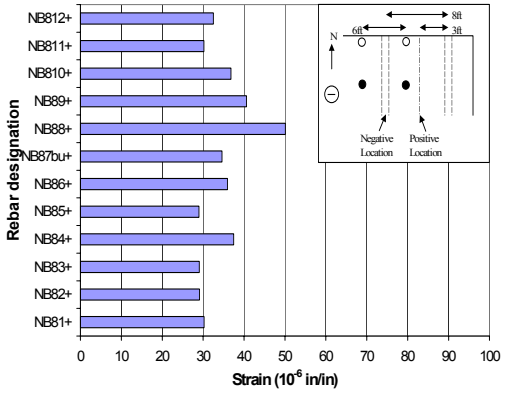

(v) Truck axle-back

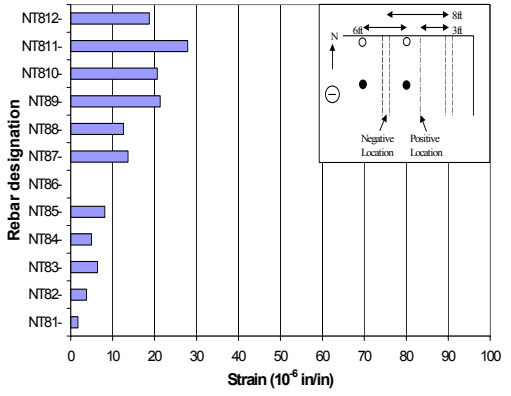

(vi) Truck axle-back

Figure 5-73: Strain profiles, HS-25 load step, negative moment loading, northeast test area; (i), (iii) and (v): bottom mat at positive location; (ii), (iv) and (vi): top mat at negative location

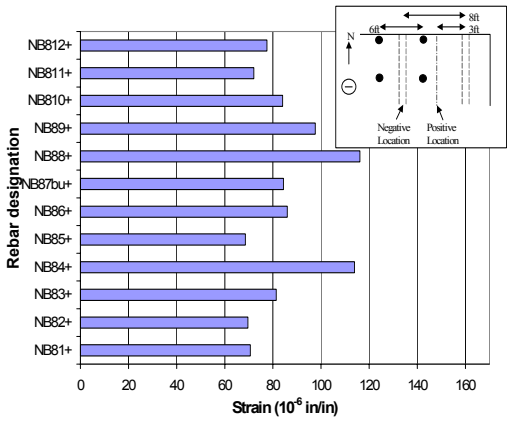

(i) Tandem

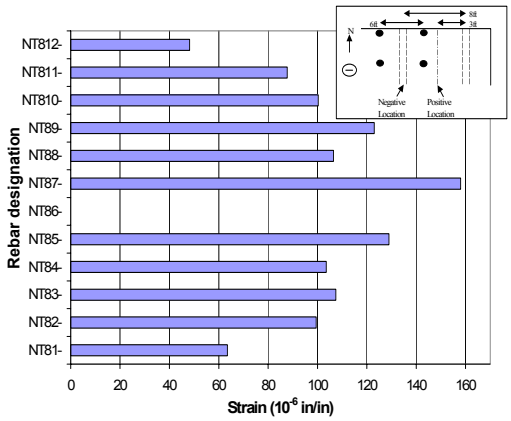

(ii) Tandem

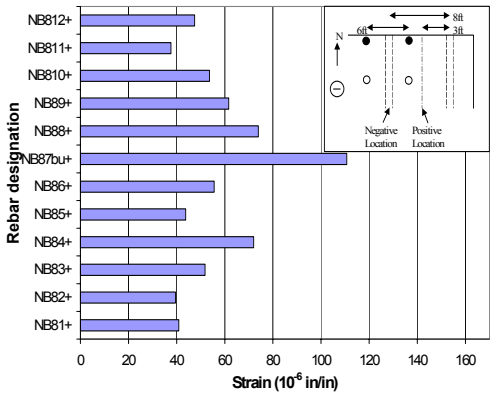

(iii) Truck axle-front

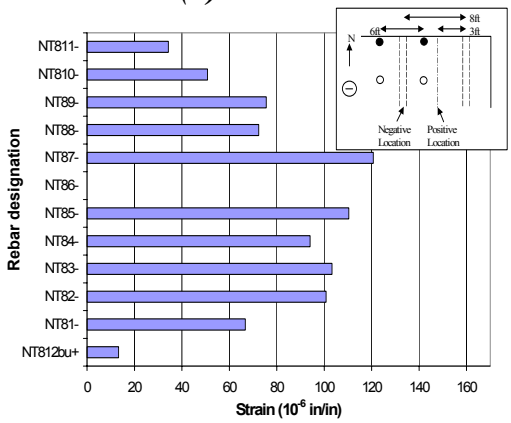

(iv) Truck axle-front

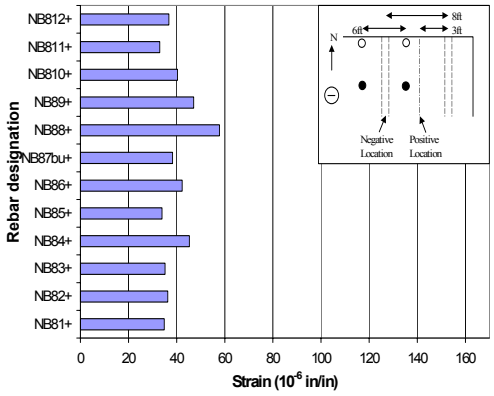

(v) Truck axle-back

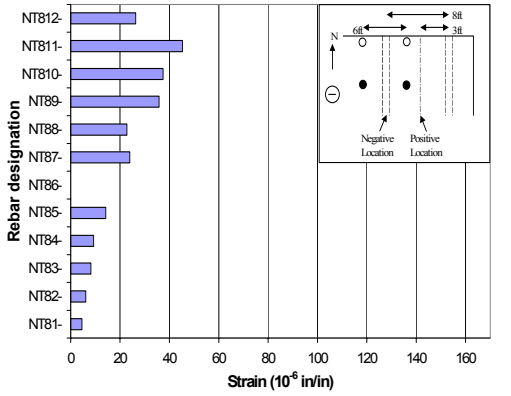

(vi) Truck axle-back

Figure 5-74: Strain profiles, 1.2xHS-25 load step, negative moment loading, northeast test area; (i), (iii) and (v): bottom mat at positive location; (ii), (iv) and (vi): top mat at negative location

5.5.2.5.3 1.75xHS-25 load step

At the 1.75xHS-25 load step, the strain readings from gauges in the negative moment section are significantly larger than those from the positive moment section (Figure 5-75). The shapes of the strain profiles are once again very similar to the HS-25 and 1.2xHS-25 strain profiles. From the 1.2xHS-25 load step to the 1.75xHS-25 load step, the strain magnitudes increased faster at the negative moment section than the positive section. The strain profiles are nearly uniform at the positive moment section.

5.5.2.5.4 3xHS-25 load step

The strain profiles changed considerably at the 3xHS-25 load step (Figure 5-76). The maximum strain at this load step remained in the middle of the slab end detail, however, the strains in the edge rebars increased considerably compared to the 1.75xHS-25 load step. As shown in the load versus deflection plots, the edge deflection increased significantly between the 1.75xHS-25 and 3xHS-25 load steps. The substantial increase in strain magnitudes at the edge bars are closely related to the relative deflection increase. The strain gradient across the slab end detail is nearly uniform at the negative moment section for the tandem loading configuration (Figure 5-76, ii).

5.5.2.5.5 Loading to failure

Strain profiles for the positive and negative moment sections, just prior to failure, are shown in Figure 5-77. At the positive moment section, the rebar strains decreased from the edge of the deck to the interior. The largest strain of 1830με (88% of yield strain of the steel) occurred at the NB84+ strain gauge. The strain profile for the negative moment section has smaller strains at the edge of the deck than in the interior (Figure 5-77, ii). The largest strain magnitudes

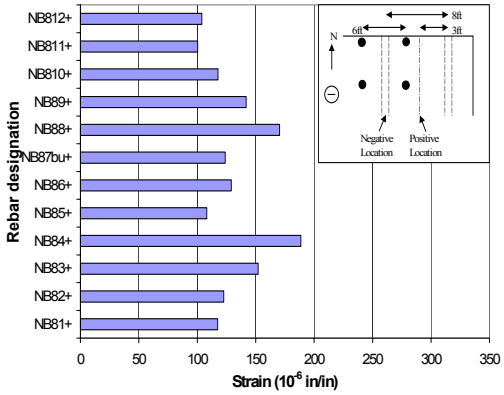

(i) Tandem

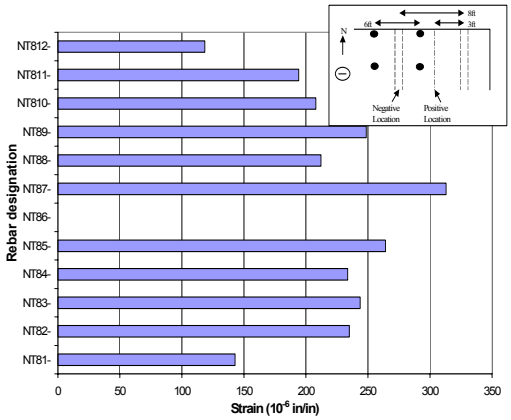

(ii) Tandem

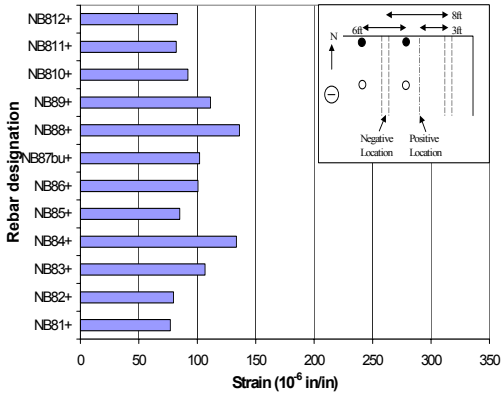

(iii) Truck axle-front

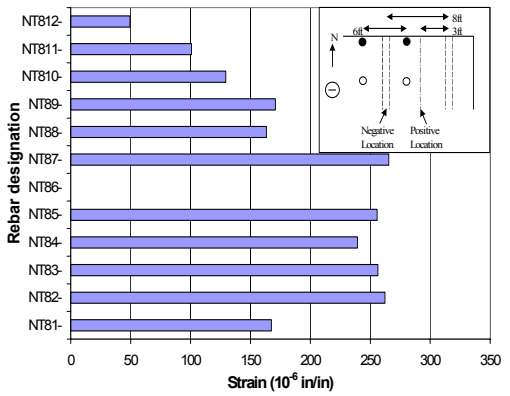

(iv) Truck axle-front

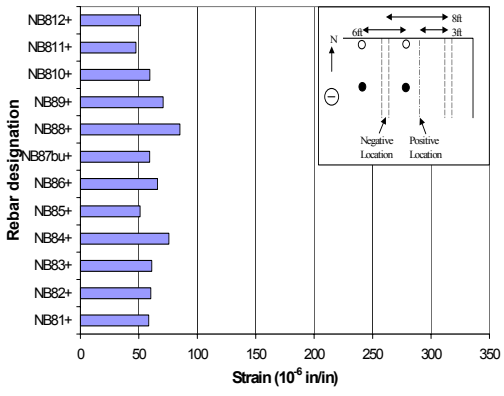

(v) Truck axle-back

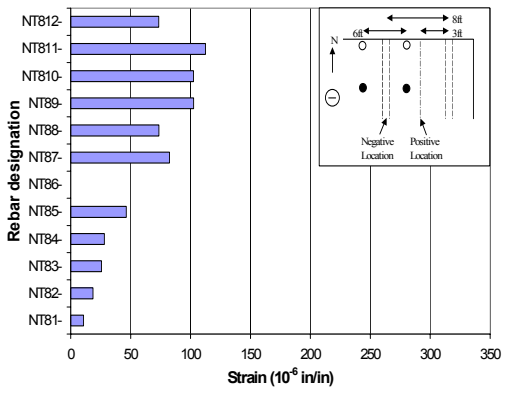

(vi) Truck axle-back

Figure 5-75: Strain profiles, 1.75xHS-25 load step, negative moment loading, northeast test area; (i), (iii) and (v): bottom mat at positive location; (ii), (iv) and (vi): top mat at negative location

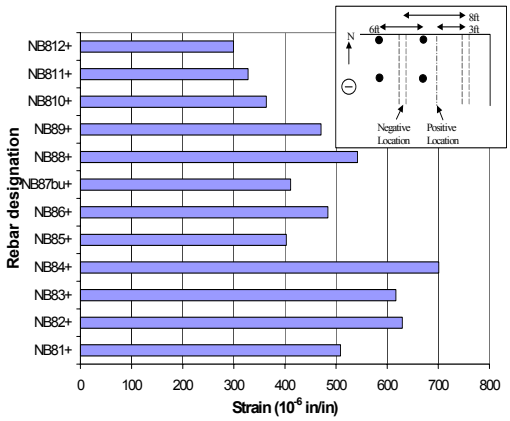

(i) Tandem

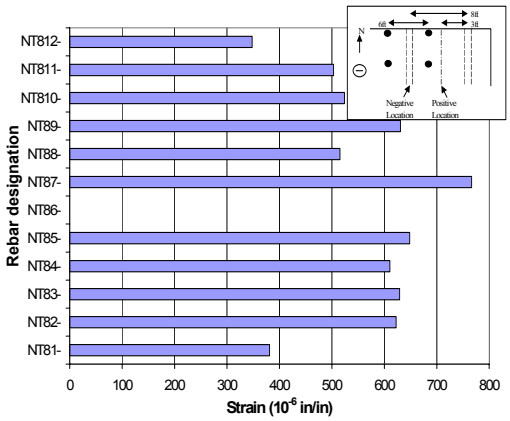

(ii) Tandem

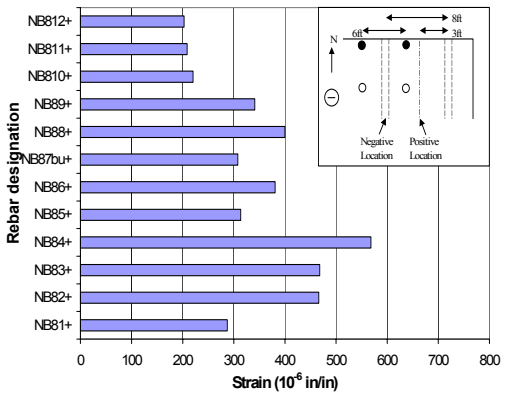

(iii) Truck axle-front

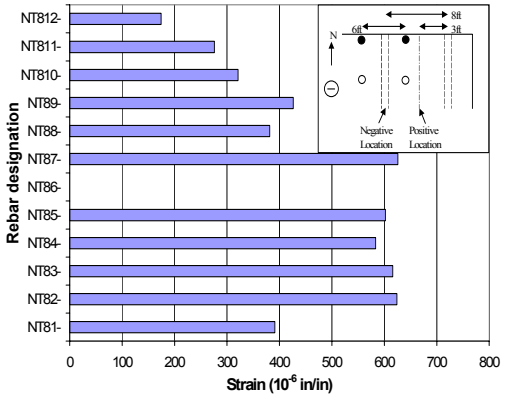

(iv) Truck axle-front

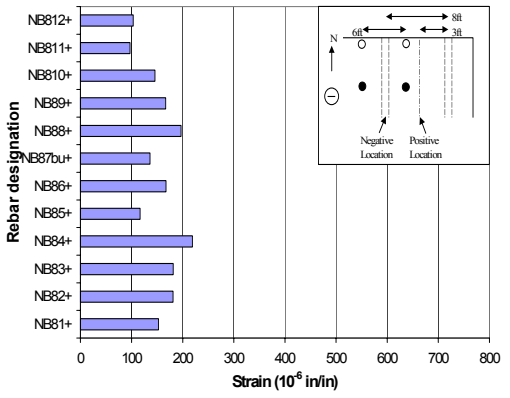

(v) Truck axle-back

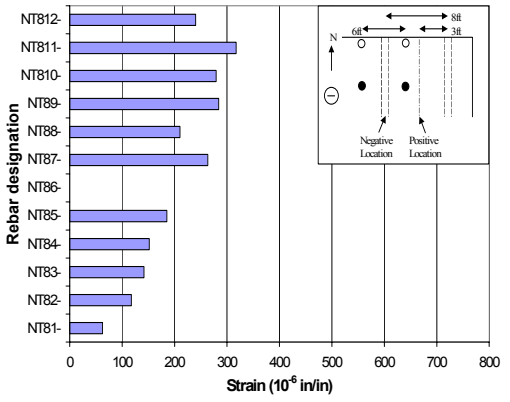

(vi) Truck axle-back

Figure 5-76: Strain profiles, 3xHS-25 load step, negative moment loading, northeast test area; (i), (iii) and (v): bottom mat at positive location; (ii), (iv) and (vi): top mat at negative location

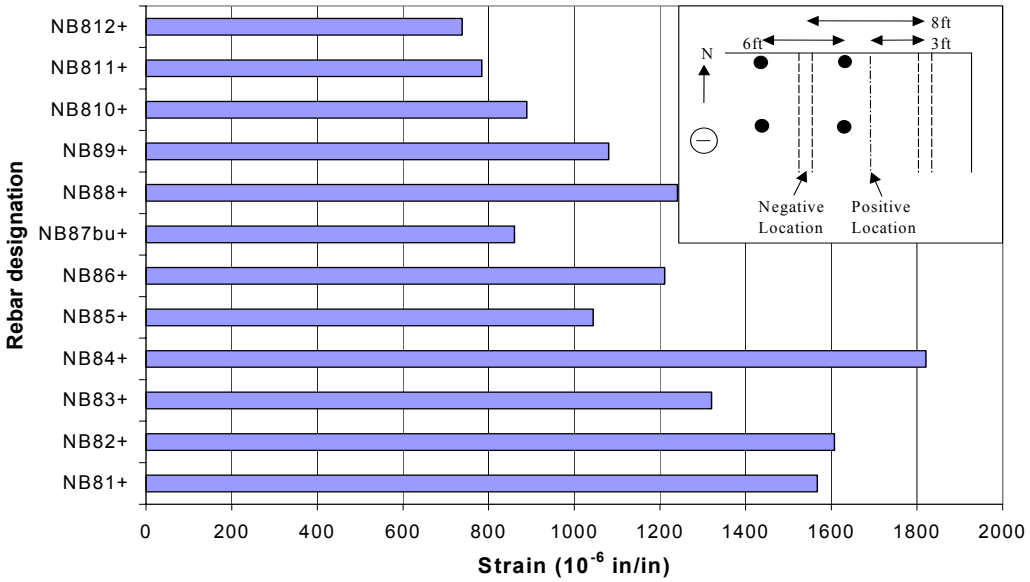

(i)Positive moment location, tandem loading configuration

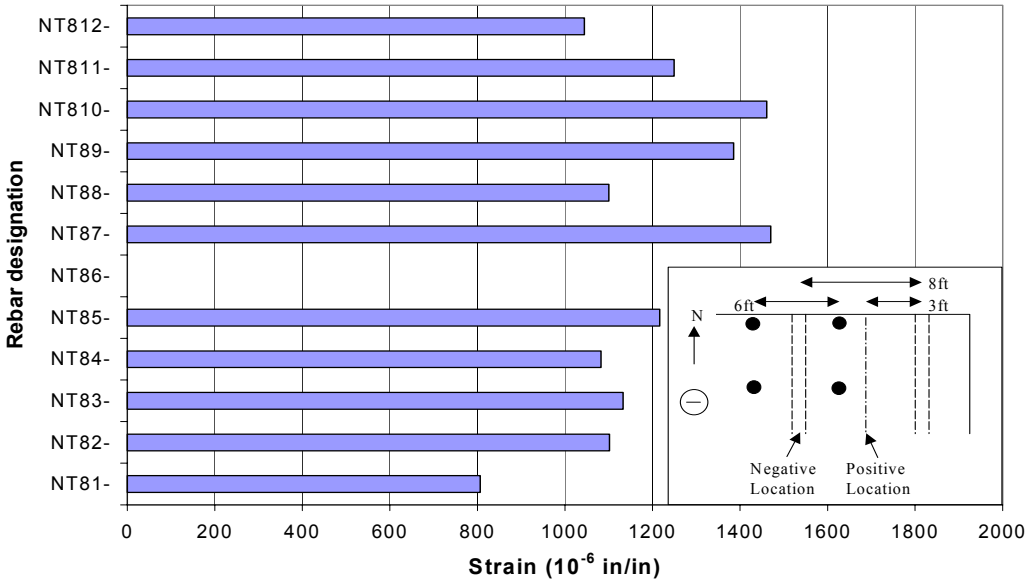

(ii)Negative moment location, tandem loading configuration

Figure 5-77: Strain profiles, loading to failure, negative moment loading, northeast test area

occurred in the 7th, 9th and 10th rebars from the edge. It is believed that the strain magnitudes at the two critical sections (of which, the section at the face of the flange was not instrumented) were comparable at failure due to redistribution of stresses.

5.5.2.6 Moment calculations

Figure 5-78 shows the moments and in-plane forces calculated using the strain gauge data. The calculated moment in the UTSE detail increases approximately linearly proportionally to the applied loads at both moment sections. At the positive moment section, the inclusion of tension in concrete effects the moment calculation until the 3xHS-25 load step. Including tension in concrete in the moment calculation has a significant effect prior to cracking. At the HS-20 and HS-25 load levels, the calculated moments at the positive moment section are approximately doubled when tension in concrete is included. From the 3xHS-25 load step to failure, the moment calculations with and without tension in concrete are almost identical. The in-plane force, P, calculated using the strain gauge data, is shown for selected load steps in Figure 5-78.

The plot of the moment calculated at the negative moment section is approximately linear. The effect of tension in concrete ends at the 1.75xHS-25 load step. The inclusion of tension in concrete doubled the calculated moments at the negative moment section prior to cracking. This section reached an ultimate moment of 965k*in. The moments calculated at the positive moment section are smaller, yet comparable to those at the negative section.

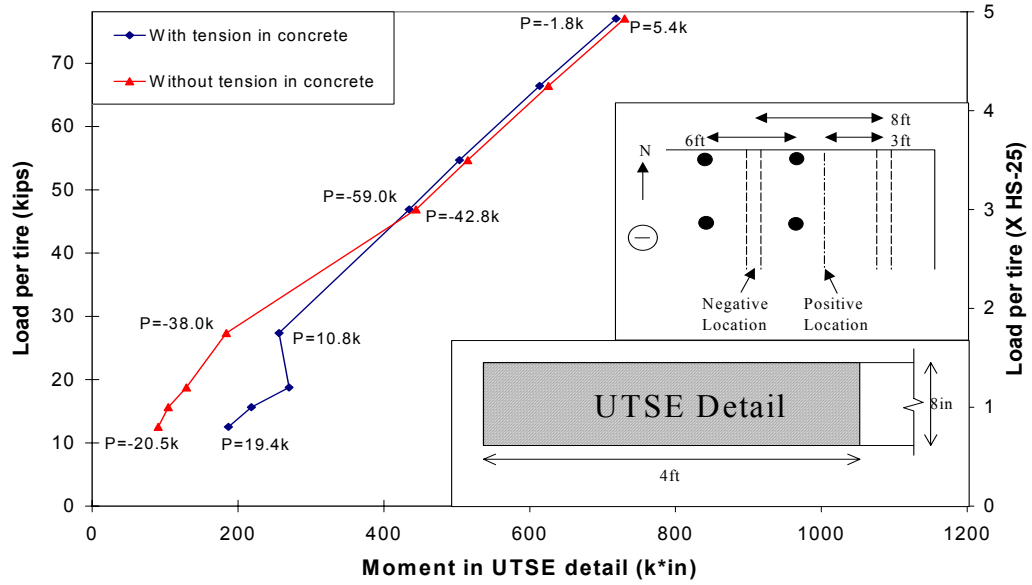

(i)Positive moment section

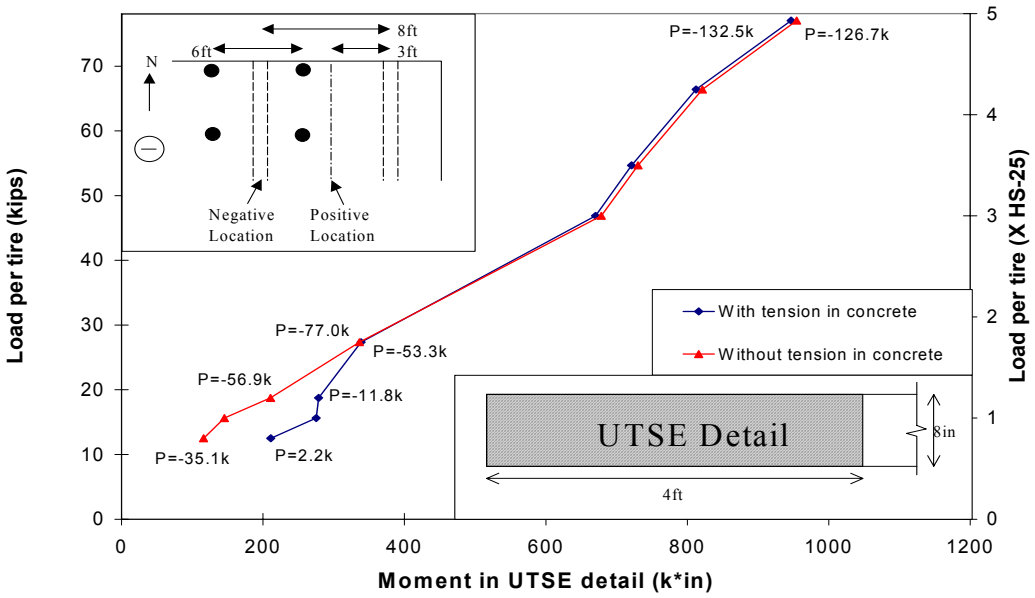

(ii)Negative moment section

Figure 5-78: Moment calculated from strain gauge readings, tandem loading configuration only

5.5.2.7 Elastic moment comparison

Section 5.2.2.7 describes the comparison of the experimentally calculated moments with the linear elastic three-span beam analysis. The northeast test area cracked at an applied load of 1.75xHS-25, therefore, the moments calculated from the strain gauges are compared to the elastic analysis at the HS-25 and 1.75xHS-25 load steps. The HS-25 load step comparison shows relatively close agreement between analysis and experiment (Figure 5-79, i). However, the comparison at the 1.75xHS-25 load step does not have as close an agreement. At the negative moment section, the experimentally calculated moment is about half the elastic moment (Figure 5-79, ii). This is due to the following two reasons:

- the location of the strain gauges (at the centerline of the girder rather than at the face of the support)
- a greater portion of the bridge deck (larger than four-feet) contributing to supporting the externally applied loads

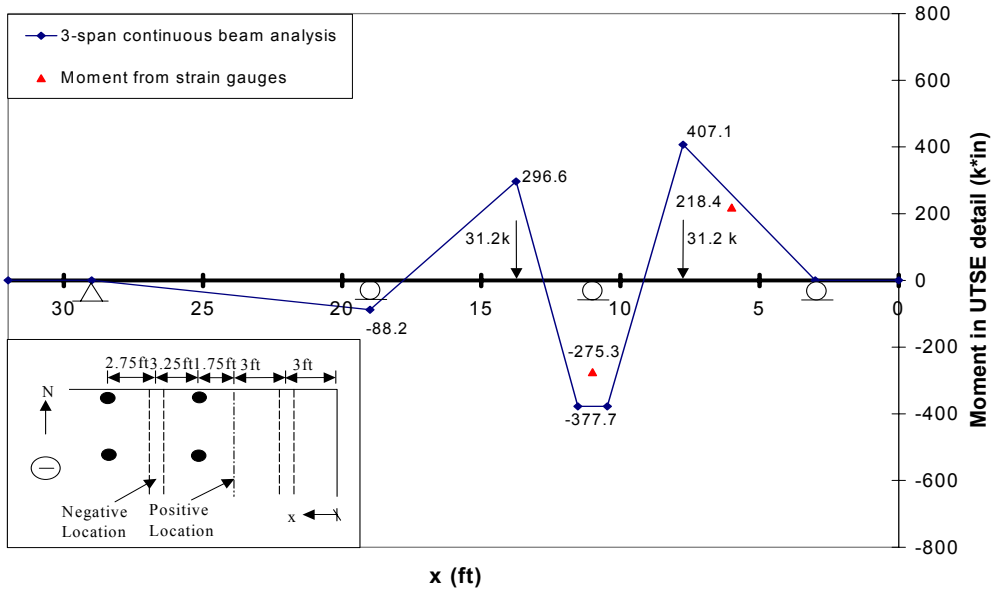

(i) HS-25 load step

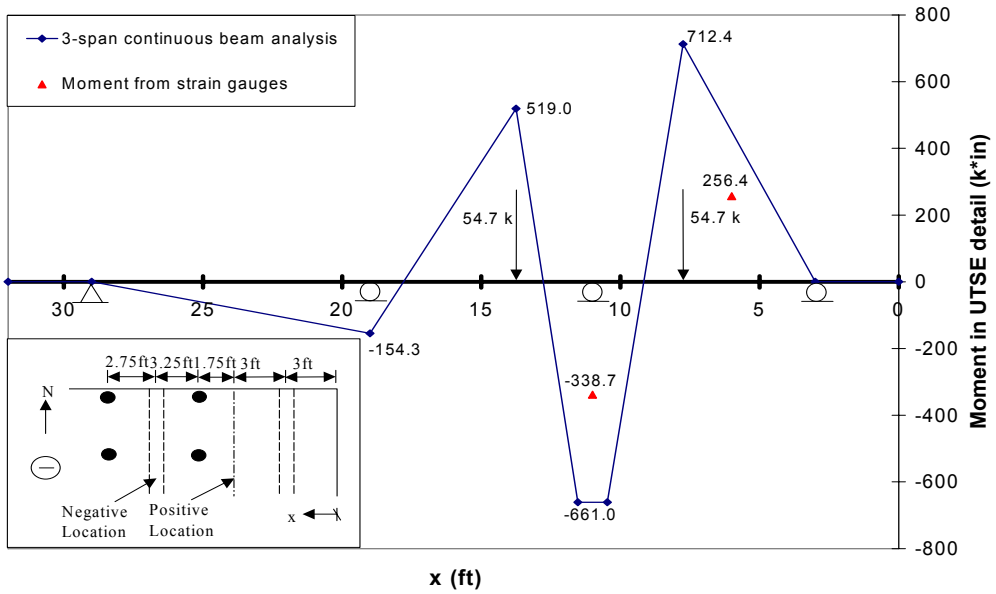

(ii) 1.75xHS-25 load step

Figure 5-79: Elastic moment compared to moment from strain gauges

5.5.2.8 Failure of the interior span

After the northeast test area failed in punching shear at the edge tire in the exterior span, the two tires in the interior span were loaded to failure. The interior deck span punched at a load of 81.5kips (5.2xHS-25) per tire. Figure 5-80 shows the failure surface at the bottom of the bridge deck. This failure surface was similar to the others that occurred on the bridge deck.

At the side of the deck, the shear cracks on the east side of the load plate were wide and extended to the flange of the girder (Figure 5-81). The shear cracks on the west side of the load plate were not as wide and they were shallow-angled (approximately 20^{o}-30^{o}) crack extending to the girder flange. The shear cracks during loading to failure formed at locations where no previous cracking had occurred. The failure surface at the top of the deck formed close around the east side of the load plate but ran adjacent to the deck edge on the west side of the load plate (Figure 5-82).

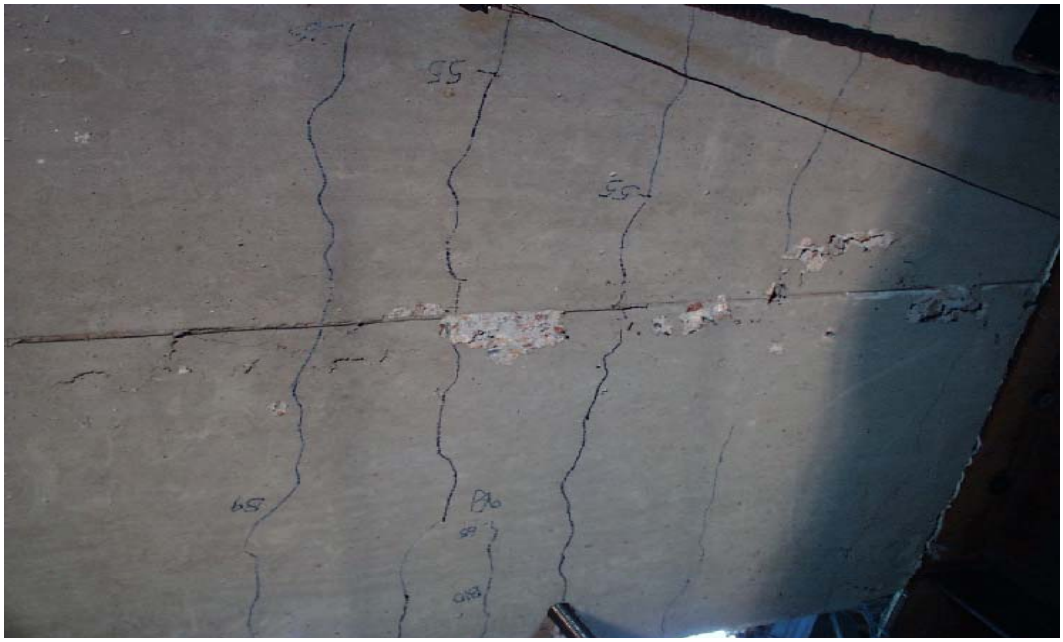

Figure 5-80: Interior span failure at bottom of deck, facing south

Figure 5-81: Interior span failure at side of deck, facing south

Figure 5-82: Interior span failure at top of deck, facing north

5.5.3 Northeast test area summary

The northeast test area contained the UTSE detail, spanning eight-feet. The deck was loaded with 10in by 20in load plates, as in the southeast test area. In addition, the northeast test area was loaded to the same design loads and overloads as the southeast test area (HS-25, 1.2xHS-25, 1.75xHS-25). The three loading configurations were applied at the 3xHS-25 load step as well. Then, the deck was loaded to failure in the tandem loading configuration at the location to maximize negative moment.

The bridge deck behavior was linear elastic during the HS-25 loading, applied at the location to maximize negative moment. The northeast test area was undamaged by the design loading applications (HS-20 and HS-25). The relative midspan deflection of the deck was not distinguishable from the noise in the data until the 1.75xHS-25 load step. At this load step, the maximum relative deflection was 0.05in. The relative deflection remained small at the 3xHS-25 load step, and at failure the relative midspan deflection was 0.33in, the smallest ultimate deflection of the four test areas. The UTSE detail was very stiff at the overloads and loading to failure.

From a serviceability standpoint, the northeast test area's behavior was excellent, with first cracking occurring at 175% of the HS-25 design load. By the 3xHS-25 load step, the bottom cracks had propagated across the slab end detail (maximum crack width of 0.004in). Just prior to failure, extensive bottom cracks formed in both deck spans, however, their widths were very small (0.005in). The largest crack widths at failure occurred in the top of the deck, over the interior girder (0.009in).

The top and bottom surfaces of the bridge deck cracked extensively prior to failing. The bridge deck failed by punching shear at the edge tire in the exterior span. The ultimate capacity of the northeast test area was 76.6kips

(4.9xHS-25 or 6.1xHS-20) per tire. The two tires in the interior span were then loaded to failure. The edge tire in this span punched at a load of 81.5kips (5.2xHS-25 or 6.5xHS-20) per tire, a slightly larger load than the initial failure load. At failure, the stiffness of the slab end detail is significant in both the positive and negative moment sections as evidenced by the load versus strain plots.

The strain profiles for the negative moment section show larger strain readings in regions close to the tire loads. At the positive moment section, the strain profiles are nearly uniform. The average strain magnitudes across the slab end detail at the two moment sections is comparable at failure.

5.6 TEST AREA COMPARISON

Table 5-5 and Table 5-6 summarize the deflections and strains measured in the southeast and northeast test areas, respectively. The variable tested in the two test areas was the slab end detail. The girder spacing in these test areas was eight-feet. Both details were very stiff at design loads and overloads. The maximum rebar strain readings measured at service loads are comparable for the southeast and northeast test areas. In general, strains in the UTSE detail were slightly smaller than comparable strains in the IBTS detail. The ultimate relative deflections measured in the two test areas were similar. The response of the IBTS detail was slightly stiffer as evidenced by the relative deflection measurements shown in Table 5-5 and Table 5-6. In addition, both slab end details were very stiff as evidenced by the large span-to-deflection ratios. Reinforcing steel was yielding in tension at the negative moment section of the IBTS detail at failure of the test area. The strains measured in the rebar in the UTSE detail did not approach the yield strain of the steel prior to punching.

For the southwest and northwest test areas, only the deflection readings have been summarized, as the strain readings were not taken at critical locations. Table 5-7 shows the maximum relative deflection measured at each load step for the two test areas. The positive bending performance of the IBTS and UTSE details can be evaluated by comparing the behavior of the bridge deck specimen in these test areas. The maximum relative deflections measured in the southwest and northwest test areas remained similar up to the 1.75xHS-25 load step. The span-to-relative deflection ratios calculated for the UTSE detail were slightly higher than those measured at the IBTS detail. At failure, the relative midspan deflection of the UTSE detail was smaller than that measured at the IBTS detail. The punching shear failure in the UTSE detail was experienced at a load of

Table 5-5: Summary of southeast test area results

	IBTS detail (Southeast test area)				
	Deflections			Strains	
	Maximum relative deflection (in)	Cracked (Yes/No)	Clear span to relative deflection ratio	Maximum strain Moment section	
				Positive	Negative
Load step				(% of steel yield strain)	
Negative HS-25	0.02	No	4800	4	4
Negative 1.2xHS-25	0.03	No	3200	5	6
Negative 1.75xHS-25	0.04	No	2400	6	18
Negative 3xHS-25*	0.09	Yes	1067	15	44
Negative Failure	0.39	Yes	246	81	108

* 2.9xHS-25 load level

Table 5-6: Summary of northeast test area results

	UTSE detail (Northeast test area)				
	Deflections			Strains	
	Maximum relative deflection (in)	Cracked (Yes/No)	Clear span to relative deflection ratio	Maximum strain Moment section	
				Positive	Negative
Load step				(% of steel yield strain)	
Negative HS-25	<0.01	No	NA	4	4
Negative 1.2xHS-25	<0.01	No	NA	6	8
Negative 1.75xHS-25	0.05	No	1920	9	15
Negative 3xHS-25	0.13	Yes	738	34	37
Negative Failure	0.36	Yes	267	88	71

Table 5-7: Summary of southwest and northwest test area results

	IBTS detail (Southwest test area)			UTSE detail (Northwest test area)		
	Deflections			Deflections		
Load step	Maximum relative deflection (in)	Cracked (Yes/No)	Clear span to relative deflection ratio	Maximum relative deflection (in)	Cracked (Yes/No)	Clear span to relative deflection ratio
Positive HS-25	0.05	No	2400	0.07	No	1714
Positive 1.2xHS-25	0.06	Yes	2000	0.07	No	1714
Positive 1.75xHS-25	0.08	Yes	1500	0.14	Yes	857
Positive 3xHS-25	0.16	Yes	750	0.34	Yes	353
Positive Failure	1.40	Yes	86	1.18	Yes	102

81.3kips (5.2xHS-25) per tire. The IBTS detail carried a load of 95.6kips (6.1xHS-25) per tire before punching. Hence, the smaller maximum load carried by the UTSE detail was accompanied by a smaller relative deflection. Overall, the UTSE detail was only slightly less stiff than the IBTS detail.

Table 5-8 compares the applied load at first cracking and failure as well as the punching shear capacities obtained from additional tests. In the eight-foot span, the IBTS detail in negative bending cracked at a 20% higher load than the UTSE detail. The top of the bridge deck cracked at applied load levels of 1.75xHS-25 and 2.1xHS-25 in the northeast and southeast test areas, respectively. The top cracks are critical for corrosion of the reinforcing steel and the minimum reserve strength for top cracking in the eight-foot span was 75% of the HS-25 design load.

During the positive bending tests conducted in the 10-foot span, the IBTS detail cracked at a lower load than the UTSE detail. This is because the interior span of the south edge of the bridge deck had failed prior to positive moment testing in the southwest test area. The discontinuity in the deck reduced the restraint and associated moment at the interior girder, thereby increasing the moment at midspan of the test area due to static equilibrium. The increased moment at midspan implies increased strains and early cracking. In short, boundary conditions in these two test areas were not identical due to failure experienced in an earlier test. However, it is reasonable to assume that, with comparable boundary conditions, the IBTS detail would crack at a higher load than the UTSE detail. Although the underside of the deck cracked under lower overloads, cracks underneath the deck are far less critical than those on the top of the deck.

The bottom cracks were relatively wide and were concentrated underneath the load plates in the southeast and southwest test areas, which test the IBTS

Table 5-8: Test area loading comparison

Test area	Variables	First cracking load (kips, xHS-25)	Failure load (kips, xHS-25)	Alternate failure load (kips, xHS-25)
Negative bending tests				
Southeast	8ft span, IBTS detail	33.0, 2.1	93.8, 6.0	90.6, 5.8
Northeast	8ft span, UTSE detail	27.3, 1.75	76.6, 4.9	81.5, 5.2
Positive bending tests				
Southwest	10ft span, IBTS detail	15.6, 1.0	95.6, 6.1	NA
Northwest	10ft span, UTSE detail	18.8, 1.2	81.3, 5.2	NA

detail (Figure 5-83, i). In the northeast and northwest test areas, which contain the UTSE detail, the cracks are narrower and they are distributed across the deck span. The top cracks were focused around the girders in the southwest and northwest test areas, whereas, the southeast and northeast test area's top cracks branched into the span of the slab end details (Figure 5-83, ii).

The failure loads for the two slab end details correspond well, with the IBTS detail withstanding approximately 20% larger loads than the UTSE detail. After the initial failure of the southeast and northeast test areas, the span that was undamaged was loaded to failure. These tests are not compared to each other as the failure in the adjacent span altered the boundary conditions of the test area. The secondary failure loads were useful in providing data for the punching shear strength of the bridge deck slab end details. These results are discussed in-depth in section 5.7.

Overall, when spanning eight-feet, the IBTS detail and the UTSE detail performed very well for both serviceability and strength criteria. Both details cracked at relatively low loads when spanning 10-feet. However, the relative deflections were small and the ultimate strength was sufficient for the 10-foot deck span. Both slab end details were very stiff at service load levels. The IBTS detail withstood larger ultimate loads than the UTSE detail due to the 10-inch deep section's larger punching shear capacity. All test areas showed significant

reserve strength, with the smallest failure load being 4.9 times the HS-25 design loading.

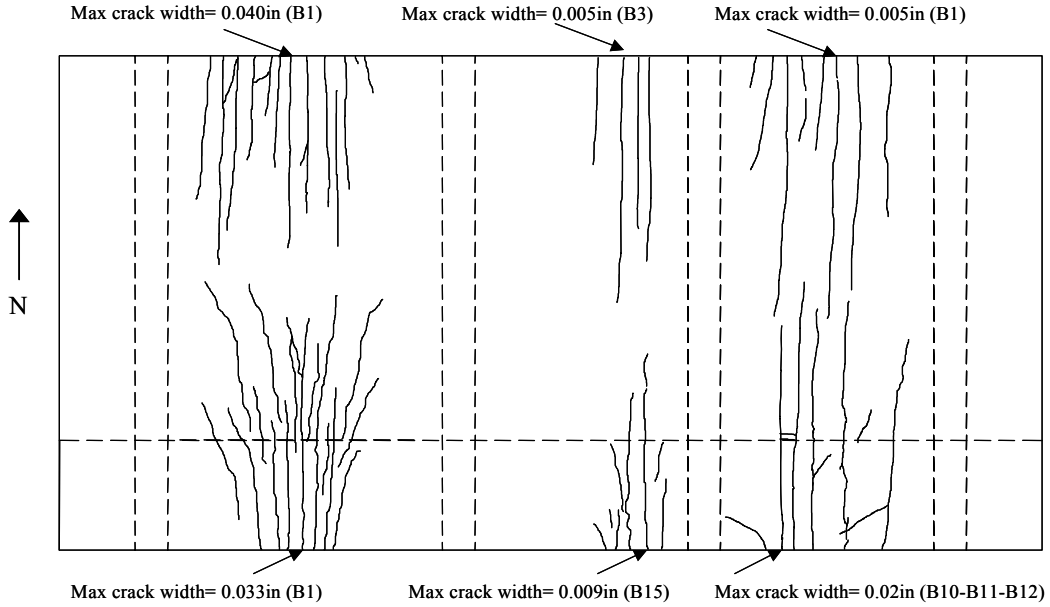

(i)Bottom surface of bridge deck

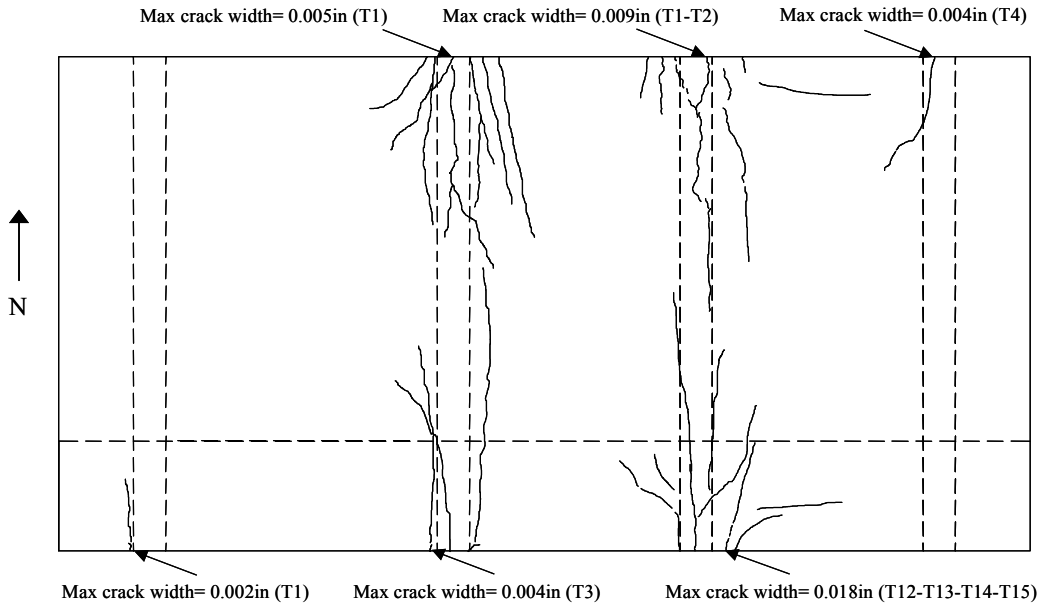

(ii)Top surface of bridge deck

Figure 5-83: Cracks at failure for all test areas

5.7 EXAMINATION OF PUNCHING SHEAR STRENGTH OF BRIDGE DECK SUBJECTED TO CONCENTRATED FORCES USING DESIGN PROVISIONS

The punching shear strength of bridge decks is handled in section 5.13.3.6 of the AASHTO LRFD Bridge Design Code. This section specifies the nominal shear resistance as the minimum of the terms in Equation 5-1:

$$v_c = \min\{4\sqrt{f_c'};\ (\frac{1}{2}+\frac{1}{B})4\sqrt{f_c'}\} \qquad \textit{Equation 5-1}$$

These equations are the same as those proposed by ACI 318-02 in section §11.12 for a uniform shear distribution (Equation 5-2). However, ACI 318-02 has one additional equation to check. For slabs subjected to concentrated loads, the critical perimeter located d/2 away from the loaded area is used to compute punching shear strength of the slab. According to this critical perimeter approach, punching shear strength can be computed as the minimum of the terms in Equation 5-2:

$$v_c = \min\{4\sqrt{f_c'};\quad (\frac{\alpha_s}{(b_o/d)}+\frac{1}{2})4\sqrt{f_c'};\quad (\frac{1}{2}+\frac{1}{B})4\sqrt{f_c'}\} \qquad \textit{Equation 5-2}$$

where f_c' is the concrete compressive strength, b_o is the critical perimeter length as shown in Figure 5-84, d is the effective depth of the slab, α_s is 40 for interior loading cases and 30 for edge loading cases, and B is the ratio of the length of the longest side of the loaded area to the shorter side. Then, the ultimate punching load carrying capacity of the slab is computed as follows:

$$V_c = v_c b_o d \qquad \textit{Equation 5-3}$$

Table 5-9 compares the punching shear capacities obtained from the bridge deck tests discussed in section 5.2 through 5.5 against predictions of the ACI 318-02 provisions (Equation 5-2 and Equation 5-3), assuming a uniform shear distribution at the critical section. It can be observed that the assumption of

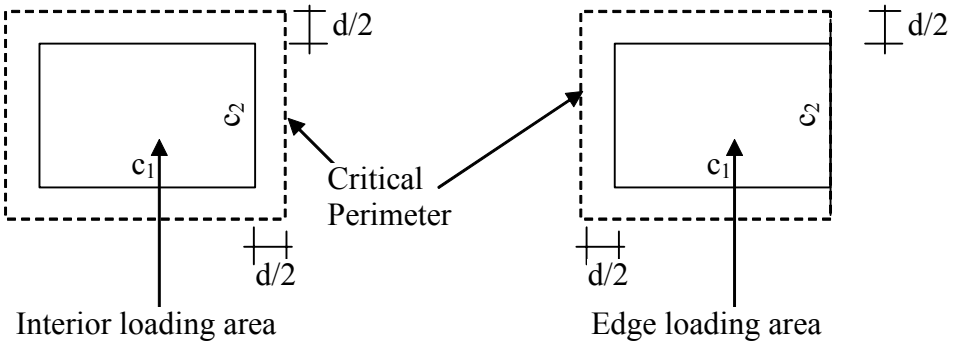

Figure 5-84: Critical perimeters used in punching shear strength calculations

Table 5-9: ACI 318-02 predictions using concentric punching shear capacity

Test Information						ACI 318-02 Predictions			
Test No	f_c' (psi)	c_1 (in)	c_2 (in.)	d (in.)	V_{test} (k)	v_c (psi)	b_o (in.)	V_{ACI} (k)	V_{exp}/V_{ACI}
1	6000	10	20	6.1	77	309.8	52.2	98.4	0.78
2	6000	10	20	6.1	81	309.8	52.2	98.4	0.82
3	6000	15	20	6.1	82	309.8	62.2	117.3	0.70
6	6000	15	20	8.1	96	309.8	66.2	165.8	0.58
4	6000	10	20	8.1	94	309.8	56.2	140.8	0.67
5	6000	10	20	8.1	91	309.8	56.2	140.8	0.64
								Mean :	0.70
								St. Dev:	0.09

a uniform stress distribution results in unsafe predictions of punching shear strength. The punching capacity of the bridge deck, when loaded at the edge, is approximately 60-80% of that predicted by ACI 318-02 and AASHTO LRFD expressions, assuming a uniform shear stress distribution.

A detailed resisting mechanism for the edge loading area is shown in Figure 5-85. According to this figure, the location of the critical section centroidal axis and the centroidal axis of the loaded area do not coincide for edge loading cases. Therefore, unbalanced moments resulting from this eccentricity naturally occur at loading areas at edges. In punching shear strength predictions, the correct use of the code expressions would necessitate the use of the eccentric

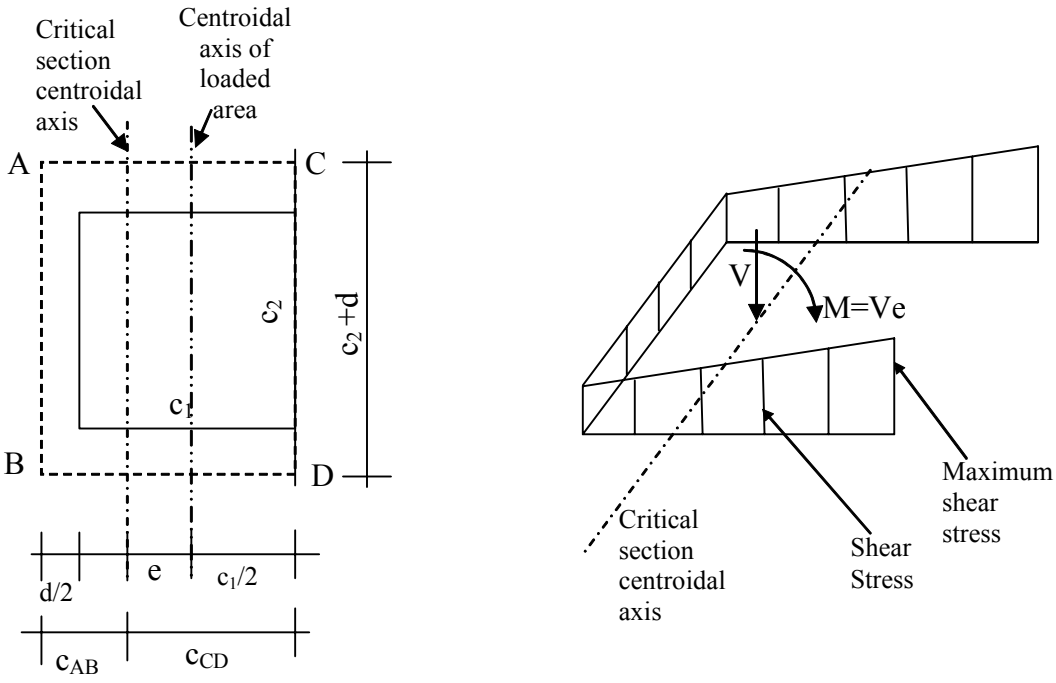

$$c_{AB} = \frac{[c_1 + d/2]^2 d}{b_o d} \qquad c_{CD} = c_1 + d/2 - c_{AB} \qquad e = c_{CD} - c_1/2$$

Figure 5-85: Shear stress resistance mechanism at edge loading areas

shear stress model, which is suggested for design of slab-column connections transferring moment.

The eccentric shear stress model in ACI 318-02 assumes that a portion of the unbalanced moment is carried by the eccentricity of the shear around the loading area. In the case of combined shear and unbalanced moment, occurring due to the eccentricity of the applied load, shear stress at a critical perimeter located d/2 away from the column face is computed using the following equation:

$$v_u = \frac{V_u}{b_o d} + \frac{\gamma_v (V_u e)}{(J / c_{CD})} \qquad \textbf{Equation 5-4}$$

where V_u is the gravity shear, b_o is the length of the critical perimeter, e is the distance between the centroidal axis of the critical section and centroidal axis of

the column as shown in Figure 5-85. The term J is analogous to the polar moment of inertia and is given as follows for edge loading areas:

$$J = \frac{d(c_1 + d/2)^3}{6} + \frac{(c_1 + d/2)d^3}{6} + d(c_2 + d)c_{AB}^2 + 2(c_1 + d/2)d\left[\frac{(c_1 + d/2)}{2} - c_{AB}\right]^2 \qquad \textit{Equation 5-5}$$

in which c_1 is the side length of the loading area perpendicular to the free edge, c_2 is the side length of the loading area parallel to the free edge, and d is the effective depth of the slab. According to Figure 5-85, the critical shear stress occurs at the free edge of the loading area and this shear stress needs to be checked against the concrete strength.

The γ_v factor, to compute the portion of the unbalanced moment transferred by eccentricity of shear, is given by the following equation for edge loading cases:

$$\gamma_v = 1 - \frac{1}{2/3 + \sqrt{(c_1 + d/2)/(c_2 + d)}} \qquad \textit{Equation 5-6}$$

Punching failure is assumed to occur when the critical shear stress, v_u, computed from Equation 5-4 exceeds the shear strength, v_c, given in Equation 5-2. Rearranging Equation 5-4, the ultimate punching shear strength of an edge loading area can be calculated as follows:

$$V_u = \frac{v_c}{\left(\frac{1}{b_o d} + \frac{\gamma_v e}{J/c_{CD}}\right)} \qquad \textit{Equation 5-7}$$

Punching shear strength predictions based on Equation 5-4 through Equation 5-7 are presented in Table 5-10. Comparisons of code predictions for two cases, neglecting the effect of unbalanced moment and considering its effect

Table 5-10: ACI 318-02 predictions considering unbalanced moments

Test No	c_1 (in.)	c_2 (in.)	d (in.)	b_o (in.)	A_c (in^2)	c_{AB} (in.)	c_{CD} (in.)	J (in^3)	v_c (psi)	γ_v	e (in.)	V_{ACI} (k)	V_{exp} (k)	V_{exp}/V_{ACI}
1	10	20	6.1	52.2	317.6	3.3	9.8	6119.5	309.8	0.27	4.8	59.3	77.0	1.30
2	10	20	6.1	52.2	317.6	3.3	9.8	6119.5	309.8	0.27	4.8	59.3	81.0	1.37
3	15	20	6.1	62.2	378.5	5.2	12.8	14141.2	309.8	0.33	5.3	73.1	82.0	1.12
6	15	20	8.1	66.2	535.2	5.5	13.6	22842.2	309.8	0.33	6.1	101.5	95.6	0.94
4	10	20	8.1	56.2	454.3	3.5	10.5	10571.8	309.8	0.27	5.5	83.7	93.8	1.12
5	10	20	8.1	56.2	454.3	3.5	10.5	10571.8	309.8	0.27	5.5	83.7	90.5	1.08
													Mean:	1.16
													St. Dev:	0.15

on punching shear strength are given in Figure 5-86. According to the predictions of ACI 318-02, when the effect of unbalanced moment is considered, ultimate strength predictions are in general agreement with the experimental results and they are conservative.

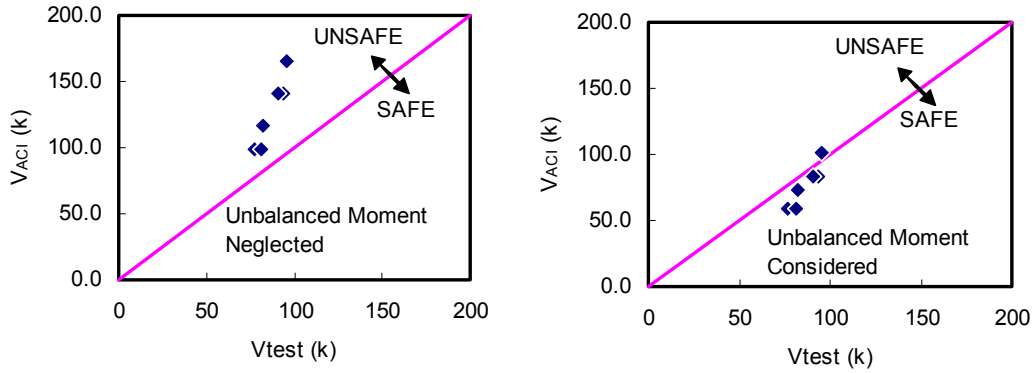

Figure 5-86: Comparisons of ACI 318-02 predictions with experimental results

The shape of the critical section assumed in the ACI 318-02 provisions for punching shear was found to be somewhat inaccurate for edge loading areas in bridge decks. The shapes of the actual failure surfaces were similar for the six punching failures. Figure 5-87 shows a plan view of a typical failure observed at the top of the bridge deck during this research.

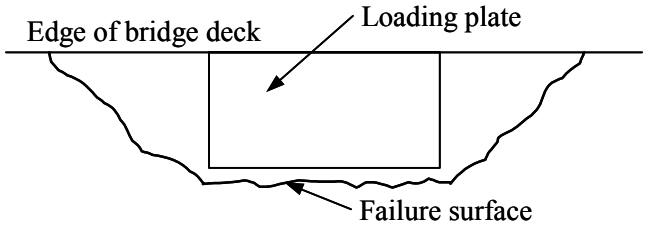

Figure 5-87: Typical bridge deck failure surface

CHAPTER 6

Conclusions and Recommendations

6.1 CONCLUSIONS

The TxDOT IBTS detail for the edge of bridge decks at expansion joints has performed satisfactorily in the field; however, its origin as well as ultimate capacity is unknown. The IBTS detail thickens a four-foot wide section of the deck at the expansion joint from eight-inches in the typical deck to 10-inches. The UTSE detail, which does not thicken the deck at the edge but increases the reinforcement ratio, was tested with the aim of increasing construction economy. A full-scale, four-girder, zero-skew, simple-span bridge deck specimen was constructed and tested in order to determine the effects of applying AASHTO design loading configurations to the edge of the deck. The test variables were the slab end detail (IBTS and UTSE) and the girder spacing (eight and 10-foot deck spans). The following conclusions can be drawn based on the research conducted:

- Serviceability performance
  - The IBTS detail, spanning eight-feet, exhibited excellent serviceability performance (i.e. cracking and deflections) when loaded in the positive and negative moment locations.
  - When subjected to positive moment loading and spanning 10-feet, the bottom surface of the IBTS detail cracked at HS-25 loading. However, the top of the deck did not crack until 3.5 times the HS-25 load level was reached.

- The Uniform Thickness Slab End (UTSE) detail was also tested and performed similarly to the IBTS detail at service loads.
- The top surface of the UTSE detail cracked at a load 75% greater than the HS-25 loading in the eight-foot span and 50% greater than the HS-25 loading in the 10-foot span.
- Both slab end details behaved linear elastically and no visible deterioration was evident up to a load 75% greater than the HS-25 load level, when spanning eight-feet.
- When spanning 10-feet, the IBTS detail remained linear elastic until the HS-25 load level and the UTSE detail cracked at a load 20% greater than HS-25 load level.
- The UTSE detail was slightly more flexible than the IBTS detail.

- Ultimate capacity
  - The ultimate load capacity of both slab end details, for both deck spans tested, was a minimum of 4.9 times the HS-25 load level.
  - At failure, the midspan edge deflection remained small for all test areas.
  - The critical failure mechanism for all test areas on this bridge deck was punching shear.

ACI 318-02 and AASHTO LRFD provisions were examined to determine the punching shear strength of the bridge deck loaded flush at the slab edge. Then, the experimental results were compared to the code predictions. The following conclusions based on punching shear can be drawn:

- The UTSE detail had about a 20% lower load carrying capacity than the IBTS detail due to the 20% difference in section depth between the two. However, the reserve strength of the UTSE detail was much higher than that typically expected in bridge design (4.9xHS-25 in eight-foot span and 5.2xHS-25 in 10-foot span).
- Unbalanced moments naturally occur at loading areas near the edge of bridge decks due to eccentricity between the centroidal axis of the critical section and the centroid of the loaded area.
- ACI 318-02 expressions considering the effect of unbalanced moment should be used to compute the punching shear strength of edge loading cases. The maximum shear stress, located at the free edge, should be checked against the permissible concrete shear stress to compute the ultimate strength of the loading area.
- ACI 318-02 and AASHTO LRFD provisions for concentrated loads do not provide safe estimations of punching shear strength for edge loading cases when unbalanced moments are neglected.
- The AASHTO LRFD Bridge Design Specification's prediction for punching shear is unsafe at the edge of bridge decks.
- Additional eccentricities caused in the direction perpendicular to the free edge need to be considered if significant unbalanced moments are transferred in this direction.

6.2 RECOMMENDATIONS FOR FUTURE RESEARCH

The behavior of a zero-skew, cast-in-place bridge deck has been discussed in this thesis. The main variables tested were the girder spacing (eight and 10-foot) and the slab end detail (IBTS and UTSE). A zero-skew bridge deck was chosen as it simplifies the boundary conditions and provides vital baseline

information needed to explain the behavior of skewed slab end details. On a skewed bridge deck, the effective span is increased and load transfer from deck to girders becomes more complicated. A full-scale, 45^{o}-skew bridge deck is currently being tested.

The behavior of the UTSE and IBTS details need to be evaluated for skewed boundary conditions. This evaluation should be done at service load and overload levels. In addition, the reserve strength of the edge detail needs to be evaluated for critical and commonly used skew angles. The presence of the armored joint at the deck edge may change the response of the edge detail to externally applied loads. This may result in reduced deflections and increased punching shear strength at the edge. These effects need to be quantified to evaluate the exact reserve strength of edge details in as-built conditions. However, if current reserve strength levels are experienced in the ongoing tests, there would be no need to evaluate the reserve strength accurately, as the reserve strengths of all test specimens were substantially higher than the AASHTO LRFD Bridge Design Specification loadings.

All the test areas failed at the edge tire, indicating the edge of the deck is a more critical location than the interior. The punching shear capacity of the bridge deck, predicted by the AAHSTO LRFD Bridge Design Specification, is inaccurate and unconservative for edge loading locations. By including the effect of unbalanced moments, as specified in ACI 318-02, the predicted punching shear capacity is both accurate and conservative. The results of the six tests performed on this bridge deck edge must be verified by additional testing as very few edge tests have been performed and there are many variables involved.

APPENDIX A

Supplemental Test Data

A.1 INTRODUCTION

After casting the bridge deck specimen, the loading location for the southwest and northwest test areas was changed. The loading location was shifted two-feet to the east, changing the critical location for strains (Figure 5-35). In addition, the negative moment section strain gauges were not at the critical section; therefore, the strain data from the southwest and northwest test areas is of limited use. The load versus strain plots, strain profiles, moment calculations and elastic moment comparisons for these two test areas are presented herein.

A.2 SOUTHWEST TEST AREA

A.2.1 Load vs. strain response

A.2.1.1 2xHS-25 load step

Figure A-1 shows load versus strain plots for the three loading configurations applied at the 2xHS-25 load step. The strains created by the loading at midspan induced much larger strains at the negative moment section than at the positive section. This contrasts the crack maps, which show cracking at midspan well before cracking at the girder. However, the strains are relatively small at this load step for both moment sections. As discussed in section 5.3.1.1, the residual strain created by the tandem loading configuration is due to microcracking within the section. The response of the bridge deck to all loading configurations at the 2xHS-25 load step was linear elastic.

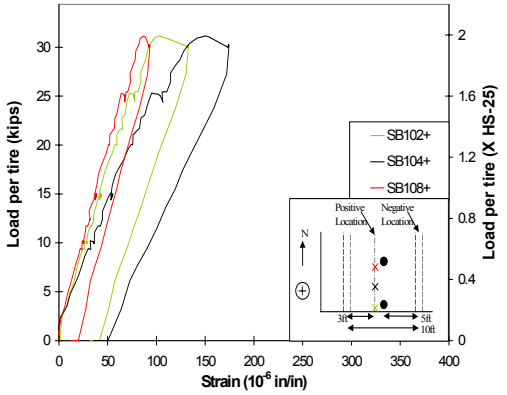

(i) Tandem

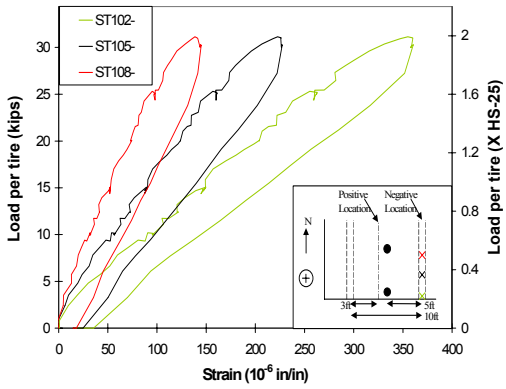

(ii) Tandem

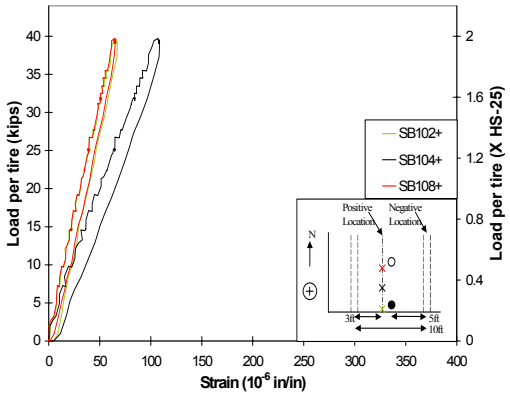

(iii) Truck axle-front

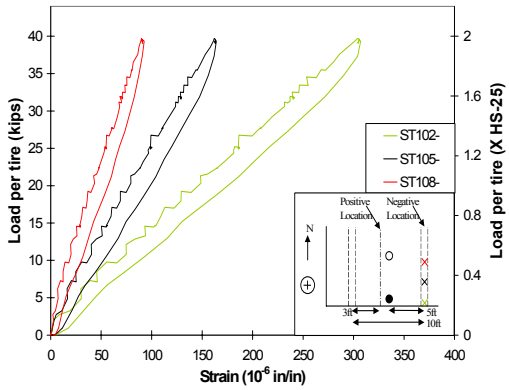

(iv) Truck axle-front

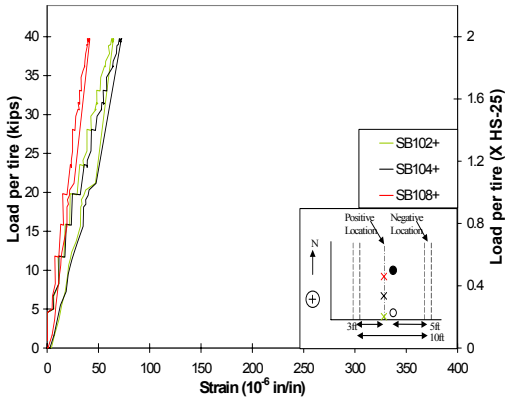

(v) Truck axle-back

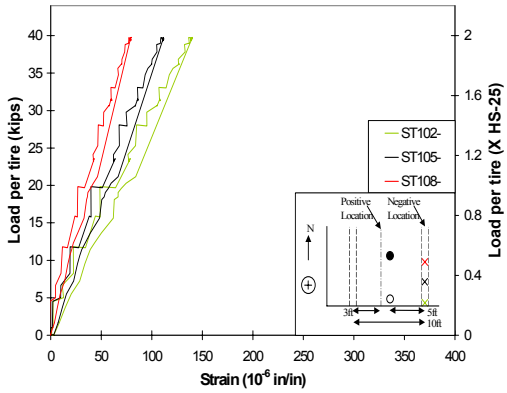

(vi) Truck axle-back

Figure A-1: Load vs. strain, 2xHS-25 load step, midspan loading location, southwest test area; (i), (iii) and (v): bottom mat at positive location; (ii), (iv) and (vi): top mat at negative location

A.2.1.2 2.4xHS-25 load step

The strain readings for the negative moment section are again significantly larger than the positive section at this load step, even though the loads are applied at midspan. The shape of the load versus strain plots in Figure A-2 are identical to the 2xHS-25 load step. The magnitude of the strains increased by 30-50% between the 2xHS-25 and 2.4xHS-25 load steps, a load increase of 20%.

The maximum strain reached at this load step was 475με (23% of yield strain in the steel) caused by the tandem loading configuration. A slight residual strain of 95με remained in the reinforcing steel after unloading. However, the unloading portion of the plot has the same slope as the loading portion, indicating the deterioration was insignificant. The behavior of the bridge deck is linear elastic at the 2.4xHS-25 load level.

A.2.1.3 3.5xHS-25 load step

the critical section for strains switched at this load step as the strains induced in the positive moment section were significantly larger than in the negative section. The maximum strain of 1255με (61% of yield strain of the steel) occurred due to the tandem loading configuration after significant non-linear behavior. The strain magnitudes recorded in the positive moment section at this load step increased by 700% compared to those at the 2xHS-25 load step, while the load increased by 175%. This is due to the non-linear behavior of the concrete after cracking.

The tandem loading configuration created a non-linear response in the bridge deck at the positive moment section (Figure A-3, i). At a load of 43kips (2.8xHS-25) per tire, there is a drastic reduction in the slope of its plot. The stiffness drops to nearly zero and then the section begins to carry more load. This

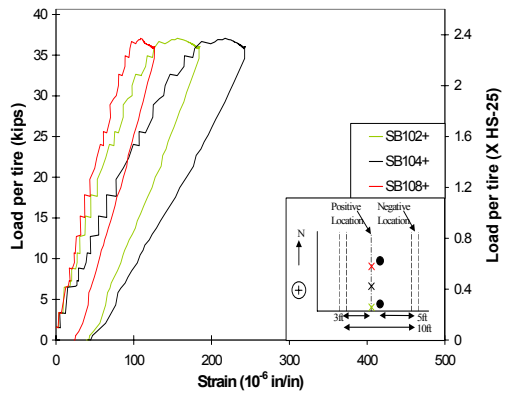

(i) Tandem

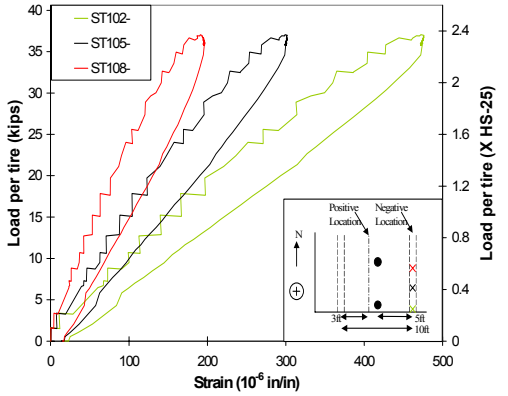

(ii) Tandem

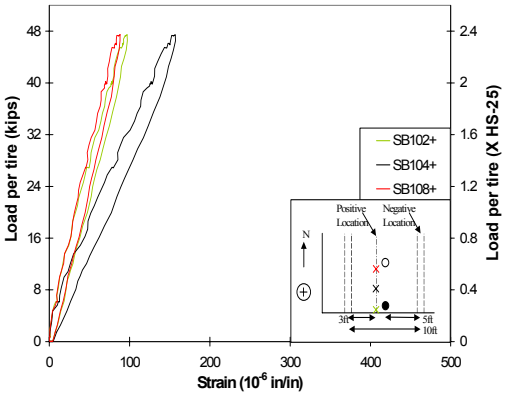

(iii) Truck axle-front

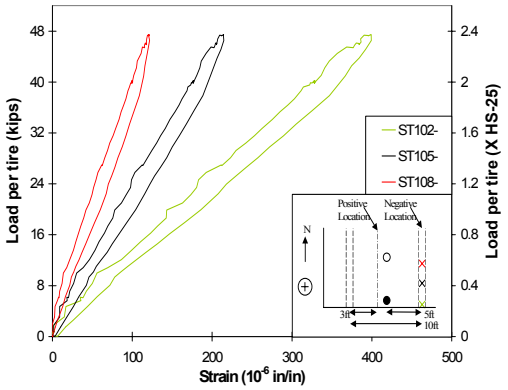

(iv) Truck axle-front

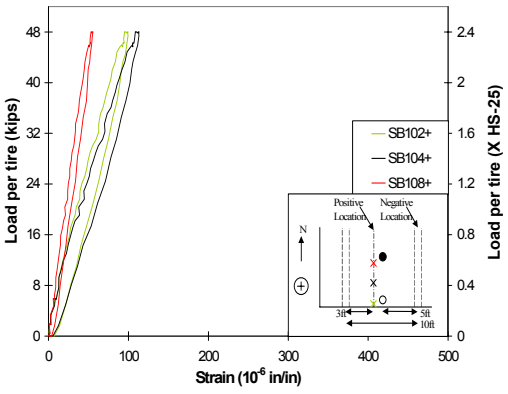

(v) Truck axle-back

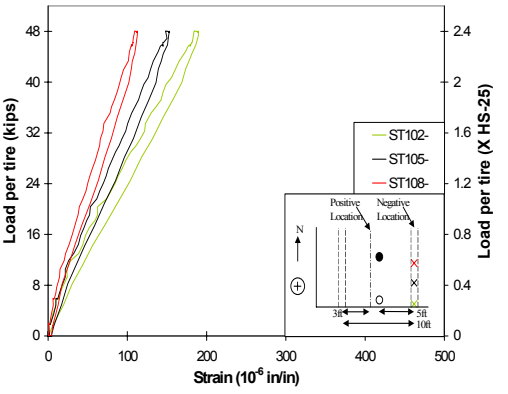

(vi) Truck axle-back

Figure A-2: Load vs. strain, 2.4xHS-25 load step, midspan loading location, southwest test area; (i), (iii) and (v): bottom mat at positive location; (ii), (iv) and (vi): top mat at negative location

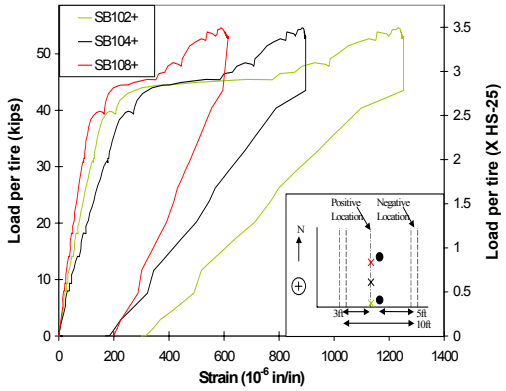

(i) Tandem

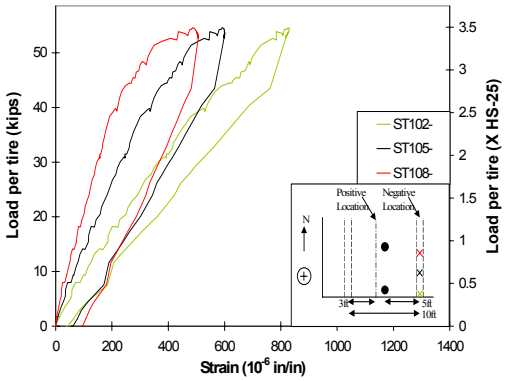

(ii) Tandem

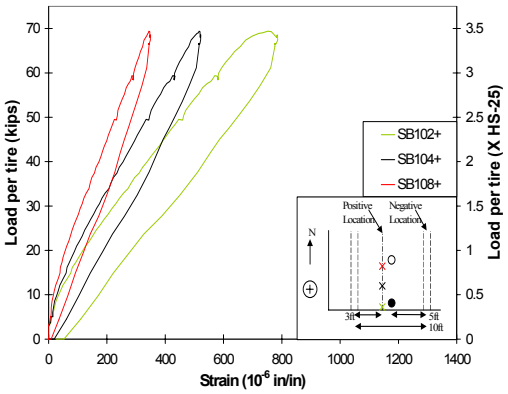

(iii) Truck axle-front

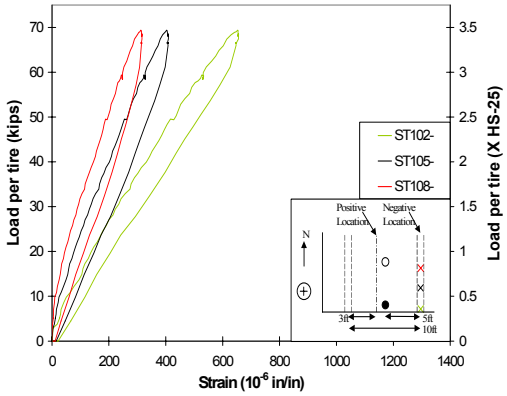

(iv) Truck axle-front

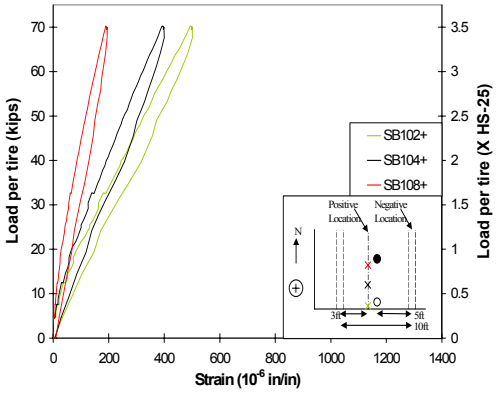

(v) Truck axle-back

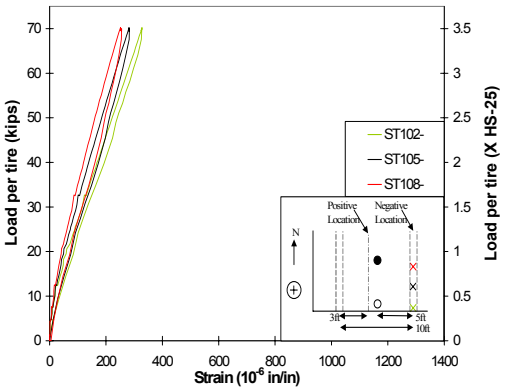

(vi) Truck axle-back

Figure A-3: Load vs. strain, 3.5xHS-25 load step, midspan loading location, southwest test area; (i), (iii) and (v): bottom mat at positive location; (ii), (iv) and (vi): top mat at negative location

deterioration is also evident in the negative moment section (Figure A-3, ii), which shows a more gradual stiffness reduction during the load application. The load versus deflection plots for this load step also show a stiffness reduction at this load level. In addition, the crack maps show the surface crack widths started to increase significantly at the 3.5xHS-25 load step after the stiffness reduction around the reinforcing steel.

The amount of deterioration caused by each loading configuration is evident by the shape of the loop created by the loading and unloading portion of the load versus strain plots. In other words, the proximity of the loading and unloading portions of the plots indicates the damage caused during the load application. The tandem loading configuration plot has the largest loop, and therefore, created the most damage at the 3.5xHS-25 load step. The truck axle-back loading configuration plot is nearly a single line, indicating very little damage due to this loading.

A.2.1.4 Loading to failure

Figure A-4 shows load versus strain plots for the three representative strain gauges at the positive and negative moment sections. The load versus strain plot for the 3.5xHS-25 load step is also plotted in order to include residual strains induced in the reinforcing steel. The gauge closest to the interior of the bridge deck (SB108+) shows a change in stiffness at a load of about 61kips (3.9xHS-25) per tire (Figure A-4, i). The other two strain gauge readings shown do not imitate this stiffness change, however, their stiffness is already reduced significantly. The crack maps show that the previous load steps deteriorated the edge of the slab end detail.

The ultimate strains at the positive and negative moment sections were very similar in magnitude due to redistribution of stresses near failure. The

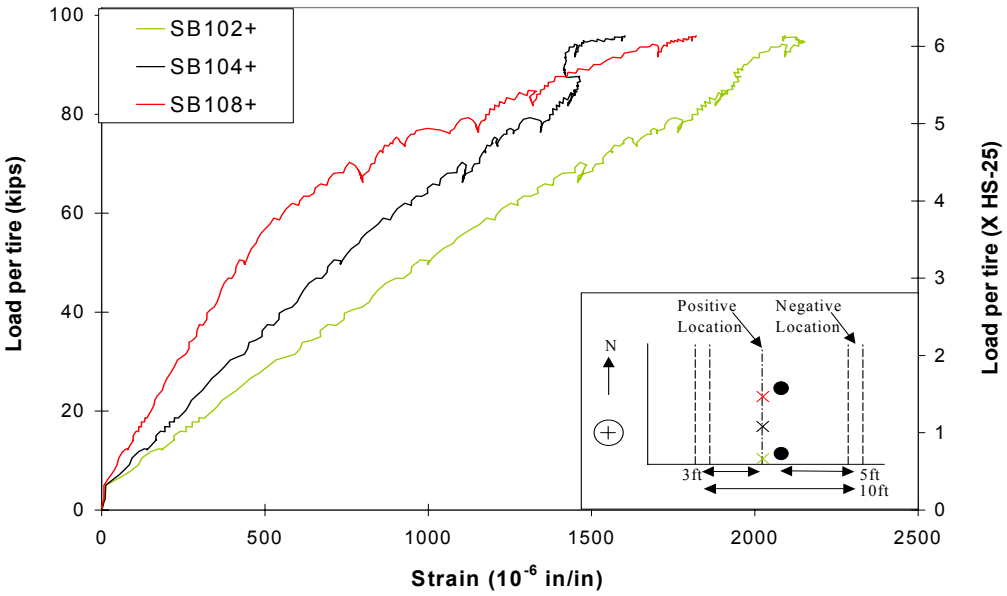

(a) Strain gauges in bottom mat at positive moment section, tandem vehicle

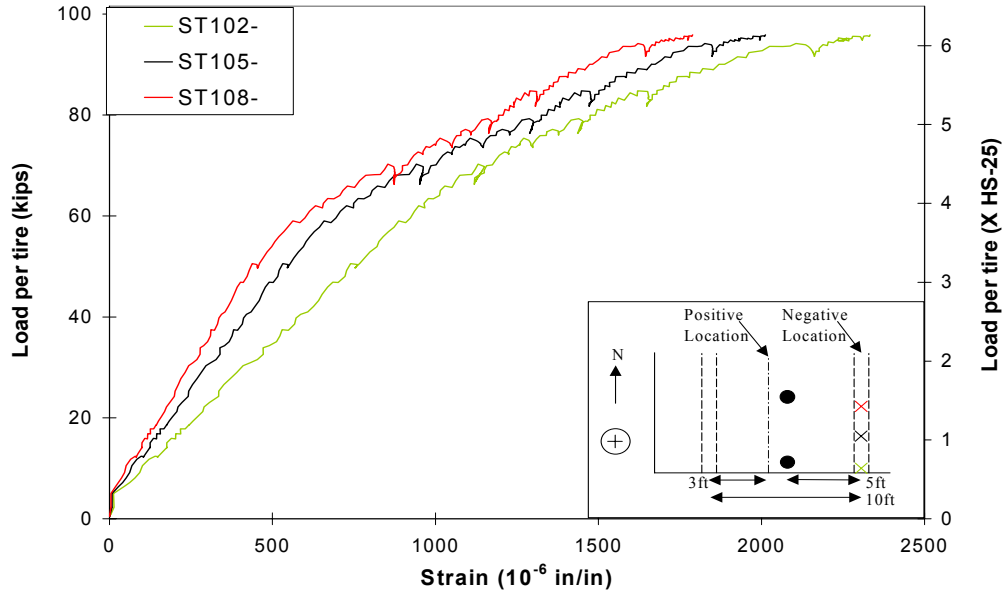

(b) Strain gauges in top mat at negative moment section, tandem vehicle

Figure A-4: Load vs. strain, loading to failure, midspan loading location, southwest test area

maximum strain created in the southwest test area was 2300με in the edge-most rebar at the negative moment section (Figure A-4, ii). This rebar is yielding since the yield strain of the reinforcing steel is 2069με. In addition, the stiffness of the this reinforcing bar changes to nearly zero at a strain magnitude of approximately 2000με, showing yielding of the rebar. The shape of the load versus strain plots in Figure A-4 (ii) for the three representative strain gauges are similar. A stiffness change is mirrored through the three representative strain gauges.

A.2.2 Strain profiles

A.2.2.1 2xHS-25 load step

Figure A-5 shows strain profiles for the three loading configurations applied at the 2xHS-25 load step. The average strain at the negative moment section is approximately three times larger than at the positive moment section, even though the load is being applied at midspan. The tandem loading configuration created a larger average strain across the section than the truck axle-front configuration. The truck axle-back loading configuration created comparable strains to the other loading configurations, however, the magnitude of all the strain readings at this load step were insignificant.

The largest strain created at this load step was 355με (17% of yield strain in the steel), caused by the tandem loading configuration. However, the truck axle-front loading configuration created a comparable maximum strain of 304με (15% of yield strain in the steel). The largest strain readings obtained at the positive moment section (Figure A-5, i, iii and v) were from the SB104+ gauge, located in the middle of the thickened edge. However, at the negative moment section, the strains decline moving into the thickened edge.

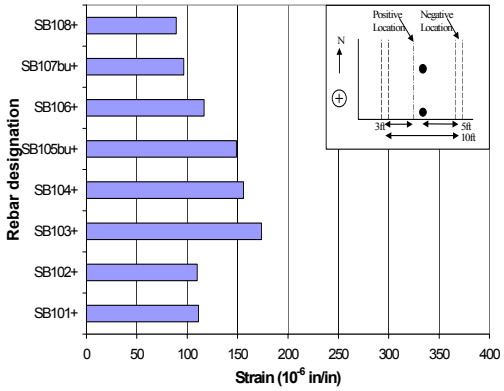

(i) Tandem

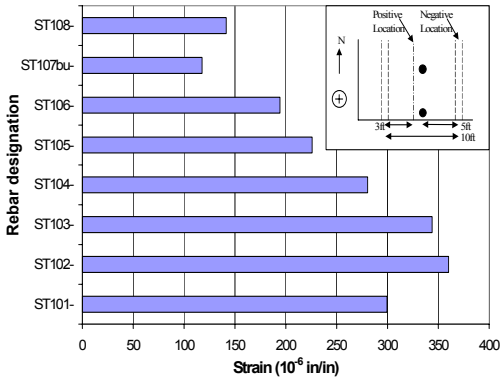

(ii) Tandem

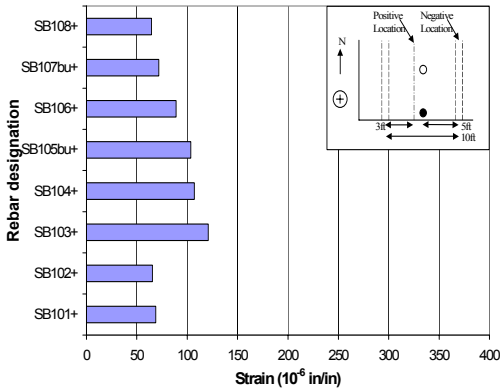

(iii) Truck axle-front

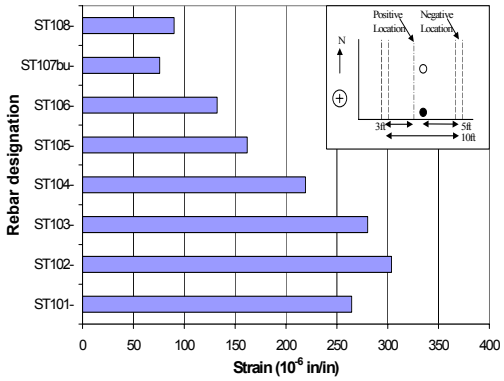

(iv) Truck axle-front

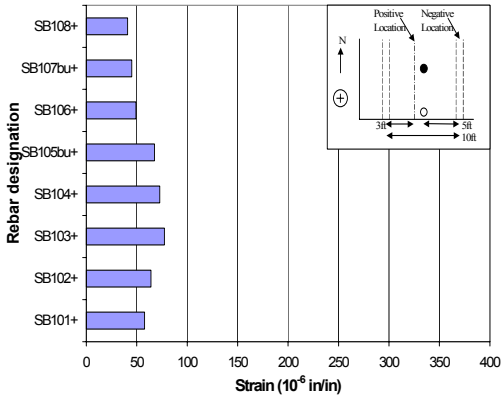

(v) Truck axle-back

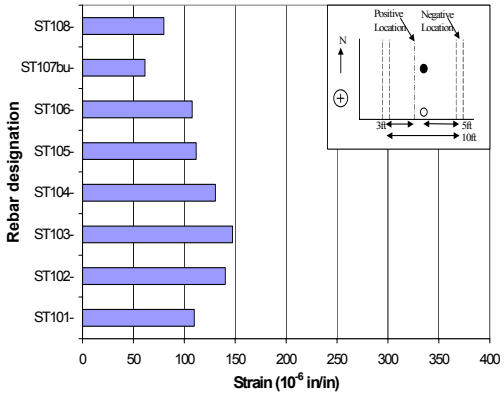

(vi) Truck axle-back

Figure A-5: Strain profiles, 2xHS-25 load step, midspan loading location, southwest test area; (i), (iii) and (v): bottom mat at positive location; (ii), (iv) and (vi): top mat at negative location

A.2.2.2 2.4xHS-25 load step

The strain profiles for the tandem and truck axle-front loading configurations at the negative moment section (Figure A-6, ii and iv) show a large strain gradient across the thickened edge. The strain profiles for these two loading configurations at the positive moment section are much more uniform (Figure A-6, i and iii). Although the strain profiles at the positive section are close to uniform for all loading configurations, the most critically strained gauges are in the middle of the thickened edge.

The maximum strain created in the thickened edge due to the 2.4xHS-25 load step was in the ST102- strain gauge, which was plotted and discussed in the load versus strain section. The strains in the bars near the edge of the deck at the negative moment section are much more critical than at any other location in the test area.

A.2.2.3 3.5xHS-25 load step

The most critically strained moment section switched from the negative section to the positive section at this load step. All the strain profiles in Figure A-7 show a reduction in strains from the edge of the slab end detail to the interior. The largest strain was again created in the SB102+ strain gauge. The strains caused by the tandem loading configuration were more critical than those caused by the truck loading configurations. Therefore, the southwest test area was taken to failure in the tandem loading configuration.

A.2.2.4 Loading to failure

The SB105bu+ strain gauge recorded bizarre strains during the loading to failure, and therefore, was removed from the failure strain profiles in Figure A-8. Residual strains are not included in the failure strain profile as there were only

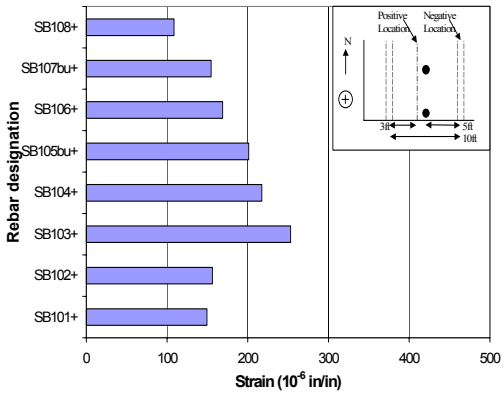

(i) Tandem

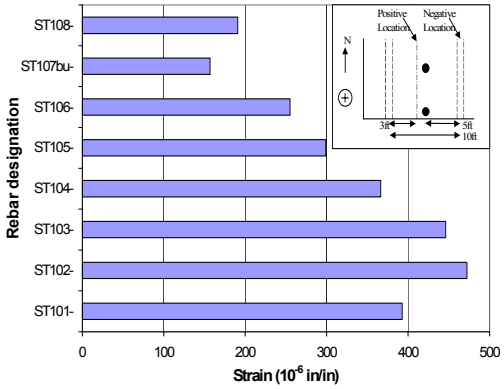

(ii) Tandem

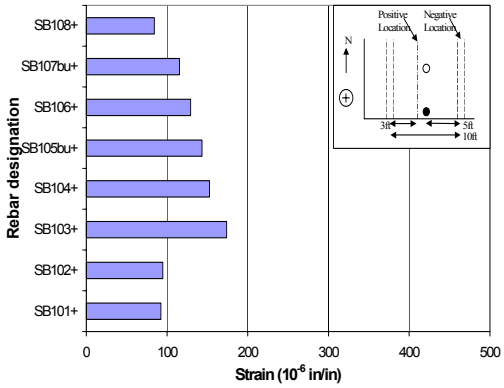

(iii) Truck axle-front

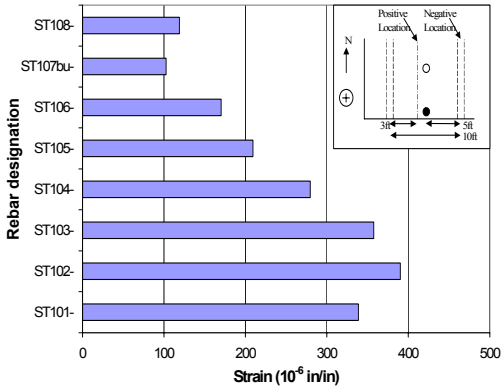

(iv) Truck axle-front

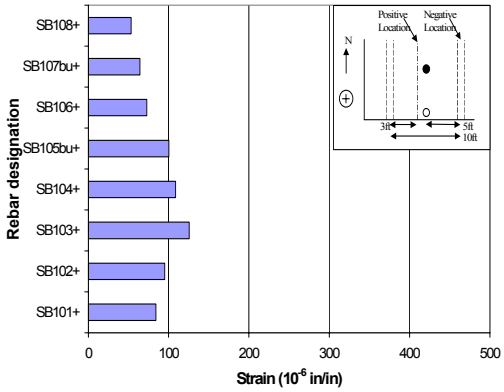

(v) Truck axle-back

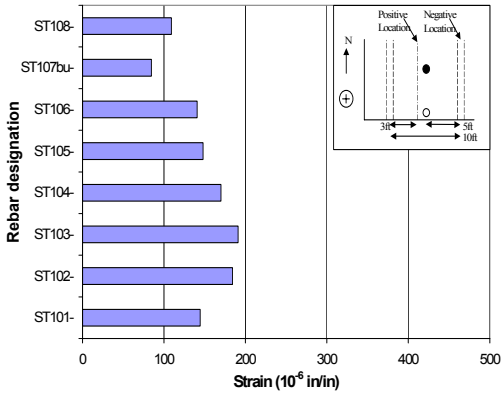

(vi) Truck axle-back

Figure A-6: Strain profiles, 2.4xHS-25 load step, midspan loading location, southwest test area; (i), (iii) and (v): bottom mat at positive location; (ii), (iv) and (vi): top mat at negative location

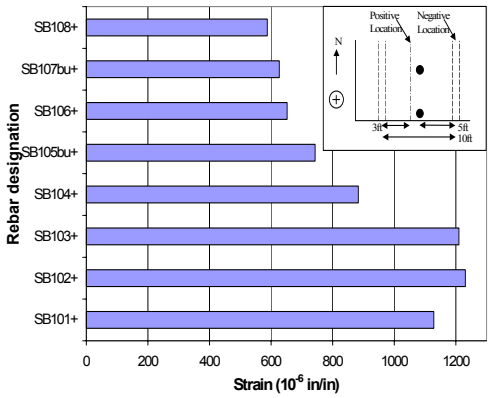

(i) Tandem

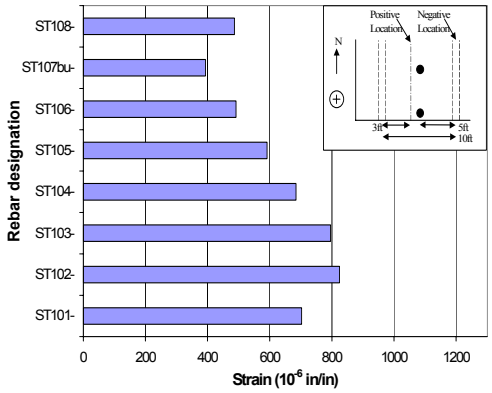

(ii) Tandem

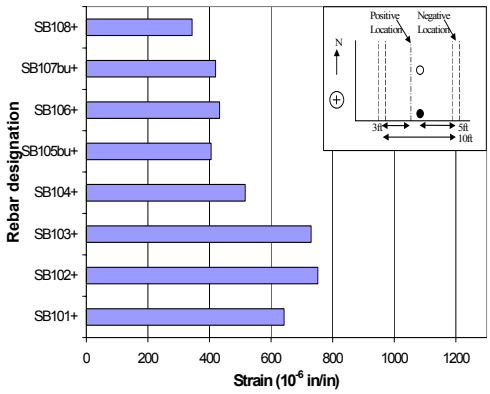

(iii) Truck axle-front

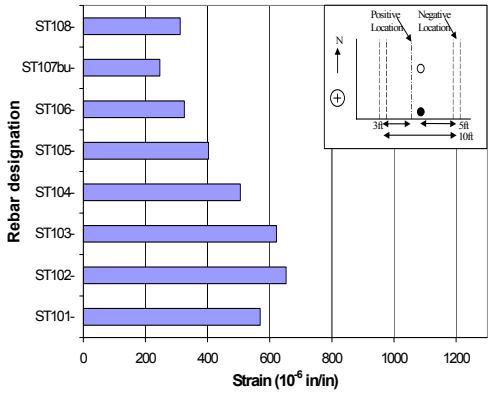

(iv) Truck axle-front

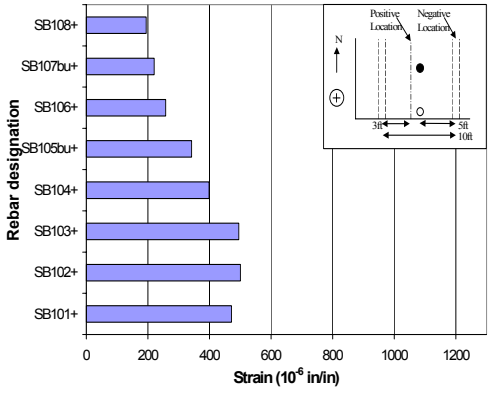

(v) Truck axle-back

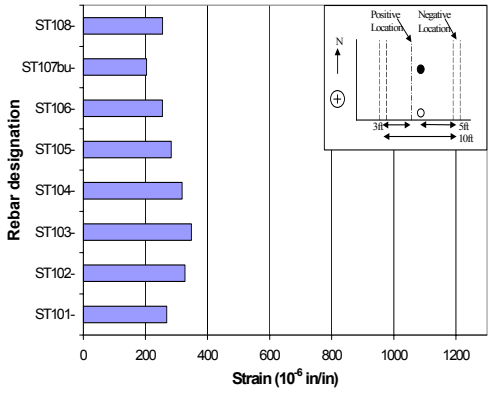

(vi) Truck axle-back

Figure A-7: Strain profiles, 3.5xHS-25 load step, midspan loading location, southwest test area; (i), (iii) and (v): bottom mat at positive location; (ii), (iv) and (vi): top mat at negative location

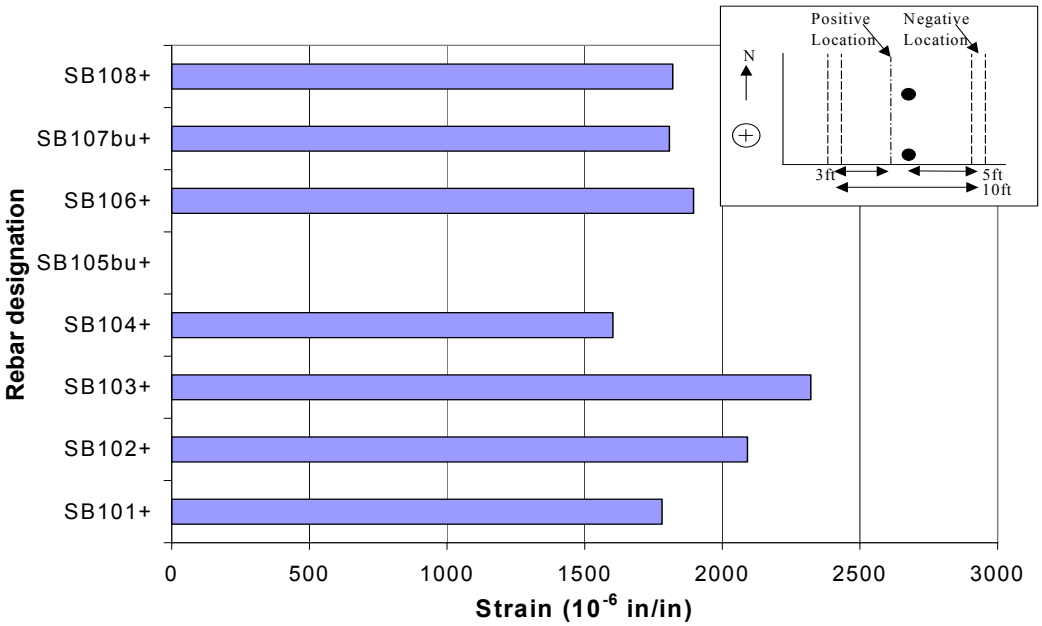

(i)Bottom mat at the positive section

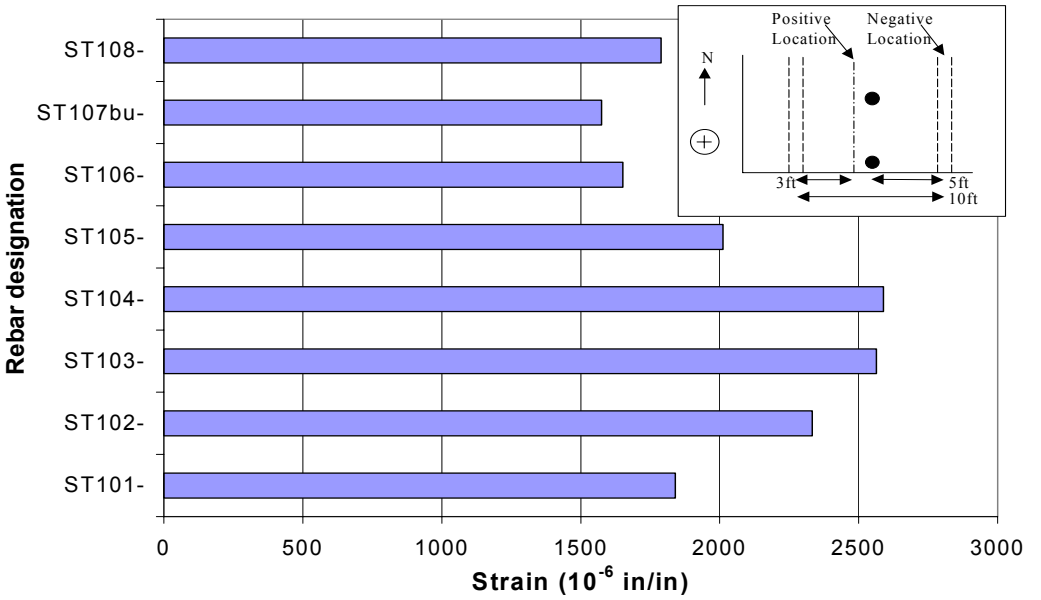

(ii)Top mat at the negative section

Figure A-8: Strain profiles, loading to failure, midspan loading location, southwest test area

small residual strains induced at the lower load steps. Just prior to failure of the bridge deck, the strain magnitudes at the negative moment section slightly exceeded those at the positive moment section. However, strains at the two sections had similar magnitudes due to redistribution of stresses near failure. In addition, the strain profiles are relatively uniform at failure due to redistribution. The maximum strain induced in the southwest test area was 2600με in the #4 rebar. Three strain gauges in each moment section recorded strains greater than 2069με, the yield strain of the reinforcing steel. This indicates substantial yielding of the reinforcing steel in the thickened edge occurred prior to the punching shear failure of the edge-most tire. This is verified by the load versus deflection plot for loading to failure, which reduced to zero stiffness just prior to failure.

A.2.3 Moment calculation

The results of the moment calculation for the southwest test area are shown in the plots in Figure A-9. As discussed previously, the moments in the positive and negative moment sections are calculated using the strain gauge data and "plane stresses remain plane" principle. The moments at the positive and negative sections are similar up to the 3xHS-25 load step. However, the maximum moments calculated for the positive and negative moment sections are 750k*in and 1500k*in, respectively. The maximum moment at the positive section is half the maximum moment at the negative section. This is partially due to the location of the strain gauges, which is not at the critical section for this loading location, as discussed in section 5.3.

At the positive moment section, the experimentally calculated moment plot is nearly vertical. Therefore, a large increase in loading creates a small increase in the moment induced in the section (Figure A-9, i). The effect of

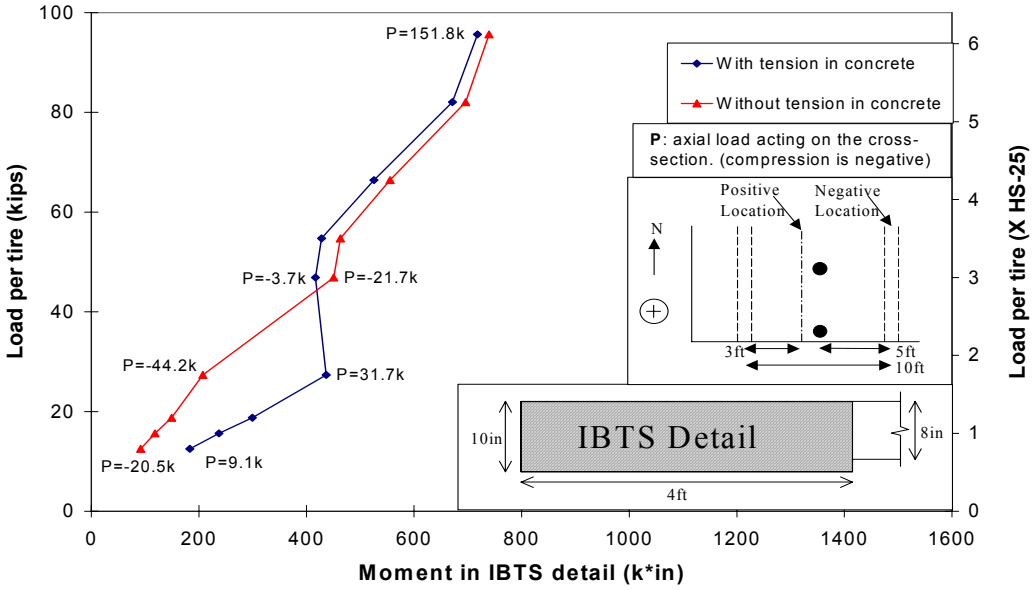

(i)Positive moment location

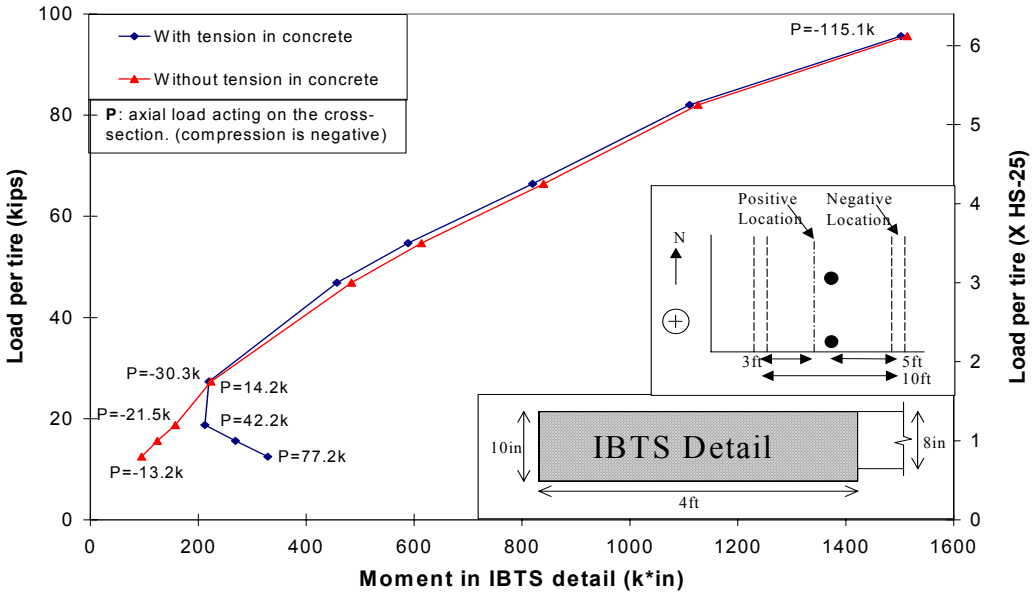

(ii)Negative moment location

Figure A-9: Moment calculated from strain gauge readings, tandem vehicle only, southwest test area

including tension in concrete is significant until the 3xHS-25 load step. At the 1.75xHS-25 load step, the moment when tension is included is over twice as large as when it is ignored. The in-plane force at the positive moment section results in a large tension force at failure, after switching between tension and compression at the lower load steps.

The plot for the moments in the negative section is linear when tension in the concrete is ignored (Figure A-9, ii). When tension in concrete is included, the calculated moments are larger prior to cracking. Then, they join with the linear plot ignoring tension in concrete. The in-plane force is initially in tension when tension in concrete is included and small compression when it is ignored. At failure, the in-plane force at the negative moment section is a large compression force of –115.1kips.

A.2.4 Elastic moment comparison

The moments calculated from the strain gauges are compared to an elastic 3-span beam analysis in Figure A-10. Cracking in the southwest test area occurred at a load of HS-25, therefore, this load step is compared, as the deck is uncracked at this load. The experimentally calculated moments are very close to the elastic analysis at both moment sections. The moments from the strain gauges are less than the elastic moment analysis. This can be attributed to two-way action of the deck as some of the load is resisted by the interior of the bridge deck.

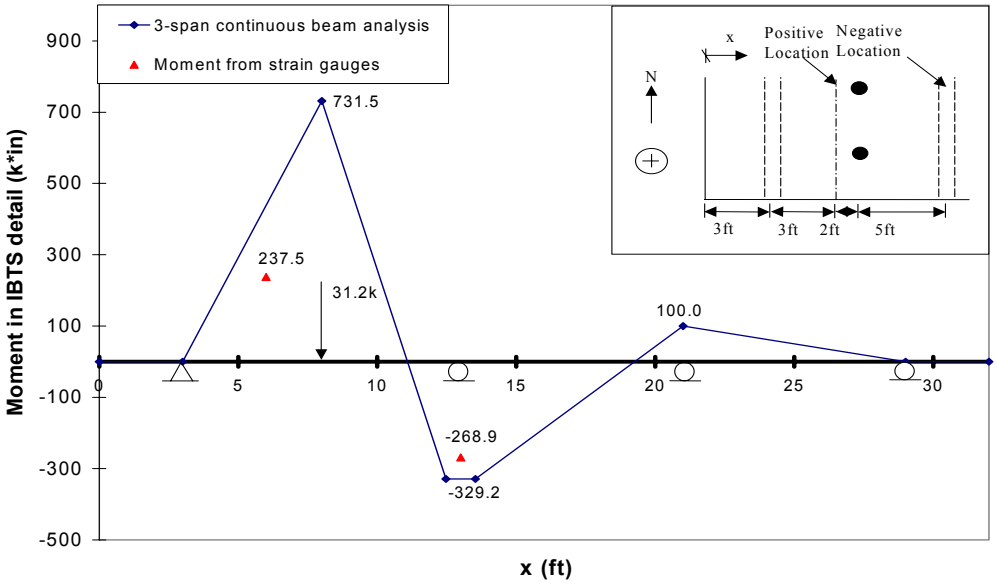

Figure A-10: Elastic moment compared to moment from strain gauges, HS-25 load step

A.3 NORTHWEST TEST AREA

A.3.1 Load vs. strain response

After analyzing the data, three representative strain gauges were chosen to display in the load versus strain plots in this section.

A.3.1.1 HS-25 load step

Figure A-11 shows plots of load versus strain for the HS-25 load step. The largest strain occurs at the positive moment section for the tandem and truck axle-back loading configurations. However, the truck axle-front loading configuration created larger strains at the negative moment section. The strains at the two moment sections are close for all loading configurations.

The maximum strain created at this load step was 335με (16% of yield strain of the steel), due to the tandem loading configuration. There is a non-linearity and residual strain shown in the #1 and #6 rebars during the application of the tandem loading configuration. This is the first loading applied to the northwest test area; therefore, the non-linearity is likely due to microcracking within the thickened edge. In addition, the plots for the truck loading configurations (Figure A-11, iii, iv, v and vi) showed linear elastic behavior. The application of the tandem HS-25 loading configuration created some shifting within the section (i.e. microcracking), however, the overall behavior of the UTSE detail was elastic and the strain magnitudes were small.

A.3.1.2 1.2xHS-25 load step

The strains induced at the positive moment section during the tandem loading application are smaller for the 1.2xHS-25 load step than the HS-25 load step. In addition, all of the plots in Figure A-12 show linear elastic behavior at the 20% overload. The shape of the load versus deflection plots show a close

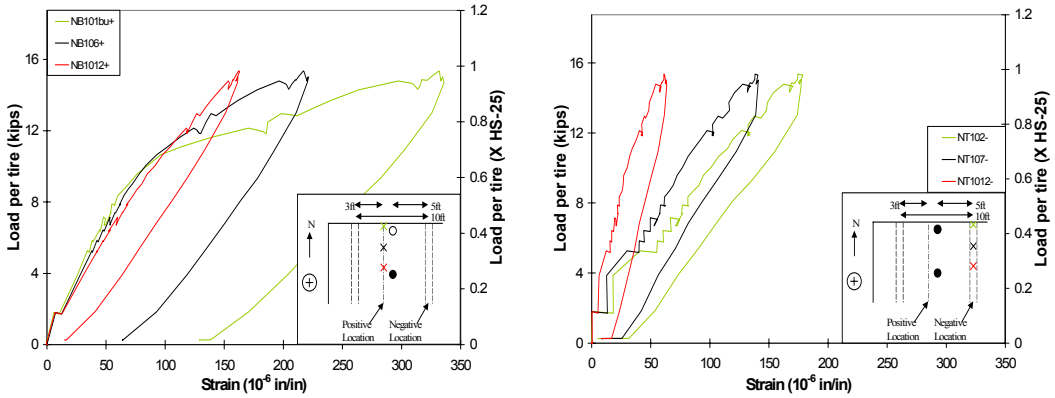

(i) Tandem

(ii) Tandem

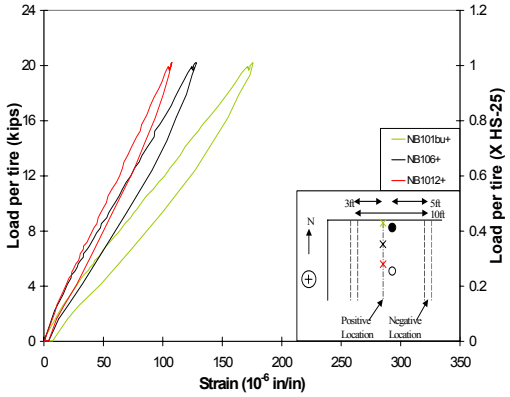

(iii) Truck axle-front

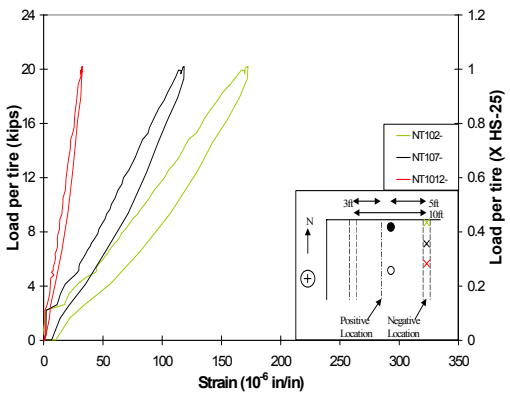

(iv) Truck axle-front

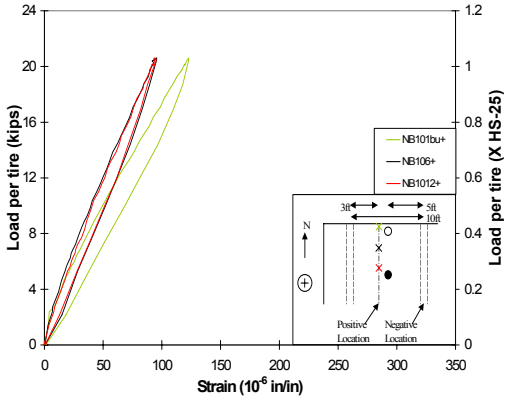

(v) Truck axle-back

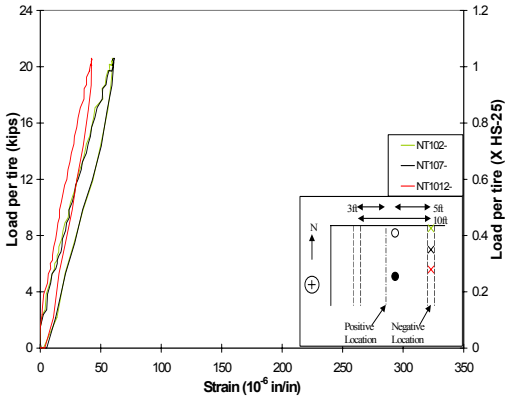

(vi) Truck axle-back

Figure A-11: Load vs. strain, HS-25 load step, midspan loading location, northwest test area; (i), (iii) and (v): bottom mat at positive location; (ii), (iv) and (vi): top mat at negative location

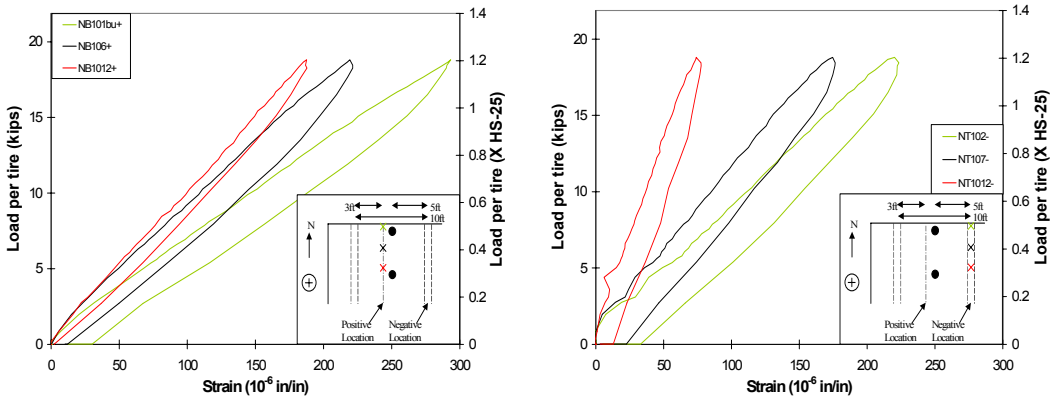

(i) Tandem

(ii) Tandem

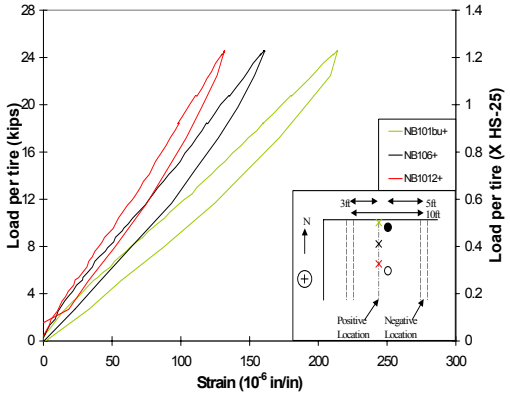

(iii) Truck axle-front

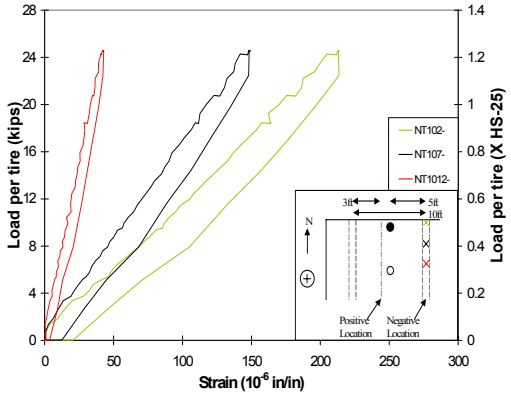

(iv) Truck axle-front

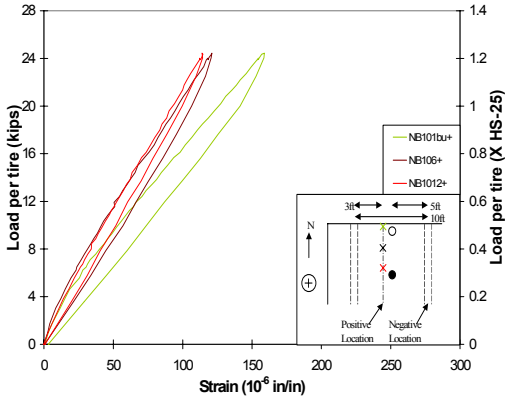

(v) Truck axle-back

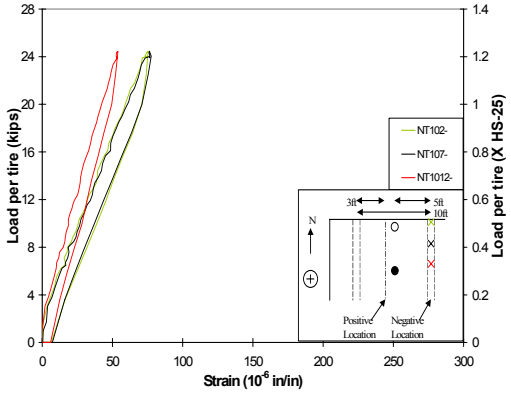

(vi) Truck axle-back

Figure A-12: Load vs. strain, 1.2xHS-25 load step, midspan loading location, northwest test area; (i), (iii) and (v): bottom mat at positive location; (ii), (iv) and (vi): top mat at negative location

loop indicating no deterioration occurred within the section during the load application. This supports the microcracking explanation for the non-linear behavior which occurred at the HS-25 load step.

The maximum strain created at the 1.2xHS-25 load step was 294με (14% of yield strain of the steel), due to the tandem loading configuration at the positive moment section (Figure A-12, i). The strain magnitudes at the positive and negative moment sections were relatively equal for all loading configurations. The truck axle-back loading configuration created strains comparable to the other configurations at this load step.

A.3.1.3 1.75xHS-25 load step

The strains induced by the tandem loading configuration at the positive moment section where approximately 26% larger at this load step than at the HS-25 load step. However, the other loading locations all showed a strain increase relative to the load increase. The maximum strain created at this load step is 424με (20% of yield strain of the steel), at the positive moment section due to the tandem loading configuration (Figure A-13, i). The UTSE detail was linear elastic at the 1.75xHS-25 load step.

A.3.1.4 3xHS-25 load step

Figure A-14 shows that the behavior of the bridge deck was again linear elastic at the 3xHS-25 load step. In the load versus strain plots, the response of the bridge deck to the tandem loading configuration (Figure A-14, i) does not show a distinct change in stiffness. However, there is a slight reduction in stiffness between the start of the load application and the 3xHS-25 load level. The slope of the unloading portion of the plot is roughly the same as the initial loading portion, indicating the section is not substantially deteriorated. However,

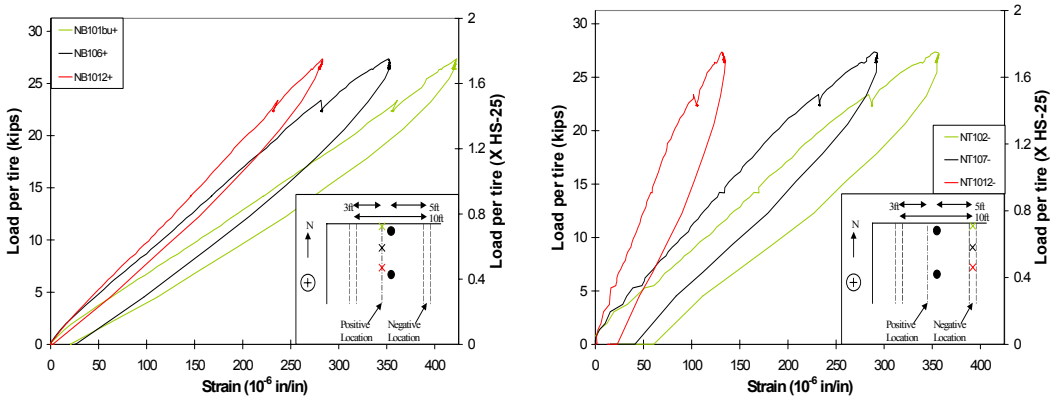

(i) Tandem

(ii) Tandem

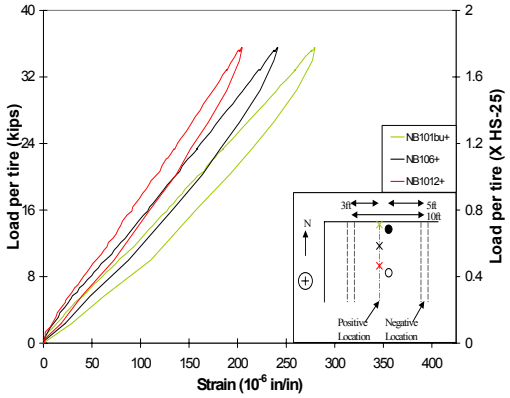

(iii) Truck axle-front

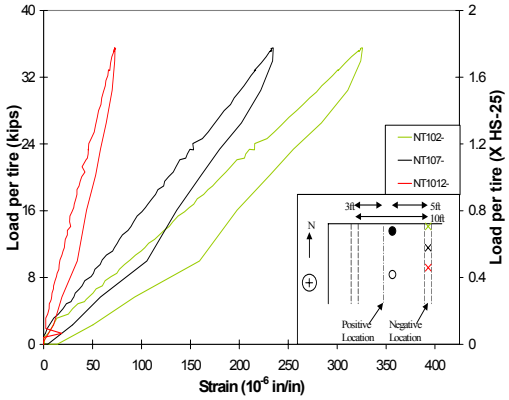

(iv) Truck axle-front

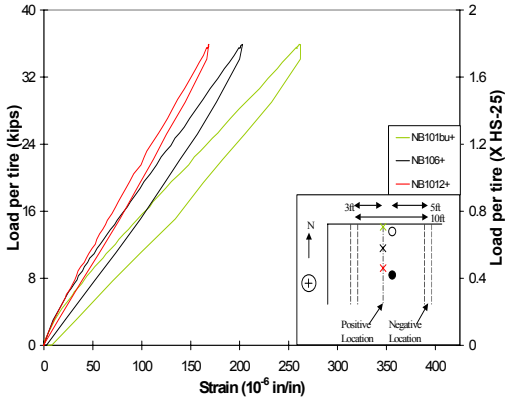

(v) Truck axle-back

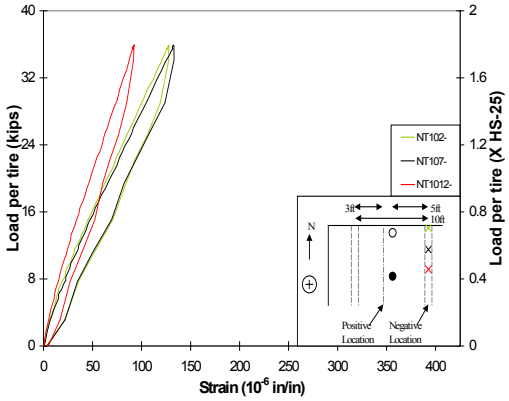

(vi) Truck axle-back

Figure A-13: Load vs. strain, 1.75xHS-25 load step, midspan loading location, northwest test area; (i), (iii) and (v): bottom mat at positive location; (ii), (iv) and (vi): top mat at negative location

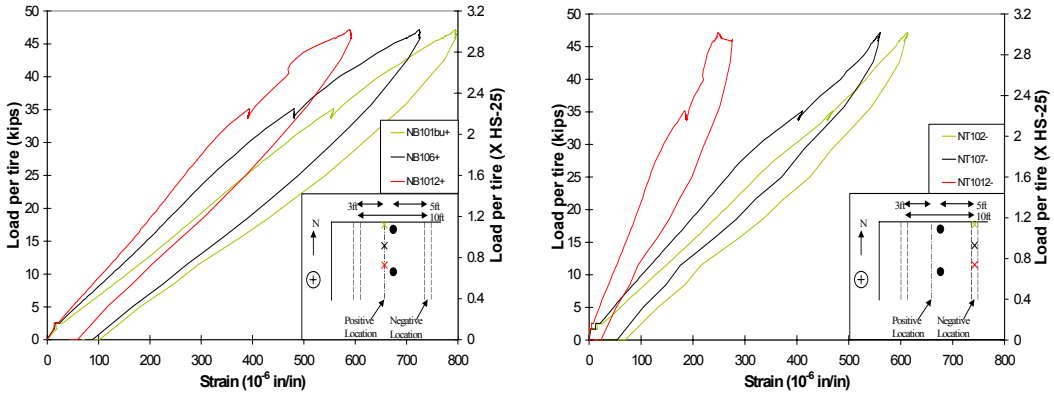

(i) Tandem

(ii) Tandem

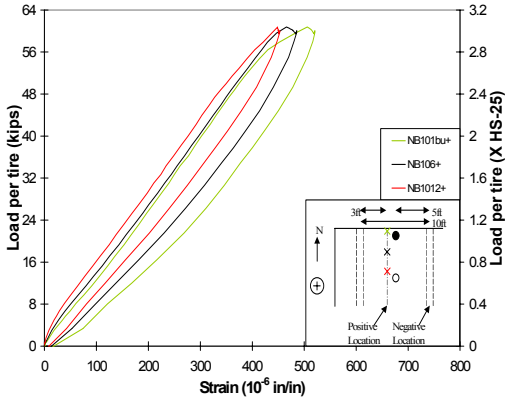

(iii) Truck axle-front

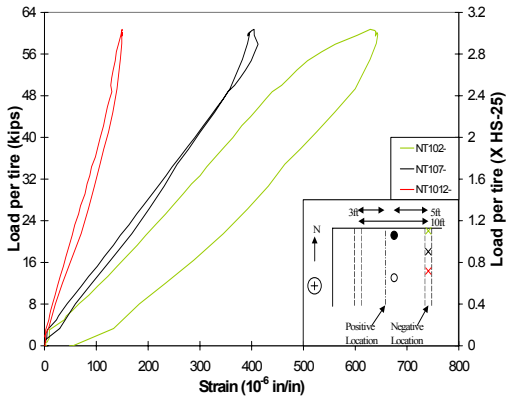

(iv) Truck axle-front

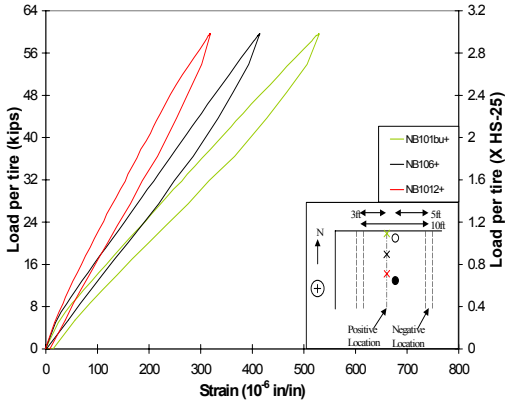

(v) Truck axle-back

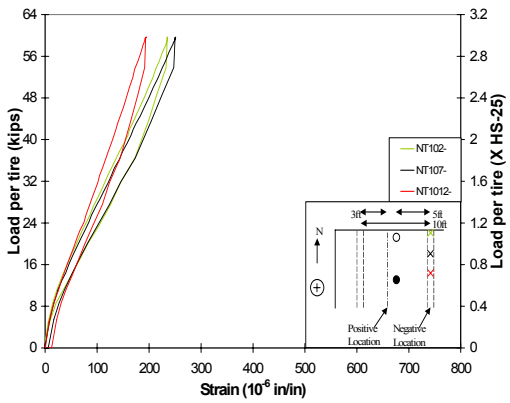

(vi) Truck axle-back

Figure A-14: Load vs. strain, 3xHS-25 load step, midspan loading location, northwest test area; (i), (iii) and (v): bottom mat at positive location; (ii), (iv) and (vi): top mat at negative location

there is a 100με residual strain induced by the tandem loading configuration at the positive moment section.

The tandem loading configuration caused a maximum strain of 800με (39% of yield strain in the steel) in the positive moment section, the largest strain created at this load step. The strains induced at the 3xHS-25 load step are relatively close in magnitude for the three loading configurations.

A.3.1.5 Loading to failure

Figure A-15 shows the load versus strain plots for the NB101bu+ and NT102- strain gauges during loading to failure. The plots include the residual strains created by the 3xHS-25 load step. The two load steps have the same stiffness, indicating there was no significant deterioration in the section when loaded to failure.

The load versus strain plot for the gauge at the positive moment section (Figure A-15, i) shows no indication of significant cracking or deterioration within the section even though there were widespread surface cracks. The readings from the NT102- strain gauge (Figure A-15, ii) show a gradual stiffness reduction, although just prior to failure, the stiffness is still substantial. The maximum strain at failure of the bridge deck occurred at the negative moment section (1500με, 72% of yield strain in the steel). The reinforcing steel was not close to yielding when the tire punched.

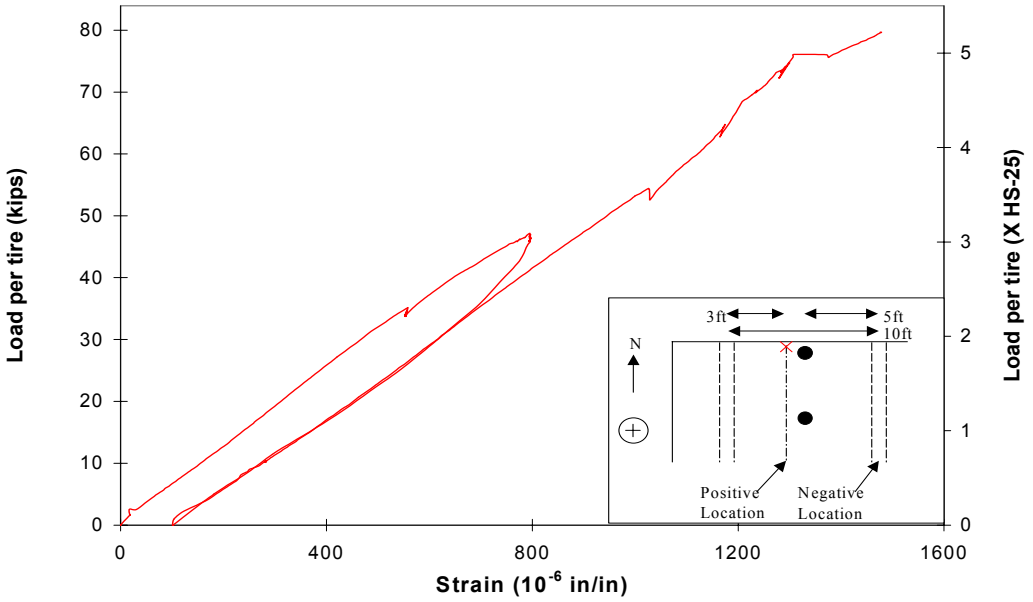

(a) NB101bu+ strain gauge in bottom mat at positive location, tandem vehicle

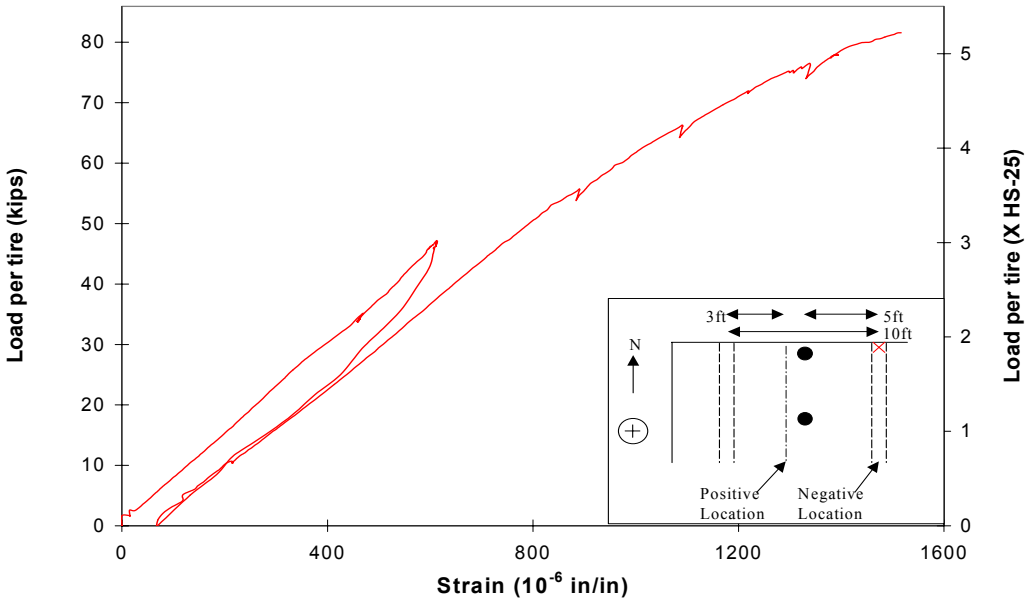

(b) NT102- strain gauge in top mat at negative location, tandem vehicle

Figure A-15: Load vs. strain, loading to failure, midspan loading location, northwest test area

A.3.2 Strain profiles

A.3.2.1 HS-25 load step

Figure A-16 shows the strain profiles for the HS-25 load step. The profile is relatively uniform across the slab end detail for all plots at this load step. Even the strain profile for the truck axle-front loading configuration, with its loads at the edge of the deck, has a flat strain profile. The tandem loading configuration's strain profile at the positive moment section (Figure A-16, i) shows the largest gradient, ranging from 300με at the edge or the deck to roughly half that at the interior side of the detail.

The strains induced across the slab end detail by the truck axle-back loading configuration at the positive moment section are close in magnitude to the truck axle-front configuration. At other test areas, the truck axle-back loading configuration did not create strains this large relative to the other configurations. The strains induced across the detail at this load step are insignificant compared to the yield strain of the reinforcing steel.

A.3.2.2 1.2xHS-25 load step

The strains at the positive and negative moment sections are well balanced at the 1.2xHS-25 load step (Figure A-17). The strain profiles at the positive moment section are uniform for all the loading configurations. The tandem loading configuration created the largest average strain across the UTSE detail at the positive moment section, however, the truck axle-back loading configuration created a comparable profile at the negative moment section.

A.3.2.3 1.75xHS-25 load step

The shape of the strain profiles at the 1.75xHS-25 load step (Figure A-18) are similar to the HS-25 and 1.2xHS-25 load steps. The maximum strain at this

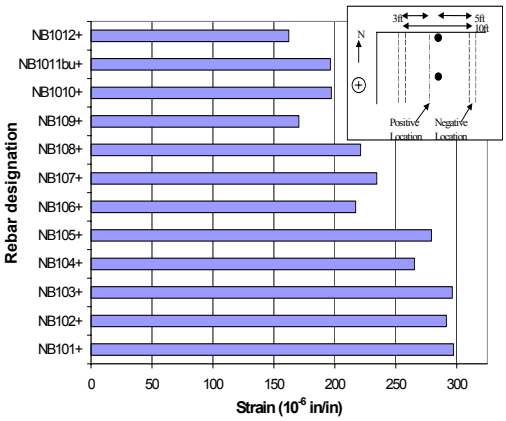

(i) Tandem

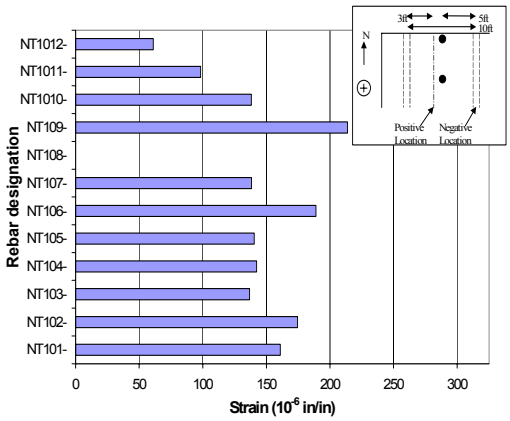

(ii) Tandem

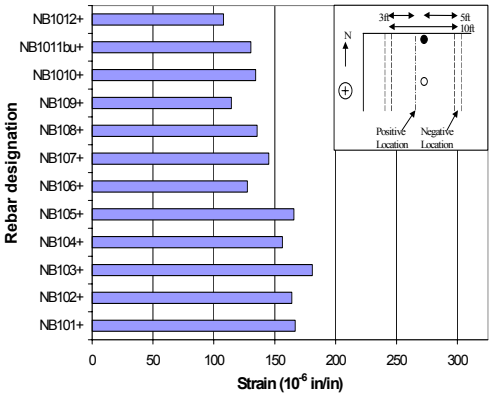

(iii) Truck axle-front

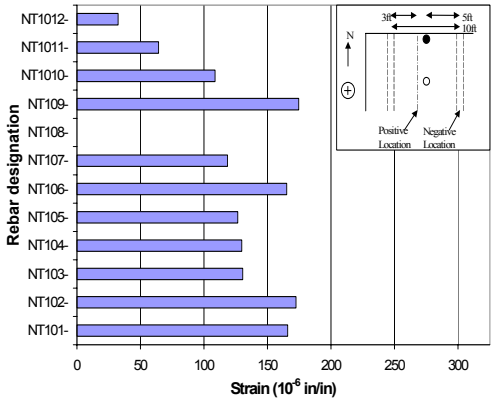

(iv) Truck axle-front

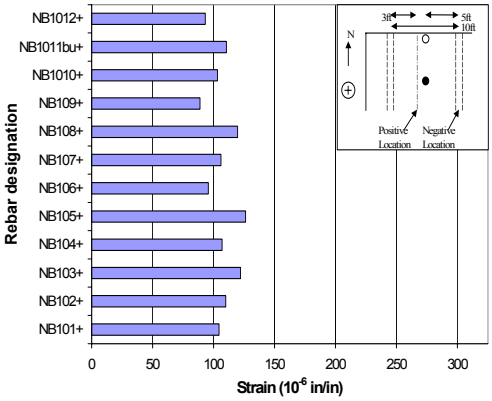

(v) Truck axle-back

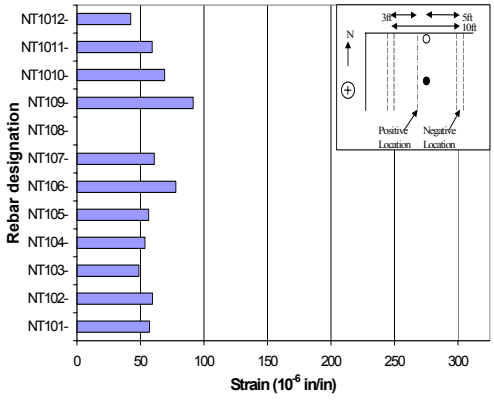

(vi) Truck axle-back

Figure A-16: Strain profiles, HS-25 load step, midspan loading location, northwest test area; (i), (iii) and (v): bottom mat at positive location; (ii), (iv) and (vi): top mat at negative location

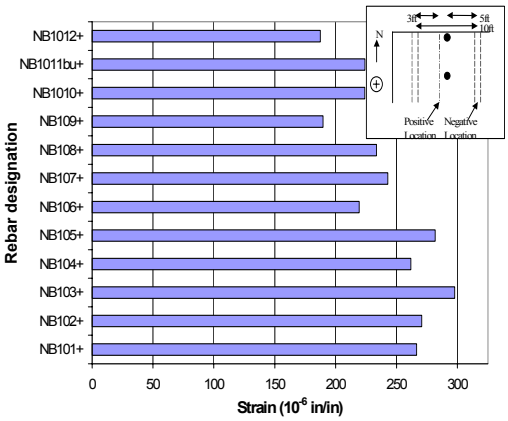

(i) Tandem

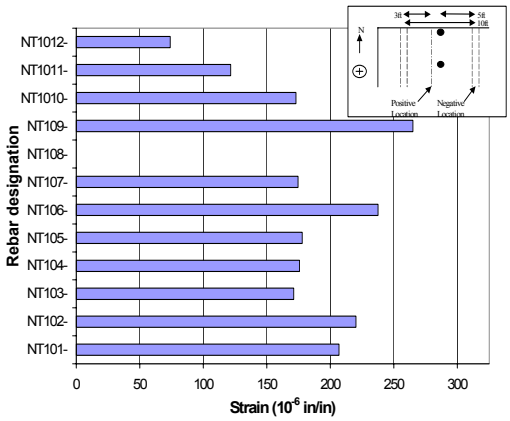

(ii) Tandem

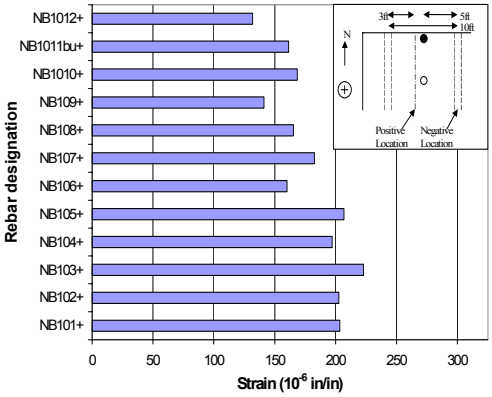

(iii) Truck axle-front

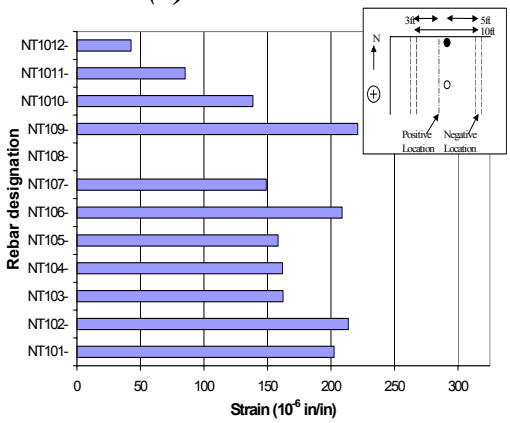

(iv) Truck axle-front

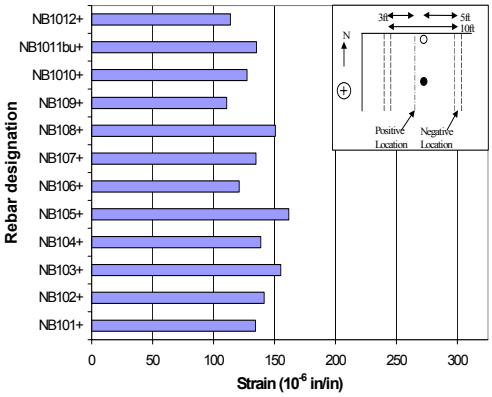

(v) Truck axle-back

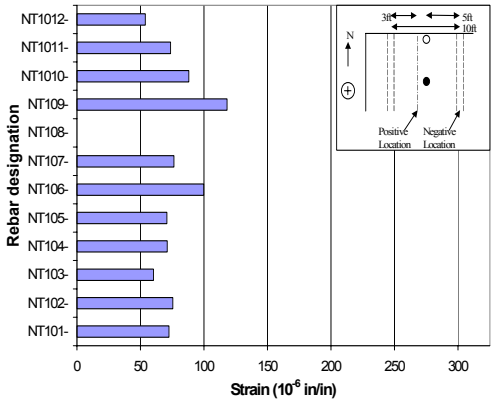

(vi) Truck axle-back

Figure A-17: Strain profiles, 1.2xHS-25 load step, midspan loading location, northwest test area; (i), (iii) and (v): bottom mat at positive location; (ii), (iv) and (vi): top mat at negative location

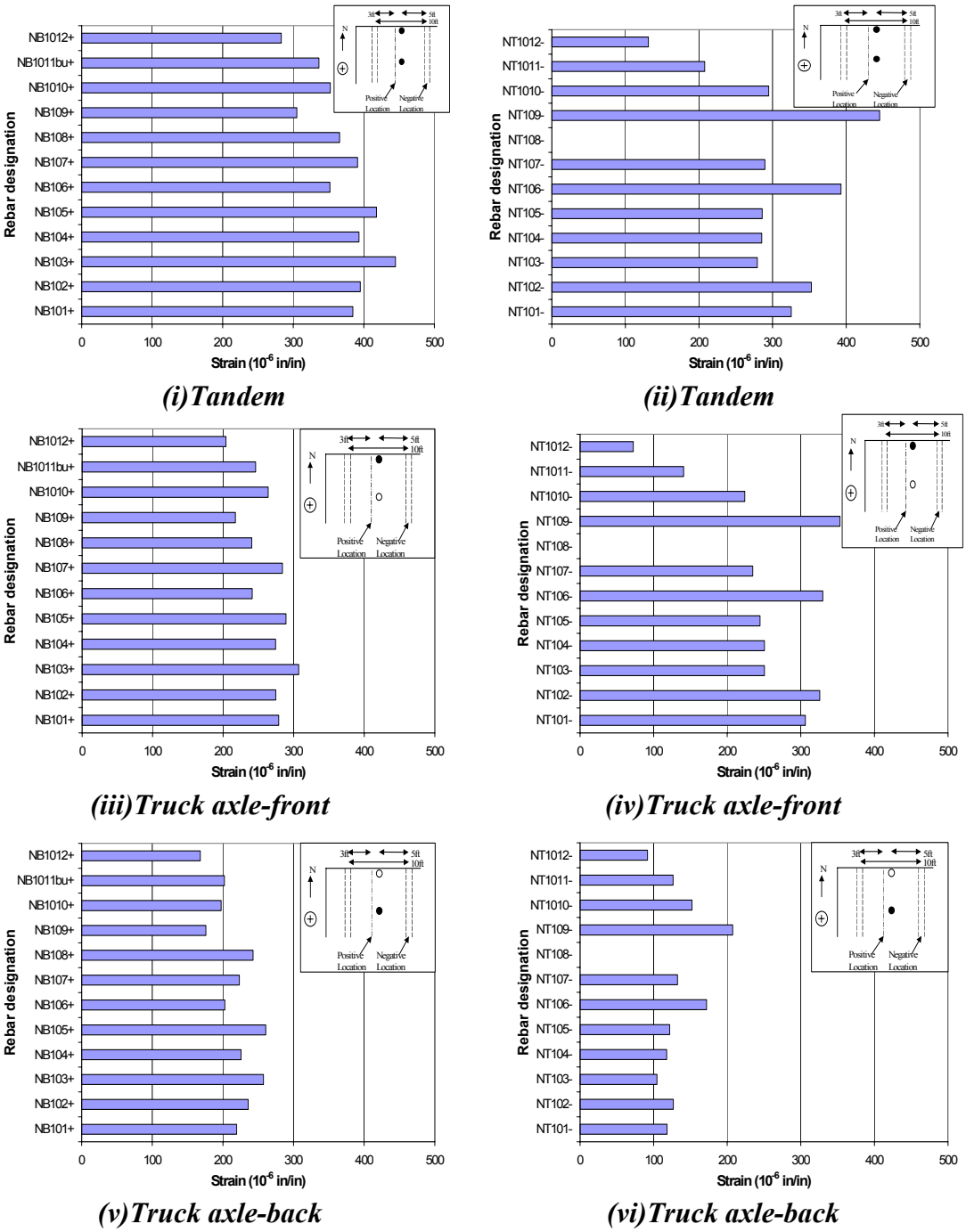

Figure A-18: Strain profiles, 1.75xHS-25 load step, midspan loading location, northwest test area; (i), (iii) and (v): bottom mat at positive location; (ii), (iv) and (vi): top mat at negative location

load step occurred in the NT109- gauge, located at the negative moment section. However, the average strain across the UTSE detail is larger at the positive moment section. The strain magnitudes at this load step are insignificant in relation to the yield strain of the steel.

A.3.2.4 3xHS-25 load step

The strain profiles in Figure A-19 for the 3xHS-25 load step are a mirror image of the 1.75xHS-25 strain profiles, with the strain magnitudes increased in proportion to the load. The strain profiles at the positive moment section are again uniform across the section. The average strain across the section at the positive moment section is relatively close for the three loading configurations.

A.3.2.5 Loading to failure

The strain profiles at failure are close to uniform and have comparable strains at the two moment sections due to redistribution of stresses. The maximum strain of 1780με (86% of yield strain in the steel) occurred at the positive moment section in the NB107+ strain gauge (Figure A-20, i). The rebar in the UTSE detail at both moment sections was not yielding when the load plate punched.

The increase in average strain across the section from the HS-25 loading to the failure loading was approximately 550% and 900% for the positive and negative moment sections, respectively. Since the load increased 420% between the two load steps, there was some non-linear behavior prior to failure. These results agree well with the load versus strain plots for the loading to failure. The plot for the strain gauge at the positive moment section (Figure A-15, i) shows a small amount of non-linear behavior prior to failure, whereas the strain gauge at the negative moment section (Figure A-15, ii) shows a larger amount of non-linear behavior.

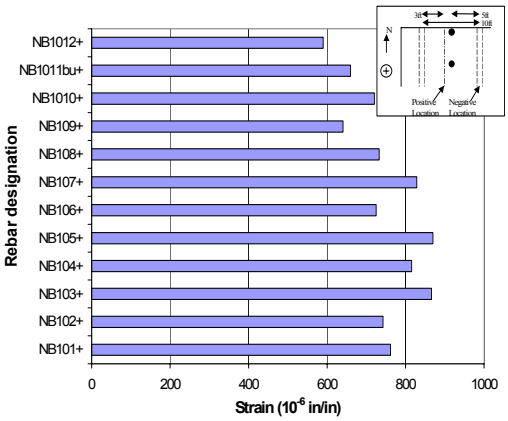

(i) Tandem

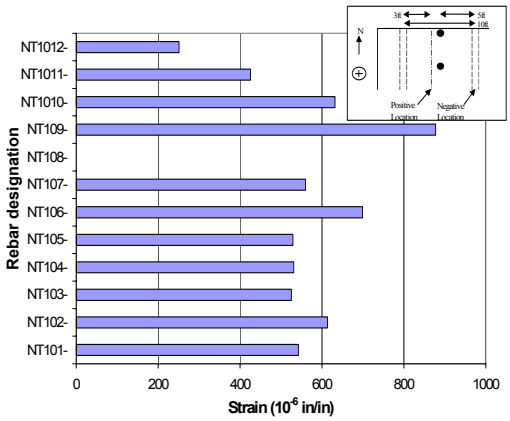

(ii) Tandem

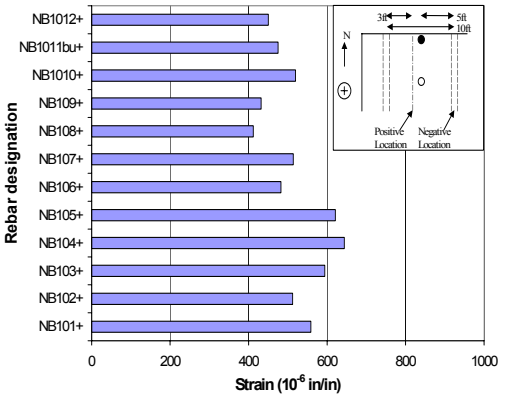

(iii) Truck axle-front

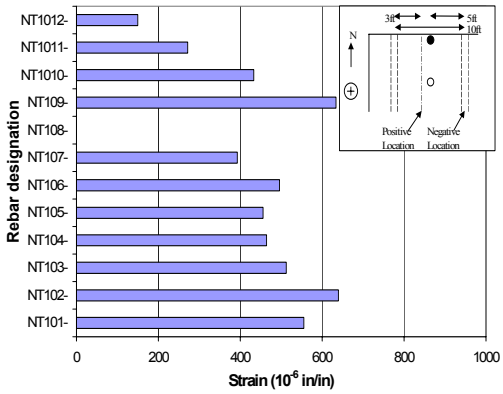

(iv) Truck axle-front

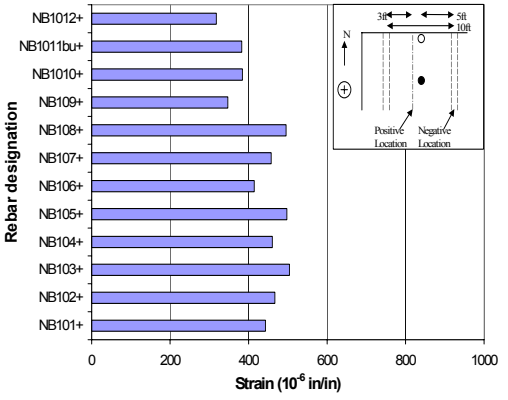

(v) Truck axle-back

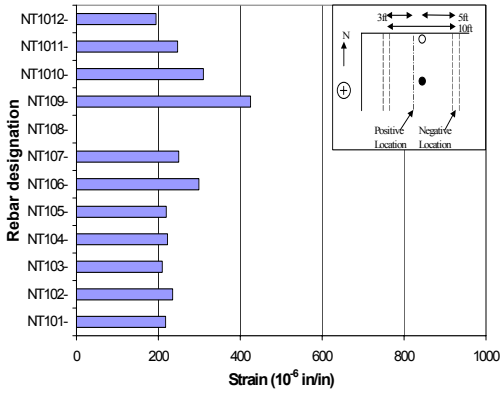

(vi) Truck axle-back

Figure A-19: Strain profiles, 3xHS-25 load step, midspan loading location, northwest test area; (i), (iii) and (v): bottom mat at positive location; (ii), (iv) and (vi): top mat at negative location

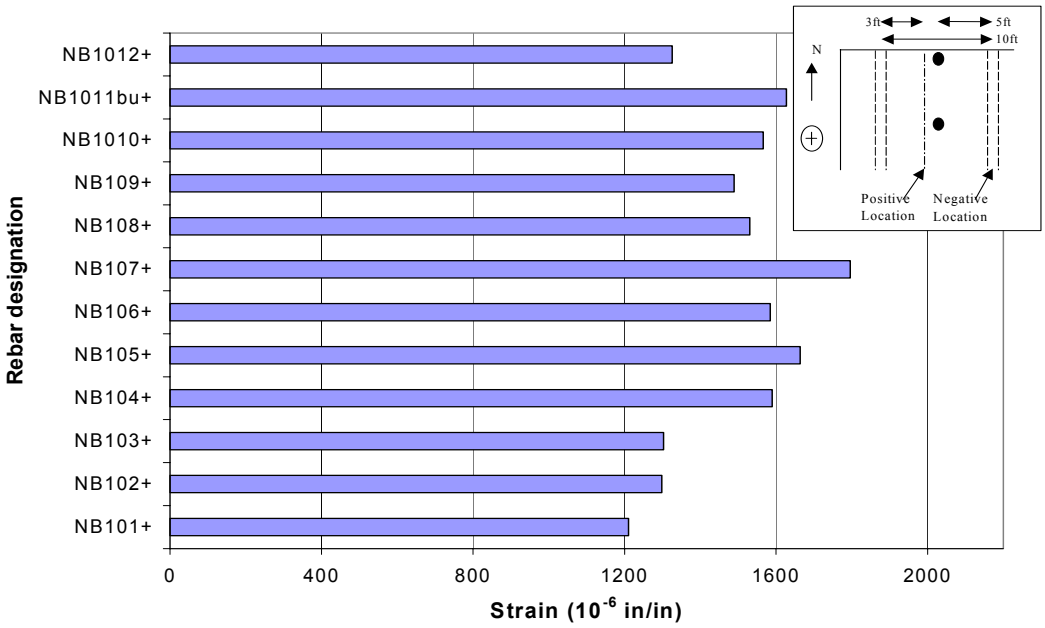

(i)Bottom mat at the positive section

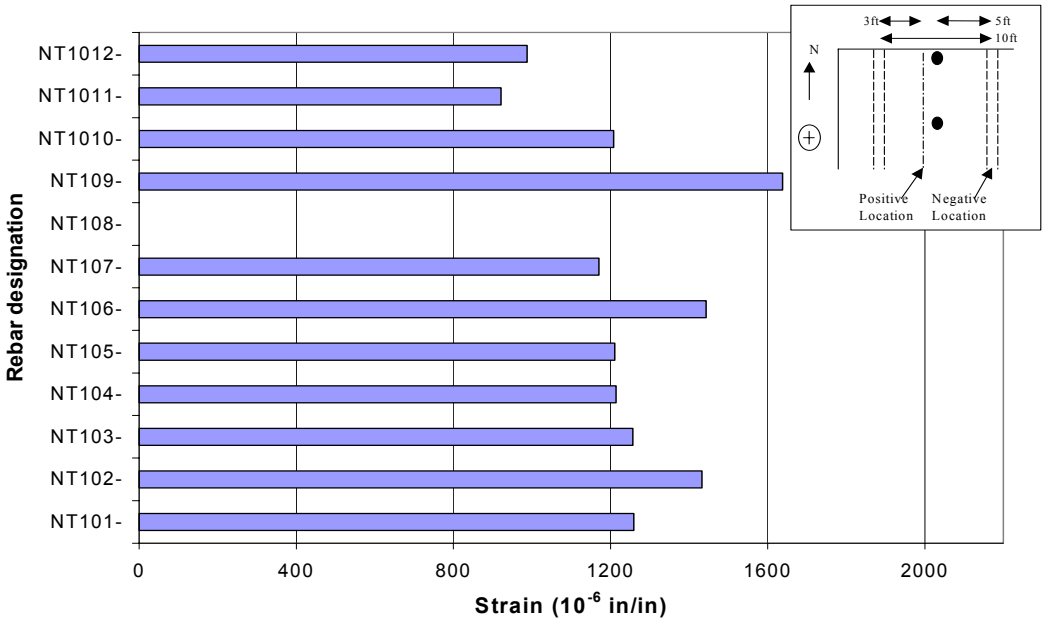

(ii)Top mat at the negative section

Figure A-20: Strain profiles, loading to failure, midspan loading location, northwest test area

A.3.3 Moment calculations

Section 5.2.2.6 describes the method used to calculate the moment in the slab end detail at the positive and negative moment sections. The moment increases linearly with the applied load increase at both moment sections. At the positive moment section, the inclusion of tension in concrete effects the moment calculated at the HS-20 load level (Figure A-21, i). However, by the HS-25 load level, the concrete is sufficiently cracked that it does not contribute a significant tension force. The maximum moment reached at the positive moment section, according to the strain gauge calculation, was 825k*in.

Also shown on the plot is the in-plane force, P, which was calculated from the strain gauge readings. The sign of P is positive for tension. The in-plane force behaved randomly at the positive moment section, switching between tension and compression as the load increases. This calculation is very sensitive to the depth of the section; the deck may be thicker than 10-inches at the positive moment section, increasing the compression zone of the section.

The plot of the moment at the negative section (Figure A-21, ii) is similar to the positive section both in shape and magnitude. The ultimate moment at this section is 885k*in. The effect of tension in concrete is present until the 1.2xHS-25 load step, a slightly larger load than in the positive moment section due to the different rebar covers at the top and bottom of the detail. The in-plane force behaves more predictably at the negative moment section. Initially, prior to cracking, the in-plane force is tension. Then, after cracking, the in-plane force increases in compression as the load increases.

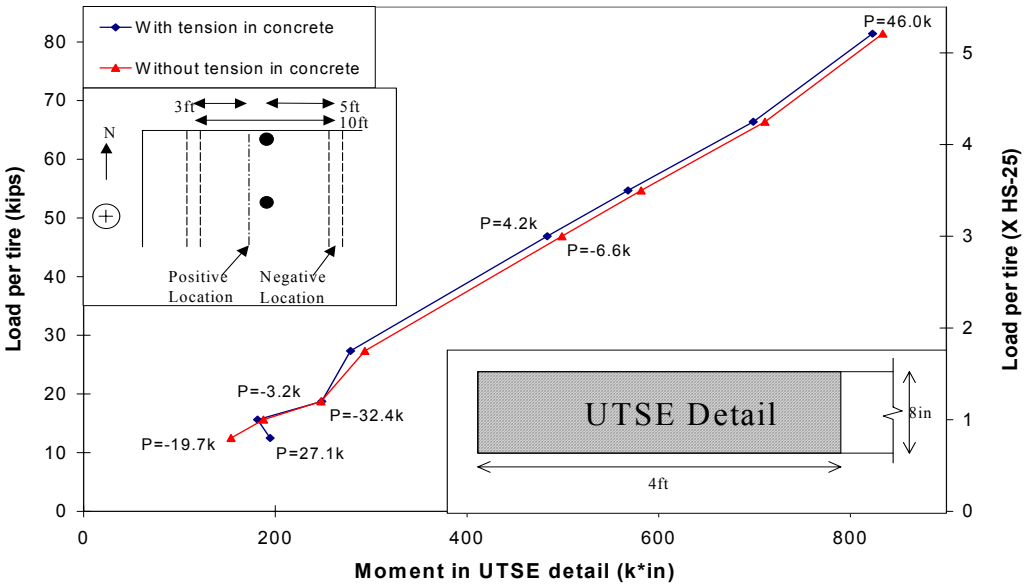

(i)Positive moment section

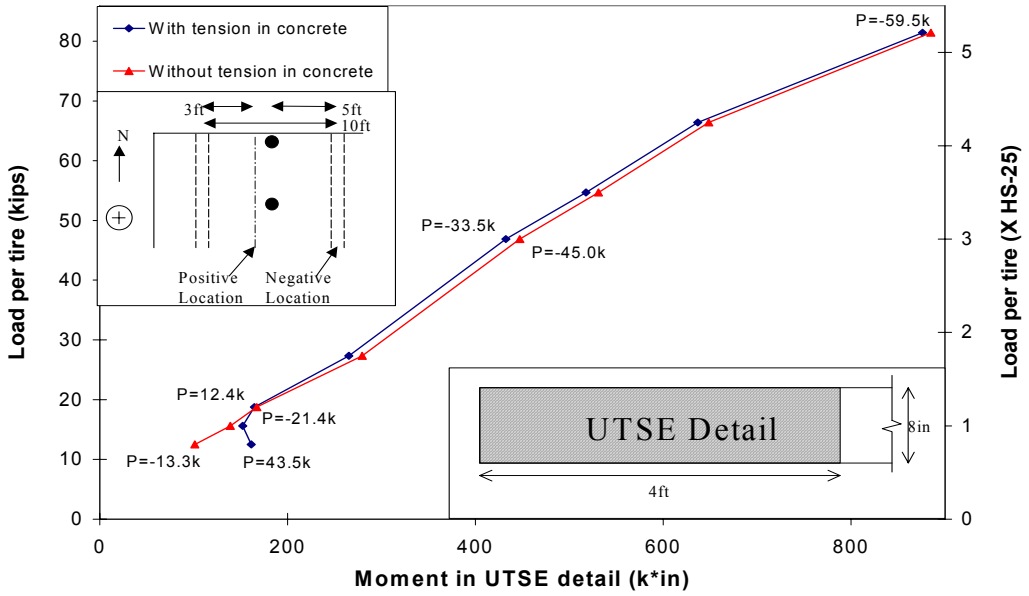

(ii)Negative moment section

Figure A-21: Moment calculated from strain gauge readings, tandem loading configuration only

A.3.4 Elastic moment comparison

The moments calculated from the strain gauges were compared to results from a linear elastic, three-span continuous beam analysis as described in section 0. This is only relevant prior to cracking of the bridge deck. For this reason, the elastic moment comparison was only performed for the HS-25 load step since the first crack was observed at a load of 1.2xHS-25.

Figure A-22 shows a comparison of the test results to the linear elastic analysis. The moments calculated using the strain data are lower than the prediction of the linear elastic analysis. This is reasonable since the model accounted for a four-foot wide section in the deck while a wider portion of the deck may contribute. In fact, the finite element analysis conducted to size the specimen in section 3.3.2 indicated this. These calculations are not aimed at reproducing the results from the linear elastic analysis. Instead, they can be used to estimate the percentage of the loads carried within the four-foot wide section of the bridge deck at the expansion joint. An examination of Figure A-22 indicates that roughly 41% of the applied loads were resisted by the four-foot wide slab end detail.

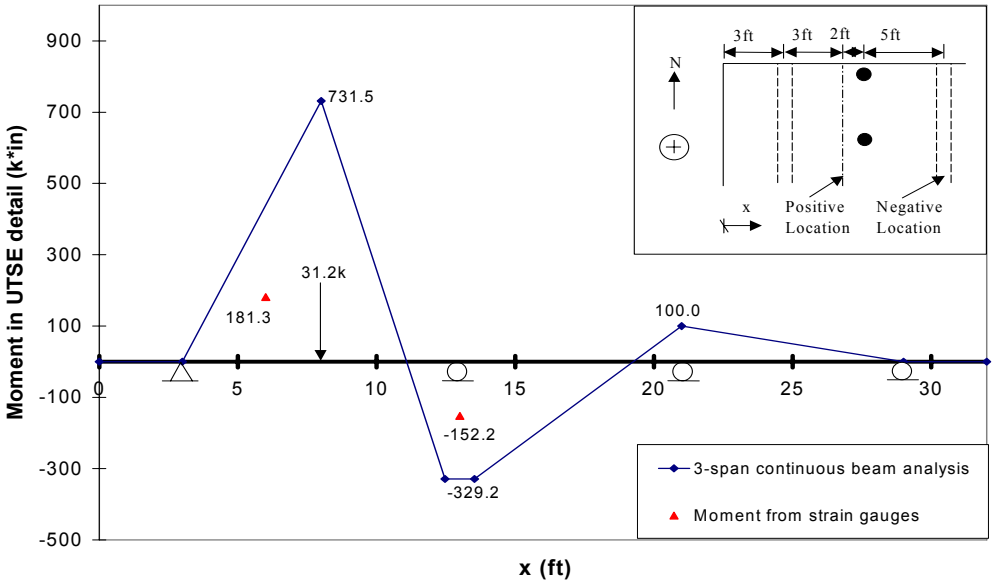

Figure A-22: Elastic moment compared to moment from strain gauges HS-25 load step

References

1. "AASHTO LRFD Bridge Design Specifications," 2nd Edition, American Association of State Highway and Transportation Officials, 1998.

2. Youn, Seok-Goo and Chang, Sung-Pil, "Behavior of Composite Bridge Decks Subjected to Static and Fatigue Loading," ACI Structural Journal, vol. 95, no. 3, May-June 1998, pg. 249-258.

3. Ockleston, A. J., "Load Tests on a Three Story Concrete Building in Johannesburg," The Structural Engineer, vol. 33, No. 10, October 1955, pg. 304-322.

4. Ockleston, A. J., "Arching Action in Reinforced Concrete Slabs," The Structural Engineer, vol. 36, no. 6, June 1958, pg. 197-201.

5. Graddy, John Conley, "Factors Affecting the Design Thickness of Bridge Slabs," Thesis Presented to the Faculty of the Graduate School of The University of Texas at Austin in Partial Fulfillment of the Requirements for the Degree of Master of Science in Engineering, May 1995.

6. Leibenberg, A. C., "Arching Action in Concrete Slabs," National Building Research Institute, Council for Scientific and Industrial Research, Report 234, Johannesburg, South Africa, 1966.

7. Park, R. and Gamble, W. L., "Reinforced Concrete Slabs, 2nd Edition,"2000.

8. Christianson, K. P., "The Effect of Membrane Stresses on the Ultimate Strength of the Internal Panel in a Reinforced Concrete Slab," The Structural Engineer, vol. 41, no. 8, August 1963, pg. 261-265.

9. Hewitt, Brian E. and Batchelor, Barrington deV., "Punching Shear Strength of Restrained Slabs," Proceedings, ASCE, ST9, September 1975, pg. 1837-1853.

10. Batchelor, Barrington deV. and Hewitt, Brian E., "Tests of Model Composite Bridge Decks," ACI Journal, vol. 73, no. 6, June 1976, pg. 340-343.

11. "Standard Specifications for Highway Bridges," 11th Edition, American Association of State Highway and Transportation Officials, 1973.

12. Ontario Bridge Design Code, Ontario Ministry of Transportation and Communications,1983, Section 7.

13. Beal, David B., "Load Capacity of Concrete Bridge Decks," Proceedings, ASCE, ST4, April 1982, pg. 814-831.

14. Azad, Abul K., Baluch, Mohammed H., Abbasi, Mohammed S. A. and Kareem, Kaiser, "Punching Capacity of Deck Slabs in Girder-Slab Bridges," ACI Structural Journal, vol. 91, no. 6, November-December 1994, pg. 656-662.

15. Fang, I-Kuang, "Behavior of Ontario-Type Bridge Deck on Steel Girders," Dissertation presented to the Faculty of the Graduate School of The University of Texas at Austin in Partial Fulfillment of the requirements for the Degree of Doctor of Philosophy, December 1985.

16. Fang, I.-K., Worley, J., Burns, N. H., and Klingner, R. E., "Behavior of Isotropic R/C Bridge Decks on Steel Girders," Journal of Structural Engineering, vol. 116, no. 3, March 1990, pg. 659-678.

17. Fang, I-Kuang, Lee, Ju-Hsin, and Chen, Chun-Ray, "Behavior of Partially Restrained Slabs under Concentrated Load, ACI Structural Journal, vol. 91, no. 2, March-April 1994, pg.133-139.

18. Mufti, Aftab A., Newhook, John P., "Punching Shear Strength of Restrained Concrete Bridge Deck Slabs," ACI Structural Journal, vol. 95, no.4, July-August 1998, pg. 375-381.

19. Petrou, Michael F. and Perdikaris, Philip C., "Punching Shear Failure in Concrete Decks as Snap-Through Instability," Journal of Structural Engineering, vol. 122, no. 9, September 1996, pg. 998-1005.

20. "TXDOT Bridge Design Manual," http://manuals.dot.state.tx.us/dynaweb/colbridg/des/@Generic__BookView;cd=2, 2001.

21. Lin, T. Y. and Burns, Ned H., "Design of Prestressed Concrete Structures," 3rd Edition, 1981.

22. ACI Committee 318, "Building Code Requirements for Structural Concrete (ACI 318-02)." American Concrete Institute, Farmington Hills, Michigan, 2002.

23. Moehle, J.P., Kreger, M.E., Leon, R., "Background to Recommendations for Design of Reinforced Concrete Slab-Column Connections," ACI Structural Journal, vol. 85, no. 6, pg. 636-644.

Vita

Jeremy Lee Ryan was born in Gallup, New Mexico on August 2, 1979, the son of William Lee Ryan and Jane Ilene Ryan. Soon after, his family moved to Anchorage, Alaska, where he lived until graduating from West Anchorage High School in 1997. Then, he attended Oregon State University in Corvallis, Oregon, where he majored in civil engineering. During the summer of 2000, he interned with KPFF Consulting Engineers in Portland, OR, performing structural design and detailing. He interned with Hoffman Construction Company in Portland, OR, during the summer of 2001. After receiving his Bachelor of Science degree from Oregon State University in 2001, he entered The Graduate School at The University of Texas at Austin.

Permanent Address: 11322 Modoc Road
White City, OR 97503

This thesis was typed by the author.